Synthesis of Thiostannates, Oxo-Thiostannates and Tin-Sulfides Applying Transition Metal Complexes Containing Macrocyclic Amine Molecules

Development of new synthetic routes to synthesize Sn-S and S-Sn-O compounds and investigation of their properties

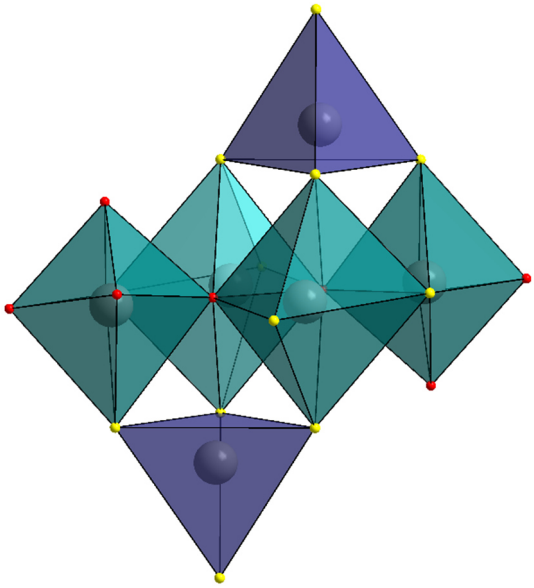

Dissertation submitted to the

Faculty of Mathematics and Natural Sciences of the Christian-Albrechts-University of Kiel, Germany

for the degree of

Doctor rer. nat.

by

Assma Benkada

Kiel 2020

Referent: Prof. Dr. Wolfgang Bensch

Koreferent: Prof. Dr. Norbert Stock

Tag der mündlichen Prüfung: 20.10.2020

Zum Druck genehmigt: Kiel, 20.10.2020

Prof. Dr. Frank Kempken, Dekan der Mathematisch-Naturwissenschaftlichen Fakultät

The present dissertation was supervised by

Prof. Dr. Wolfgang Bensch

from November 2016 to July 2020

at the Institute of Inorganic Chemistry

at the Christian-Albrechts- Albrechts-University of Kiel.

Abstract

The aims of the present work were the synthesis and characterization of new thiostannates, oxo-thiostannates and tin-sulfide compounds. The salt $Na_4SnS_4 \cdot 14H_2O$ was used as precursor, which was reacted with transition metal complexes containing macrocyclic amine ligands. The advantage of macrocyclic amine ligands is on the one hand they form very stable complexes and on the other hand they provide one or two free coordination sites so that a bond formation between thiostannate anion and transition metal cation is possible, if the transition metal cation prefers an octahedral environment.

The formation of $Na_4SnS_4 \cdot 14H_2O$ was investigated demonstrating that $Na_4SnS_4 \cdot 14H_2O$ could be prepared through a new simple procedure reacting $Na_2S \cdot 9H_2O$ with $SnCl_4 \cdot 5H_2O$ in H_2O at room temperature. For the precipitation of the product dried acetone was added to the aqueous solution. Furthermore, the stability of $Na_4SnS_4 \cdot 14H_2O$ was investigated indicating that $Na_4SnS_4 \cdot 14H_2O$ transforms slowly to the new compound $Na_4Sn_2S_6 \cdot 5H_2O$ in the solid state. The formation of $Na_4Sn_2S_6 \cdot 5H_2O$ probably requires a protonation of the terminal S^{2-} anions and condensation of the protonated species under release of H_2S. In addition, the stability of $Na_4SnS_4 \cdot 14H_2O$ in H_2O was investigated by ^{119}Sn-NMR spectroscopy demonstrating that the $[Sn_2S_6]^{4-}$ anions were formed very fast in aqueous solution.

$Na_4SnS_4 \cdot 14H_2O$ was reacted with the complexes $[Ni(cyclen)](ClO_4)_2$ and $[Ni(cyclen)(H_2O)_2](ClO_4)_2 \cdot H_2O$ under hydrothermal conditions leading to the generation of new oxo-thiostannate compounds: $\{[Ni(cyclen)]_6[Sn_6S_{12}O_2(OH)_6]\} \cdot 2(ClO_4) \cdot 19H_2O$ and $[Ni(cyclen)(H_2O)_2]_4[Sn_{10}S_{20}O_4] \cdot \sim 13H_2O$ (cyclen = 1,4,7,10-tetraazacyclo-dodecane). The crystal structure of $\{[Ni(cyclen)]_6[Sn_6S_{12}O_2(OH)_6]\} \cdot 2(ClO_4) \cdot 19H_2O$ is constructed by the rare cluster $[Sn_6S_{12}O_2(OH)_6]^{10-}$ and six Ni^{2+} centered complexes which are covalently bonded to the cluster *via* Ni–S und Ni–OH bonds. In $[Ni(cyclen)(H_2O)_2]_4[Sn_{10}S_{20}O_4] \cdot \sim 13H_2O$ only isolated cations and anions are observed. Both compounds display good photocatalytic activity for H_2 generation. Investigations of the thermal properties of both compounds indicate that the water molecules of $[Ni(cyclen)(H_2O)_2]_4[Sn_{10}S_{20}O_4] \cdot \sim 13H_2O$ can be reversibly removed and incorporated without structural collapse. However, the crystal water of $\{[Ni(cyclen)]_6[Sn_6S_{12}O_2(OH)_6]\} \cdot 2(ClO_4) \cdot 19H_2O$ cannot be reversibly removed and

treatment with small amounts of water was required leading to the generation of the pristine material and an unidentified phase.

Using the $[Cu(cyclam](ClO_4)_2$ complex (cyclam = 1,4,8,11-tetraazacyclotetradecane) the new layered compound $\{[Cu(cyclam)]_2[Sn_2S_6]\}_n \cdot 2nH_2O$ could be obtained, which is the first thiostannate compound containing Cu(II) cations. $\{[Cu(cyclam)]_2[Sn_2S_6]\}_n \cdot 2nH_2O$ was synthesized at room temperature using H_2O as solvent. In the crystal structure distorted CuN_4S_2 octahedra are observed. The distortion of the octahedra was confirmed by EPR spectroscopy. The sample can be dehydrated and rehydrated without changing the crystallinity of the material.

Similar to the synthesis of $\{[Cu(cyclam)]_2[Sn_2S_6]\}_n \cdot 2nH_2O$, syntheses were performed using the complexes $[Ni(L_1)](ClO_4)_2$ and $[Ni(L_2)](ClO_4)_2$ (L_1 = 1,8-dimethyl-1,3,6,8,10,13-hexaazacyclotetradecane and L_2 = 1,8-diethyl-1,3,6,8,10,13-hexaazacyclotetradecane) at room temperature leading to crystallization of new compounds: $[Ni(L_1)][Ni(L_1)Sn_2S_6]_n \cdot 2H_2O$ and $[Ni(L_2)]_2[Sn_2S_6] \cdot 4H_2O$. Since the complexes $[Ni(L_1)](ClO_4)_2$ and $[Ni(L_2)](ClO_4)_2$ are poorly soluble in water but exhibit a good solubility in organic solvents like acetonitrile or dimethylsulfoxide, syntheses were carried out by overlaying an aqueous solution of $Na_4SnS_4 \cdot 14H_2O$ with the $[Ni(L_1)](ClO_4)_2$ complex dissolved in acetonitrile or by overlaying a solution of the $[Ni(L_2)](ClO_4)_2$ complex dissolved in dimethylsulfoxid with an aqueous solution of $Na_4SnS_4 \cdot 14H_2O$.

Kurzzusammenfassung

Die Ziele der vorliegenden Arbeit waren die Synthese und Charakterisierung neuer Thiostannate, Oxo-Thiostannate und Zinn-Sulfid-Verbindungen. Als Precursor wurde das Salz $Na_4SnS_4 \cdot 14H_2O$ verwendet, welcher mit Übergangsmetallkomplexen zur Reaktion gebracht wurde. Die Komplexe beinhalteten ausschließlich makrozyklische Amin-Liganden, da diese einerseits sehr stabile Komplexe bilden und andererseits eine oder zwei freie Koordinationsstellen zur Verfügung stellen, so dass die Bildung einer kovalenten Bindung zwischen dem Thiostannat-Anion und dem Übergangsmetallkation möglich ist, falls das Übergangsmetallkation eine oktaedrische Umgebung bevorzugt.

Die Untersuchungen der Bildung von $Na_4SnS_4 \cdot 14H_2O$ haben gezeigt, dass $Na_4SnS_4 \cdot 14H_2O$ durch ein neues einfaches Verfahren synthetisiert werden kann. Bei diesem Verfahren wurde $Na_2S \cdot 9H_2O$ mit $SnCl_4 \cdot 5H_2O$ in H_2O bei Raumtemperatur zur Reaktion gebracht und zur Fällung des Produktes wurde trockenes Aceton zugegeben. Des Weiteren wurde die Stabilität von $Na_4SnS_4 \cdot 14H_2O$ untersucht. $Na_4SnS_4 \cdot 14H_2O$ wandelt sich langsam im festen Zustand in die neue Verbindung $Na_4Sn_2S_6 \cdot 5H_2O$ um. Die Bildung von $Na_4Sn_2S_6 \cdot 5H_2O$ erfordert wahrscheinlich eine Protonierung der terminalen S^{2-}-Anionen und die Kondensation der protonierten Spezies unter Freisetzung von H_2S. Darüber hinaus wurde die Stabilität von $Na_4SnS_4 \cdot 14H_2O$ in H_2O mit ^{119}Sn-NMR Spektroskopie untersucht. Die Ergebnisse der Untersuchungen zeigten, dass sich $[Sn_2S_6]^{4-}$-Anionen sehr schnell in Lösung bilden.

Bei der Reaktion von $Na_4SnS_4 \cdot 14H_2O$ mit den Komplexen $[Ni(cyclen)](ClO_4)_2$ und $[Ni(cyclen)(H_2O)_2](ClO_4)_2 \cdot H_2O$ unter hydrothermalen Bedingungen konnten zwei neue Oxo-Thiostannate hergestellt werden: $\{[Ni(cyclen)]_6[Sn_6S_{12}O_2(OH)_6]\} \cdot 2(ClO_4) \cdot 19H_2O$ und $[Ni(cyclen)(H_2O)_2]_4[Sn_{10}S_{20}O_4] \cdot \sim 13H_2O$ (cyclen = 1,4,7,10-Tetraazacyclododecan). Die Kristallstruktur der Verbindung $\{[Ni(cyclen)]_6[Sn_6S_{12}O_2(OH)_6]\} \cdot 2(ClO_4) \cdot 19H_2O$ besteht aus dem bisher nicht beobachteten Cluster $[Sn_6S_{12}O_2(OH)_6]^{10-}$ und aus sechs Ni^{2+}-zentrierten Komplexen, welche kovalent am Cluster *via* Ni–S- und Ni–OH-Bindungen gebunden sind. In der Struktur von $[Ni(cyclen)(H_2O)_2]_4[Sn_{10}S_{20}O_4] \cdot \sim 13H_2O$ hingegen werden isolierte Kationen und Anionen beobachtet. Beide Verbindungen zeigten gute photokatalytische Aktivität für die H_2-Generierung. Untersuchungen der thermischen

Eigenschaften belegten, dass das Kristallwasser der Verbindung $[Ni(cyclen)(H_2O)_2]_4[Sn_{10}S_{20}O_4]\cdot\sim13H_2O$ ohne Kollaps der Kristallstruktur reversibel entfernt und wieder eingebaut werden kann. Das Kristallwasser der Verbindung $\{[Ni(cyclen)]_6[Sn_6S_{12}O_2(OH)_6]\}\cdot2(ClO_4)\cdot19H_2O$ hingegen konnte nicht unter ambienten Bedingungen in die Struktur eingelagert werden, und erst nach der Behandlung der wasserfreien Probe mit wenig Wasser bildeten sich das Ausgangsmaterial und eine unbekannte Nebenphase.

Bei der Verwendung von $[Cu(cyclam](ClO_4)_2$ (cyclam = 1,4,8,11-tetraazacyclotetradecan) konnte die Schichtverbindung $\{[Cu(cyclam)]_2[Sn_2S_6]\}_n\cdot2nH_2O$ synthetisiert werden. Diese stellt das erste Thiostannat dar, welches Cu in der Oxidation Stufe +II aufweist. $\{[Cu(cyclam)]_2[Sn_2S_6]\}_n\cdot2nH_2O$ konnte bei Raumtemperatur und unter Verwendung von H_2O als Lösungsmittel synthetisiert werden. In der Kristallstruktur liegen verzerrte CuN_4S_2-Oktaeder vor. Die Verzerrung der Oktaeder konnte mittels EPR-Spektroskopie bestätigt werden. Die Wassermoleküle, welche sich zwischen den Schichten befinden, können thermisch entfernt und anschließend wieder eingelagert werden. Dabei kommt es zu keiner Änderung der Kristallinität des Materiales.

Analog zu der Synthese von $\{[Cu(cyclam)]_2[Sn_2S_6]\}_n\cdot2nH_2O$ wurden Synthesen bei Raumtemperatur durchgeführt, in denen die Komplexe $[Ni(L_1)](ClO_4)_2$ und $[Ni(L_2)](ClO_4)_2$ (L_1 = 1,8-dimethyl-1,3,6,8,10,13-hexaazacyclotetradecan und L_2 = 1,8-diethyl-1,3,6,8,10,13-hexaazacyclotetradecan) verwendet wurden. Dabei konnten die neuen Verbindungen $[Ni(L_1)][Ni(L_1)Sn_2S_6]_n\cdot2H_2O$ und $[Ni(L_2)]_2[Sn_2S_6]\cdot4H_2O$ erhalten werden. Da die Komplexe $[Ni(L_1)](ClO_4)_2$ und $[Ni(L_2)](ClO_4)_2$ eine schlechte Löslichkeit in Wasser aufweisen, aber in organischen Lösungsmitteln wie Acetonitril oder Dimethylsulfoxid sehr gut löslich sind, wurde eine wässrige Lösung von $Na_4SnS_4\cdot14H_2O$ mit einer Lösung von $[Ni(L_1)](ClO_4)_2$, gelöst in Acetonitril, oder eine Lösung von $[Ni(L_2)](ClO_4)_2$, gelöst in Dimethylsulfoxid, mit einer wässrigen Lösung von $Na_4SnS_4\cdot14H_2O$ überschichtet. Mit diesem synthetischen Vorgehen konnten die beiden Verbindungen erfolgreich hergestellt werden.

Contents

1. Introduction 1

1.1 Motivation 1

1.2 Thiostannates 1

1.2.1 Metal cations 2

1.2.2 Protonated amine molecules 3

1.2.3 Transition metal complexes 4

1.3 Tin-sulfides 5

1.4 Oxo-Thiostannates 7

1.5 Aims of this work 8

1.5.1 Utilization of building units 8

1.5.2 Utilization of macrocyclic amines 9

1.5.3 Alternative synthetic approach: Room temperature synthesis 10

2. Experimental Section 12

2.1 Chemicals 12

2.2 Characterization Methods 13

2.3 Programs 15

2.4 Synthetic approaches 16

2.4.1 Solvothermal synthesis 16

2.4.2 Room temperature synthesis 16

3. Publications 17

3.1 “New Transition Metal Oxo-Thiostannate: Synthesis, Characterization, and Investigation of its Photocatalytic Properties” 17

3.2 “Synthesis and Characterization of a Rare Transition-Metal Oxothiostannate and Investigation of its Photocatalytic Properties” 25

3.3 “The First Thiostannate Compound with Copper(II) Synthesized Under Ambient Conditions: Crystal Structure, Electronic and Thermal Properties” VIP Paper 35

3.4 “Room temperature synthesis of new thiostannates by slow interdiffusion of different solvents” 42

3.5 “Transformation of $Na_4SnS_4 \cdot 14H_2O$ into $Na_4Sn_2S_6 \cdot 5H_2O$ at room temperature in the solid state: Synthesis and Crystal Structure of the new compound $Na_4Sn_2S_6 \cdot 5H_2O$” 51

4. Conclusions and Outlook 60

5. References 62

6. Appendix 68

6.1 Supporting Information 68

6.1.1 “New Transition Metal Oxo-Thiostannate: Synthesis, Characterization, and Investigation of its Photocatalytic Properties” 68

6.1.2 “Synthesis and Characterization of a Rare Transition-Metal Oxothiostannate and Investigation of Its Photocatalytic Properties” 82

6.1.3 “The First Thiostannate Compound with Copper(II) Synthesized Under Ambient Conditions: Crystal Structure, Electronic and Thermal Properties” 98

6.1.4 “Room temperature synthesis of new thiostannates by slow interdiffusion of different solvents” 111

6.1.5 “Transformation of $Na_4SnS_4 \cdot 14H_2O$ into $Na_4Sn_2S_6 \cdot 5H_2O$ at room temperature in the solid state: Synthesis and Crystal Structure of the new compound $Na_4Sn_2S_6 \cdot 5H_2O$” 130

6.2 List of Publications 147

6.3 Acknowledgements 148

6.4 Declaration 149

1. Introduction

1.1 Motivation

The preparation of chalcogenide-based open framework materials was motivated by their applications in gas adsorption, ion exchange, electrical conductivity and photocatalysis.[1] The first microporous sulfides with germanium and tin were reported by Bedard *et al.*[2] These compounds were obtained under hydrothermal conditions in the presence of amine molecules acting as template agents.[2] Under mild solvothermal conditions molecular building units remain intact und can be interconnected by corner- and/or edge-sharing to networks containing pores. The interest in the class of thiometalates is to combine the typical exchange and catalytic properties of zeolite-like materials and the optoelectronic features of chalcogenidometalates.[3] However, the low thermal stability (< 500 °C) of chalcogenide-based open framework materials limits their applications very often.[1] Nevertheless, there are many thiometalate compounds that show reasonably good properties in catalysis, ion exchange, ion conductivity and as absorber material. For example, $Cu_2Sn_{1-x}Si_xS_3$ ($0.4 \leq x \leq 0.6$; band gaps of 1.25, 1.35 and 1.45 eV) and $[dienH_2][Cu_2Sn_2S_6]$ (dien = diethylenetriamine) display potential as absorber for photovoltaic devices,[4,5] the compound $[H_3O]_4[Cu_8Sn_3S_{12}]$ exhibits high proton conductivity,[6] $[CH_3NH_3]_2[Ag_4Sn_3S_8]$ reveals photocatalytic activity for degradation of crystal violet under visible-light irradiation,[7] $K_6Sn[Zn_4Sn_4S_{17}]$ displays exceptional ion exchange properties for Cs^+ and NH_4^+ cations,[8] in $[Me_2NH_2]_{1.33}[Me_3NH]_{0.67}[Sn_3S_7]\cdot 1.25H_2O$ the protonated amine molecules can be exchanged by UO_2^{2+} ions[9] and the compound $[DMA][H^+\text{-}TMA]_{18}[H_2O]_{14}[Sn_{40}O_{16}S_{73}]$[10] (DMA = dimethylamine, TMA = trimethylamine) reveals photoluminescence emission.

1.2 Thiostannates

Thiostannates are compounds containing isolated cations and anions.[11] In the crystal structure of thiostannates, different building units like a tetrahedron (coordination = 4), a trigonal-bipyramid (coordination = 5) or an octahedron (coordination = 6) are observed. Examples for thiostannate compounds with the $[SnS_4]^{4-}$ tetrahedron are $Na_4SnS_4\cdot 14H_2O$,[12] $K_4SnS_4\cdot 4H_2O$, $Rb_4SnS_4\cdot 4H_2O$, $Ba_2SnS_4\cdot 11H_2O$ and $Cs_4SnS_4\cdot 3H_2O$.[13] Condensation of two $[SnS_4]^{4-}$ tetrahedra *via* a common edge leads

to the generation of the dimeric $[Sn_2S_6]^{4-}$ anion. Additionally to the anions $[SnS_4]^{4-}$ and $[Sn_2S_6]^{4-}$, diverse anions generated by condensation were reported such as $[Sn_2S_5]^{2-}$, $[Sn_2S_7]^{6-}$, $[Sn_2S_8]^{2-}$, $[Sn_3S_7]^{2-}$, $[Sn_4S_9]^{2-}$, $[Sn_5S_{12}]^{4-}$ or $[Sn_4S_{10}]^{4-}$.[11,14–16] In the $[Sn_2S_7]^{6-}$ and $[Sn_4S_{10}]^{4-}$ anions, Sn atoms are tetrahedrally coordinated by S atoms while in the anions $[Sn_2S_5]^{2-}$ and $[Sn_3S_7]^{2-}$, the Sn atoms exhibit a trigonal-bipyramidal environment. Mixed-coordination numbers of 4 and 6, 4 and 5, and 5 and 6 for Sn are observed in $[Sn_2S_8]^{2-}$, $[Sn_4S_9]^{2-}$ and $[Sn_5S_{12}]^{4-}$, respectively.[11,14–16] The condensation of small structural units to large aggregates depends mainly on the pH value and concentration ratios of the components.[11] In thiostannate and tin-sulfide compounds Sn occurs in three oxidation states: +II, +III and +IV. In the above-mentioned examples for thiostannate anions Sn exhibits only the oxidation state +IV. However, there are thiostannate and tin-sulfide compounds, in which Sn adopts the oxidation states +II/IV or +III/IV.[17–20] Such compounds are called mixed-valent. The variable coordination number as well as the variable oxidation state of Sn lead to a versatility of the crystal structures of thiostannates and tin-sulfide compounds, in which three types of cations compensating the negative charge of $[Sn_xS_y]^{n-}$ anions can be distinguished: metal cations, protonated amine molecules or transition metal complexes.

1.2.1 Metal cations

Thiostannates containing metal cations for charge compensation are e.g. $Na_4SnS_4 \cdot 14H_2O$,[12] $K_4SnS_4 \cdot 4H_2O$, $Rb_4SnS_4 \cdot 4H_2O$, $Cs_4SnS_4 \cdot 3H_2O$, $Ba_2SnS_4 \cdot 11H_2O$,[13] $K_2Sn_2S_5$,[14] $Na_4Sn_2S_6 \cdot 14H_2O$,[21] $A_2Sn_2S_8$ (A = K and Rb),[14] $Na_4Sn_3S_8$[22] and $Cs_4Sn_5S_{12} \cdot 2H_2O$,[23] which include isolated anions such as $[SnS_4]^{4-}$, $[Sn_2S_5]^{2-}$, $[Sn_2S_6]^{4-}$, $[Sn_2S_8]^{2-}$, $[Sn_3S_8]^{4-}$ and $[Sn_5S_{12}]^{4-}$. In $[Sn_2S_5]^{2-}$ only SnS_5 trigonal-bipyramids are observed. These bipyramids are connected *via* two common edges consisting of one axial S and one equatorial S atom generating chains $[SnS_3]^{2-}$, which are cross-bound by the remaining equatorial S atoms of SnS_5 forming an anionic 3D framework. In this anionic framework, 1D tunnels are observed, in which the K^+ cations are found.[14] The $[Sn_2S_6]^{4-}$ units are generated by edge-sharing of two $[SnS_4]^{4-}$ tetrahedra.[21] The structure of the $[Sn_2S_8]^{2-}$ anion consists of SnS_4 tetrahedra and SnS_6 octahedra, which are linked *via* sulfide as well as polysulfide anions (S_4^{2-}) forming a layered framework. The metal cations K^+ and Rb^+ are positioned between the layers.[14] Similarly, the $[Sn_5S_{12}]^{4-}$ anion exhibits a layered structure. However, the Sn atoms are

fourfold and sixfold coordinated. The Cs^+ cations and H_2O molecules are located between the layers.[23] In contrast, the $[Sn_3S_8]^{4-}$ units feature a 3D structure, in which Sn atoms have a tetrahedral as well as trigonal-bipyramidal environment.[22]

The compounds $A_nB_mSn_xS_y$ present a further class of thiostannates with charge compensating metal cations, in which one kind of metal cations is integrated in the anionic frameworks and the other type balances the negative charge. Examples are: A_2CdSnS_4 (A = Li and Na), $Na_6CdSn_4S_{12}$,[24] $Rb_2Cu_2SnS_4$, $Rb_2Cu_2Sn_2S_6$, $K_2Au_2SnS_4$ and $K_2Au_2Sn_2S_6$.[25] These compounds feature 1D, 2D and 3D structures. Most of these compounds are synthesized by high-temperature reaction or by molten flux synthesis. Under solvothermal conditions, amine molecules can be used as structure-directing reagents generating new thiostannate compounds with crystal structures, which are not available using high-temperature reaction or molten flux synthesis.

1.2.2 Protonated amine molecules

Compounds with protonated amine molecules as charge balancing cations enclose mostly layered anions. The most prominent examples are R-SnS-1 and R-SnS-3, where R represents the type of cations. In these materials, the layered anions $[Sn_3S_7]^{2-}$ and $[Sn_4S_9]^{2-}$, respectively are observed (Figure 1).[26,27] Prominent examples include $[DABCOH]_2[Sn_3S_7]$ (DABCO = 1,8-diazabicyclooctane),[15,27] $[ATEA]_2[Sn_3S_7]$ (ATEA = ammonium-tetraethylammonium), $[TEA]_2[Sn_3S_7]$ (TEA = tetraethylammonium),[15] $[TMA]_2[Sn_3S_7]$ (TMA = tetramethylammonium),[28] $[trenH]_2[Sn_3S_7]$ (tren = tris(2-aminoethyl)amine),[29] $[1AEP]_2[Sn_3S_7]$ (1AEP = 1-(2-aminoethyl)piperidine),[30] $[TPA]_2[Sn_4S_9]$ (TPA = tetrapropylammonium), $[TBA]_2[Sn_4S_9]$ (TBA = tetrabutylammonium).[15] The structure of the $[Sn_3S_7]^{2-}$ anion consists of the clusters $\{Sn_3S_4\}$, where Sn atoms are in trigonal-bipyramidal environment. The linkage of $\{Sn_3S_4\}$ *via* $(\mu\text{-}S)_2$ leads to the generation of negatively charged layers, in which hexagonal rings with 24 atoms are observed. Similarly, the structure of the $[Sn_4S_9]^{2-}$ anion is composed of the clusters $\{Sn_3S_4\}$, which are interconnected by $(\mu\text{-}S)_2$ as well as by $(\mu\text{-}S_2SnS_2)$ units forming elliptically shaped 32-atom rings. In contrast to $[Sn_3S_7]^{2-}$ layers, the Sn atoms are in a tetrahedral as well as a trigonal-bipyramidal coordination. The negative charge of the layers is balanced by protonated amine cations located between the layers. In addition to both materials, there are also thiostannates with protonated amine molecules containing $[Sn_2S_6]^{4-}$, e.g. $[CHAH]_4[Sn_2S_6]$ (CHA =

cyclohexylamine),[31] $[enH]_4[Sn_2S_6]$,[32] $[enH]_4[Sn_2S_6]\cdot en$ (en = ethylenediamine),[33] $[C_{12}H_{25}NH_3]_4[Sn_2S_6]\cdot 2H_2O$[34] and $[trenH_2]_2[Sn_2S_6]$.[35] In the presence of transition metal cations, complexes were often obtained, which are *in-situ* formed and act as counterions.

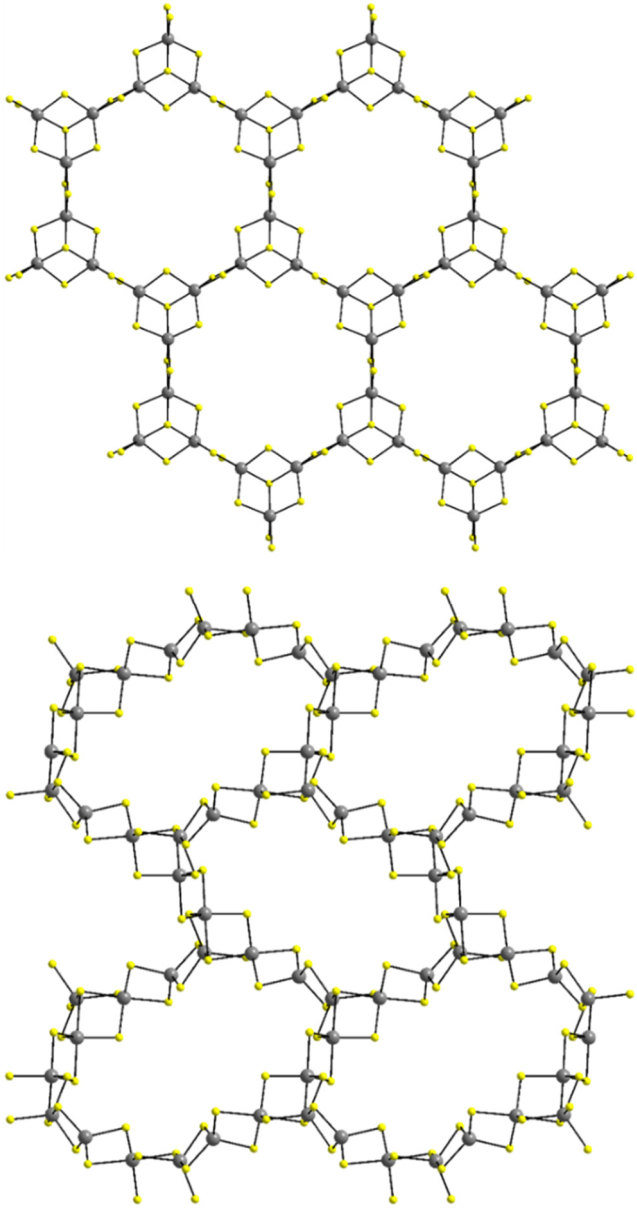

Figure 1: Crystal structures of the layered $[Sn_3S_7]^{2-}$ (top) and $[Sn_4S_9]^{2-}$ anions (bottom). Yellow: S atoms, grey: Sn atoms.

1.2.3 Transition metal complexes

Thiostannate compounds with transition metal complexes are listed in Table 1. As can be seen numerous compounds involve Ni^{2+} centered complexes as counterions. Moreover, only a few thiostannates contain Co^{2+}, Mn^{2+} or Zn^{2+} centered complexes

and no thiostannates with $Ag^{+/2+}$, $Cu^{+/2+}$ or Fe^{2+} complexes are observed. According to Table 1, bi-, tri- and hexadentate amine molecules such as 2amp (2amp = 2-(aminomethyl)pyridine), 1,2-dach (1,2-dach = 1,2-diaminocyclohexane), dap (dap = 1,2-diaminopropane), dien, en, aepa (aepa = N-2-aminoethyl-1,3-propandiamine) or peha (peha = pentaethylenehexamine) prefer to form saturated complexes with the transition metal cations Co^{2+}, Mn^{2+}, Ni^{2+} and Zn^{2+}. In contrast, tetra- and pentadentate amine molecules like cyclam (cyclam = 1,4,8,11-tetraazacyclotetradecane), tren, trien (trien = triethylenetetramine) or tepa (tepa = tetraethylenepentamine) favor to generate complexes with free coordination sites enabling the S^{2-} anions of the anionic unit to coordinate to the metal cation forming tin-sulfide compounds (see below). In the case of thiostannates comprising Ni^{2+} cations, various amine ligands with different denticities are observed demonstrating that the affinity of Ni^{2+} cations for N atoms is higher than for S atoms.

1.3 Tin-sulfides

Tin-sulfide compounds with transition metal complexes include mainly the $[Sn_2S_6]^{4-}$ anion (Table 1). The transition metal cations and the thiostannate anions are covalently bonded by three connection modes: a) two *trans* terminal S^{2-} anions of the thiostannate unit have bonds to two transition metal centers, b) one transition metal center is coordinated by N atoms of the amine molecule and by two S^{2-} anions, or c) each metal center is coordinated by one S^{2-} anion. Many tin-sulfide compounds contain Mn^{2+} centered complexes, in which mostly bidentate amine ligands are present, indicating that Mn^{2+} cations exhibit approximately the same affinity to S atoms and to N atoms. Tin-sulfide compounds with Ag^{+} complexes are not observed until now and only compounds with integrated Ag^{+} in the anionic framework were reported such as [1,4-dabH$_2$][Ag$_2$SnS$_4$] (1,4-dab = 1,4-diaminobutane),[36] [enH$_2$][Ag$_2$SnS$_4$][37] and [NH$_4$]$_2$[Ag$_6$Sn$_3$S$_{10}$].[38] Similarly, there are many tin-sulfide frameworks with integrated Cu^{+} in the anionic framework like in [enH][Cu$_2$AgSnS$_4$],[39] [enH]$_3$[Cu$_7$Sn$_4$S$_{12}$], [enH]$_{6+n}$[Cu$_{40}$Sn$_{15}$S$_{60}$],[18] [enH$_2$]$_2$[Cu$_8$Sn$_3$S$_{12}$],[40] [dienH$_2$][Cu$_2$Sn$_2$S$_6$],[5] [DBUH][CuSnS$_3$] (DBU = 1,8-diazabicyclo[5.4.0]undec-7-ene), [1,4-dabH$_2$][Cu$_2$SnS$_4$],[41] [H$_3$tren][Cu$_7$Sn$_4$S$_{12}$].[18] In both tin-sulfide types, Ag and Cu atoms are in the oxidation state +I. Cu(II) thiostannates and tin-sulfides have not been observed due to the reduction of Cu(II) by S^{2-} anions to Cu(I).

Table 1: Thiostannate and tin-sulfide compounds containing transition metal complexes.

Thiostannates
$Ag^{+/2+}$

Co^{2+}
$[Co(en)_3]_2[Sn_2S_6]$,[42] $[Co(dien)_2]_2[Sn_2S_6]$,[43] $[Co(dien)_2](dienH_2)Sn_2S_6$,[44] $[Co(2amp)_3]_2[Sn_2S_6]\cdot 10H_2O$, $[Co(1,2\text{-dach})_3]_2[Sn_2S_6]\cdot 8H_2O$[45]
$Cu^{+/2+}$

Fe^{2+}

Mn^{2+}
$[Mn(en)_3]_2[Sn_2S_6]$,[42] $[Mn(en)_3]_2[Sn_2S_6]\cdot 2H_2O$, $[Mn(dien)_2]_2[Sn_2S_6]$, $[Mn(dien)_2][MnSnS_4]$[46]
Ni^{2+}
$[Ni(en)_3]_2[Sn_2S_6]$,[47,48] $[Ni(dien)_2]_2[Sn_2S_6]$,[47] $[Ni(1,2\text{-dap})_3]_2[Sn_2S_6]\cdot 2H_2O$,[48] $[Ni(1,2\text{-dach})_3]_2[Sn_2S_6]\cdot 4H_2O$,[43] $[Ni(peha)]_2[Sn_2S_6]\cdot H_2O$,[43] $[Ni(tren)(en)]_2[Sn_2S_6]\cdot 2H_2O$,[49] $[Ni(aepa)_2]_2[Sn_2S_6]$,[43] $[Ni(tren)(1,2\text{-dap})]_2[Sn_2S_6]\cdot 4H_2O$,[49] $[Ni(tren)(en)]_2[Sn_2S_6]\cdot 6H_2O$,[49] $[Ni(tren)(2amp)]_2[Sn_2S_6]\cdot 10H_2O$,[49] $[Ni(tren)(1,2\text{-dach})]_2[Sn_2S_6]\cdot 4H_2O$,[49] $[Ni(tren)(1,2\text{-dach})]_2[Sn_2S_6]\cdot 3H_2O$,[49] $[Ni(2amp)_3]_2[Sn_2S_6]\cdot 9.5H_2O$,[50] $[Ni(tren)(ma)(H_2O)]_2[Sn_2S_6]\cdot 4H_2O$,[51] $[Ni(tren)(1,2\text{-dap})]_2[Sn_2S_6]\cdot 2H_2O$,[51] $[Ni(tren)_2]_2[Sn_2S_6]\cdot 8H_2O$,[52] $[Ni(tren)(2amp)]_2[Sn_2S_6]$[52]
Zn^{2+}
$[Zn(en)_3]_2[Sn_2S_6]$[42]
Tin-sulfides
$Ag^{+/2+}$

Co^{2+}
$\{[Co(tren)]_2[Sn_2S_6]\}$,[48] $\{[Co(tepa)]_2[Sn_2S_6]\}$,[53] $\{[Co(Phen)_2]_2[Sn_2S_6]\}$,[54] $\{[Co(Phen)_2]_2[Sn_2S_6]\}\cdot Phen\cdot H_2O$,[54] $\{[Co(cyclam)]_2[Sn_2S_6]\}_n\cdot 2nH_2O$[55]
$Cu^{+/2+}$

| --- |
| **Fe^{2+}** |
| {[Fe(tepa)]$_2$[Sn_2S_6]},[53] {[Fe(Phen)$_2$]$_2$[Sn_2S_6]},[54] {[Fe(Phen)$_2$]$_2$[Sn_2S_6]}·Phen·H_2O,[54] {[Fe(1,2-dach)$_2$][Sn_2S_6]}$_n$·2n(1,2-dachH)[56] |
| **Mn^{2+}** |
| {[Mn(tren)]$_2$[Sn_2S_6]},[29] {[Mn(trien)]$_2$[SnS_4]}·4H_2O,[57] {[Mn(trien)]$_2$[SnS_4]},[43] {[Mn(2,2'-bipy)$_2$]$_2$[Sn_2S_6]},[56] {[Mn(1,2-dach)$_2$][Sn_2S_6]}$_n$·2ndachH,[58] {[Mn(1,2-dach)$_2$(H_2O)]$_2$[Sn_2S_6]},[58] {[Mn(Phen)$_2$]$_2$[Sn_2S_6]},[59] {[Mn(Phen)$_2$]$_2$[Sn_2S_6]}·Phen·H_2O,[59] {[Mn(Phen)$_2$]$_2$[SnS_4]$_2$[Mn(Phen)]$_2$}·H_2O,[59] {[Mn(Phen)$_2$]$_2$[Sn_2S_6]}·Phen,[59] {[Mn(phen)]$_2$[SnS_4]}$_n$·nH_2O,[60] {[Mn(en)$_2$]$_2$[Sn_2S_6]},[61] {[Mn(en)$_2$]$_2$(μ-en)(μ-Sn_2S_6)}$_\infty$,[62] {[Mn(tepa)]$_2$[Sn_2S_6]},[63] {[Mn(1,2-dap)$_2$]$_2$[Sn_2S_6]},[46] {[Mn(1,2-dap)$_2$(H_2O)]$_2$[Sn_2S_6]}[64] |
| **Ni^{2+}** |
| {[Ni(tepa)]$_2$[Sn_2S_6]},[53] {o[Ni(tepa)]$_2$[Sn_2S_6]},[43] {[Ni(phen)$_2$]$_2$[Sn_2S_6]}·2,2'-bipy,[65] {[Ni(Phen)$_2$]$_2$[Sn_2S_6]}·4,4'-bipy·0.5H_2O,[65] {[Ni(phen)$_2$]$_2$[Sn_2S_6]}·biph,[56] {[Ni(phen)$_2$]$_2$[Sn_2S_6]}·phen·H_2O,[56] {[Ni(cyclam)]$_2$[Sn_2S_6]}$_n$·2nH_2O,[56] {[Ni(tren)]$_2$[Sn_2S_6]}[48] |
| **Zn^{2+}** |
| {[Zn(tren)]$_2$[Sn_2S_6]}[44] |

ma: methylamine, 2,2'-bipy: 2,2'-bipyridine , 4,4'-bipy: 4,4'-bipyridine, biph: biphenyl, phen: 1,10- phenanthroline.

1.4 Oxo-Thiostannates

In oxo-thiostannate compounds the anions $[Sn_xS_yO_z]^{n-}$ are observed, in which the SnS_x polyhedra are connected *via* O^{2-} anions. For example, the anion $[Sn_{10}S_{20}O_4]^{8-}$ is composed of ten corner linked SnS_4 tetrahedra forming the T3-type supertetrahedron $[Sn_{10}S_{20}]$. The O^{2-} anions are positioned between the SnS_4 tetrahedra and exhibit a tetrahedral coordination of Sn atoms.[11,66–68] The Sn_4O tetrahedra are connected *via* corners forming an anti-T2 cluster.[69] Isolated anionic clusters $[Sn_{10}S_{20}O_4]^{8-}$ with inorganic cations compensating the negative charge are observed in $[Li_8(H_2O)_{29}][Sn_{10}S_{20}O_4]\cdot 2H_2O$[66] and $[Cs_8(H_2O)_{13}][Sn_{10}S_{20}O_4]$.[67] Only in the compound {[Ni(1,2-dach)$_2$(ma)]$_4$[$Sn_{10}S_{20}O_4$]}, the $[Sn_{10}S_{20}O_4]^{8-}$ cluster is covalently bound *via* S

atoms to Ni^{2+} cations.[69] In addition to this cluster, there are further oxo-clusters, in which Cl^- anions or sulfur containing organic molecules are integrated in the cluster like in $[Sn_{10}S_{16}O_4Cl_4]^{4-}$,[70] $[Sn_8S_{12}O_4(SPh)_6]^{6-}$ (Ph = phenyl)[71] and $[Sn_8S_{12}O_2(OH)_2Cl_6]^{4-}$[70] (Figure 2).

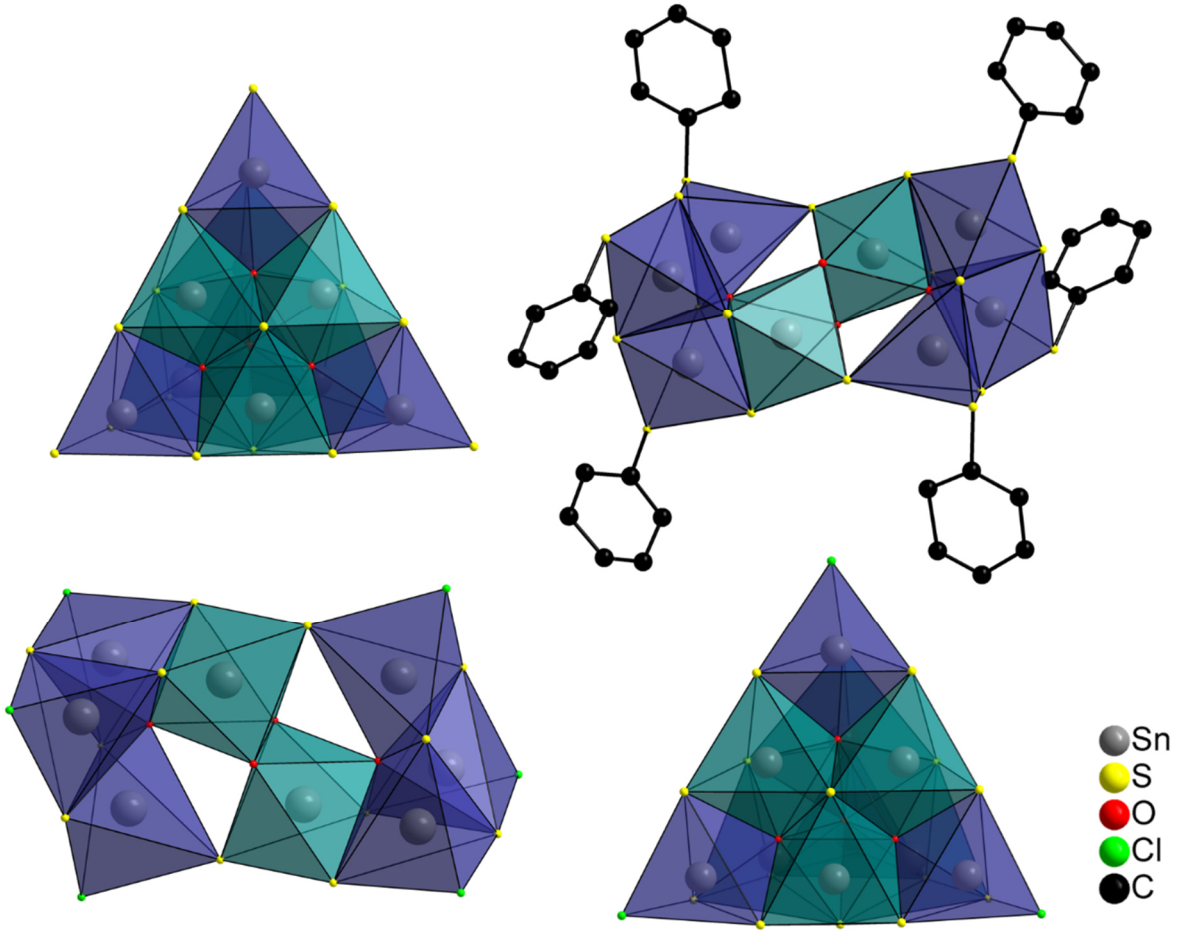

Figure 2: View of the clusters $[Sn_{10}S_{20}O_4]^{8-}$ (top left), $[Sn_8S_{12}O_4(SPh)_6]^{6-}$ (top right), $[Sn_8S_{12}O_2(OH)_2Cl_6]^{4-}$ (bottom left) and $[Sn_{10}S_{16}O_4Cl_4]^{10-}$ (bottom right). The teal colored polyhedra highlighting the octahedrally coordinated Sn, the blue polyhedra highlight the trigonal bipyramidal coordinated Sn.

1.5 Aims of this work

1.5.1 Utilization of building units

Many thiostannate and tin-sulfide compounds were synthesized applying the elements Sn, S and transition metals or transition metal salts under solvothermal conditions.[72] Using the elements Sn and S as starting materials basic conditions are required to form polysulfide anions which are able to react with Sn yielding thiostannate anions.[31]

The needed basic conditions are achieved using amine molecules in water as solvents, which can also act as structure directing agents and charge compensating cations. Moreover, SnS_2[23,73,74] and salts like $SnCl_4 \cdot 5H_2O$[42,47,62,75] or $SnCl_2 \cdot 2H_2O$[53,76] were utilized as Sn sources. To minimize the reaction parameters of solvothermal reactions, building units were applied. For example, the compound $\{[Ni(tren)]_2[Sn_2S_6]\}_n$ was applied as precursor leading to the formation of new thiostannate compounds at room temperature.[51,52] The drawback of this precursor is the restricted product diversity. Applying $Na_4SnS_4 \cdot 14H_2O$ as precursor thiostannate and tin-sulfide compounds could be obtained under solvothermal conditions as well as at room temperature.[49,50,56] The use of such building units can simplify the planning of the reactions leading to the generation of thiostannates and/or tin-sulfide compounds, if these building units are stable in the used solvents.

1.5.2 Utilization of macrocyclic amines

In this work, transition metal complexes including macrocyclic amine ligands like cyclen (cyclen = 1,4,7,10-tetraazacyclododecane), cyclam, 1,8-Dimethyl- (L_1) and 1,8-Diethyl-1,3,6,8,10,13-hexaazacyclotetradecane (L_2) were applied as charge balancing agents (Figure 3). The advantage of macrocyclic ligands is that they form stable complexes and provide two free coordination sites on transition metal cations and if these cations favor an octahedral environment, the coordination of S^{2-} anions of the $[Sn_xS_y]^{n-}$ and $[Sn_xS_yO_z]^{n-}$ moieties to transition metal cations is achievable. In fact, in the compounds $\{[M(cyclam)]_2[Sn_2S_6]\}_n \cdot 2nH_2O$ (M = Co and Ni), the $[M(cyclam)]^{2+}$ cations are covalently bonded to the $[Sn_2S_6]^{4-}$ anions according to connection mode c) (see chapter 1.3 Tin-Sulfides) generating layers.[55,56] The N_4Cu/Ni moieties in $[Cu(cyclam)]^{2+}$, $[Ni(L_1)]^{2+}$ and $[Ni(L_2)]^{2+}$ complex cations are coplanar, whereas the coplanarity of N_4Ni units in $[Ni(cyclen)]^{2+}$ is not achieved. Cyclen is the smallest ligand of the macrocyclic amine molecules. This could be the reason why the coplanarity of the N_4Ni units in compounds containing cyclen ligands decrease and thus the cis-stereochemistry is preferred, which is indeed observed in the complex $[Ni(cyclen)(H_2O)_2](ClO_4)_2 \cdot 2H_2O$[77].

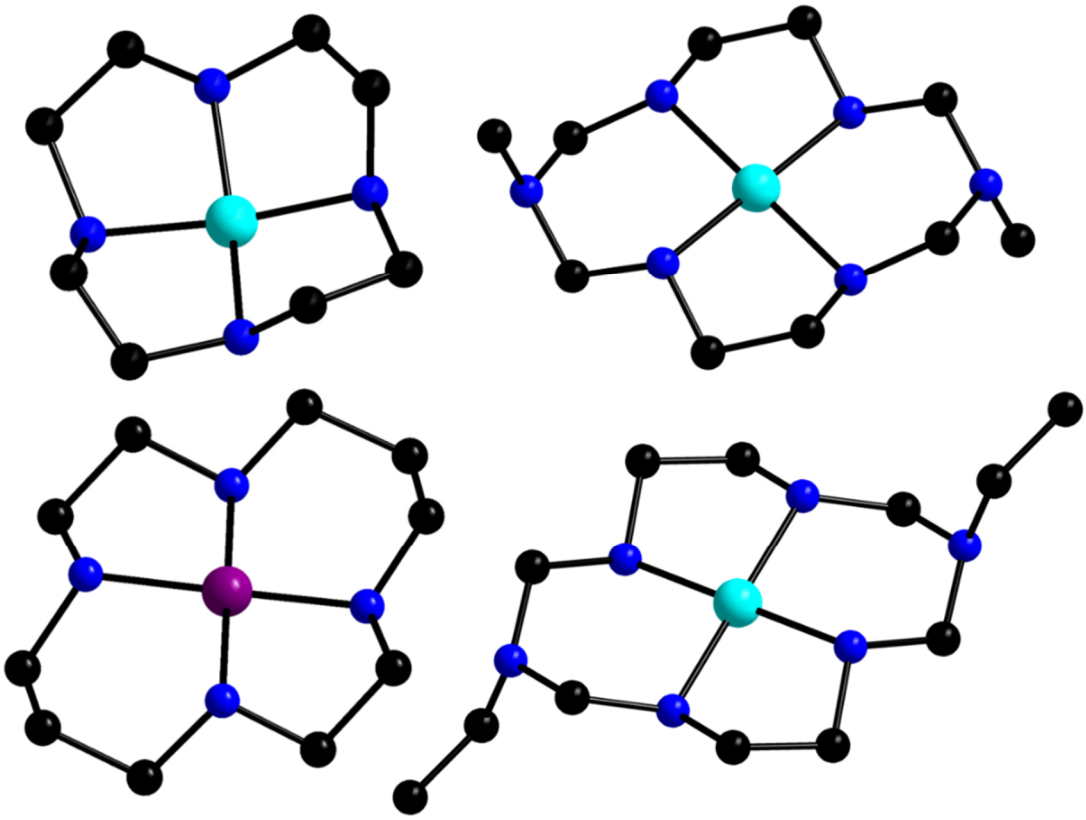

Figure 3: Molecular structures of $[Ni(cyclen)]^{2+}$ (top left), $[Ni(L_1)]^{2+}$ (top right), $[Cu(cyclam)]^{2+}$ (bottom left) and $[Ni(L_1)]^{2+}$ complex cations (bottom right). H atoms are omitted for clarity. Blue: N atoms, black: C, cyan: Ni and violet: Cu.

1.5.3 Alternative synthetic approach: Room temperature synthesis

Pure inorganic thiostannate and tin-sulfide frameworks were generally prepared applying either the high-temperature synthesis or polysulfide flux approach.[14,24,78–81] In contrast to the high-temperature synthesis (T > 600 °C) that leads to the preparation of mainly thermodynamically stable products,[82,83] the polychalcogenide fluxes (200-600 °C) and solvothermal approaches (T < 400 °C) allow the generation of kinetically stable structures.[82,84] The incorporation of protonated amine molecules in the structure of thiostannate and tin-sulfide compounds is achieved only under solvothermal conditions.[72] However, the solvothermal synthesis is a complex reaction system and product formation depends on many parameters like temperature, pressure, pH-Wert, concentration of the educts, nature of the solvents etc.[84] All these parameters made a product prediction impossible. In the past, room temperature syntheses were performed yielding new thiostannate compounds like $[dda]_4[Sn_2S_6]\cdot 2H_2O$ (dda = dodecylamine),[34] $[(CH_3)_2NH_2(NH_4)][SnS_3]$,

$[CH_3C(NH_2)_2]_8[Sn_2S_6SnS_4]$ and $[NH_4]_6[Sn_3S_9]\cdot 1.3H_2O$.[85] However, the formation of these compounds required few months. In another synthetic approach, the reaction of $Na_4SnS_4\cdot 14H_2O$ with $[Ni(amine)_3]^{2+}$ complexes (amine = 2-(aminomethyl)pyridine, 1,2-diaminocyclohexane, 1,2-diaminopropane, ethylenediamine) in tren amine aqueous solution led to the generation of new thiostannate compounds in a short reaction time (1-7 days).[49]

The aims of this work were the development of new synthetic routes, the synthesis and characterization of new oxo-thiostannate compounds, the application of macrocyclic ligands to form new thiostannate and tin-sulfide compounds and investigation of their properties.

2. Experimental Section

2.1 Chemicals

All chemicals used in this doctoral thesis are listed in Table 2.

Table 2: Overview of the used chemicals.

Chemicals	Purity	Manufacturer
Acetone (C_3H_6O)	>99.8 %	Fisher Chemical
Acetonitrile (C_2H_3N)	>99.5 %	Fischer Chemical
Copper(II) perchlorate hexahydrate ($Cu(ClO_4)_2 \cdot 6H_2O$)	98 %	abcr
Cyclen ($C_8H_{20}N_4$)	>98 %	Strem Chemicals, Inc.
Cyclam ($C_{10}H_{24}N_4$)	>98 %	Alfa Aesar
Dimethyl sulfoxide (C_2H_6OS)	99 %	Grüssing
Ethanol (C_2H_5OH)	99 %	Walter-CMP
Ethylamine ($C_2H_5NH_2$)	70 % aq. solution	Merck
Ethylenediamine ($C_2H_8N_2$)	99 %	Grüssing
Formaldehyde (CH_2O)	37 % in MeOH	Grüssing
Glycerine ($C_3H_8O_3$)	99 %	Grüssing
Sodium sulfide nonahydrate ($Na_2S \cdot 9H_2O$)	>98 %	Acros Organics
Nickel(II) chloride hexahydrate ($NiCl_2 \cdot 6H_2O$)	>97 %	Merck
Nickel(II) perchlorate hexahydrate ($Ni(ClO_4)_2 \cdot 6H_2O$)	99 %	abcr
Methanol (CH_3OH)	99 %	Walter-CMP
Methylamine (CH_3NH_2)	40 % aq. solution	abcr
Tin(IV) chloride pentahydrate ($SnCl_4 \cdot 5H_2O$)	>98 %	Acros Organics
Tris(2,2‘-bipyridine)ruthenium(II) hexafluorophosphate ($[Ru(bpy)_3](PF_6)_2$)	97 %	Aldrich
Triethylamine ($(C_2H_5)_3N$)	99 %	Grüssing

2.2 Characterization Methods

In order to investigate the educts and products diverse standard characterization methods were applied like: X-ray powder diffraction (XRPD), single crystal analysis, scanning electron microscope equipped with energy-dispersive X-ray spectroscopy (SEM/EDX), elemental analysis (EA), IR-, UV/Vis-, Raman-, Electron Paramagnetic Resonance (EPR)- and ^{119}Sn-NMR spectroscopy, differential thermoanalysis and thermogravimetry (DTA-TG), H_2O- and N_2 sorption and *in-situ* investigation. All applied methods are summarized in Table 3.

Table 3: Overview of the characterization methods utilized in this work.

Methods	Equipment	Description
XRPD	Stoe Stadi-P	Transmission geometry, Cu-Kα_1 (λ=1.5406 Å) Ge-monochromator Mythen 1K-Detector
single crystal analysis	Stoe IPDS-2	Mo-Kα radiation (λ = 0.71073 Å) Graphite monochromator
SEM/EDX	Philips ESEM XL30	Scanning electron microscope with XL-30 EDX detector
EA	Elemental Analyzer EURO EA, EURO VECTOR	Burning in O_2 at 1000 °C, Detection by GC with a thermal conductivity detector
IR	Bruker Vertex70 FT-IR spectrometer	Range: 80-6000 cm^{-1}
UV/Vis	1. Cary 5 UV/Vis/NIR two channel spectrometer, Varian Techtron Pty. Darmstadt 2. Agilent 8453 spectrometer	1. Reference: $BaSO_4$ 250-2000 nm 2. 190-1100 nm, Deviation: ± 0.5 nm, Wavelength reproducibility: ± 0.02 nm
Raman	Bruker RAM II FT-Raman spectrometer	equipped with a N_2 cooled, highly sensitive Ge detector Radiation: 1064 nm

		Resolution: 3 cm^{-1}
EPR	Bruker EMXplus spectrometer	cooled with N_2 and equipped with a PremiumX microwave bridge and a Bruker dual mode X-band cavity
^{119}Sn-NMR	Bruker Avance3 400 HD spectrometer	in D_2O at 149 MHz, pulse width: 11 µs at 30.974 W, relaxation delay: 1 s, number of scans: 256, T_{max} = 80 ºC
DTA-TG	Linseis STA PT1600	Heating rate: 0.1, 1, 4 and 16 K/min, N_2-flow
H_2O sorption	Belsorp$_{max}$, BEL JAPAN INC.	T = 303 K
N_2 sorption	Belsorp$_{max}$, BEL JAPAN INC.	T = 77 K
In-situ investigation	EasyMax reactor system (Mettler Toledo GmbH, Giessen, Germany), equipped with a pH and redox electrode	stirring = 300 rpm, T = 90 ºC (5 K/min), pH electrode: InLab Semi-Micro, Mettler Toledo; sensor type, combined pH electrode; reference system, Argenthal (0−100 °C) redox electrode: InLab Redox Micro (Mettler Toledo); sensor type, combined ORP electrode with platinum ring; reference system, Argenthal (ceramic diaphragm, 3 M KCl as the reference electrolyte (0−100 °C)

2.3 Programs

All programs utilized in this work are listed in Table 4.

Table 4: Overview of the utilized programs.

Programs	Description
SHELXS-97[86]	Solution of crystal structures
SHELXL-2014[87]	Refinement of crystal structures
STOE WinXPow[88]	Calculation of X-ray powder diffractograms from data of single crystal analysis, visualization of powder diffractograms and software for data collection
Diamond 3.2k[89]	Visualization of crystal structures
Olex^2 [90]	Calculation of the solvent accessible space in a crystal structure
TOPAS Academics[91]	Indexing of X-ray powder diffractograms, solving of crystal structures and refinements by Rietveld method
EXPO2009[92]	Determination of the positions of atoms using direct methods
Materials Studio[93]	Molecular modeling and optimization by calculation of force-field
Platon[94]	Calculation of the solvent accessible space in structures containing voids
PIEFACE[95]	Software to analyze the distortion of polyhedra and to calculate the MBE (minimum bounding ellipsoid)

2.4 Synthetic approaches

2.4.1 Solvothermal synthesis

Some of the compounds presented in this work were synthesized under hydrothermal conditions. The thiostannate salt $Na_4SnS_4 \cdot 14H_2O$ and the transition metal (TM) complexes were transferred in a DURAN© culture tube (V = 11 mL, T_{max} = 180 ºC) including PBT (Polybutylene terephthalate) screw cap and PTFE (Polytetrafluoroethylene) gasket. Water was added and the reaction mixture was shaken for 1 min and heated up to 120 ºC either under static (≤ 7 d) or under dynamic (under stirring, ≥ 2 h) conditions. The reaction products were filtered off, washed with small amounts of water and dried in air.

The advantage of dynamic syntheses is that they allow a visual monitoring of the reaction. Furthermore, owing to the continuous stirring of the reaction medium an homogeneous mixture is obtained enabling a rapid reaction of the reactants leading to an increase of the yield and reduction of the reaction time. Under dynamic conditions crystalline precipitate is often obtained. Crystals suitable for single crystal structure analysis were formed under static conditions.

2.4.2 Room temperature synthesis

Room temperature reactions were carried out in snap cap bottles (V = 5 mL). The thiostannate salt $Na_4SnS_4 \cdot 14H_2O$ was dissolved in water and added to an aqueous solution of TM^{n+} complex. The reaction mixture was stirred for ~ 20 min. and kept at room temperature until crystalline precipitate was generated. Since several TM^{n+} complexes are poorly soluble in water and display a good solubility in organic solvents, syntheses were performed by dissolving $Na_4SnS_4 \cdot 14H_2O$ in water and dissolving the TM^{n+} complexes either in acetonitrile (CH_3CN) or in dimethylsulfoxide (DMSO). Using DMSO as solvent, the organic phase was overlayed with the aqueous solution. However, if CH_3CN is utilized as solvent, the aqueous phase was overlayed with the organic phase. The reaction products were filtered, washed with water and ethanol and dried in air. $Na_4SnS_4 \cdot 14H_2O$ and TM^{n+} complexes were synthesized according to literature procedures.[77,96–99]

3. Publications

3.1 “New Transition Metal Oxo-Thiostannate: Synthesis, Characterization, and Investigation of its Photocatalytic Properties”

The reaction of $Na_4SnS_4 \cdot 14H_2O$ with the complex $[Ni(cyclen)](ClO_4)_2$ under hydrothermal conditions led to crystallization of a new transition metal oxo-thiostannate compound with the formula $\{[Ni(cyclen)]_6[Sn_6S_{12}O_2(OH)_6]\} \cdot 2(ClO_4) \cdot 19H_2O$. The crystal structure of this compound is composed of the cation $\{[Ni(cyclen)]_6[Sn_6S_{12}O_2(OH)_6]\}^{2+}$ and perchlorate anions. In addition, a complex hydrogen-bonding network is observed, which stabilizes the structure. The cation $\{[Ni(cyclen)]_6[Sn_6S_{12}O_2(OH)_6]\}^{2+}$ contains the rare anion $[Sn_6S_{12}O_2(OH)_6]^{10-}$, which is constructed by two $SnS_2O(OH)_3$, two SnS_4O_2 octahedra and two SnS_4 tetrahedra. Six Ni^{2+} complexes are covalently bonded to the anion *via* Ni-S and Ni-OH bridges. Heating $\{[Ni(cyclen)]_6[Sn_6S_{12}O_2(OH)_6]\} \cdot 2(ClO_4) \cdot 19H_2O$ to 150 ºC and treating the residue with small amounts of H_2O led to the recrystallization of $\{[Ni(cyclen)]_6[Sn_6S_{12}O_2(OH)_6]\} \cdot 2(ClO_4) \cdot 19H_2O$ and to the generation of an unidentified crystalline phase. Moreover, the compound reveals good photocatalytic activity for H_2 production. The H_2 generation reached 26.6 $mmol \cdot g^{-1}$ after 3 h irradiation time. During the photocatalytic reactions nanoparticles were formed. Since the photocatalytic reaction is a complex system, it is not clear whether the compound or the nanoparticles are the active species.

Reprinted with permission from A. Benkada, M. Poschmann, C. Näther, W. Bensch, New Transition Metal Oxo-Thiostannate: Synthesis, Characterization, and Investigation of its Photocatalytic Properties, *Z. Anorg. Allg. Chem.*, **2019**, *645*, 433-439. DOI: 10.1002/zaac.201800475. Copyright 2019 John Wiley & Sons.

Journal of Inorganic and General Chemistry
ZAAC
Zeitschrift für anorganische und allgemeine Chemie
DOI: 10.1002/zaac.201800475
ARTICLE

New Transition Metal Oxo-Thiostannate: Synthesis, Characterization, and Investigation of its Photocatalytic Properties

Assma Benkada,[a] Michael Poschmann,[a] Christian Näther,[a] and Wolfgang Bensch*[a]

Abstract. The new transition metal oxo-thiostannate $\{[Ni(cyclen)]_6[Sn_6S_{12}O_2(OH)_6]\}\cdot 2(ClO_4)\cdot 19H_2O$ (**1**) was prepared under hydrothermal conditions using $Na_4SnS_4\cdot 14H_2O$ and $[Ni(cyclen)](ClO_4)_2$ as reactants. In the crystal structure the rare $[Sn_6S_{12}O_2(OH)_6]^{10-}$ anion is observed, which is composed of $SnS_2O(OH)_3$ and SnS_4O_2 octahedra, and SnS_4 tetrahedra sharing edges and corners. The anion is expanded by six Ni^{2+} centered complexes via Ni–S and Ni–OH bonds. The photocatalytic properties for the visible light driven hydrogen evolution reaction shows that 26.6 mmol·g^{-1} H_2 were evolved after 3 h.

Introduction

Thiostannates, oxo-thiostannates and tin-sulfur compounds are an interesting group among the group of thiometalates compounds that show a versatile structural behavior and are promising candidates as catalysts, ion exchangers, absorbers and as sensors.[1–4] Due to the variable coordination number and oxidation state of tin, the different tin building units like tetrahedron, trigonal bipyramid, and octahedron are observed in the crystal structures of thiostannates.[5] The most thiostannates(IV) and tin-sulfur compounds contain the $[Sn_2S_6]^{4-}$ anion,[6] which is formed by two edge-sharing $[SnS_4]^{4-}$ tetrahedra. The $[Sn_2S_6]^{4-}$ anion is either isolated as in $Na_4Sn_2S_6\cdot 14H_2O$,[7] $[Ni(2amp)_3][Sn_2S_6]\cdot 9.5H_2O$,[8] $[Ni(tren)(amine)]_2[Sn_2S_6]\cdot nH_2O$ [amine = 1,2-diaminocyclohexane (1,2-dach); 2-(aminomethyl)pyridine (2amp); ethylendiamine (en); 1,2-diaminopropane (1,2-dap); n = 2, 3, 4, 6, 10],[9] $[Ni(aepa)_2]_2[Sn_2S_6]$ (aepa = *N*-2-aminoethyl-1,3-propandiamine), $[Ni(peha)][Sn_2S_6]\cdot H_2O$ (peha = pentaethylenehexamine), $[Co(dien)_2]_2[Sn_2S_6]$ (dien = diethylenetriamine),[10] $[M(en)_3]_2[Sn_2S_6]$ (M = Co, Mn, Zn),[11] or is bonded covalently to transition metal cations such as in $\{[M(tepa)]_2[Sn_2S_6]\}$ (M = Co, Fe, Ni; tepa = tetraethylenepentamine)[12] forming neutral complexes.

In addition to the $[Sn_2S_6]^{4-}$ anion, different other thiostannate anions like $[SnS_3]^{2-}$, $[SnS_4]^{4-}$, $[Sn_2S_5]^{2-}$, $[Sn_2S_7]^{6-}$, $[Sn_2S_8]^{2-}$, $[Sn_3S_7]^{2-}$, $[Sn_4S_9]^{2-}$, $[Sn_5S_{12}]^{4-}$ [13–17] or the tetrameric adamantane-like unit $[Sn_4S_{10}]^{4-}$ are known.[13] In the above mentioned anions tin is in the oxidation state IV. However, in the compounds $BaLnSn_2S_6$ (Ln = Ce, Pr, Nd),[18] $(trenH_3)Cu_7Sn_4S_{12}$,[19] $[(Ph_3PCu)_6\{(CH_2)_4SnS_2\}_6Cu_4Sn]$,[20] $[(R^2Sn)_2SnS_4]$, $\{[(R^2Sn)(R^{fC4}Sn)SnS_4]_2FeR^{fCO}\}$ {R^2 = $C(Me)_2CH_2C(Me)=NNH_2$, R^{fC4} = $[C(Me)_2CH_2C(Me)=N–NHC(O)]fC[C(O)NH–NH_2$, and R^{fCO} = $[fC(COO)_2]^{2-}$},[21] $[(CuPPh_3)_2(Sn^{II}Cl)_2\{(RSn^{IV})_2Se_4\}_2]$, $[(CuPPh_3)_2(Sn^{II}Cu_2)\{(R^1Sn^{IV})_2Se_4\}_3]$, $[(CuPPh_3)_2(Sn^{II}Cl)_2\{(R^1Sn^{IV}Cl)Se_2\}_2]$ and $[Cu(CuPPh_3)(Sn^{II}Cu_2)\{(R^1Sn^{IV})_2Se_4\}_3]$ [R^1 = $CMe_2CH_2C(O)Me$] [22] tin adopts the oxidation states II and IV, whereas in $[\{(CMe_2CH_2C(O)Me)Sn)_2(\mu\text{-}S)_2\}Sn_2S_6]$,[23] Sn^{III} and Sn^{IV} cations are observed.

In contrast to $[Sn_xS_y]^{n-}$ anions, oxo-thiostannate anions $[Sn_xS_yO_z]^{n-}$ are relatively rare and much less investigated. Prominent representatives are $[Sn_{10}S_{20}O_4]^{8-}$,[24,25] $[Sn_{10}S_{16}O_4Cl_4]^{4}$,[26] $[Sn_8S_{12}O_4(SPh)_6]^{6-}$,[27] $[Sn_8S_{12}O_2(OH)_2Cl_6]^{4-}$,[26] and $[Sn_4S_5(S_3)OCl_4]^{2-}$.[28] Among these anions the $[Sn_{10}S_{20}O_4]^{8-}$ anionic cluster is most common. It has an idealized T_d symmetry and can be described as a supertetrahedral cluster (denoted as T3) formed by ten corner-linked SnS_4 polyhedra. Four empty sites are occupied by O^{2-} anions expanding the coordination number of Sn from four to five or six.[24,25,29] All Sn-O-S compounds contain isolated $[Sn_{10}S_{20}O_4]^{8-}$ anionic clusters with inorganic cations compensating the negative charges like in $[Cs_8(H_2O)_{13}][Sn_{10}S_{20}O_4]$[29] and $[Li_8(H_2O)_{29}][Sn_{10}S_{20}O_4]\cdot 2H_2O$,[24] and only in $\{[Ni(1,2\text{-}dach)_2(ma)]_4[Sn_{10}S_{20}O_4]\}$ (1,2-dach = 1,2-diaminocyclohexane; ma = methylamine)[30] the cluster is expanded via sulfur atoms to Ni^{2+} centered complexes.

In this context, we have reported on a new oxo-thiostannate with the composition $[Ni(cyclen)(H_2O)_2]_4[Sn_{10}S_{20}O_4]\cdot ca\cdot 13H_2O$ that consists of a T3-type $[Sn_{10}S_{20}O_4]$ cluster anion. The negative charge is compensated by Ni^{2+} cations that are coordinated by four nitrogen atoms of a cyclen ligand. The octahedral Ni coordination is completed by two additional water molecules that occupies the axial positions, leading to the formation of a $[Ni(cyclen)(H_2O)_2]^{2+}$ cation. Therefore, they are not connected to the cluster anion. Surprisingly, the oxothiostannate cluster has formed only by the reaction of $[Ni(cyclen)(H_2O)_2](ClO_4)_2\cdot H_2O$ with $Na_4SnS_4\cdot 14H_2O$ in water. The reaction mechanism for the formation of this oxo-cluster is still not fully understood, but it is assumed that

* Prof. Dr. W. Bensch
Fax: +49-431-880-1520
E-Mail: wbensch@ac.uni-kiel.de
[a] Institute of Inorganic Chemistry
Christian-Albrechts-University of Kiel
Max-Eyth-Str. 2
<postCode/24118 Kiel, Germany
Supporting information for this article is available on the WWW under **http://dx.doi.org/10.1002/zaac.201800475** or from the author.

Journal of Inorganic and General Chemistry
ZAAC
Zeitschrift für anorganische und allgemeine Chemie

ARTICLE

$[SnS_3(OH)]^{3-}$ is formed, which condense to generate $[Sn_2S_5O]^{4-}$ that further reacts with $[Sn_2S_7]^{6-}$ yielding $[Sn_4S_{10}O]^{6-}$ anions. These anions might be further linked by sulfur atoms leading to the formation of the $[Sn_{10}S_{20}O_4]^{8-}$ cluster.[31] Based on these assumptions the question arises, whether additional oxo-thiostannate clusters can be synthesized using these reactants and if bond formation between the Ni^{2+} cations and the cluster anions can be enforced by using slightly different synthesis conditions, e.g. less water in the slurry. Therefore, we reacted $Na_4SnS_4{\cdot}14H_2O$ with $[Ni(cyclen)](ClO_4)_2$ under hydrothermal conditions and we obtained a new oxo-thiostannate cluster with the composition $\{[Ni(cyclen)]_6[Sn_6S_{12}O_2(OH)_6]\}$. Finally, this compound shows promising photocatalytic properties and therefore, such investigations were also conducted. Herein we report on these investigations.

Experimental Section

$Na_4SnS_4{\cdot}14H_2O$ and $[Ni(cyclen)](ClO_4)_2$ were synthesized according to literature methods.[32,33] Generally, the reaction products were filtered off, washed with tiny amounts of water, and dried at ambient conditions.

Caution: Perchlorates are potentially explosive if heated and must be handled with care.

Synthesis of $\{[Ni(cyclen)]_6[Sn_6S_{12}O_2(OH)_6]\}{\cdot}2(ClO_4){\cdot}19H_2O$ (1): $Na_4SnS_4{\cdot}14H_2O$ (147.8 mg, 0.25 mmol) and $[Ni(cyclen)](ClO_4)_2$ (107.5 mg, 0.25 mmol) were reacted in a glass tube with 2 mL H_2O for 7 d at 120 °C. The mixture was cooled down to room temperature, filtered off, and the blue-green mother liquor was kept in a refrigerator until blue-green block-like crystals were formed (12% yield based on Sn). Elemental analysis: calcd. C: 18.26, H 5.23, N 10.64%; found C 17.33, H 4.94, N 10.07%.

Structure Determination: Data for compound **1** were collected with a STOE IPDS-1 (Imaging Plate Diffraction System) with graphite monochromated Mo-K_α radiation (λ = 0.7107 Å) at 170(2) K. The structure was solved with direct methods using the program SHELXS-97,[34] and the refinements were done with SHELXL-2014.[35] All non-hydrogen atoms were refined anisotropically. The C–H hydrogen atoms were positioned with idealized geometry and were refined isotropically with $U_{iso}(H) = 1.2\ U_{eq}(C)$ using a riding model. The hydroxy hydrogen atoms were located in the difference Fourier maps, their bond lengths were set to ideal values and finally they were refined isotropically with $U_{iso}(H) = 1.5\ U_{eq}(O)$ using a riding model. The water hydrogen atoms were not located but considered in the calculation of the formula and the molecular weight. One of the perchlorate anions is disordered on a center of inversion and was refined using a split model. The position of the other perchlorate anion seems to be disordered with water molecules and was refined with only half occupation. Several water molecules are also disordered and were refined using a split model with in part not full occupation (Table S1, Supporting Information).

Crystallographic data (excluding structure factors) for the structure in this paper have been deposited with the Cambridge Crystallographic Data Centre, CCDC, 12 Union Road, Cambridge CB21EZ, UK. Copies of the data can be obtained free of charge on quoting the depository number CCDC-1863370 (Fax: +44-1223-336-033; E-Mail: deposit@ccdc.cam.ac.uk, http://www.ccdc.cam.ac.uk).

Characterization Methods

X-ray powder Diffractometry: The powder diffraction patterns were collected with a STOE Stadi P diffractometer equipped with a MYTHEN 1 K detector (DECTRIS) using germanium monochromatized Cu-$K_{\alpha1}$ radiation (λ = 1.540598 Å). The experimental and the calculated patterns using the single-crystal X-ray data match perfectly indicating phase purity of the samples (Figure S1, Supporting Information).

Energy dispersive X-ray Spectroscopy (EDX): EDX analyses (Table S2, Supporting Information) were performed with a Philips Environmental Scanning Electron Microscope ESEM XL30 equipped with an EDX detector.

Elemental Analysis: CHNS elemental analyses were performed with a EURO EA Elemental Analyzer (EURO VECTOR Instruments and Software).

Infrared Spectroscopy: IR spectra were measured in a region from 400 to 4000 cm^{-1} with a Bruker Alpha P spectrometer.

UV/Vis Spectroscopy: UV/Vis analyses were performed at room temperature with an UV/Vis/NIR two channel spectrometer Cary 5 (Varian Techtron Pty., Darmstadt, 200–3000 cm^{-1}) using $BaSO_4$ as reference material. The UV/Vis reflectance data were transformed applying the Kubelka–Munk function.

Thermogravimetric Analysis: Thermogravimetric analysis was performed with a Linseis STA PT1600 instrument. The sample was heated in a nitrogen atmosphere with a heating rate of 4 $K{\cdot}min^{-1}$.

Photocatalytic Hydrogen Evolution: In the photocatalytic experiments, **1** (10 mg, 3.2 µmol) or $[Ni(cyclen)(H_2O)_2](ClO_4)_2{\cdot}H_2O$ (9.3 mg, 19.2 µmol) and $[Ru(bpy)_3](PF_6)_2$ (8.6 mg, 1 µmol) as photosensitizer were transferred in a double-walled thermostatically controlled vessel. Triethylamine (10 mL) and acetonitrile (10 mL) were dried with CaH_2, distilled in a nitrogen atmosphere, and added to the mixture. Subsequently, degassed H_2O (3 mL) was added. The reaction mixture was stirred in the dark for 1 h and irradiated with UV light (330 W Xe lamp with a 400 nm cut-off filter) at 30 °C. The evolved gas was collected after distinct reaction times and was quantified by gas chromatography using an Agilent 6890 Plus gas chromatograph with a 5 Å molecular sieves column and TCD detector with argon as carrier gas.

Supporting Information (see footnote on the first page of this article): Crystal data and refinement results; X-ray powder pattern of the title compound; Tables with distances and angles; IR and UV-Vis spectra; X-ray powder patterns of the pristine samples, dehydrated and rehydrated; additional photocatalysis curves.

Results and Discussion

Crystal Structure

The compound $\{[Ni(cyclen)]_6[Sn_6S_{12}O_2(OH)_6]\}{\cdot}2(ClO_4){\cdot}19H_2O$ (**1**) crystallizes in the monoclinic space group *C*2/*c* with four formula units per unit cell. The $[Sn_6S_{12}O_2(OH)_6]^{10-}$ anionic building unit is located on a center of inversion and consists of three crystallographically independent Sn cations that exhibit different coordination arrangements (Figure 1 top).

Journal of Inorganic and General Chemistry
ZAAC
Zeitschrift für anorganische und allgemeine Chemie

ARTICLE

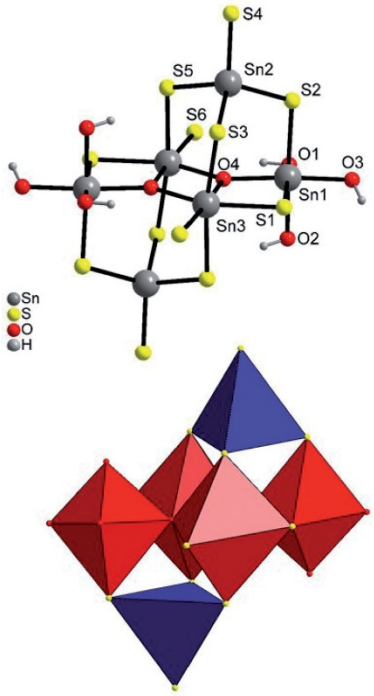

Figure 1. The structure of the $[Sn_6S_{12}O_2(OH)_6]^{10-}$ anion with labelling (top) and in polyhedral representation (bottom) in compound **1**. Only the crystallographically unique atoms are labeled.

Sn1 is coordinated by three terminally bonded OH^- anions, two μ_2-bridging S atoms, and one μ_3-O atom to form a $SnS_2O(OH)_3$ octahedron. Sn3 is also octahedrally coordinated, but by one terminal and three μ_2-bridging S atoms as well as two μ_3-O atoms forming SnS_4O_2 units. Sn2 is in a tetrahedral environment of four S atoms. Each two SnS_4O_2 octahedra are linked via two O atoms sharing common edges forming a double octahedron (Figure 1 bottom). The double octahedron is further connected to two $SnS_2O(OH)_3$ units by μ_3-oxo and μ_2-S atoms sharing common edges into tetranuclear units, in which the Sn atoms are coplanar. The two SnS_4 tetrahedra are located above and below this plane and are linked to two SnS_4O_2 and one $SnS_2O(OH)_3$ octahedra by common corners.

The Sn–S bond lengths are in the range of 2.386(2) to 2.623(2) Å for bridging S^{2-}, whereas the bonds to terminal S^{2-} are between 2.327(2) and 2.408(2) Å (Table S3, Supporting Information). The μ_3-O-Sn bonds are between 2.075(5) and 2.128(5) Å. Similar values have also been reported in literature.[7,30,36,37,38] The Sn–OH bond lengths range from 2.066(6) to 2.102(6) Å and are significantly shorter than for bridged OH^- anions (2.310 and 2.348 Å) (Figure S2, Supporting Information). According to BVS. analysis, the oxidation states of the O atoms of the hydroxyl groups are between 0.68 and 0.77 (average: 0.71) and the oxidation state of the μ_3-O atom is 2.08, which is in agreement with bridging O^{2-} and terminal OH^- anions **1**. In the two different Sn octahedra, the angles around Sn indicate a severe distortion (Table S3, Supporting Information). The S–Sn–S angles in the SnS_4 tetrahedron are between 105.42(7) and 109.05(9)° indicating a moderate distortion.

The $Sn_6S_{12}O_2(OH)_6$ cluster anions are expanded by six $[Ni(cyclen)]^{2+}$ cations, of which four are coordinated by S^{2-} and by two OH^- anions into $\{[Ni(cyclen)]_6[Sn_6S_{12}O_2(OH)_6]\}^{2+}$ cations and the positive charge is compensated by two ClO_4^- anions (Figure 2). The Ni^{2+} cations within these clusters form a trigonal antiprism (Figure S3, Supporting Information). The cluster is stabilized by strong intramolecular O–H···S and N–H···S hydrogen bonds between the S atoms and the hydroxyl and amino hydrogen atoms (Figure 2 bottom and Table S4, Supporting Information). There are additional weak

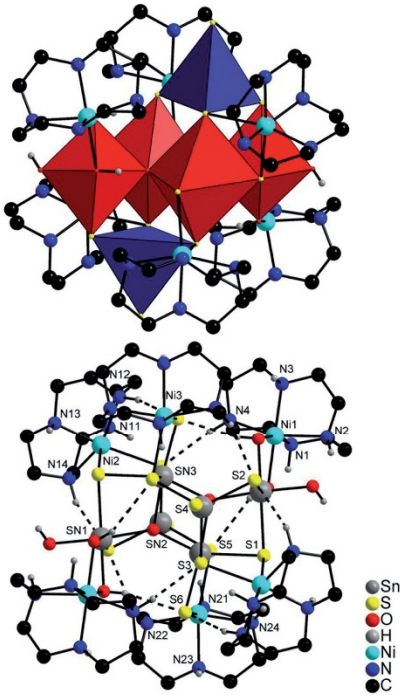

Figure 2. $\{[Ni(cyclen)]_6[Sn_6S_{12}O_2(OH)_6]\}^{2+}$ cluster cation with view along (top) and perpendicular (bottom) to the plane formed by the octahedral coordinated Sn cations in the crystal structure of **1**. Intramolecular O–H···S and N–H···S hydrogen bonding is shown as dashed lines and C–H hydrogen atoms are omitted for clarity.

Journal of Inorganic and General Chemistry
ZAAC
Zeitschrift für anorganische und allgemeine Chemie

ARTICLE

C–H···S contacts but the H···S distances and C–H···S angles indicate that this is only a weak interaction (Table S5, Supporting Information).

In the [Ni(cyclen)S_2] and [Ni(cyclen)$(OH)_2$] units the Ni–N, Ni–O, and Ni–S bond lengths are in the range of 2.071(9)–2.144(10), 2.107(6)–2.115(6), and 2.459(2)–2.543(2) Å agreeing well with literature data.[39–41] The octahedra NiN_4S_2 and $NiN_4(OH)_2$ (Figure 3) are distorted as evidenced by the angles around the Ni^{2+} cations (Table S6, Supporting Information). These values are in good agreement with those reported in literature.[41–43] The distortion of NiN_4S_2 and $NiN_4(OH)_2$ can be quantified using two parameters: the octahedral angle variance $\sigma_{\theta<oct>}{}^2$ and the mean octahedral quadratic elongation λ_{oct}.[44] The values of $\sigma_{\theta<oct>}{}^2$ = 85.310, λ_{oct} = 1.025 for Ni1, $\sigma_{\theta<oct>}{}^2$ = 95.035, λ_{oct} = 1.037 for Ni2, and $\sigma_{\theta<oct>}{}^2$ = 103.119, λ_{oct} = 1.039 for Ni3 confirm a strong distortion of the octahedra. In this context, it is important to notice that Sn–OH–Ni units have been rarely observed so far.

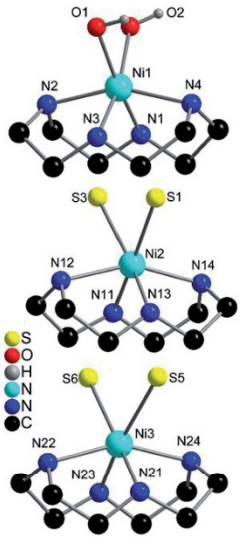

Figure 3. Coordination sphere of the three octahedrally coordinated Ni cations in the crystal structure of **1**. The C–H hydrogen atoms are omitted for clarity.

In the crystal structure of **1** the $\{[Ni(cyclen)]_6[Sn_6S_{12}O_2(OH)_6]\}^{2+}$ cations are linked into chains by centrosymmetric pairs of C–H···S hydrogen bonds (Figure S4 and Table S5, Supporting Information). Between the chains the perchlorate anions are located that are hydrogen bonded to the cations (Figure 4). This includes one strong N–H···O hydrogen bond with a H···O distance of 2.32 Å and the corresponding N–H···O angle of 158.4° as well as a number of weaker C–H···O interactions (Table S5). By this arrangement cavities are formed, in which the water molecules are embedded. These water molecules are linked only to the perchlorate anions via strong intermolecular N–H···O and weaker C–H···O hydrogen bonding (Table S5).

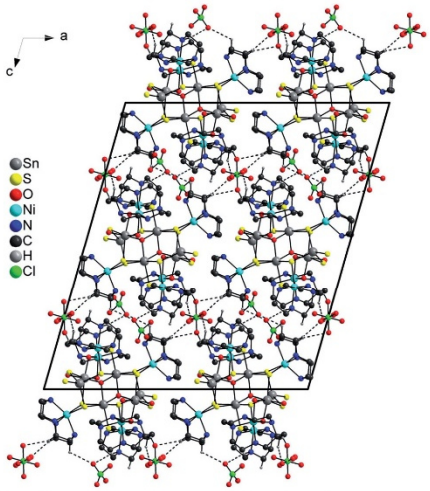

Figure 4. Crystal structure of **1** with view along the crystallographic *b* axis showing the arrangement of the $\{[Ni(cyclen)]_6[Sn_6S_{12}O_2(OH)_6]\}^{2+}$ cations and the perchlorate anions with intermolecular hydrogen bonding shown as dashed line. For clarity, only the hydrogen atoms involved in intermolecular hydrogen bonding are shown. Please note, that the one of the two crystallographically independent ClO_4^- anions is disordered.

Since the hydrogen atoms of the H_2O molecules could not be located, for all O···O separations up to 3.2 Å intermolecular O–H···O hydrogen bonding interactions were assumed, which is also supported experimentally by IR spectroscopic investigations, where a broad band is observed at about 3387 cm^{-1} (see below). If all hydrogen bonds are considered a complex hydrogen bonding network is formed (Figure 5).

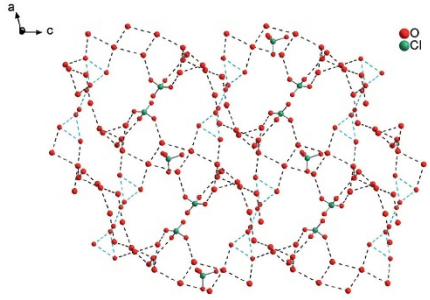

Figure 5. View of the hydrogen-bonded network generated by intermolecular O···O interactions between the water molecules, perchlorate anions, and the anionic $[Sn_6S_{12}O_2(OH)_6]^{10-}$ anions (dotted grey lines) as well as within the anionic unit (dotted turquoise lines).

Journal of Inorganic and General Chemistry
ZAAC
Zeitschrift für anorganische und allgemeine Chemie
ARTICLE

Spectroscopic Properties

The typical bands of the cyclen molecule in compound **1** can be identified in the IR spectra (Figure S5 and Table S7, Supporting Information). The broad absorption at approximately 3387 cm^{-1} is assigned to the OH stretching vibration of the water molecules. The N–H stretching vibration of cyclen occurs around 3149 cm^{-1} and the Ni–N stretching mode is observed around 426 cm^{-1}. The UV/Vis spectrum shows the expected d–d transitions. For the high spin complex $[Ni(H_2O)_6]^{2+}$ these transitions are located at about 1.05 eV (1176 nm, $^3A_{2g} \rightarrow {}^3T_{2g}$), 1.71 eV (724 nm, $^3A_{2g} \rightarrow {}^3T_{1g}$ (F)), and 3.14 eV (395 nm, $^3A_{2g} \rightarrow {}^3T_{1g}$ (P)).[45] For **1** the d–d transitions occur at 1.21 eV (1024 nm), 2.11 eV (587 nm) and 3.45 eV (359 nm) (Figure S6, Supporting Information). The latter absorption seems to be too intense and too broad for a d–d transition indicating that a charge-transfer band is superimposed. The color of the crystals is caused by the transition at 2.11 eV (587 nm) which corresponds to green. The strong absorption at 4.11 eV may be regarded as HOMO–LUMO transition.

Thermogravimetric Analysis

To get some information on the stability of compound **1** and to investigate if the water molecules can be reversibly removed, measurements using simultaneously differential thermoanalysis and thermogravimetry (DTA-TG) were performed. Upon heating two mass steps are observed in the TG curve, of which the first one is accompanied by two endothermic signals in the DTA curve at peak temperatures of ca. 75 and 106 °C (Figure 6). The mass loss of 10.5 % in the first step is in good agreement with that calculated for the removal of nineteen H_2O molecules (calcd. 10.8 %). In the second TG step the anhydrate formed as intermediate decomposes at 250 °C in an exothermic reaction. In a further experiment, heating was stopped after the first TG step at 150 °C and the residue was investigated by X-ray powder diffraction, and the powder pattern reveals some similarities to that of the pristine compound. The anhydrate does not show water uptake on storage at room temperature and therefore, it was treated with small amounts of water. The X-ray powder pattern of this residue consists of a mixture of the pristine compound **1** as the major phase and a small amount of an additional unknown crystalline phase (Figure S7, Supporting Information).

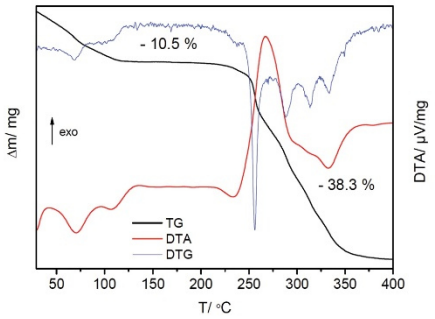

Figure 6. TG (black), DTA (red), and DTG (blue) curves of compound **1**.

Photocatalytic Hydrogen Evolution

The photocatalytic experiments were performed using **1**, $[Ru(bpy)_3](PF_6)_2$ as photosensitizer, the sacrificial agent triethylamine as electron donor, H_2O as proton source, and CH_3CN as solvent for the photosensitizer. The photocatalytically evolved H_2 (Figure 7) increases with increasing irradiation time, and then levels-off reaching 26.6 mmol·g^{-1} after 3 h irradiation. During the reaction the orange solution turned brown leading to a reduced absorption of the incident light, which may explain the decline of the initially steep evolution curve. Such color change demonstrates the photodegradation of $[Ru(bpy)_3](PF_6)_2$ as reported previously.[46–51] Because **1** is soluble in water one may assume that the photocatalytic reaction is homogeneous. Hence, the stability of **1** in both H_2O and a mixture of trimethylamine, acetonitrile and H_2O was investigated by storing the sample for 1 d at room temperature, but **1** could not be recovered after evaporation of the solvents indicating decomposition of the compound.

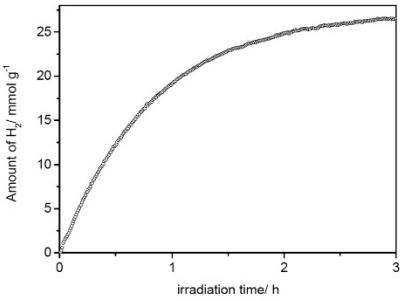

Figure 7. Photocatalytic hydrogen evolution using compound **1**, $[Ru(bpy)_3](PF_6)_2$ as photosensitizer, triethylamine as sacrificial, water as proton donor, and acetonitrile as solvent.

Indeed, the Tyndall effect could be detected after the photocatalytic reaction confirming the presence of nanoparticles, i.e. such particles were generated during the catalytic test. It was reported in the literature that transition metal complexes may be destroyed during the photocatalytic reaction and nanoparticles are generated, which are the active species.[52] Such complexes may be regarded as pre-catalysts which are in-situ transformed into the catalytically active species. Therefore, we assumed that during chemical decomposition the Ni^{2+} centered complex is released, and therefore a photocatalytic experiment was performed with the mixture $[Ni(cyclen)(H_2O)_2](ClO_4)_2 \cdot H_2O/[Ru(bpy)_3](PF_6)_2$ (Figure S8, Supporting Information). For this system 14.2 mmol·g^{-1} H_2 were obtained after 1.5 h irradiation time. In the present case the situation is more com-

Journal of Inorganic and General Chemistry
ZAAC
Zeitschrift für anorganische und allgemeine Chemie

ARTICLE

Table 1. Comparison of the photocatalytic activity of different catalysts at various conditions.

Catalyst	Reaction mixture / Light source	Activity/TON
1	Triethylamine, acetonitrile, water, $[Ru(bpy)_3](PF_6)_2$/ 330 W Xe lamp, cut-off filter ($\lambda > 400$ nm)	83.1
$[Ni(cyclen)(H_2O)_2](ClO_4)_2 \cdot H_2O$ [a]	Triethylamine, acetonitrile, water, $[Ru(bpy)_3](PF_6)_2$/ 330 W Xe lamp, cut-off filter ($\lambda > 400$ nm)	44.4
$[Co(N4Py)(OH_2)]^{3+}$ [54]	H_2A/NaHA, pH = 4, $[Ru(bpy)_3]Cl_2$/ 150 W Xe lamp, cut-off filter ($\lambda > 400$ nm)	65
$[Co(N4Py)(NCMe)]^{3+}$ [54]	H_2A/NaHA, pH = 4, $[Ru(bpy)_3]Cl_2$/ 150 W Xe lamp, cut-off filter ($\lambda > 400$ nm)	67
$[Co(N4Py)(N_3)]^{2+}$ [54]	H_2A/NaHA, pH = 4, $[Ru(bpy)_3]Cl_2$/ 150 W Xe lamp, cut-off filter ($\lambda > 400$ nm)	75
$[Co(N4Py)(NCS)]^{2+}$ [54]	H_2A/NaHA, pH = 4, $[Ru(bpy)_3]Cl_2$/ 150 W Xe lamp, cut-off filter ($\lambda > 400$ nm)	73
$[Co(N4Py)Cl]^{2+}$ [54]	H_2A/NaHA, pH = 4, $[Ru(bpy)_3]Cl_2$/ 150 W Xe lamp, cut-off filter ($\lambda > 400$ nm)	65
$[Co(N4Py)Br]^{2+}$ [54]	H_2A/NaHA, pH = 4, $[Ru(bpy)_3]Cl_2$/ 150 W Xe lamp, cut-off filter ($\lambda > 400$ nm)	68
$[Ni(bpy)_3]^{2+}$ [55]	Acetonitrile-water: 8/2, TEOA, pH = 9, $[Ir(dfppy)_2(Hdcbpy)]$ [b] / 30 W white LED lamp ($\lambda = 420$ nm)	118
$[Ni(bpet)(CH_3CN)_2](ClO_4)_2$ [56] [c]	DMA/ascorbate buffer (pH = 4.0), $[Ru(bpy)_3]Cl_2$/ 6 W diode LED lamp ($\lambda = 450$ nm)	36
$[Ni(bppt)(CH_3CN)_2](BPh_4)_2$ [56] [c]	DMA/ascorbate buffer (pH = 4.0), $[Ru(bpy)_3]Cl_2$/ 6 W diode LED lamp ($\lambda = 450$ nm	3.8

a) N4Py = 1,1-bis(pyridin-2-yl)-*N*,*N*-bis(pyridin-2ylmethyl)methanamine. b) dfppy = 2-(3,4-difluorophenyl)pyridine; Hdcbpy = 4-carboxy-2,2′-bipyridine-4′-carboxylate. c) bpet = bis(2-pyridylmethyl)-1,2-ethanedithiol, bppt = bis(2-pyridylmethyl)-1,3-propane-dithiol.

plex than only using a Ni^{2+} centered complex and the sensitizer because the anion may also decompose and the nanoparticles generated contain both Ni and Sn.

A comparison of the photocatalytic activity with data reported in literature is difficult because the activity depends on a large number of parameters like, e.g., the solvents, the amount of the catalyst, the co-catalyst, the photosensitizer, the intensity and wavelength of the light source, the sacrificial compound, pH value etc. In addition, the amount of hydrogen produced is reported as different quantities like e·g·mmol·g^{-1}, mmol, mL, TON (turnover number, Table 1) or TOF (turnover frequency).[53] Nevertheless, the TON of 83.1 for the title compound is in the range of data reported for Ni^{2+} and Co^{2+} centered complexes (Table 1).

Conclusions

The presented work was motivated by previous investigations, in which a new oxo-thiostannate was accidently obtained simply by the reaction of $[Ni(cyclen)(H_2O)_2](ClO_4)_2 \cdot H_2O$ with $Na_4SnS_4 \cdot 14H_2O$. Therefore, we investigated if other oxo-thiostannate compounds can be synthesized by this route and whether the Ni^{2+} cations can be bonded to the cluster anion. Under similar conditions the new oxo-thiostannate $\{[Ni(cyclen)]_6[Sn_6S_{12}O_2(OH)_6]\} \cdot 2(ClO_4) \cdot 19H_2O$ was obtained, in which the Ni^{2+} cations are covalently bonded to the cluster anion. The photocatalytic experiments show a high activity for H_2 generation. Since the catalytic system is complex the nature of the catalytic process could not be determined.

Acknowledgements

Financial support by the State of Schleswig-Holstein is gratefully acknowledged. We thank *Aleksej Jochim* for the TG measurements.

Keywords: $[Sn_6S_{12}O_2(OH)_6]^{10-}$; Hydrothermal synthesis; Single crystal structure; Spectroscopic and thermal properties; Photocatalytic hydrogen evolution

References

[1] T. Jiang, A. Lough, G. A. Ozin, *Adv. Mater.* **1998**, *10*, 42–46.
[2] H. Ahari, G. A. Ozin, R. L. Bedard, S. Petrov, D. Young, *Adv. Mater.* **1995**, *7*, 370–374.
[3] P. Enzel, G. S. Henderson, G. A. Ozin, R. L. Bedard, *Adv. Mater.* **1995**, *7*, 64–68.
[4] J. B. Parise, Y. H. Ko, J. Rijssenbeek, D. M. Nellis, K. M. Tan, S. J. Koch, *J. Chem. Soc., Chem. Commun.* **1994**, 527.
[5] W. S. Sheldrick, *J. Chem. Soc., Dalton Trans.* **2000**, *18*, 3041–3052.
[6] B. Seidlhofer, N. Pienack, W. Bensch, *Z. Naturforsch. B* **2010**, *65*, 937–975.
[7] B. Krebs, S. Pohl, W. Schiwy, *Z. Anorg. Allg. Chem.* **1972**, *393*, 241–252.
[8] J. Hilbert, C. Näther, W. Bensch, *Z. Anorg. Allg. Chem.* **2017**, *643*, 1861–1866.
[9] J. Hilbert, C. Näther, W. Bensch, *Cryst. Growth Des.* **2017**, *17*, 4766–4775.
[10] N. Pienack, H. Lühmann, B. Seidlhofer, J. Ammermann, C. Zeisler, F. Danker, C. Näther, W. Bensch, *Solid State Sci.* **2014**, *33*, 67–72.
[11] D. X. Jia, Y. Zhang, J. Dai, Q. Y. Zhu, Y. M. Gu, *Z. Anorg. Allg. Chem.* **2004**, *630*, 313–318.
[12] N. Pienack, S. Lehmann, H. Lühmann, M. El-Madani, C. Näther, W. Bensch, *Z. Anorg. Allg. Chem.* **2008**, *634*, 2323–2329.
[13] B. Krebs, *Angew. Chem.* **1983**, *95*, 113–134.
[14] W. Schiwy, S. Pohl, B. Krebs, *Z. Anorg. Allg. Chem.* **1973**, *402*, 77–86.
[15] J.-H. Liao, C. Varotsis, M. G. Kanatzidis, *Inorg. Chem.* **1993**, *32*, 2453–2462.
[16] T. Jiang, A. Lough, G. A. Ozin, R. L. Bedard, R. Broach, *J. Mater. Chem.* **1998**, *8*, 721–732.
[17] Y. Ko, C. L. Cahill, J. B. Parise, *J. Chem. Soc., Chem. Commun.* **1994**, 69–70.
[18] K. Feng, X. Zhang, W. Yin, Y. Shi, J. Yao, Y. Wu, *Inorg. Chem.* **2014**, *53*, 2248–2253.

Journal of Inorganic and General Chemistry
ZAAC
Zeitschrift für anorganische und allgemeine Chemie

ARTICLE

[19] M. Behrens, M.-E. Ordolff, C. Näther, W. Bensch, K.-D. Becker, C. G.-Deudon, A. Lafond, J. A. Cody, *Inorg. Chem.* **2010**, *49*, 8305–8309.
[20] H. P. Nayek, W. Massa, S. Dehnen, *Inorg. Chem.* **2008**, *47*, 9146–9148.
[21] Z. You, K. Harms, S. Dehnen, *Eur. J. Inorg. Chem.* **2015**, 5322–5328.
[22] N. Rinn, L. Guggolz, J. Lange, S. Chatterjee, T. Block, R. Pöttgen, S. Dehnen, *Chem. Eur. J.* **2018**, *24*, 5840–5848.
[23] Z. H. Fard, C. Müller, T. Harmening, R. Pöttgen, S. Dehnen, *Angew. Chem.* **2009**, *121*, 4507–4511.
[24] T. Kaib, M. Kapitein, S. Dehnen, *Z. Anorg. Allg. Chem.* **2011**, *637*, 1683–1686.
[25] J. B. Parise, Y. Ko, *Chem. Mater.* **1994**, *6*, 718–720.
[26] J.-J. Zhang, S.-M. Hu, X.-T. Wu, W.-X. Du, R.-B. Fu, L.-S. Wang, *Inorg. Chem. Commun.* **2003**, *6*, 744–747.
[27] L. Wu, L. Chen, J. Dai, C. Cui, Z. Fu, X. Wu, *Inorg. Chem. Commun.* **2001**, *4*, 574–576.
[28] W. Bubenheim, U. Müller, *Z. Anorg. Allg. Chem.* **1993**, *619*, 779–785.
[29] W. Schiwy, B. Krebs, *Angew. Chem.* **1975**, *87*, 451–452.
[30] J. Hilbert, C. Näther, W. Bensch, *Curr. Inorg. Chem.* **2016**, *6*, 181–186.
[31] A. Benkada, H. Reinsch, M. Poschmann, J. Krahmer, N. Pienack, W. Bensch, *Inorg. Chem.* **2018**, under revision.
[32] Y. Oh, S. Bag, C. D. Malliakas, M. G. Kanatzidis, *Chem. Mater.* **2011**, *23*, 2447–2456.
[33] J. H. Coates, D. A. Hadi, S. F. Lincoln, H. W. Dodgen, J. P. Hunt, *Inorg. Chem.* **1981**, *20*, 707–711.
[34] G. M. Sheldrick, *SHELXS-97*, Program for the Solution of Crystal Structures; University of Göttingen, Göttingen, Germany, **1997**.
[35] G. M. Sheldrick, *SHELXL-2014*, Program for the Refinement of Crystal Structures, University of Göttingen, Göttingen, Germany, **2014**.
[36] B. Krebs, W. Schiwy, *Z. Anorg. Allg. Chem.* **1973**, *398*, 63–71.
[37] H. Puff, H. Reuter, *J. Organomet. Chem.* **1989**, *368*, 173–183.
[38] H. Puff, H. Reuter, *J. Organomet. Chem.* **1989**, *373*, 173–184.
[39] M. Behrens, S. Scherb, C. Näther, W. Bensch, *Z. Anorg. Allg. Chem.* **2003**, *629*, 1367–1373.
[40] B. Scott, K. J. Brewer, L. O. Spreer, C. A. Craig, J. W. Otvos, M. Calvin, S. Taylor, *J. Coord. Chem.* **1990**, *21*, 307–313.
[41] J. Hilbert, C. Näther, W. Bensch, *Dalton Trans.* **2015**, *44*, 11542–11550.
[42] J. Hilbert, N. Pienack, H. Lühmann, C. Näther, W. Bensch, *Z. Anorg. Allg. Chem.* **2016**, *642*, 1427–1434.
[43] J. Hilbert, C. Näther, R. Weihrich, W. Bensch, *Inorg. Chem.* **2016**, *55*, 7859–7865.
[44] K. Robinson, G. V. Gibbs, P. H. Ribbe, *Science* **1971**, *172*, 567–570.
[45] F. A. Holleman, E. Wiberg, N. Wiberg, *Lehrbuch der Anorganischen Chemie*, 102nd., Walter de Gruyter, Berlin, **2007**.
[46] B. B. Beyene, C.-H. Hung, *Sustainable Energy Fuels* **2018**, *2*, 2036–2043.
[47] M. Nippe, R. S. Khnayzer, J. A. Panetier, D. Z. Zee, B. S. Olaiya, M. Head-Gordon, C. J. Chang, F. N. Castellano, J. R. Long, *Chem. Sci.* **2013**, *4*, 3934–3945.
[48] B. Durham, J. V. Caspar, J. K. Nagle, T. J. Meyer, *J. Am. Chem. Soc.* **1982**, *104*, 4803–4810.
[49] L. J. Henderson, M. Ollino, V. K. Gupta, G. R. Newkome, W. R. Cherry, *J. Photochem.* **1985**, *31*, 199–210.
[50] A. Vaidyalingam, P. K. Dutta, *Anal. Chem.* **2000**, *72*, 5219–5224.
[51] F. Niefind, J. Djamil, W. Bensch, B. R. Srinivasan, I. Sinev, W. Grünert, M. Deng, L. Kienle, A. Lotnyk, M. B. Mesch, J. Senker, L. Dura, T. Beweries, *RSC Adv.* **2015**, *5*, 67742–67751.
[52] M. A. Asraf, H. A. Younus, M. Yusubovc, F. Verpoort, *Catal. Sci. Technol.* **2015**, *5*, 4901–4925.
[53] M. Dave, A. Rajagopal, M. Damm-Ruttensperger, B. Schwarz, F. Nägele, L. Daccache, D. Fantauzzi, T. Jacob, C. Streb, *Sustainable Energy Fuels* **2018**, *2*, 1020–1026.
[54] W. K. C. Lo, C. E. Castillo, R. Gueret, J. Fortage, M. Rebarz, M. Sliwa, F. Thomas, C. J. McAdam, G. B. Jameson, D. A. McMorran, J. D. Crowley, M.-N. Collomb, A. G. Blackman, *Inorg. Chem.* **2016**, *55*, 4564–4581.
[55] Y.-J. Yuan, H.-W. Lu, J.-R. Tu, Y. Fang, Z.-T. Yu, X.-X. Fan, Z.-G. Zou, *ChemPhysChem* **2015**, *16*, 2925–2930.
[56] D. Hong, Y. Tsukakoshi, H. Kotani, T. Ishizuka, K. Ohkubo, Y. Shiota, K. Yoshizawa, S. Fukuzumi, T. Kojima, *Inorg. Chem.* **2018**, *57*, 7180–7190.

Received: November 12, 2018
Published Online: January 23, 2019

3.2 “Synthesis and Characterization of a Rare Transition-Metal Oxothiostannate and Investigation of its Photocatalytic Properties”

The hydrothermal reaction of $Na_4SnS_4 \cdot 14H_2O$ with the complex $[Ni(cyclen)(H_2O)_2](ClO_4)_2 \cdot H_2O$ led to the generation of the new oxo-thiostannate compound $[Ni(cyclen)(H_2O)_2]_4[Sn_{10}S_{20}O_4] \cdot \sim 13H_2O$. Its structure consists of isolated cations $[Ni(cyclen)(H_2O)_2]^{2+}$ and cluster anions $[Sn_{10}S_{20}O_4]^{8-}$, which include ten $[SnS_4]^{4-}$ tetrahedra connected *via* corners. The O^{2-} anions are placed between these tetrahedra and exhibit a tetrahedral environment of Sn atoms. ^{119}Sn NMR investigations of an aqueous solution of $Na_4SnS_4 \cdot 14H_2O$ revealed only the presence of the anions $[SnS_4]^{4-}$ and $[Sn_2S_6]^{4-}$ up to 120 °C and the presence of the complex $[Ni(cyclen)(H_2O)_2](ClO_4)_2 \cdot H_2O$ is required for the formation of the anion $[Sn_{10}S_{20}O_4]^{8-}$. Thermal investigations of the compound demonstrate that the water molecules located in tunnels directed along [001] can be reversibly removed. The crystallinity remains unchanged. Furthermore, $[Ni(cyclen)(H_2O)_2]_4[Sn_{10}S_{20}O_4] \cdot \sim 13H_2O$ exhibits a high activity for hydrogen formation and reached 18.7 $mmol.g^{-1}$ after 3 h.

Reprinted with permission from A. Benkada, H. Reinsch, M. Poschmann, J. Krahmer, N. Pienack, and W. Bensch, Synthesis and Characterization of a Rare Transition-Metal Oxothiostannate and Investigation of Its Photocatalytic Properties, *Inorg. Chem.*, **2019**, *58*, 2354-2362. DOI: 10.1021/acs.inorgchem.8b02773.

Inorganic Chemistry
Cite This: Inorg. Chem. 2019, 58, 2354−2362
Article
pubs.acs.org/IC

Synthesis and Characterization of a Rare Transition-Metal Oxothiostannate and Investigation of Its Photocatalytic Properties

Assma Benkada, Helge Reinsch, Michael Poschmann, Jan Krahmer, Nicole Pienack, and Wolfgang Bensch*

Institute of Inorganic Chemistry, Christian-Albrechts University of Kiel, Max-Eyth-Strasse 2, 24118 Kiel, Germany

Supporting Information

ABSTRACT: The new transition-metal oxothiostannate $[Ni(cyclen)(H_2O)_2]_4[Sn_{10}S_{20}O_4]\cdot\sim 13H_2O$ (**1**) was prepared under hydrothermal conditions using $Na_4SnS_4\cdot 14H_2O$ as the precursor in the presence of $[Ni(cyclen)(H_2O)_2](ClO_4)_2\cdot H_2O$. Compound **1** comprises the $[Sn_{10}S_{20}O_4]^{8-}$ anion constructed by the T3-type supertetrahedron $[Sn_{10}S_{20}]$ and the $[Sn_{10}O_4]$ anti-T2 cluster. Channels host the H_2O molecules, and the sample can be reversibly dehydrated and rehydrated without significantly affecting the crystallinity of the material. ^{119}Sn NMR spectroscopy of an aqueous solution of $Na_4SnS_4\cdot 14H_2O$ evidences that between 25 and 120 °C only $[SnS_4]^{4-}$ and $[Sn_2S_6]^{4-}$ anions are present. In further experiments, hints were found that the formation of tin oxosulfide ions depends on the Ni^{2+}-centered complexes. Compound **1** exhibits promising photocatalytic properties for the visible-light-driven hydrogen evolution reaction, with 18.7 mmol·g^{-1} H_2 being evolved after 3 h.

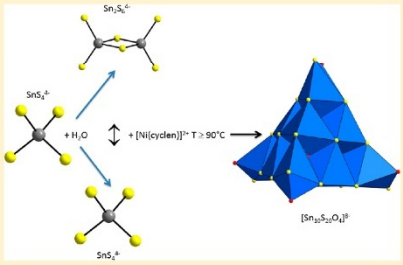

INTRODUCTION

Thiostannates exhibit a pronounced structural flexibility due to the variable oxidation state and coordination of Sn^{n+} (n = 2, 4) cations. Hence, SnS_x primary structural building units like a tetrahedron, a trigonal bipyramid, and an octahedron are observed.[1] In the crystal structures of thiostannates(IV), mainly the $[SnS_4]^{4-}$ tetrahedron occurs, which is either isolated as in $Na_4SnS_4\cdot 14H_2O$,[2] $K_4SnS_4\cdot 4H_2O$, $Rb_4SnS_4\cdot 4H_2O$, or $Cs_4SnS_4\cdot 3H_2O$[3] or condensed, forming the $[Sn_2S_6]^{4-}$ anion such as in $Na_4Sn_2S_6\cdot 14H_2O$.[4] Compounds with isolated $[Sn_2S_6]^{4-}$ anions combined with inorganic, organic, or complex cations for charge compensation form the most frequent class of thiostannates(IV). Depending on the pH value, various SnS_x polyhedra are formed in aqueous solution. Thus, in addition to the $[SnS_4]^{4-}$ and $[Sn_2S_6]^{4-}$ anions, different condensation products are observed like, e.g., $[SnS_3]^{2-}$, $[Sn_2S_5]^{2-}$, $[Sn_2S_7]^{6-}$, $[Sn_2S_8]^{2-}$, $[Sn_3S_7]^{2-}$, $[Sn_4S_9]^{2-}$, and $[Sn_5S_{12}]^{4-}$ anions[5−8] or the tetrameric adamantane-like moiety $[Sn_4S_{10}]^{4-}$.[5] In thiostannate compounds, three types of cations for charge compensation are distinguished: (i) metal cations, (ii) protonated organic molecules and metal complexes, or (iii) transition-metal cations with bonds to the anionic frameworks. Examples for group i are $Na_4SnS_4\cdot 14H_2O$,[2] $Na_4Sn_2S_6\cdot 14H_2O$,[4] $Cs_4Sn_5S_{12}\cdot 2H_2O$[8] or $Rb_2Sn_3S_7\cdot 2H_2O$,[9] with isolated anions like $[SnS_4]^{4-}$, $[Sn_2S_6]^{4-}$, $[Sn_5S_{12}]^{4-}$, and $[Sn_3S_7]^{2-}$, layered materials like $M_2Cu_2Sn_2S_6$ (M = Na, K, Cs, and Rb)[10] or three-dimensional structures as observed in $K_2Sn_2S_5$[6] and $Na_4Sn_3S_8$.[11] Group ii covers materials like $[Ni(dap)_3]_2Sn_2S_6\cdot 2H_2O$ (dap = 1,2-diaminopropane),[12] $[M(en)_3]_2Sn_2S_6$ (M = Ni, Co, Mn, and Zn; en = ethylenediamine),[12,13] and $[M(dien)_2]_2Sn_2S_6$ (M = Ni and Mn; dien = diethylenetriamine)[14,15] with discrete $[Sn_2S_6]^{4-}$ anions and compounds with layered anions, e.g., $(Et_4N)_2Sn_3S_7$, $(DABCOH)_2Sn_3S_7$ (DABCO = 1,4-diazabicyclo[2.2.2]-octane),[7] and $(trenH)_2Sn_3S_7$.[16] In group iii, transition-metal cations have bonds to the anionic framework exemplified by $Rb_2Cu_2SnS_4$, $M_2Cu_2Sn_2S_6$ (M = Na, K, Cs, and Rb)[10] $Cu_2CdSn_3S_8$,[17] $\{[Mn(2,2'\text{-bipy})_2]_2[Sn_2S_6]\}$ (2,2′-bipy = 2,2′-bipyridine),[18] $\{[M(1,10'\text{-phen})_2]_2[Sn_2S_6]\}$ (M = Mn, Fe, and Co; 1,10′-phen = 1,10′-phenanthroline),[19,20] $\{[Ni(cyclam)]_2[Sn_2S_6]\}_n\cdot 2nH_2O$ (cyclam = 1,4,8,11-tetraazacyclotetradecane),[18] $(1,4\text{-dabH}_2)Ag_2SnS_4$ (1,4-dab = 1,4-diaminobutane),[21] or $(dienH_2)Cu_2Sn_2S_6$.[22]

In most thiostannates, Sn adopts oxidation state IV, but there are some mixed-valent thiostannates in which Sn occurs in oxidation states II/IV or III/IV, e.g., $BaLnSn_2S_6$ (Ln = Ce, Pr, and Nd),[23] $(trenH_3)Cu_7Sn_4S_{12}$ (tren = tris(2-aminoethyl)-amine),[24] $[(Ph_3PCu)_6\{(CH_2)_4SnS_2\}_6Cu_4Sn]$,[25] and $[\{(CMe_2CH_2COMe)Sn_2(\mu\text{-}S)_2\}Sn_2S_6]$.[26] In the first five compounds, $Sn^{II/IV}$ is observed, while in the sixth Sn adopts oxidation states III and IV.

Another group of tin compounds contain sulfide and oxide anions, and prominent representatives are $[Sn_{10}S_{20}O_4]^{8-}$,[27,28] $[Sn_{10}S_{16}O_4Cl_4]^{4-}$,[29] $[Sn_8S_{12}O_4(SPh)_6]^{6-}$,[30] $[Sn_8S_{12}O_2(OH)_2Cl_6]^{4-}$,[29] and $[Sn_4S_5(S_3)OCl_4]^{2-}$.[31] Among these anions, the $[Sn_{10}S_{20}O_4]^{8-}$ moiety is the most common. It has an idealized T_d symmetry and can be described as a

Received: September 29, 2018
Published: January 31, 2019

DOI: 10.1021/acs.inorgchem.8b02773
Inorg. Chem. 2019, 58, 2354−2362

supertetrahedral cluster (denoted as T3) formed by 10 corner-linked SnS_4 polyhedra. Four empty sites are occupied by O^{2-} anions expanding the coordination number of Sn^{IV} from 4 to 5 or 6.[27,28,32]

While many thiostannate compounds were prepared using the molten flux approach like, e.g., $Cs_2Sn_4S_9$, $Rb_2Sn_4S_9$, $K_2Sn_4S_9$, and Li_2CdSnS_4[33,34] or high-temperature synthesis, e.g., $AGaSnS_4$ (A = Na, K, Rb, Cs, and Tl),[35] $BaCdSnS_4$,[36] and Au_2BaSnS_4,[37] the solvothermal approach allows the preparation of inorganic−organic hybrid compounds containing amine molecules and/or in situ generated transition-metal complexes, and this synthetic method led to an enormous expansion of the chemical and structural diversity of thiostannates.[38] Many of these compounds were synthesized by applying the elements Sn and S and transition metals or salts like $SnCl_4{\cdot}5H_2O$ and $Na_2S{\cdot}9H_2O$ in aqueous amine solutions.[38] Here we present a new rare oxothiostannate, which was synthesized under hydrothermal conditions using $Na_4SnS_4{\cdot}14H_2O$ as the precursor and the $[Ni(cyclen)(H_2O)_2](ClO_4)_2{\cdot}H_2O$ complex. The potential of $Na_4SnS_4{\cdot}14H_2O$ as single-source precursor for the generation of thiostannates has only been explored a little. Hence, we investigated the behavior of this salt in H_2O from room temperature up to 120 °C using ^{119}Sn NMR spectroscopy in order to monitor the stability. In addition to the synthesis and crystal structure of the new compound $[Ni(cyclen)(H_2O)_2]_4[Sn_{10}S_{20}O_4]{\cdot}{\sim}13H_2O$ (**1**), we report an in situ investigation of the formation of **1**, its thermal and H_2O sorption behavior, and the photocalytic properties of the title compound as well.

■ EXPERIMENTAL SECTION

$Na_4SnS_4{\cdot}14H_2O$ and $[Ni(cyclen)](ClO_4)_2$ were synthesized according to literature methods.[39,40] $[Ni(cyclen)(H_2O)_2](ClO_4)_2{\cdot}H_2O$ was prepared by dissolving $[Ni(cyclen)](ClO_4)_2$ in a H_2O/ethanol (1:1) mixture and allowing the solvent to evaporate slowly until purple crystals formed. Cyclen (Strem Chemicals, Inc., 98%) and $Ni(ClO_4)_2{\cdot}6H_2O$ (abcr, 99%) were used without further purification. Generally, the reaction product was filtered off, washed with tiny amounts of H_2O, and dried at ambient conditions. ***Caution!*** *One should keep in mind that perchlorate compounds are potentially explosive if heated and must be handled with care.*

Synthesis of $[Ni(cyclen)(H_2O)_2]_4[Sn_{10}S_{20}O_4]{\cdot}{\sim}13H_2O$ (1). For the synthesis of **1**, 120.9 mg (0.25 mmol) of $[Ni(cyclen)(H_2O)_2](ClO_4)_2{\cdot}H_2O$ was dissolved in 10 mL of H_2O. A total of 147.8 mg (0.25 mmol) of $Na_4SnS_4{\cdot}14H_2O$ also dissolved in 10 mL of H_2O was added dropwise to the $[Ni(cyclen)(H_2O)_2](ClO_4)_2{\cdot}H_2O$ solution. The mixture was filtered off to remove the black solid, and the reaction was then carried out under dynamic conditions (2 h at 120 °C). The product was cooled to room temperature, the green powder of compound **1** was filtered off, and the green mother liquor was again heated for 2 h to 120 °C until the solution became light pink and green crystals of **1** were formed (27% yield based on Sn). Compound **1** could also be obtained by using $Ni(ClO_4)_2{\cdot}6H_2O$ (91.0 mg, 0.25 mmol) and cyclen (43.0 mg, 0.25 mmol) instead of the complex. The salt and ligand were dissolved in 10 mL of H_2O and stirred at room temperature for 20 min. $Na_4SnS_4{\cdot}14H_2O$ (147.8 mg, 0.25 mmol) was added portionwise to the solution. The slurry was filtered to remove a black solid, and the clear brown solution was heated under dynamic conditions (120 °C). Compound **1** crystallized as green crystals after 2 h in a similar yield. We performed syntheses below 120 °C and observed that crystallization of compound **1** already occurred at 90 °C. Elem anal. Found: C, 12.58%; H, 3.21%; N, 7.33%; S. 20.54%. Calcd: C, 12.03%; H, 3.85%; N, 7.02%; S, 20.08%.

Structure Determination from Powder X-ray Diffraction (PXRD) Data. The PXRD pattern of compound **1** could be successfully indexed with a tetragonal unit cell using *TOPAS Academics*,[41] and the reflection extinction conditions point to space group $I4_1/a$. Using the lattice parameters and composition based on the energy-dispersive X-ray (EDX) data and CHNS analysis, the positions of the heavy Sn, S/O, and Ni atoms could be determined using direct methods, as implemented in *EXPO2009*.[42] This initial model was further complemented by the missing atoms of the cyclen ligand and the H_2O molecules of the nickel complex, which were inserted using the molecular modeling software *Materials Studio*.[43] The obtained model was further optimized by force-field calculations using the universal force field,[44] as implemented in the forcite routine in *Materials Studio*. The structurally optimized starting model was subsequently refined by the Rietveld method using a Thompson−Cox−Hasting profile shape function and an 18th-order polynomial background function. The positions of all atoms of the $\{Sn_{10}S_{20}O_4\}$ cluster were freely refined using only bond restraints. The nickel complex was refined as rigid body. Attempts to position the complex so that Ni−O/S bonds to the cluster are formed led to a significant decline of the figures of merit. The comparably high values for the displacement parameters were refined element-specific or as a group for the nickel complex. The crystallographic details and resulting reliability factors are summarized in Table S1, and the results of the Rietveld refinement are shown in Figure S1. In the difference Fourier map, only weak electron densities could be observed, indicating that for disordered H_2O, which was not considered in the refinement. Hence, the final structure contained voids, and using the program suite *PLATON*, a solvent-accessible space of 2050 $Å^3$ was calculated (23% of the unit cell volume).[45] Assuming that a H_2O molecule requires 40 $Å^3$ space, app. 13 H_2O molecules occupy the voids (Figure S2). The structural data have been deposited in the Cambridge Crystallographic Data Centre as CCDC 1863577 (**1**).

Characterization Methods. *PXRD.* The PXRD patterns were collected with a STOE Stadi-P diffractometer equipped with a MYTHEN 1K detector (DECTRIS) using monochromatized Cu $K\alpha_1$ radiation (λ = 1.540598 Å). The experimental and calculated patterns using the results of the Rietveld refinement matched perfectly, indicating the phase purity of the sample (Figure S3).

EDX Spectroscopy. EDX analysis (Table S2) was performed with a Philips ESEM XL30 environmental scanning electron microscope equipped with an EDX detector.

Elemental Analysis. CHNS elemental analyses were performed with a EURO EA elemental analyzer (EURO VECTOR Instruments and Software).

^{119}Sn NMR Spectroscopy. ^{119}Sn NMR spectra were recorded in D_2O at 149 MHz using a Bruker Avance3 400 HD spectrometer (T_{max} = 80 °C) and at different temperatures. The pulse width was 11 μs at 30.974 W, the relaxation delay 1 s, and the number of scans 256. The NMR samples were prepared in a 5 mm tube and referenced to $SnCl_4$ [$\delta(^{119}Sn)$ = −150 ppm]. To be consistent with literature data, the NMR shifts were corrected using $SnMe_4$ as the standard (0 ppm).

In Situ Investigation of the Formation of Compound 1. The crystallization of compound **1** was investigated in situ using an EasyMax reactor system (Mettler Toledo GmbH, Giessen, Germany), which allowed control of the temperature, dosing of the solution, and stirring. With this cell, simultaneous measurements of, e.g., pH value, redox potential, ion conductivity, in situ IR spectroscopy, and in situ luminescence, can be performed.[46,47] In the present experiment, the precursor was dissolved in H_2O and placed inside the glass reactor vessel. $[Ni(cyclen)(H_2O)_2](ClO_4)_2{\cdot}H_2O$ was also dissolved in H_2O and then added dropwise to the reactor vessel under constant stirring (300 rpm). The solution was slowly heated to 90 °C (5 K·min^{-1}). The pH value and redox potential were measured with a pH electrode [InLab Semi-Micro, Mettler Toledo; sensor type, combined pH electrode; reference system, Argenthal (0−100 °C as the temperature range)] and a redox electrode [InLab Redox Micro (Mettler Toledo); sensor type, combined ORP electrode with platinum ring; reference system, Argenthal (ceramic diaphragm, 3 M KCl as the reference electrolyte, and 0−100 °C as the temperature range)].

IR Spectroscopy. IR spectra were measured in the region from 400 to 4000 cm^{-1} with a Bruker Alpha P spectrometer.

DOI: 10.1021/acs.inorgchem.8b02773
Inorg. Chem. 2019, 58, 2354−2362

UV/Vis Spectroscopy. UV/vis analysis was performed at room temperature with a Cary 5 UV/vis−near-IR two-channel spectrometer (Varian Techtron Pty., Darmstadt, Germany, 200−3000 cm^{-1}) using $BaSO_4$ as the reference material. The UV/vis diffuse-reflectance data were transformed by applying the Kubelka−Munk function.

Thermogravimetric Analysis (TGA). TGA was performed with a Linseis STA PT1600 instrument. The samples were heated in a N_2 atmosphere with a heating rate of 4 $K{\cdot}min^{-1}$.

N_2 and H_2O Sorption Measurements. The N_2 and H_2O sorption isotherms of compound **1** were measured by a Belsorpmax instrument (BEL Japan Inc., Toyonaka, Japan) at 77 K (N_2) and 303 K (H_2O). The samples were pretreated by heating to 130 °C in a vacuum for 16 h to remove H_2O molecules.

Photocatalytic Hydrogen Evolution. In the photocatalytic experiments, a double-walled thermostatically controlled vessel with **1** (10 mg, 3.13 μmol) or $[Ni(cyclen)(H_2O)_2](ClO_4)_2{\cdot}H_2O$ (6.0 mg, 12.5 μmol) and $[Ru(bpy)_3](PF_6)_2$ (8.6 mg, 1.00 μmol) as the photosensitizer were used. Triethylamine (10 mL) and acetonitrile (10 mL) were dried with CaH_2, distilled under N_2, and added to the mixture. Subsequently, degassed H_2O (3 mL) was added. The system was stirred in the dark for 1 h and irradiated after equilibration with UV light (330 W Xe lamp with a 400 nm cutoff filter) at 30 °C. Evolved gas was collected after a distinct reaction time and quantified by gas chromatography (Agilent 6890 Plus gas chromatograph with a 5 Å molecular sieve column and a thermal conductivity detector; the carrier gas was argon).

RESULTS AND DISCUSSION

Synthetic Aspects and In Situ Investigations. To prove which species might form when the precursor was dissolved in H_2O, measurements using ^{119}Sn NMR spectroscopy were performed. Depending on the reaction conditions, one can expect that different thiostannates or oxothiostannates can form, which can easily be distinguished because the chemical shift is sensitive whether only S^{2-} anions or mixed anions are present. In the ^{119}Sn NMR spectra, the chemical shifts of thiostannate and oxothiostannate ions are in the range of −1000 to +1000 ppm.[48,49] If the precursor $Na_4SnS_4{\cdot}14H_2O$ is dissolved in H_2O, two signals occur at approximately 69 and 74 ppm, indicating that the Sn^{IV} cations in the solution are in a tetrahedral environment (literature data: 49−74 ppm;[50] Figures 1 and S4). The signal at 69 ppm can be assigned to the $[Sn_2S_6]^{4-}$ anion and that at 74 ppm to $[SnS_4]^{4-}$. This observation suggests that a relatively fast protonation and condensation reaction must occur, in which H_2S is emitted and

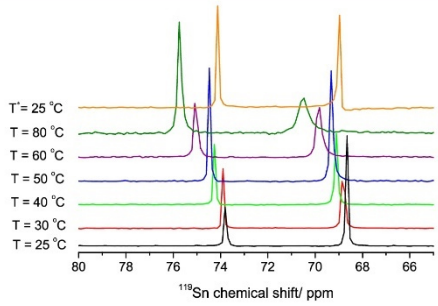

Figure 1. ^{119}Sn NMR spectra of the precursor $Na_4SnS_4{\cdot}14H_2O$ dissolved in D_2O measured at the indicated temperatures in the range of 80 to 65 ppm (*: ^{119}Sn NMR spectrum of the precursor solution, which was heated at 120 °C for 1 h and cooled to room temperature).

$[Sn_2S_6]^{4-}$ anions are formed. The evolution of H_2S could be proven with wet lead acetate paper. With increasing temperature, the signals occurred at slightly larger chemical shifts because the Sn−S bond lengths increased, leading to a change of the nuclear magnetic shielding.[51] Upon heating of $[Sn_2S_6]^{4-}$, the equilibrium was shifted to $[SnS_4]^{4-}$, and integration of both signals confirmed that with increasing temperature the amount of $[Sn_2S_6]^{4-}$ was reduced (Table S3). However, no tin oxosulfide ions were detected, demonstrating the stability of Sn^{IV} in the S^{2-} environment up to at least 80 °C. In another experiment, the precursor solution was heated at 120 °C for 1 h, and after cooling to room temperature, the ^{119}Sn NMR spectrum (Figure 1) showed only the signals of $[Sn_2S_6]^{4-}$ and $[SnS_4]^{4-}$, while tin oxosulfide species were absent because they should show signals between −200 and −500 ppm.[49] The two signals exhibited different intensities compared to the spectrum recorded at the beginning of the experiments (T = 25 °C) and now the two anions were present in a nearly 1:1 ratio (Table S3). The main conclusions of the ^{119}Sn NMR investigations are that, in the presence of H_2O, no tin oxosulfides are generated and that $[SnS_4]^{4-}$ and $[Sn_2S_6]^{4-}$ anions are stable up to 120 °C.

In the following, an in situ experiment monitoring the redox potential, pH value, and temperature of the solution simultaneously was performed (Figure 2). Dissolution of the

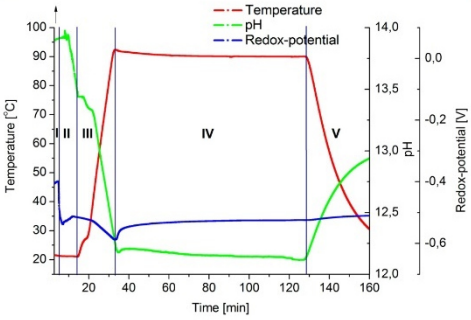

Figure 2. In situ investigation of the crystallization of compound **1**. The temperature (red), pH value (green), and redox potential (blue) were recorded simultaneously: (I) showing the precursor solution before the solution containing the Ni^{2+} complex was added (II); (III) heating the solution to 90 °C; (IV) keeping the temperature constant; (V) cooling the solution to room temperature.

precursor in H_2O (region I) yields an initial pH value of 13.9 and a redox potential of −0.40 V. After addition of the dissolved Ni^{2+} complex (region II), the pH value drops to 13.4, which can be explained by dilution of the solution. Simultaneously the redox potential reaches −0.51 V, indicating the release of reducing species like, e.g., HS^- formed according to $H_2S + H_2O \Leftrightarrow HS^- + H_3O^+$.[52] In region III, the temperature is successively increased, which is accompanied by a reduction of the pH value to 12.3 and of the redox potential to −0.59 V at T = 90 °C (region III). The pH value drop is caused by the temperature dependence of the pH and eventually by further release of H_2S. Alteration of the redox potential can also be traced back to the increased temperature. In region IV, the slight decrease of the pH (12.1) can be explained by further generation of H_2S, and the minute change

DOI: 10.1021/acs.inorgchem.8b02773
Inorg. Chem. 2019, 58, 2354−2362

of the redox potential may be caused by the consumption of, e.g., HS^-. Finally, lowering the temperature to room temperature (region V) is accompanied by an increase of the pH value. The PXRD pattern of the solid recovered from the slurry demonstrates that **1** already crystallized at 90 °C (Figure S5).

For an explanation of the formation of the tin oxosulfide species, the chemical reactivity of organotin compounds R_3SnX (R = organic molecule; X = electronegative ligand) in H_2O may serve as a model. For example, the hydrolysis of R_3SnX leads to the formation of $R_3Sn(OH)$, which further reacts to $R_3SnOSnR_3$.[53,54] In analogy, one may propose that $[SnS_3(OH)]^{3-}$ is formed and then condenses to generate $[Sn_2S_5O]^{4-}$. This anion reacts with $[Sn_2S_7]^{6-}$, yielding $[Sn_4S_{10}O]^{6-}$. The connection of these anions via S atoms leads to formation of the $[Sn_{10}S_{20}O_4]^{8-}$ cluster (Scheme 1).

Scheme 1. Proposed Mechanism for the Formation of $[Sn_{10}S_{20}O_4]^{8-}$ Starting from the $[SnS_4]^{4-}$ Anion

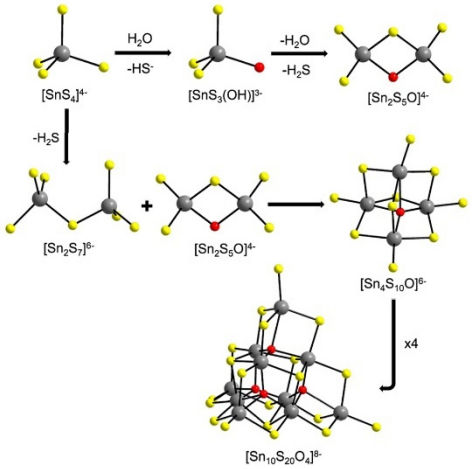

To confirm this suggestion, the pH value of the precursor solution without the Ni^{2+} complex was adjusted to 12.3 (with 0.2 M HCl) and the solution was heated at 90 °C for 1 h. After cooling to room temperature, a ^{119}Sn NMR spectrum was recorded (Figure S6), which shows only the signal of $[Sn_2S_6]^{4-}$ at 55 ppm and no signal for $[SnS_4]^{4-}$ or any possible oxo species. Therefore, one may assume that the Ni^{2+} complex plays a crucial role for the formation of the oxosulfide species.

Crystal Structures. Compound **1** crystallizes in the tetragonal space group $I4_1/a$ with three unique Sn atoms, five independent S atoms, three unique O atoms, and one independent Ni atom. The structure of the $[Sn_{10}S_{20}O_4]^{8-}$ anion consists of ten $[SnS_4]^{4-}$ tetrahedra, which are linked via corners, yielding the T3-type supertetrahedron $[Sn_{10}S_{20}]$[55−57] (Figure 3, top). The O atoms are located between the SnS_4 tetrahedra (Figure 3, bottom) and are in a tetrahedral environment of Sn atoms. The arrangement of the O atoms can be described as an anti-T2 cluster[57] (Figure 4, bottom).

In the $[Sn_{10}S_{20}O_4]^{8-}$ cluster, Sn1 and Sn3 are in an octahedral environment, while a trigonal-bipyramidal coordi-

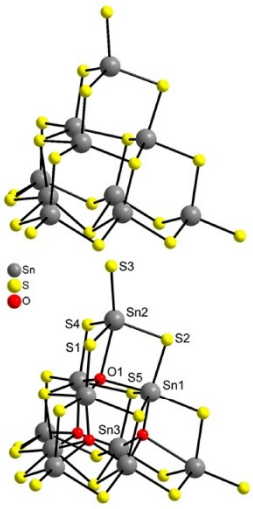

Figure 3. View of the T3 supertetrahedral cluster $[Sn_{10}S_{20}]$ in the structure of **1** (top) and the O atoms located in the voids of the cluster (bottom). Only crystallographically unique atoms are labeled.

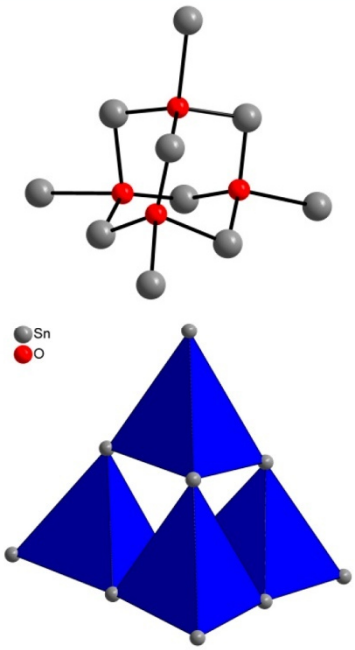

Figure 4. Structure (top) and a polyhedral representation (bottom) of the anti-T2 cluster formed by the tetrahedral environments of the O atoms in the structure of **1**.

DOI: 10.1021/acs.inorgchem.8b02773
Inorg. Chem. 2019, 58, 2354−2362

nation is observed for Sn2. In the $Sn1S_4O_2$ octahedron, the O atoms are in the trans positions, while in $Sn3S_4O_2$, the O atoms occupy the cis positions. In the two octahedra, the Sn−S/Sn−O bonds in the basal plane and Sn−S/Sn−O bonds to the apical atoms (Table S4) are comparable with data reported in the literature.[32,55] For the SnS_4O trigonal bipyramid, the Sn−O/S bonds are slightly larger than those in the octahedra. The S−Sn−S/S−Sn−O/O−Sn−O angles (Table S4) in the three polyhedra indicate distortions from ideal geometry, as were also observed in similar compounds.[32,55] The Sn_4O tetrahedron is strongly distorted, as evidenced by the Sn−O bond lengths (2.001(7)−2.681(1) Å) and the Sn−O−Sn angles (92.95(6)−128.77(6)°). One cluster of **1** is located on each corner and another in the middle of the unit cell, and two clusters are positioned on the middle of the faces (010) and (001) (Figure 5).

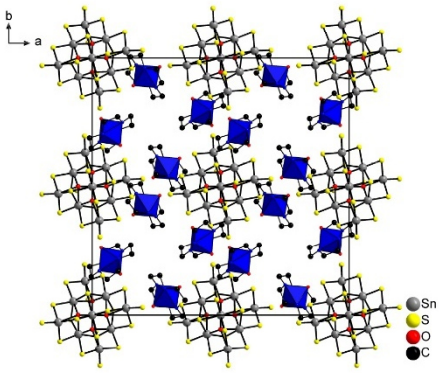

Figure 5. View of the arrangement of the $\{Sn_{10}S_{20}O_4\}$ moieties and Ni^{2+}-centered complexes (blue octahedra) in the unit cell of compound **1**. H atoms are not shown.

The $[Sn_{10}S_{20}O_4]^{8-}$ clusters on the corner and in the middle of the unit cell are arranged in rods along the *b* axis, and the remaining clusters form rods along [100]. The cations and H_2O molecules occupy the empty spaces between the anions. The size of the channel along [001] is about 5.5 $Å^2$ measured from coordinate-to-coordinate. In **1**, charge compensation is achieved by the Ni^{2+} cation, which is in an octahedral environment of four N atoms of the cyclen ligands and two O atoms of the H_2O molecules (Figure 6).

We note that all Sn−O−S compounds contain isolated $[Sn_{10}S_{20}O_4]^{8-}$ clusters with inorganic cations compensating for the negative charges like in $[Cs_8(H_2O)_{13}][Sn_{10}S_{20}O_4]$[32] and $[Li_8(H_2O)_{29}][Sn_{10}S_{20}O_4]\cdot 2H_2O$,[27] and only in $\{[Ni(1,2\text{-dach})_2(ma)]_4[Sn_{10}S_{20}O_4]\}$ (1,2-dach = 1,2-diaminocyclohexane; ma = methylamine)[55] is the cluster expanded via S atoms to Ni^{2+}-centered complexes. In this compound, the Ni^{2+} cation is in an octahedral environment of five N atoms of the amine ligands and of one S atom of the $[Sn_{10}S_{20}O_4]^{8-}$ cluster.

Spectroscopy Properties. The typical bands of the cyclen molecule in **1** can be identified in the IR spectrum (Figure S7 and Table S5). The OH band of H_2O molecules in compound **1** is located at 3373 cm^{-1}. The N−H stretching vibration of cyclen occurs around 3199 cm^{-1}, and the Ni−N stretching mode is observed around 417 cm^{-1}. The UV/vis spectrum

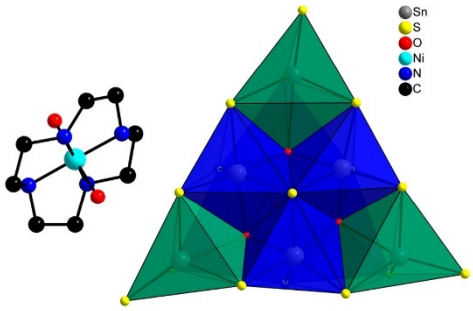

Figure 6. Views of the $[Ni(cyclen)(H_2O)_2]^{2+}$ complex (left) and the $[Sn_{10}S_{20}O_4]^{8-}$ anion (right). Nearly trigonal-bipyramidal SnS_4O: polyhedra, green; octahedra, blue.

shows the expected d−d transitions. For the high-spin complex $[Ni(H_2O)_6]^{2+}$, the d−d transitions are located at 1.05 eV (1176 nm, $^3A_{2g} \rightarrow {}^3T_{2g}$), 1.71 eV (724 nm, $^3A_{2g} \rightarrow {}^3T_{1g}$ (F)), and 3.14 eV (395 nm, $^3A_{2g} \rightarrow {}^3T_{1g}$ (P)).[52] For **1**, these transitions are found at 1.16 eV (1068 nm), 2.03 eV (610 nm), and 3.11 eV (398 nm) (Figure S8); i.e., the color stems from d−d transitions at 2.03 eV (610 nm), explaining the green color of the crystals. The absorption band at 3.11 eV is too intense for a d−d transition and is mostly the sum of the d−d and HOMO−LUMO transition.[52] The strong absorption at 3.72 eV may be regarded as a charge-transfer band.[58]

TGA. The TGA, differential thermal analysis (DTA), and derivative thermogravimetry curves of **1** are displayed in Figure S9. A mass loss of 4.5% is observed in the first step, which is accompanied by a broad endothermic event ($T_{peak} \approx 75$ °C) and corresponds to the removal of eight crystal H_2O molecules (calcd 4.6%). The second decomposition step with a mass loss of 26.7% is also accompanied by an endothermic event (T_{peak} = 335 °C) and corresponds to the removal of eight H_2O molecules that coordinate to the Ni^{2+} cation and four cyclen ligands (calcd 26.6%). To confirm the emission of individual constituents of the compound, the black residue of the decomposition product (T = 500 °C) was investigated by PXRD and IR spectroscopy. According to the PXRD pattern, the residue consists of NiO, SnS, $Ni_3Sn_2S_2$, and an unknown phase (Figure S10). Furthermore, in the IR spectrum, no bands of H_2O molecules and cyclen ligands are observed (Figure S11). According to the void space, the crystal H_2O content should be app. 13. An experiment was performed with a freshly prepared compound, which was weighed at room temperature for about 1 day at regular time intervals. The weight was reduced within several minutes, which may explain the difference between the observed and expected H_2O content in the TGA curve. In a further experiment, decomposition was stopped at 130 °C and a PXRD pattern was collected. Afterward, the residue was stored for 1 day in a H_2O atmosphere, and again a PXRD pattern was measured (Figures S12 and S13). The removal of H_2O is accompanied by a slight shift of the positions of the Bragg reflections (Figure S12, bottom), while rehydration leads to a PXRD pattern in full agreement with that of the pristine material.

N_2 and H_2O Sorption. The N_2 adsorption−desorption curves of **1** were recorded, but the Brunauer−Emmett−Teller surface area was only app. 20 $m^2 \cdot g^{-1}$; i.e., the sample is

DOI: 10.1021/acs.inorgchem.8b02773
Inorg. Chem. 2019, 58, 2354−2362

nonporous (Figure S14, bottom). Nevertheless, the H_2O sorption−desorption was measured, and ca. 13 H_2O molecules were adsorbed at $p/p_0 = 0.9$ (Figure S14, top). The desorption branch exhibits a divergent shape, and at $p/p_0 = 0.1$, the sample still contained about 4 H_2O molecules. After H_2O uptake, a PXRD pattern was recorded that matches that collected for the pristine material (Figure S15); i.e., the sample is stable. The observed H_2O isotherm does not follow the typical isotherms according to the IUPAC nomenclature. At the moment, no straightforward explanation can be given, but we will assume that kinetics play an important role and strong interactions between H_2O and atoms of the host material lead to the observed isotherm. Similarly, the low N_2 adsorption (Figure S14, bottom) may be a kinetic phenomenon because the measurement is performed at 77 K, and additionally N_2 and H_2O exhibit different kinetic diameters (N_2, 3.64 Å; H_2O, 2.65 Å[59]). We note that the observation made here is not unusual, and, e.g., MOF-802,[60] Ni-CAU-29,[61] or STA-12[62] did not show N_2 adsorption but good H_2O uptake. We calculated the Connolly surface (Figure S16) for H_2O as the probe molecule (probe radius 1.32 Å) using *Materials Studio*. The calculated accessible volume for this guest molecule is 19.3% of the total volume, being proportional to a maximum H_2O content of approximately 9 wt %. These data clearly support the experimental findings.

Photocatalytic Hydrogen Evolution. Photocatalytic experiments were carried out with **1**, $[Ru(bpy)_3](PF_6)_2$ as the photosensitizer, the sacrificial agent triethylamine as the electron donor, H_2O as the proton source, and CH_3CN as the solvent for the photosensitizer. The photocatalytically evolved H_2 (Figure 7) increases with increasing irradiation and then levels off, reaching 18.7 mmol·g^{-1} after 3 h of irradiation time, and longer irradiation yields a constant H_2 evolution up to 5 h. During the reaction, the light-orange solution turned brown, leading to a reduced absorption of incident light, which may explain the decline of the initially steep curve. Such a color change indicates photodegradation of the sensitizer, as reported in several publications.[63−68] The compound could be recovered after photocatalysis, but the PXRD pattern indicates low crystallinity (Figure S17). When new solvents are applied to the recovered material, the hydrogen evolution reaches only 3.2 mmol·g^{-1}. This observation is an indication that the compound is destroyed during the photocatalytic reaction. Therefore, the stability of **1** in the solution of triethylamine/acetonitrile/H_2O was investigated by storing the sample for 1 day at room temperature. The PXRD pattern shows a modulated background besides reflections of **1**, suggesting the formation of an amorphous solid. This observation supports the assumption that **1** is not stable under the basic conditions for a longer time and irradiation may accelerate the amorphization process. We assume that during chemical decomposition the Ni^{2+}-centered complex is released, and therefore a photocatalytic experiment was performed with the mixture $[Ni(cyclen)(H_2O)_2](ClO_4)_2 \cdot H_2O/[Ru(bpy)_3](PF_6)_2$ (Figure S18). For this system, 18.9 mmol·g^{-1} H_2 was obtained after 3 h of irradiation time, and longer irradiation yields a constant H_2 evolution up to 5 h. However, it was reported that transition-metal complexes may be destroyed during the photocatalytic reaction and nanoparticles are generated, which are the active species.[69] Such complexes may be regarded as precatalysts, which are in situ transformed into the catalytically active species. The appearance of the Tyndall effect after the photocatalytic reaction confirms the presence of nanoparticles. In the present case, the situation is more complex than only using a Ni^{2+}-centered complex because the anion may also be decomposed and the amorphous particles generated may contain both Ni and Sn. A possible photocatalytic mechanism has already been discussed for the $[Ni(bpy)_3]^{2+}$ complex (bpy = 2,2′-bipyridine)[70] and on the basis of this proposed mechanism, we assume a similar mechanism for the $[Ni(cyclen)(H_2O)_2]^{2+}$ complex (Scheme 2).

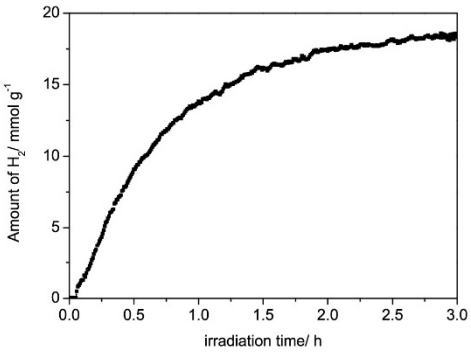

Figure 7. Photocatalytic hydrogen evolution using compound **1**, $[Ru(bpy)_3](PF_6)_2$ as the photosensitizer, triethylamine as the sacrificial agent, H_2O as the proton donor, and acetonitrile as the solvent.

Scheme 2. Proposed Mechanism for Photocatalytic Hydrogen Generation Using the $[Ni(cyclen)(H_2O)_2]^{2+}$ Complex[a]

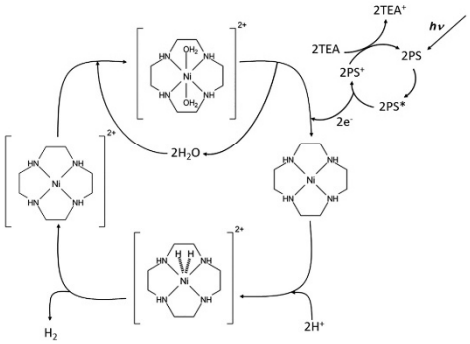

[a]PS = $[Ru(bpy)_3](PF_6)_2$; TEA = triethylamine. The scheme was adapted from ref 70.

A comparison of the photocatalytic activity with data reported in the literature is difficult because the activity depends on a large number of parameters like solvents, the amount of the catalyst, the cocatalyst, the photosensitizer, the intensity and wavelength of the light source, the sacrificial compound, the pH value, etc. In addition, the amount of H_2

DOI: 10.1021/acs.inorgchem.8b02773
Inorg. Chem. 2019, 58, 2354−2362

produced is reported as different quantities like, e.g., mmol·g^{-1}, mmol, mL, turnover number, or turnover frequency.[71] Nevertheless, the amount of H_2 of 138 μmol·h^{-1} is in the range of data reported for sulfidic compounds or composites (Table 1).

Table 1. Comparison of the Photocatalytic Activity of Different Catalysts at Various Conditions

catalyst	reaction mixture/light source	activity/ μmol·h^{-1}
compound **1**	triethylamine, acetonitrile, H_2O, $[Ru(bpy)_3](PF_6)_2$, 330 W Xe lamp, cutoff filter (λ > 400 nm)	138
colloidal MoS_2[72]	scorbic acid, acetonitrile, methanol, $[Ru(bpy)_3](PF_6)_2$, 300 W Xe lamp, cutoff filter (λ > 420 nm)	420
TiO_2/MoS_2/graphene[73]	ethanol, H_2O, 350 W Xe lamp	165
MoS_xC_y[74]	triethylamine, acetonitrile, H_2O, $[Ru(bpy)_3](PF_6)_2$, 300 W Xe lamp, cutoff filter (λ > 420 nm)	120
MoS_2/SiO_2[75]	KOH, TiO_2, H_2O, methanol, medium-pressure Hg lamp	860
CoS_x/graphene[76]	TEOA, H_2O, Eosin Y/300 W Xe lamp, cutoff filter (λ > 455 nm)	300
$[Co_4(C_6H_{14}N)_4(\mu_4\text{-}S_2)_2(\mu_2\text{-}S_2)_4]\cdot 4H_2O$[77]	triethylamine, acetonitrile, H_2O, $[Ru(bpy)_3](PF_6)_2$, 330 W Xe lamp	98
CoS/mpg-CN (mpg = mesoporous graphitic)[78]	H_2O, triethanolamine, 300 W Xe lamp	37

CONCLUSION

In this work, we present the structure of a new rare oxothiostannate **1**, which was prepared by the reaction of $Na_4SnS_4\cdot 14H_2O$ with $[Ni(cyclen)(H_2O)_2](ClO_4)_2\cdot H_2O$ under hydrothermal conditions. The anion is constructed by a T3 supertetrahedron and an anti-T2 cluster. In the structure, tunnels are directed along [001], which host H_2O molecules. The sample can be reversibly dehydrated and rehydrated without significant loss of crystallinity. ^{119}Sn NMR investigations of an aqueous solution of $Na_4SnS_4\cdot 14H_2O$ demonstrate that only $[SnS_4]^{4-}$ and $[Sn_2S_6]^{4-}$ anions exist in solution, and they are stable up to 120 °C. The formation of $[Sn_2S_6]^{4-}$ occurs via a condensation reaction, and H_2S is released. One must postulate that generation of the oxosulfide $[Sn_{10}S_{20}O_4]^{8-}$ ion requires the presence of the Ni^{2+}-centered complex in the reaction mixture. In situ investigations of the formation show that crystallization already occurs at 90 °C and pH 12.3. The photocatalytic experiments show a high activity for hydrogen generation, and the catalysis is most probably heterogeneous.

ASSOCIATED CONTENT

Supporting Information

The Supporting Information is available free of charge on the ACS Publications website at DOI: 10.1021/acs.inorgchem.8b02773.

Crystal data and refinement results, tables with interatomic distances, IR and UV/vis spectra, DTA–TGA curves, N_2 and H_2O sorption curves, PXRD patterns of the pristine samples (dehydrated and rehydrated), and additional photocatalytic curves (PDF)

Accession Codes

CCDC 1863577 contains the supplementary crystallographic data for this paper. These data can be obtained free of charge via www.ccdc.cam.ac.uk/data_request/cif, or by emailing data_request@ccdc.cam.ac.uk, or by contacting The Cambridge Crystallographic Data Centre, 12 Union Road, Cambridge CB2 1EZ, UK; fax: +44 1223 336033.

AUTHOR INFORMATION

Corresponding Author

*E-mail: wbensch@ac.uni-kiel.de. Phone: +49 431 880-2419. Fax: +49 431 880-1520.

ORCID

Helge Reinsch: 0000-0001-5288-1135

Wolfgang Bensch: 0000-0002-3111-580X

Notes

The authors declare no competing financial interest.

ACKNOWLEDGMENTS

Financial support by the State of Schleswig-Holstein is gratefully acknowledged. We thank Aleksej Jochim for the TGA measurements and Philipp Polzin and Dr. Huayna Terraschke for support.

REFERENCES

(1) Sheldrick, W. S. Network self-assembly patterns in Main Group metal chalcogenide-based materials. *J. Chem. Soc., Dalton Trans.* **2000**, 3041–3052.

(2) Schiwy, W.; Pohl, S.; Krebs, B. Darstellung und Struktur von $Na_4SnS_4\bullet 14H_2O$. *Z. Anorg. Allg. Chem.* **1973**, *402*, 77–86.

(3) Ruzin, E.; Jakobi, S.; Dehnen, S. Syntheses, Structures and Reactivity of Novel Hydrates of *ortho*-Sulfidostannate Salts. *Z. Anorg. Allg. Chem.* **2008**, *634*, 995–1001.

(4) Krebs, B.; Pohl, S.; Schiwy, W. Darstellung und Struktur von $Na_4Ge_2S_6\bullet 14H_2O$ und $Na_4Sn_2S_6\bullet 14H_2O$. *Z. Anorg. Allg. Chem.* **1972**, *393*, 241–252.

(5) Krebs, B. Thio- und Selenoverbindungen von Hauptgruppenelementen – neue anorganische Oligomere und Polymere. *Angew. Chem.* **1983**, *95*, 113–134.

(6) Liao, J.-H.; Varotsis, C.; Kanatzidis, M. G. Syntheses, Structures, and Properties of Six Novel Alkali Metal Tin Sulfides: $K_2Sn_2S_8$, α-$Rb_2Sn_2S_8$, β-$Rb_2Sn_2S_8$, $K_2Sn_3S_8$, $Cs_2Sn_2S_6$, and Cs_2SnS_{14}. *Inorg. Chem.* **1993**, *32*, 2453–2462.

(7) Jiang, T.; Lough, A.; Ozin, G. A.; Bedard, R. L.; Broach, R. Synthesis and structure of microporous layered tin(IV) sulfide materials. *J. Mater. Chem.* **1998**, *8*, 721–732.

(8) Ko, Y.; Cahill, C. L.; Parise, J. B. Novel Layered Sulfides of Tin: Synthesis and Structural Characterization of $Cs_4Sn_5S_{12}\bullet 2H_2O$ and $Sn_5S_{12}(N_2C_4H_{11})_2(N_4C_{10}H_{24})$. *J. Chem. Soc., Chem. Commun.* **1994**, 69–70.

(9) Sheldrick, W. S.; Schaaf, B. Darstellung und Kristallstruktur von $Rb_2Sn_3S_7\bullet 2H_2O$ und $Rb_4Sn_2Se_6$. *Z. Anorg. Allg. Chem.* **1994**, *620*, 1041–1045.

(10) Liao, J.-H.; Kanatzidis, M. G. Quaternary $Rb_2Cu_2SnS_4$, $A_2Cu_2Sn_2S_6$ (A = Na, K, Rb, Cs), $A_2Cu_2Sn_2Se_6$ (A = K, Rb), $K_2Au_2SnS_4$, and $K_2Au_2Sn_2S_6$. Syntheses, Structures, and Properties of New Solid-state Chalcogenides Based on Tetrahedral $[SnS_4]^{4-}$ Units. *Chem. Mater.* **1993**, *5*, 1561–1569.

(11) Jumas, J.-C.; Philippot, E.; Maurin, M. Etude Structurale de $Na_4Sn_3S_8$. Evolution de la Coordination de l'Etain dans le Système Na_2S-SnS_2. *J. Solid State Chem.* **1975**, *14*, 152–159.

(12) Behrens, M.; Scherb, S.; Näther, C.; Bensch, W. On the Incorporation of Transition Metal Atoms into Thiostannates: Synthesis, Crystal Structures and Spectroscopic Properties of $[Ni(en)_3]_2Sn_2S_6$, $[Ni(dap)_3]_2Sn_2S_6\cdot 2H_2O$, $[Co(tren)]_2Sn_2S_6$, and $[Ni(tren)]_2Sn_2S_6$. *Z. Anorg. Allg. Chem.* **2003**, *629*, 1367–1373.

DOI: 10.1021/acs.inorgchem.8b02773
Inorg. Chem. 2019, 58, 2354–2362

(13) Jia, D.-X.; Zhang, Y.; Dai, J.; Zhu, Q.-Y.; Gu, Y.-M. Solvothermal Syntheses and Characterization of Thiostannates $[M(en)_3]_2Sn_2S_6$ (M = Mn, Co, Zn), the Influence of Metal Ions on the Crystal Structure. *Z. Anorg. Allg. Chem.* **2004**, *630*, 313−318.
(14) Jia, D.-X.; Dai, J.; Zhu, Q.-Y.; Zhang, Y.; Gu, X.-M. Syntheses, crystal structures and thermoanalyses of thiostannates $[Ni(en)_3]_2Sn_2S_6$ and $[Ni(dien)_2]_2Sn_2S_6$. *Polyhedron* **2004**, *23*, 937−942.
(15) Fu, M.-L.; Guo, G.-C.; Liu, B.; Wu, A.-Q.; Huang, J.-S. Two New Thiostannates Templated by Transition Metal Complexes. *Chin. J. Inorg. Chem.* **2005**, *21*, 25−29.
(16) Pienack, N.; Schinkel, D.; Puls, A.; Ordolff, M.-E.; Lühmann, H.; Näther, C.; Bensch, W. New Thiostannates Synthesized Under Solvothermal Conditions: Crystal Structures of $(trenH)_2Sn_3S_7$ and $\{[Mn(tren)]_2Sn_2S_6\}$. *Z. Naturforsch., B: J. Chem. Sci.* **2012**, *67b*, 1098−1106.
(17) Chykhrij, S. I.; Sysa, L. V.; Parasyuk, O. V.; Piskach, L. V. Crystal structure of the $Cu_2CdSn_3S_8$ compound. *J. Alloys Compd.* **2000**, *307*, 124−126.
(18) Hilbert, J.; Pienack, N.; Lühmann, H.; Näther, C.; Bensch, W. Transition Metal Complexes with Linkage to the Thiostannate Units Forced by Suitable Amine Molecules. *Z. Anorg. Allg. Chem.* **2016**, *642*, 1427−1434.
(19) Hilbert, J.; Näther, C.; Bensch, W. Influence of the Synthesis Parameters onto Nucleation and Crystallization of Five New Tin−Sulfur Containing Compounds. *Inorg. Chem.* **2014**, *53*, 5619−5630.
(20) Hilbert, J.; Näther, C.; Bensch, W. The $[Sn_2S_6]^{4-}$ Anion Acting as Tetradentate Linker: Solvothermal Synthesis and Selected Properties of $\{[TM(phen)_2]_2Sn_2S_6\}$ and $\{[TM(phen)_2]_2Sn_2S_6\}\cdot phen\cdot H_2O$ (TM = Fe, Co). *Z. Anorg. Allg. Chem.* **2014**, *640*, 2858−2863.
(21) Pienack, N.; Bensch, W. The new silver thiostannate $(1,4\text{-dab}H_2)Ag_2SnS_4$: Solvothermal Synthesis, Crystal Structure and Spectroscopic Properties. *Z. Anorg. Allg. Chem.* **2006**, *632*, 1733−1736.
(22) Pienack, N.; Puls, A.; Näther, C.; Bensch, W. The layered thiostannate $(dienH_2)Cu_2Sn_2S_6$ − a Photoconductive Inorganic-Organic Hybrid Compound. *Inorg. Chem.* **2008**, *47*, 9606−9611.
(23) Feng, K.; Zhang, X.; Yin, W.; Shi, Y.; Yao, J.; Wu, Y. New Quaternary Rare-Earth Chalcogenides $BaLnSn_2Q_6$ (Ln = Ce, Pr, Nd, Q = S; Ln = Ce, Q = Se): Synthesis, Structure, and Magnetic Properties. *Inorg. Chem.* **2014**, *53*, 2248−2253.
(24) Behrens, M.; Ordolff, M.-E.; Näther, C.; Bensch, W.; Becker, K.-D.; Guillot-Deudon, C.; Lafond, A.; Cody, J. A. New Three-Dimensional Thiostannates Composed of Linked Cu_8S_{12} Clusters and the First Example of a Mixed-Metal Cu_7SnS_{12} Cluster. *Inorg. Chem.* **2010**, *49*, 8305−8309.
(25) Nayek, H. P.; Massa, W.; Dehnen, S. A Heterometallic, Heterovalent $Cu^I/Sn^{II/IV}/S$ Cluster with an Unprecedented Cu_4Sn Core and Stannacyclopentane Units. *Inorg. Chem.* **2008**, *47*, 9146−9148.
(26) Hassanzadeh Fard, Z.; Müller, C.; Harmening, T.; Pöttgen, R.; Dehnen, S. Knüpfung von Thiostannat-Sn-Sn-Bindungen in Lösung: In-situ-Bildung des gemischtvalenten funktionalisierten Komplexes $[\{(RSn^{IV})_2(\mu\text{-}S)_2\}_3Sn^{III}_2S_6]$. *Angew. Chem.* **2009**, *121*, 4507−4511.
(27) Kaib, T.; Kapitein, M.; Dehnen, S. Synthesis and Crystal Structure of $[Li_8(H_2O)_{29}][Sn_{10}O_4S_{20}]\cdot 2H_2O$. *Z. Anorg. Allg. Chem.* **2011**, *637*, 1683−1686.
(28) Parise, J. B.; Ko, Y. Material Consisting of Two Interwoven 4-Connected Networks: Hydrothermal Synthesis and Structure of $[Sn_5S_9O_2][HN(CH_3)_3]_2$. *Chem. Mater.* **1994**, *6*, 718−720.
(29) Zhang, J.-J.; Hu, S.-M.; Wu, X.-T.; Du, W.-X.; Fu, R.-B.; Wang, L.-S. A simple method for the preparation of octanuclear tin (IV) oxosulfide cluster and the conversion of it to decanuclear cluster. *Inorg. Chem. Commun.* **2003**, *6*, 744−747.
(30) Wu, L.; Chen, L.; Dai, J.; Cui, C.; Fu, Z.; Wu, X. The first octanuclear tin(IV)-oxosulfide cluster. *Inorg. Chem. Commun.* **2001**, *4*, 574−576.
(31) Bubenheim, W.; Müller, U. Reaktionen von Zinnchloriden mit Polysulfiden. Die Kristallstrukturen von $(PPh_4)_2[SnCl_2(S_6)_2]$, $(PPh_4)_2[Sn_4Cl_4S_5(S_3)O]$ und $(PPh_4)_2[SnCl_6]\bullet S_8\bullet 2CH_3CN$. *Z. Anorg. Allg. Chem.* **1993**, *619*, 779−785.
(32) Schiwy, W.; Krebs, B. $[Sn_{10}O_4S_{20}]^{8-}$: Ein neuer Typ eines Polyanions. *Angew. Chem.* **1975**, *87*, 451−452.
(33) Marking, G. A.; Evain, M.; Petricek, V.; Kanatzidis, M. G. New Layered Compounds through Polysulfide Flux Synthesis; $A_2Sn_4S_9$ (A = K, Rb, Cs) Present a New Form of the $[Sn_4S_9]^{2-}$ Network. *J. Solid State Chem.* **1998**, *141*, 17−28.
(34) Devi, M. S.; Vidyasagar, K. First examples of sulfides in the quaternary A/Cd/Sn/S (A = Li, Na) systems: molten flux synthesis and single crystal X-ray structures of Li_2CdSnS_4, Na_2CdSnS_4 and $Na_6CdSn_4S_{12}$. *J. Chem. Soc., Dalton Trans.* **2002**, 2092−2096.
(35) Kumari, A.; Vidyasagar, K. Solid-state synthesis, structural variants and transformation of three-dimensional sulfides, $AGaSnS_4$ (A = Na, K, Rb, Cs, Tl) and $Na_{1.263}Ga_{1.263}Sn_{0.737}S_4$. *J. Solid State Chem.* **2007**, *180*, 2013−2019.
(36) Teske, C. L. Darstellung und Kristallstruktur von Barium-Cadmium-Thiostannat (IV) $BaCdSnS_4$. *Z. Anorg. Allg. Chem.* **1980**, *460*, 163−168.
(37) Teske, C. L. Darstellung und Kristallstruktur von Gold-Barium-Thiostannat (IV), Au_2BaSnS_4. *Z. Anorg. Allg. Chem.* **1978**, *445*, 193−201.
(38) Seidlhofer, B.; Pienack, N.; Bensch, W. Synthesis of Inorganic-Organic Hybrid Thiometallate Materials with a Special Focus on Thioantimonates and Thiostannates and in *situ* X-Ray Scattering Studies of their Formation. *Z. Naturforsch., B: J. Chem. Sci.* **2010**, *65b*, 937−975.
(39) Oh, Y.; Bag, S.; Malliakas, C. D.; Kanatzidis, M. G. Selective Surfaces: High-Surface-Area Zinc Tin Sulfide Chalcogels. *Chem. Mater.* **2011**, *23*, 2447−2456.
(40) Coates, J. H.; Hadi, D. A.; Lincoln, S. F.; Dodgen, H. W.; Hunt, J. P. Oxygen-17 Magnetic Resonance and Temperature-Jump Spectrophotometric Study of the Square Planar-Octahedral Equilibrium in the 1,4,7,10-Tetraaza-cyclododecanenickel(II) System. *Inorg. Chem.* **1981**, *20*, 707−711.
(41) *Topas Academics 4.2*; Coelho Software: Brisbane, Australia, 2007.
(42) Altomare, A.; Camalli, M.; Cuocci, C.; Giacovazzo, C.; Moliterni, A.; Rizzi, R. EXPO2009: structure solution by powder data in direct and reciprocal space. *J. Appl. Crystallogr.* **2009**, *42*, 1197−1202.
(43) *Materials Studio*, version 5.0; Accelrys Inc.: San Diego, CA, 2009.
(44) Rappe, A. K.; Casewit, C. J.; Colwell, K. S.; Goddard, W. A., III; Skiff, W. M. UFF, a full periodic table force field for molecular mechanics and molecular dynamics simulations. *J. Am. Chem. Soc.* **1992**, *114*, 10024−10035.
(45) Spek, A. L. Single-crystal structure validation with the program PLATON. *J. Appl. Crystallogr.* **2003**, *36*, 7−13.
(46) Pienack, N.; Ruiz Arana, L.; Bensch, W.; Terraschke, H. In Situ Studies on Phase Transitions of Tris(acetylacetonato)-Aluminum(III) $Al(acac)_3$. *Crystals* **2016**, *6*, 157−158.
(47) Terraschke, H.; Ruiz Arana, L.; Lindenberg, P.; Bensch, W. Development of a new *in situ* analysis technique applying luminescence of local coordination sensors: principle and application for monitoring metal-ligand exchange processes. *Analyst* **2016**, *141*, 2588−2594.
(48) Mundus, C.; Taillades, G.; Pradel, A.; Ribes, M. A ^{119}Sn solid-state nuclear magnetic resonance study of crystalline tin sulphides. *Solid State Nucl. Magn. Reson.* **1996**, *7*, 141−146.
(49) Davies, A. G.; Gielen, M.; Pannell, K. H.; Tiekink, E. R. T. *Tin Chemistry: Fundamentals, Frontiers, and Applications*, 1st; John Wiley & Sons, Ltd.: London, 2008.
(50) Protesescu, L.; Nachtegaal, M.; Voznyy, O.; Borovinskaya, O.; Rossini, A. J.; Emsley, L.; Copéret, C.; Günther, D.; Sargent, E. H.; Kovalenko, M. V. Atomistic Description of Thiostannate-Capped CdSe Nanocrystals: Retention of Four-Coordinate SnS4Motif and Preservation of Cd-Rich Stoichiometry. *J. Am. Chem. Soc.* **2015**, *137*, 1862−1874.

DOI: 10.1021/acs.inorgchem.8b02773
Inorg. Chem. 2019, 58, 2354−2362

(51) Mason, J. *Multinuclear NMR*, 1st; Plenum Press: New York, 1987.
(52) Holleman, F. A.; Wiberg, E.; Wiberg, N. *Lehrbuch der Anorganischen Chemie*, 102nd; Walter de Gruyter: Berlin, 2007.
(53) Haj, S. B. Functionalized Organotin Compounds as Synthons for Tin-containing Heterocycles and Periphery-functionalized Organotinoxo Clusters. Ph.D. Thesis, University of Dortmund, Dortmund, Germany,2015.
(54) Powell, P. *Principles of Organometallic Chemistry*, 2nd; Springer: London, 1988.
(55) Hilbert, J.; Näther, C.; Bensch, W. {[Ni(1,2-dach)$_2$(ma)]$_4$[$Sn_{10}S_{20}O_4$]} An Example of the Tin-Oxo-Sulfide Cluster with Uncommon Connection Mode Towards the Charge Compensating Ni(II) Complex. *Curr. Inorg. Chem.* **2017**, *6*, 181−186.
(56) Cahill, C. L.; Parise, J. B. On the formation of framework indium sulfides. *J. Chem. Soc., Dalton Trans.* **2000**, 1475−1482.
(57) Bu, X.; Zheng, N.; Feng, P. Tetrahedral Chalcogenide Clusters and Open Frameworks. *Chem. - Eur. J.* **2004**, *10*, 3356−3362.
(58) Vijayan, P.; Viswanathamurthi, P.; Velmurugan, K.; Nandhakumar, R.; Balakumaran, M. D.; Kalaichelvan, P. T.; Malecki, J. G. Nickel(II) and copper(II) complexes constructed with N_2S_2 hybrid benzamidine−thiosemicarbazone ligand: synthesis, X-ray crystal structure, DFT, kinetico-catalytic and *in vitro* biological applications. *RSC Adv.* **2015**, *5*, 103321−103342.
(59) Ismail, A. F.; Khulbe, K. C.; Matsuura, T. *Gas Separation Membranes: Polymeric and Inorganic*; Springer International Publishing, 2015.
(60) Furukawa, H.; Gandara, F.; Zhang, Y.-B.; Jiang, J.; Queen, W. L.; Hudson, M. R.; Yaghi, O. M. Water Adsorption in Porous Metal−Organic Frameworks and Related Materials. *J. Am. Chem. Soc.* **2014**, *136*, 4369−4381.
(61) Rhauderwiek, T.; Wolkersdörfer, K.; Øien-Ødegaard, S.; Lillerud, K.-P.; Wark, M.; Stock, N. Crystalline and permanently porous porphyrin-based metal tetraphosphonates. *Chem. Commun.* **2018**, *54*, 389−392.
(62) Wharmby, M. T.; Pearce, G. M.; Mowat, J. P. S.; Griffin, J. M.; Ashbrook, S. E.; Wright, P. A.; Schilling, L.-H.; Lieb, A.; Stock, N.; Chavan, S.; Bordiga, S.; Garcia, E.; Pirngruber, G. D.; Vreeke, M.; Gora, L. Synthesis and crystal chemistry of the STA-12 family of metal N,N′-piperazinebis(methylenephosphonate)s and applications of STA-12(Ni) in the separation of gases. *Microporous Mesoporous Mater.* **2012**, *157*, 3−17.
(63) Beyene, B. B.; Hung, C.-H. Photocatalytic hydrogen evolution from neutral aqueous solution by a water-soluble cobalt(II) porphyrin. *Sustainable Energy Fuels* **2018**, *2*, 2036−2043.
(64) Nippe, M.; Khnayzer, R. S.; Panetier, J. A.; Zee, D. Z.; Olaiya, B. S.; Head-Gordon, M.; Chang, C. J.; Castellano, F. N.; Long, J. R. Catalytic proton reduction with transition metal complexes of the redox-active ligand bpy2PYMe. *Chem. Sci.* **2013**, *4*, 3934−3945.
(65) Durham, B.; Caspar, J. V.; Nagle, J. K.; Meyer, T. J. Photochemistry of tris(2,2′-bipyridine)ruthenium(2+) ion. *J. Am. Chem. Soc.* **1982**, *104*, 4803−4810.
(66) Henderson, L. J.; Ollino, M.; Gupta, V. K.; Newkome, G. R.; Cherry, W. R. Effect of chelate ring size on the photoanation reaction of polypyridine ruthenium complexes. *J. Photochem.* **1985**, *31*, 199−210.
(67) Vaidyalingam, A.; Dutta, P. K. Analysis of the Photodecomposition Products of $[Ru(bpy)_3]^{2+}$ in Various Buffers and upon Zeolite Encapsulation. *Anal. Chem.* **2000**, *72*, 5219−5224.
(68) Niefind, F.; Djamil, J.; Bensch, W.; Srinivasan, B. R.; Sinev, I.; Grünert, W.; Deng, M.; Kienle, L.; Lotnyk, A.; Mesch, M. B.; Senker, J.; Dura, L.; Beweries, T. Room temperature synthesis of an amorphous MoS_2 based composite stabilized by N-donor ligands and its light-driven photocatalytic hydrogen production. *RSC Adv.* **2015**, *5*, 67742−67751.
(69) Asraf, Md. A.; Younus, H. A.; Yusubov, M.; Verpoort, F. Earth-abundant metal complexes as catalysts for water oxidation; is it homogeneous or heterogeneous? *Catal. Sci. Technol.* **2015**, *5*, 4901−4925.
(70) Yuan, Y.-J.; Lu, H.-W.; Tu, J.-R.; Fang, Y.; Yu, Z.-T.; Fan, X.-X.; Zou, Z.-G. A Noble-Metal-Free Nickel(II) Polypyridyl Catalyst for Visible-Light-Driven Hydrogen Production from Water. *ChemPhysChem* **2015**, *16*, 2925−2930.
(71) Dave, M.; Rajagopal, A.; Damm-Ruttensperger, M.; Schwarz, B.; Nägele, F.; Daccache, L.; Fantauzzi, D.; Jacob, T.; Streb, C. Understanding homogeneous hydrogen evolution reactivity and deactivation pathways of molecular molybdenum sulfide catalysts. *Sustainable Energy Fuels* **2018**, *2*, 1020−1026.
(72) Zong, X.; Na, Y.; Wen, F.; Ma, G.; Yang, J.; Wang, D.; Ma, Y.; Wang, M.; Sun, L.; Li, C. Visible light driven H_2 production in molecular systems employing colloidal MoS_2 nanoparticles as catalyst. *Chem. Commun.* **2009**, 4536−4538.
(73) Xiang, Q.; Yu, J.; Jaroniec, M. Synergetic Effect of MoS_2 and Graphene as Cocatalysts for Enhanced Photocatalytic H_2 Production Activity of TiO_2 Nanoparticles. *J. Am. Chem. Soc.* **2012**, *134*, 6575−6578.
(74) Djamil, J.; Segler, S. A.; Dabrowski, A.; Bensch, W.; Lotnyk, A.; Schürmann, U.; Kienle, L.; Hansen, S.; Beweries, T. The influence of carbon content on the structure and properties of MoS_xC_y photocatalysts for light-driven hydrogen generation. *Dalton Trans.* **2013**, *42*, 1287−1292.
(75) Sobczynski, A. Molybdenum Disulfide as a Hydrogen Evolution Catalyst for Water Photodecomposition on Semiconductors. *J. Catal.* **1991**, *131*, 156−166.
(76) Kong, C.; Min, S.; Lu, G. Dye-sensitized cobalt catalysts for high efficient visible light hydrogen evolution. *Int. J. Hydrogen Energy* **2014**, *39*, 4836−4844.
(77) Pienack, N.; Lühmann, H.; Djamil, J.; Permien, S.; Näther, C.; Haumann, S.; Weihrich, R.; Bensch, W. Two Pseudopolymorphic Star-Shaped Tetranuclear Co^{3+} Compounds with Disulfide Anions Exhibiting Two Different Connection Modes and Promising Photocatalytic Properties. *Chem. - Eur. J.* **2015**, *21*, 13637−13645.
(78) Zhu, Y.; Xu, Y.; Hou, Y.; Ding, Z.; Wang, X. Cobalt sulfide modified graphitic carbon nitride semiconductor for solar hydrogen production. *Int. J. Hydrogen Energy* **2014**, *39*, 11873−11879.

DOI: 10.1021/acs.inorgchem.8b02773
Inorg. Chem. 2019, 58, 2354−2362

3.3 “The First Thiostannate Compound with Copper(II) Synthesized Under Ambient Conditions: Crystal Structure, Electronic and Thermal Properties” VIP Paper

The first Cu(II) thiostannate compound, $\{[Cu(cyclam)]_2[Sn_2S_6]\}_n \cdot 2nH_2O$, was obtained at room temperature by reacting $Na_4SnS_4 \cdot 14H_2O$ with $[Cu(cyclam)](ClO_4)_2$ in aqueous solution. The compound was formed in good yield after only 2 h reaction time. The crystal structure is composed of the $[Sn_2S_6]^{4-}$ anions and the $[Cu(cyclam)]^{2+}$ cations, which are connected *via* Cu-S bonds forming layers along the a-axis. Between these layers water molecules are located. The Cu^{2+} cations have a distorted octahedral coordination sphere formed by four N atoms of the cyclam ligand and two S^{2-} anions of the $[Sn_2S_6]^{4-}$ anion. According to EPR spectroscopy the unpaired electron is in the $d_{x^2-y^2}$ orbital demonstrating that the CuN_4S_2 octahedron is distorted along the z-axis. In the UV/Vis spectrum only one d-d transition is observed, which is the overlap of the three possible transitions: $^2B_{1g} \rightarrow {}^2A_{1g}$, $^2B_{1g} \rightarrow {}^2B_{2g}$ and $^2B_{1g} \rightarrow {}^2E_g$. Heating $\{[Cu(cyclam)]_2[Sn_2S_6]\}_n \cdot 2nH_2O$ to 165 ºC and storing the residue in air led to recovery of the pristine material indicating that the water molecules can be reversibly removed.

Reprinted with permission from A. Benkada, H. Reinsch, W. Bensch, The First Thiostannate Compound with Copper(II) Synthesized Under Ambient Conditions: Crystal Structure, Electronic and Thermal Properties, *Eur. J. Inorg. Chem.*, **2019**, 4427-44432. DOI: 10.1002/ejic.201900924. Copyright 2019 John Wiley & Sons.

ChemPubSoc Europe

DOI: 10.1002/ejic.201900924

EurJIC European Journal of Inorganic Chemistry

Full Paper

Layered Compounds | *Very Important Paper* |

The First Thiostannate Compound with Copper(II) Synthesized Under Ambient Conditions: Crystal Structure, Electronic and Thermal Properties

Assma Benkada,[a] Helge Reinsch,[a] and Wolfgang Bensch*[a]

Abstract: The new compound $\{[Cu(cyclam)]_2[Sn_2S_6]\}_n \cdot 2nH_2O$ containing Cu(II) was synthesized at room temperature reacting aqueous solutions of $Na_4SnS_4 \cdot 14H_2O$ and of $[Cu(cyclam)](ClO_4)_2$. A crystalline precipitate consisting of small crystallites was formed after a very short reaction time of 2 h. Structure analysis reveals that $[Sn_2S_6]^{4-}$ anions are joined by the $[Cu(cyclam)]^{2+}$ cations via Cu–S bonds generating layers which are stacked along the crystallographic a-axis. The Cu(II) centers are in a distorted octahedral environment of four N and two S atoms. The distortion is reflected in the EPR spectrum that displays the $A_{||}$ lines characteristic for Cu^{2+} (I = 3/2) and due to $g_{||} > g_{\perp} > 2.0023$, the unpaired electron is located in the $d_{x^2-y^2}$ orbital. The crystal water molecules can be removed at elevated temperatures, while crystallinity of the sample is mainly retained. Storage of the dehydrated sample on air leads to water uptake and recovery of the pristine compound.

Introduction

The integration of transition metals into thiostannate frameworks significantly alters the crystal structures and properties of the inorganic framework. Pure inorganic bulk thiostannates, respectively tin sulfides containing transition metals are prepared using the high temperature route,[1] by reaction of elements in an inert flux,[2] in reactive fluxes[3] or by mechanical alloying combined with spark plasma sintering.[4] In the past, it was demonstrated that the solvothermal method is most promising for the generation of thiostannates containing transition metal complexes. Considering only compounds that contain the $[Sn_2S_6]^{4-}$ anion, saturated complexes with the cations Mn^{2+}, Co^{2+}, Ni^{2+} and Zn^{2+} are observed with bi- and tridentate amine molecules like en (en = ethylenediamine), dap (dap = 1,2-diaminopropane), 1,2-dach (1,2-dach = 1,2-diaminocyclohexane), 2amp (2amp = 2-(aminomethyl)pyridine), dien (dien = diethylenetriamine) and aepa (aepa = *N*-2-aminoethyl-1,3-propandiamine), as exemplified by the compounds $[M(en)_3]_2[Sn_2S_6]$ (M = Mn, Co, Ni and Zn),[5,6] $[Ni(dap)_3]_2[Sn_2S_6] \cdot 2H_2O$,[6] $[Ni(1,2\text{-dach})_3]_2[Sn_2S_6] \cdot 4H_2O$,[7] $[M(dien)_2]_2[Sn_2S_6]$ (M = Co and Ni),[7,8] $[Ni(2amp)_3]_2[Sn_2S_6] \cdot 9.5H_2O$[9] and $[Ni(aepa)_2]_2[Sn_2S_6]$.[7] In contrast, tetra- and pentadentate amines like tren (tren = tris(2-aminoethyl)amine), trien (trien = triethylenetetramine), cyclam (cyclam = 1,4,8,11-tetraazacyclotetradecane) or tepa (tepa = tetraethylenepentamine) form unsaturated metal complexes allowing the coordination of S^{2-} of the inorganic framework to metal cation. Examples include $[M(tren)]_2Sn_2S_6$ (M = Mn, Co and Ni),[6,10] $\{[Mn(trien)]_2[SnS_4]\}_n$,[7] $\{[M(cyclam)]_2[Sn_2S_6]\}_n \cdot 2nH_2O$ (M = Co and Ni)[11,12] and $\{[M(tepa)]_2[Sn_2S_6]\}$ (M = Co, Fe and Ni).[13] All these compounds contain the anionic $[Sn_2S_6]^{4-}$ unit, which occurs as an isolated anion like in $[Ni(tren)_2]_2[Sn_2S_6] \cdot 8H_2O$ and $[Ni(tren)(2amp)]_2[Sn_2S_6]$,[14] or is linked to the transition metal complexes by covalent M–S bonds. The linkage is realized by three different modes: A) two *trans* terminal S^{2-} anions form a bond such in $\{[Fe(1,2\text{-dach})_2][Sn_2S_6]\}_n \cdot 2n$1,2-dach;[12] B) all four terminal S^{2-} are involved in bonds and two S^{2-} anions bind to two transition metal complexes like in $\{[M(phen)_2]_2[Sn_2S_6]\} \cdot phen \cdot H_2O$ (M = Co, Fe and Mn)[15] or in $\{[Ni(phen)_2]_2[Sn_2S_6]\} \cdot 2,2'$-pipy;[16] C) each S^{2-} anion binds to one complex, so that four complexes are bound to one $[Sn_2S_6]^{4-}$ unit as observed in $\{[M(cyclam)]_2[Sn_2S_6]\}_n \cdot 2nH_2O$ (M = Co and Ni).[12]

Only a few thiostannate and tin sulfide compounds containing Cu or Ag are known so far, whereby both metals exhibit the oxidation state +I. In addition, Cu(I) and Ag(I) cations have bonds to the S^{2-} anions of the thiostannate ions like in $[1,4\text{-dabH}_2][Ag_2SnS_4]$ (1,4-dab = 1,4-diaminobutane),[17] $[H_2en][Ag_2SnS_4]$,[18] $[enH][Cu_2AgSnS_4]$,[19] $[dienH_2][Cu_2Sn_2S_6]$,[20] $[enH]_{6+n}[Cu_{40}Sn_{15}S_{60}]$,[21] $[enH]_3[Cu_7Sn_4S_{12}]$,[21] $[trenH_3][Cu_7Sn_4S_{12}]$,[21] $[DBUH][CuSnS_3]$ (DBU = 1,8-diazabicyclo[5.4.0]undec-7-ene),[22] $[H_2en]_2[Cu_8Sn_3S_{12}]$,[23] $[1,4\text{-dabH}_2][Cu_2SnS_4]$,[22] where protonated amine molecules provide charge balance and act as structure directing agents. All these compounds were synthesized under solvothermal conditions using the elements Sn, S, Cu or Cu_2S in amine solvents. The compounds $Cu_2Sn_{1-x}Si_xS_3$

[a] *Institute of Inorganic Chemistry, Christian-Albrechts-University of Kiel, Max-Eyth-Str. 2, 24118 Kiel, Germany*
E-mail: wbensch@ac.uni-kiel.de
http://www.ac.uni-kiel.de/de/bensch

Supporting information and ORCID(s) from the author(s) for this article are available on the WWW under https://doi.org/10.1002/ejic.201900924.

ChemPubSoc Europe

EurJIC European Journal of Inorganic Chemistry

Full Paper

($0.4 \le x \le 0.6$) with band gaps of 1.25, 1.35 and 1.45 eV[24] as well as $(dienH_2)Cu_2Sn_2S_6$,[20] reveal potential as absorber materials for photovoltaic devices.

The existence of Cu(II) in thiostannates and tin sulfides has not been observed until now. The reason is that Cu(II) is reduced by S^{2-} anions to Cu(I). Our challenge was to find an amine ligand that forms stable complexes with Cu(II) leaving sites at the Cu(II) center free for bond formation to S^{2-}. Indeed, after a research in the Cambridge Structural Database (CSD) we found that cyclam generates stable complexes with transition metal cations and especially with Cu(II) ($\log K = 27.2$,[25] see Synthetic aspects). Encouraged by this observation we performed syntheses with the $[Cu(cyclam)](ClO_4)_2$ complex under hydrothermal conditions as well as at room temperature. Herein, we present the first copper(II) containing tin-sulfide compound $\{[Cu(cyclam)]_2[Sn_2S_6]\}_n{\cdot}2nH_2O$, which exhibits a 2D structure. This compound was prepared by using $Na_4SnS_4{\cdot}14H_2O$ as precursor and the stable complex $[Cu(cyclam)](ClO_4)_2$ in water at room temperature. In addition, electronic and thermal properties of the title compound were investigated and the results are presented herein.

Results and Discussions

Synthetic Aspects

The overwhelming number of thiostannates were synthesized using elemental Sn and S in aqueous amine solutions.[26] The basic conditions are necessary to generate polysulfide anions, which react with Sn to form thiostannate ions.[27] Applying $Na_4SnS_4{\cdot}14H_2O$ as precursor the addition of amine is not necessary, and recently we have shown that $[SnS_4]^{4-}$ condenses very fast to form $[Sn_2S_6]^{4-}$ units under release of H_2S.[9,28] Reacting $[Ni(cyclen)](ClO_4)_2$ (cyclen = 1,4,7,10-tetrazacyclododecane) and $Na_4SnS_4{\cdot}14H_2O$ under hydrothermal conditions we successfully prepared $\{[Ni(cyclen)]_6[Sn_6S_{12}O_2(OH)_6]\}{\cdot}2(ClO_4){\cdot}19H_2O$.[29] Cyclen is a tetraaza macrocyclic ligand that forms TM^{n+} centred complexes with two free coordination sites and if TM^{n+} prefers an octahedral coordination, bond formation to thiostannate anions is possible, which is observed in the structure where $[Ni(cyclen)]^{2+}$ cations are bound to the central core unit via S^{2-} and OH^- anions.[29] Encouraged by this observation we used in the present work the $[Cu(cyclam)]^{2+}$ complex with a planar environment around Cu(II) and the two apical positions are free for bond formation. The compounds $\{[Ni(cyclam)]_2[Sn_2S_6]\}_n{\cdot}2nH_2O$ and $\{[Co(cyclam)]_2[Sn_2S_6]\}_n{\cdot}2nH_2O$ were prepared under solvothermal conditions by reacting $[Ni(cyclam)](ClO_4)_2$ with $Na_4SnS_4{\cdot}14H_2O$ or by reacting $[Co(cyclam)Cl_2]Cl$ with elemental Sn and S. For comparison, we heated an aqueous solution of $Na_4SnS_4{\cdot}14H_2O$ with $[Cu(cyclam)](ClO_4)_2$ at $T = 120$ °C for 1 d but no thiostannates could be obtained. In the X-ray powder pattern reflections of Cu_8S_5 could be identified indicating that $[Cu(cyclam)](ClO_4)_2$ is not stable under hydrothermal conditions. Because the $[Cu(cyclam)](ClO_4)_2$ complex exhibits a good solubility in water (solubility = 14.4 g/L, Figure S1), syntheses at room temperature were carried out by adding an aqueous solution of $Na_4SnS_4{\cdot}14H_2O$ to aqueous solution of the complex.

Comparison of the complex stability constants of the Co(II), Zn(II), Ni(II) and Cu(II) complexes (Table 1) demonstrates that the Cu(II) centered complex is most stable in this series of compounds. The high stability makes formation of Cu(II) aqua complexes unlikely which are prone to react with S^{2-} anions in solution thus leading to precipitation of CuS or Cu_2S.

Table 1. Complex stability constants ($\log K$) of Co(II), Zn(II), Ni(II) and Cu(II) complexes.

Ligand	Co^{2+} ($\log K$)[25]	Zn^{2+} ($\log K$)[25]	Ni^{2+} ($\log K$)[25]	Cu^{2+} ($\log K$)[25]
Cyclam	12.7	15.0	22.2	27.2

Crystal Structures

Compound **I**, $\{[Cu(cyclam)]_2[Sn_2S_6]\}_n{\cdot}2nH_2O$, crystallizes in the triclinic space group $P\bar{1}$ with one formula unit per unit cell. The unique Sn and S atoms of the $[Sn_2S_6]^{4-}$ anion are located on general and the Cu atoms of the complexes on special positions. The $[Sn_2S_6]^{4-}$ anion is formed by two edge-sharing $[SnS_4]^{4-}$ tetrahedra (Figure 1).

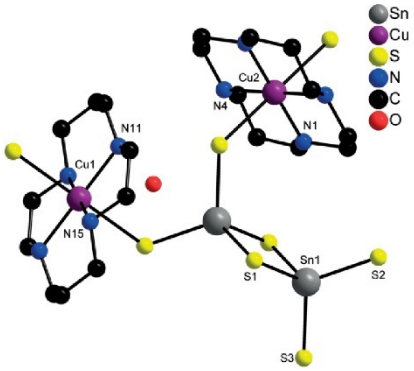

Figure 1. View of the constituent in the structure of compound **I**. Only selected atoms are labelled and H atoms are omitted for clarity.

The $Sn–S_{term}$ bond lengths vary between 2.3877 and 2.3935 Å, while the $Sn–S_{brid}$ bonds scatter between 2.4262 and 2.4946 Å (Table S1). These values are in the typical range of literature data. The S–Sn–S angles are in the range of 93.04–117.25° ($S_{term}–Sn–S_{term}$: 111.30°, $S_{brid}–Sn–S_{brid}$: 93.04°, $S_{brid}–Sn–S_{term}$: 108.95–117.25°) indicating a pronounced distortion of the tetrahedra.[5,11,30] Both Cu(II) cations are in an octahedral environment of four N and two S atoms occupying the apical positions (Figure 1). The Cu–N/S bonds are Cu–N = 1.992(2)–2.085(1) Å and Cu–S = 2.764(9)–2.782(9) Å, with corresponding angles around Cu(II) cations (Table S1) indicative for a significant distortion of the ideal octahedral geometry. However, all Cu–N and N–Cu–N values are in the range of literature data.[31] The Cu–S bonds are longer than the sum of ionic radii [Cu^{2+} (CN = 6) = 0.73 Å; S^{2-}: 1.84 Å; sum: 2.57 Å],[32] but shorter than the sum of the van der Waals radii (3.4 Å).[33] A search in the Cambridge

ChemPubSoc Europe

EurJIC European Journal of Inorganic Chemistry

Full Paper

Structural Database for the complexes with CuN_4S_2 cores (mainly thiolates and complexes with SCN^-), in which S is in the apical position, yields Cu–S separations between 2.560 and 3.258 Å. These values indicate that Cu–S bonds in the CuN_4S_2 moieties are between the sum of ionic radii and the sum of the van der Waals radii. For analyzing the distortions of polyhedra, a new method was reported by Cumby et al.,[34] in which the shape of a polyhedron is approximated by an ellipsoid (minimum bounding ellipsoid, MBE). Regardless of coordination number and geometry, the calculation of the MBE can be carried out for any polyhedron. In addition, the MBE must be the ellipsoid of smallest volume that includes all atoms. Normally, the vertices of high symmetry polyhedra are positioned on the surface of a sphere. Variation of the symmetry of polyhedra causes a transformation of the sphere into an ellipsoid. The principal ellipsoid radii are $R1 \geq R2 \geq R3$, their average $<R>$ and their variance $\sigma^2(R)$ or standard deviation $\sigma(R) = \sqrt{\sigma^2(R)}$ present the size and the distortion of the polyhedra, respectively. An important parameter to describe the distortion of the polyhedra is the shape of the ellipsoid S which is represented by $S = R3/R2 - R2/R1$. S is in the range of −1 to 1. A sphere has $S = 0$, for an axially compressed ellipsoid $S < 0$ and for an axially stretched ellipsoid $S > 0$. Table 2 shows the volumes and the shape parameters S of the two Cu centered polyhedra. As can be seen from the data the polyhedra are axially elongated and the Cu1 centered polyhedron shows the largest stretching.

Table 2. Volumes and shape parameters of the Cu^{2+} centered octahedra.

Atom	V [Å^3]	S
Cu1 (**I**)	49.8	0.227
Cu2 (**I**)	45.2	0.155

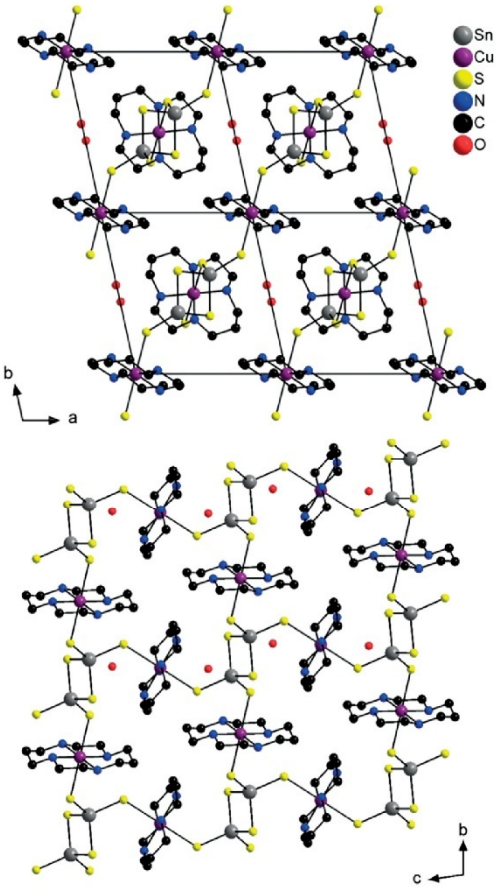

Figure 2. View of the crystal structure of compound **I** along [001] (top) and along [100] (bottom). The H atoms of the complexes are omitted for clarity.

All S_{term} atoms of the $[Sn_2S_6]^{4-}$ moiety are bonded to the Cu^{2+} cations in two different directions forming layers within the *ac* plane. The layers are stacked along [100] and in a•••AAA••• sequence with the shortest interlayer separation of ≈ 4.4 Å (measured from coordinate to coordinate).

The water molecules are located between the layers (Figure 2). Compound **I** is isostructural to the compounds $\{[M(cyclam)]_2[Sn_2S_6]\}_n \cdot 2nH_2O$ (M = Co and Ni),[11,12] and all three compounds belong to the relatively rare two-dimensional thiostannate compounds containing TM^{2+} cations, like observed in $[enH][Cu_2AgSnS_4]$,[19] $[dienH_2][Cu_2Sn_2S_6]$,[20] $K_2Ag_6Sn_3S_{10}$[35] or $[enH_2][Ag_2SnS_4]$.[18]

Spectroscopic Properties

The characteristic bands of the macrocyclic amine molecule can be identified in the IR spectrum (Figure S2; Table S2). The broad band at approximately 3441 cm^{-1} is attributable to the OH stretching vibration of H_2O. The N-H stretching vibrations of cyclam are located around 3202–3101 cm^{-1} and the Cu–N stretching mode is observed at about 424 cm^{-1}. The typical Sn–S modes occur in the Raman spectrum in the region of 400 to 100 cm^{-1}. The Sn–S_{term} stretching mode is located at 384 cm^{-1}. The Sn–S–Sn and Sn_2S_2 ring vibrations are observed at 341 and 277 cm^{-1}. The deformation and lattice vibrations of the $[Sn_2S_6]^{4-}$ unit occur between 200 and 100 cm^{-1}, however a reasonable assignment is not possible (Figure S3).

The UV/Vis spectrum of **I** displays the expected d-d transition (Figure 3). For $[Cu(H_2O)_6]^{2+}$ the transition is located at about 1.55 eV (800 nm, $^2E_g \rightarrow {}^2T_{2g}$).[36] The title compound shows a signal at 2.27 eV (546 nm) which is shifted to higher energy compared to the hexa-aqua complex caused by the differing bonding properties. Compounds with CuN_4S_2 cores, in which S is in apical position exhibit a single broad band between 1.87 and 2.26 eV,[37,38] which is the envelope of the three possible transitions: $^2B_{1g} \rightarrow {}^2A_{1g}$, $^2B_{1g} \rightarrow {}^2B_{2g}$ and $^2B_{1g} \rightarrow {}^2E_g$.[39] The color of the crystals of the title compound is caused by the transition at 2.27 eV (546 nm) which corresponds to violet color. The strong absorption at 2.87 eV (432 nm) is attributed to charge transfer transition.[37]

ChemPubSoc Europe

EurJIC European Journal of Inorganic Chemistry
Full Paper

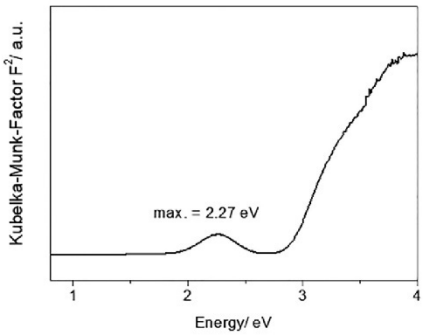

Figure 3. Kubelka–Munk-Factor F^2 as function of energy calculated from UV/Vis spectroscopic data.

Electronic Properties

The electron paramagnetic resonance (EPR) spectroscopy is an interesting method to study the coordination geometry and the electronic structure. Based on the two important parameters $g_{\parallel}$ and $g_{\perp}$ the ground state can be determined. For an elongated octahedron, a square pyramid or square planar environment of Cu(II) the ground state is $d_{x^2-y^2}$ and $g_{\parallel} > g_{\perp} > 2.0023$. When the d_{z^2} orbital is the ground state, then $g_{\perp} > g_{\parallel} = 2.0023$ and the coordination sphere is compressed octahedral or trigonal bipyramidal.[40] The EPR spectrum of **I** (Figure 4) reveals only three of the four $A_{\parallel}$ lines characteristic for Cu^{2+} ($I = 3/2$).[41] This is due to the overlap of the signals assigned to $g_{\parallel}$ with those assigned to $g_{\perp}$. Since $g_{\parallel}$ (2.26) > $g_{\perp}$ (2.02) > 2.0023, the unpaired electron is located in the $d_{x^2-y^2}$ orbital.[40] The metal hyperfine coupling $A_{\parallel}$ in this region is ≈ 205 G. These results demonstrate that the CuN_4S_2 octahedron is elongated, which is in line with relatively long Cu–S bonds (see above) and are in good agreement with those of Cu(II) complexes with distorted octahedra.[41,42]

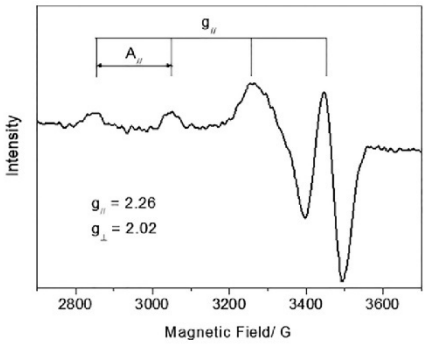

Figure 4. EPR spectrum for compound **I** in water/glycerin mixture at 77 K.

Thermogravimetric Analysis

To investigate the stability of compound **I** and if the water molecules can be reversibly removed, measurements using simultaneously differential thermoanalysis and thermogravimetry (DTA-TG) were performed. Upon heating two mass steps are observed in the TG curve (Figure S4). The first step is accompanied by an endothermic signal in the DTA curve at peak temperature of ≈ 140 °C. The mass loss of 4.0 % is in good agreement with that calculated for the removal of two H_2O molecules (calc. 3.6 %). In the second step the intermediately formed anhydrate decomposes between 200 and 400 °C in two endothermic reactions (T_p = 228 and 252 °C). The mass loss of 43.7 % probably matches with the emission of two cyclam molecules and one H_2S molecule (calc. 43.7 %). The X-ray powder pattern of the black residue obtained after heating the sample to 500 °C contains SnS, Cu_2S and Cu_8S_5 (Figure S5). In a further experiment, heating was stopped after the first step at 165 °C and the light purple powder was investigated by X-ray powder diffraction. The powder pattern is very similar to that of the pristine compound, with some reflections being shifted and broadened. Storing this sample on air at room temperature the title compound is retained, but the crystallinity is slightly reduced as can be seen comparing the pattern of the pristine material with that of the rehydrated one (Figure S6). The anhydrate was also dispersed in methanol to investigate whether a polar solvent can be incorporated. Nevertheless, the X-ray powder pattern indicates that the uptake of methanol was unsuccessful (Figure S7).

Conclusion

The first Cu(II) thiostannate was prepared at room temperature in good yield applying a simple aqueous synthesis method using $Na_4SnS_4 \cdot 14H_2O$ and $[Cu(cyclam)](ClO_4)_2$. The crystallites of the title compound were formed after 2 h reaction time, which is much faster than for classical solvothermal syntheses. In the structure of **I** the $[Sn_2S_6]^{4-}$ anions are covalently bound to the $[Cu(cyclam)]^{2+}$ cations by Cu–S bonds in *trans* position. In this way, layers are generated which are stacked along [1–10]. The Cu(II) cations are in a distorted octahedral environment which is reflected by the EPR data. According to these data, the unpaired electron is located in the $d_{x^2-y^2}$ orbital, which is typical for a distortion of the octahedron along the *z* axis. A further confirmation was provided from UV/Vis spectrum, in which only one broad band is observed which is the envelope of the three possible electronic transitions. The crystal water molecules can be thermally removed without collapse of the structure. Further experiments are under way with other Cu(II) centered complexes to check whether the new synthetic approach can be used for generation of further new compounds.

Experimental Section

$Na_4SnS_4 \cdot 14H_2O$ and $[Cu(cyclam)](ClO_4)_2$ were prepared according to literature methods.[43] Generally, the reaction products were filtered, washed with water and dried at ambient conditions. Caution: Perchlorate anions are potentially explosive if heated and must be handled with care.

Synthesis of $\{[Cu(cyclam)]_2[Sn_2S_6]\}_n \cdot 2nH_2O$ (I): $Na_4SnS_4 \cdot 14H_2O$ (59.1 mg, 0.1 mmol) was dissolved in 0.5 mL of H_2O and [Cu-

ChemPubSoc Europe

EurJIC European Journal of Inorganic Chemistry

Full Paper

(cyclam)](ClO$_4$)$_2$ (46.3 mg, 0.1 mmol) in 0.5 mL of H_2O. The Na_4SnS_4·14H_2O solution was added to the [Cu(cyclam)](ClO$_4$)$_2$ solution, stirred for 20 min. and was kept at room temperature. A violet crystalline precipitate was formed after 2 h (≈ 29 % yield based on Sn). Elemental analysis: found C: 23.90 %, H: 5.23 %, N: 11.11 %, calculated: C: 24.18 %, H: 5.28 %, N: 11.28 %.

Structure Determination: The X-ray powder pattern (PXRD) of compound **I** could be successfully indexed in a triclinic unit cell with a Goodness of Fit of 50.6 using TOPAS Academics.[44] The position of most atoms except for some carbon atoms of the cyclam ligand could be determined using direct methods as implemented in Expo 2009.[45] The missing carbon atoms of the ligand were subsequently inserted using the molecular modelling software Materials Studio.[46] The thus obtained model was further optimized by force-field calculations using the universal force-field[47] as implemented in the forcite routine in Materials Studio. This structurally optimized starting model was afterwards converted into the conventional crystallographic setting using Platon[48] and the structure could be successfully refined with the Rietveld method. The positions of all atoms were freely refined using only bond restrains. The residual electron density in the Fourier map was attributed to crystal water molecules. A preferred orientation along [1–10] was taken into account using the method of March.[49] The isotropic displacement factors were refined element specific or as a group for C and N atoms. The final Rietveld refinement plot is shown Figure S8 and some reliability factors are summarized in Table S3.

CCDC 1947342 (for compound **I**) contains the supplementary crystallographic data for this paper. These data can be obtained free of charge from The Cambridge Crystallographic Data Centre.

Characterization Methods

X-ray Powder Diffraction (PXRD): The powder diffraction patterns were measured with a STOE Stadi-P diffractometer equipped with a MYTHEN 1K detector (DECTRIS) using monochromatized Cu-$K_{\alpha1}$ radiation (λ = 1.540598 Å). The experimental and the calculated patterns using the results of the Rietveld refinement match perfectly indicating phase purity of the sample (Figures S9).

Energy Dispersive X-ray Spectroscopy (EDX): EDX analysis (Table S4) was carried out on a Philips Environmental Scanning Electron Microscope ESEM XL30 equipped with an EDX detector.

Elemental Analysis: CHNS elemental analysis was performed with an EURO EA Elemental Analyzer (EURO VECTOR Instruments and Software).

Infrared Spectroscopy: The IR spectrum was measured at room temperature from 80 to 6000 cm^{-1} with a Bruker Vertex70 FT-IR spectrometer.

Raman Spectroscopy: The Raman spectrum was collected at room temperature on a Bruker RAM II FT-Raman spectrometer equipped with a liquid nitrogen cooled, highly sensitive Ge detector. The radiation and the resolution are 1064 nm and 3 cm^{-1}, respectively.

UV/Visible Spectroscopy: UV/Vis measurement was done at room temperature with an UV/Vis/NIR two channel spectrometer Cary 5 (Varian Techtron Pty., Darmstadt, 200–3000 cm^{-1}) using $BaSO_4$ as reference. The UV/Vis data were converted applying the Kubelka–Munk function. For determination of the solubility of the complex, UV/Vis spectra were measured on an Agilent 8453 spectrometer in a range of 190 nm to 1100 nm with deviation of ±0.5 nm and wavelength reproducibility of ±0.02 nm.

Electron Paramagnetic Resonance (EPR) Spectroscopy: The EPR spectrum was collected on a Bruker EMXplus spectrometer cooled with liquid nitrogen (T = 77 K) and equipped with a PremiumX microwave bridge and a Bruker dual mode X-band cavity. The samples were dissolved in a mixture of H_2O/Glycerine (4:6) transferred into a 1 mm quartz tube and measured at 77 K.

Thermogravimetric Analysis: Thermogravimetric investigations were carried out using a Linseis STA PT1600 instrument, in which the sample was heated in a nitrogen atmosphere with a heating rate of 4 K·min^{-1}.

Acknowledgments

Financial support by the State of Schleswig-Holstein is gratefully acknowledged. We thank Inke Jess for the TG measurements. We also thank Dr. Jan Krahmer for the EPR measurement.

Keywords: Copper(II) thiostannate · Room temperature synthesis · Rietveld refinement · Electronic properties · Thermal properties

[1] a) C. L. Teske, *Z. Anorg. Allg. Chem.* **1985**, *522*, 122–130; b) C. L. Teske, *Z. Anorg. Allg. Chem.* **1976**, *419*, 67–76; c) C. L. Teske, O. Vetter, *Z. Anorg. Allg. Chem.* **1976**, *426*, 281–287; d) T. Bernert, A. Pfitzner, *Z. Kristallogr.* **2005**, *220*, 3519; e) J. A. Aitken, J. W. Lekse, J.-L. Yao, R. Quinones, *J. Solid State Chem.* **2009**, *182*, 141–146.
[2] X.-a. Chen, H. Wada, A. Sato, *Mater. Res. Bull.* **1999**, *34*, 239–247.
[3] J. H. Liao, M. G. Kanatzidis, *Chem. Mater.* **1993**, *5*, 1561–1569.
[4] C. Bourgès, P. Lemoine, O. I. Lebedev, R. Daou, V. Hardy, B. Malaman, E. Guilmeau, *Acta Mater.* **2015**, *97*, 180–190.
[5] D.-X. Jia, Y. Zhang, J. Dai, Q.-Y. Zhu, X.-M. Gu, *Z. Anorg. Allg. Chem.* **2004**, *630*, 313–318.
[6] M. Behrens, S. Scherb, C. Näther, W. Bensch, *Z. Anorg. Allg. Chem.* **2003**, *629*, 1367–1373.
[7] N. Pienack, H. Lühmann, B. Seidlhofer, J. Ammermann, C. Zeisler, F. Danker, C. Näther, W. Bensch, *Solid State Sci.* **2014**, *33*, 67–72.
[8] D.-X. Jia, J. Dai, Q.-Y. Zhu, Y. Zhang, X.-M. Gu, *Polyhedron* **2004**, *23*, 937–942.
[9] J. Hilbert, C. Näther, W. Bensch, *Z. Anorg. Allg. Chem.* **2017**, *643*, 1861–1866.
[10] N. Pienack, D. Schinkel, A. Puls, M.-E. Ordolff, H. Lühmann, C. Näther, W. Bensch, *Z. Naturforsch. B* **2012**, *67*, 1098–1106.
[11] C. Zeisler, C. Näther, W. Bensch, *CrystEngComm* **2013**, *15*, 8874.
[12] J. Hilbert, N. Pienack, H. Lühmann, C. Näther, W. Bensch, *Z. Anorg. Allg. Chem.* **2016**, *642*, 1427–1434.
[13] N. Pienack, S. Lehmann, H. Lühmann, M. El-Madani, C. Näther, W. Bensch, *Z. Anorg. Allg. Chem.* **2008**, *634*, 2323–2329.
[14] J. Hilbert, C. Näther, W. Bensch, *Inorg. Chim. Acta* **2017**, *459*, 29–35.
[15] a) J. Hilbert, C. Näther, W. Bensch, *Z. Anorg. Allg. Chem.* **2014**, *640*, 2858–2863; b) J. Hilbert, C. Näther, W. Bensch, *Inorg. Chem.* **2014**, *53*, 5619–5630.
[16] J. Hilbert, C. Näther, W. Bensch, *Dalton Trans.* **2015**, *44*, 11542–11550.
[17] N. Pienack, W. Bensch, *Z. Anorg. Allg. Chem.* **2006**, *632*, 1733–1736.
[18] Y. An, B. Menghe, L. Ye, M. Ji, X. Liu, G. Ning, *Inorg. Chem. Commun.* **2005**, *8*, 301–303.
[19] W.-W. Xiong, J. Miao, P.-Z. Li, Y. Zhao, B. Liu, Q. Zhang, *CrystEngComm* **2014**, *16*, 5989–5992.
[20] N. Pienack, A. Puls, C. Näther, W. Bensch, *Inorg. Chem.* **2008**, *47*, 9606–9611.
[21] M. Behrens, M.-E. Ordolff, C. Näther, W. Bensch, K.-D. Becker, C. Guillot-Deudon, A. Lafond, J. A. Cody, *Inorg. Chem.* **2010**, *49*, 8305–8309.
[22] N. Pienack, C. Näther, W. Bensch, *Solid State Sci.* **2007**, *9*, 100–107.
[23] R.-C. Zhang, H.-G. Yao, S.-H. Ji, M.-C. Liu, M. Ji, Y.-L. An, *Chem. Commun.* **2010**, *46*, 4550–4552.
[24] A. Lafond, J. A. Cody, M. Souilah, C. Guillot-Deudon, R. Kiebach, W. Bensch, *Inorg. Chem.* **2007**, *46*, 1502–1506.
[25] X. Liang, P. J. Sadler, *Chem. Soc. Rev.* **2004**, *33*, 246–266.
[26] B. Seidlhofer, N. Pienack, W. Bensch, *Z. Naturforsch. B* **2010**, *65*, 937–975.

[27] T. Jiang, A. Lough, G. A. Ozin, R. L. Bedard, *J. Mater. Chem.* **1998**, *8*, 733–741.

[28] a) J. Hilbert, C. Näther, W. Bensch, *Cryst. Growth Des.* **2017**, *17*, 4766–4775; b) A. Benkada, H. Reinsch, M. Poschmann, J. Krahmer, N. Pienack, W. Bensch, *Inorg. Chem.* **2019**, *58*, 2354–2362.

[29] A. Benkada, M. Poschmann, C. Näther, W. Bensch, *Z. Anorg. Allg. Chem.* **2019**, *645*, 433–439.

[30] B. Krebs, S. Pohl, W. Schiwy, *Z. Anorg. Allg. Chem.* **1972**, *393*, 241–252.

[31] a) A. W. Addison, E. Sinn, *Inorg. Chem.* **1983**, *22*, 1225–1228; b) J. C. A. Boeyens, S. M. Dobson, R. D. Hancock, *Inorg. Chem.* **1985**, *24*, 3073–3076; c) L. R. Gahan, C. H. L. Kennard, G. Smith, T. C. W. Mak, *Transition Met. Chem.* **1986**, *11*, 465–466; d) M. Koman, M. Máriássy, G. Ondrejovič, *Acta Crystallogr., Sect. C: Cryst. Struct. Commun.* **1990**, *46*, 2041–2043.

[32] R. D. Shannon, *Acta Crystallogr., Sect. A* **1976**, *32*, 751–767.

[33] L. Shen, *Acta Crystallogr., Sect. C: Cryst. Struct. Commun.* **2002**, *58*, m588–90.

[34] J. Cumby, J. P. Attfield, *Nat. Commun.* **2017**, *8*, 14235.

[35] M. Baiyin, Y. An, X. Liu, M. Ji, C. Jia, G. Ning, *Inorg. Chem.* **2004**, *43*, 3764–3765.

[36] A. F. Holleman, E. Wiberg, N. Wiberg, *Lehrbuch der anorganischen Chemie*, 102nd ed., de Gruyter, Berlin **2007**.

[37] M. Julve, M. Verdaguer, G. de Munno, J. A. Real, G. Bruno, *Inorg. Chem.* **1993**, *32*, 795–802.

[38] a) B. Machura, A. Świtlicka, J. Mroziński, B. Kalińska, R. Kruszynski, *Polyhedron* **2013**, *52*, 1276–1286; b) F. Tsague Chimaine, D. M. Yufanyi, A. Colette Benedicta Yuoh, D. B. Eni, M. O. Agwara, *Cogent Chem.* **2016**, *2*, 11108; c) S. Youngme, N. Chaichit, C. Pakawatchai, S. Booncoon, *Polyhedron* **2002**, *21*, 1279–1288; d) L. Shen, X. Feng, *Struct. Chem.* **2002**, *13*, 437–441.

[39] a) J. L. Mesa, K. Urtiaga, L. Lezama, M. I. Arriortua, M. Björkman, B. H. Forngren, T. Forngren, P. Hartvig, K. Markides, U. Yngve, et al., *Acta Chem. Scand.* **1999**, *53*, 634–638; b) P. Paoletti, L. Fabbrizzi, R. Barbucci, *Inorg. Chim. Acta* **1973**, *7*, 43–68.

[40] E. Garribba, G. Micera, *J. Chem. Educ.* **2006**, *83*, 1229.

[41] M. A. Williams, T. Daviter, *Protein-Ligand Interactions*, Vols. 1008, Humana Press, Totowa, NJ **2013**.

[42] a) F. H. O. Ishiruji, N. L. Speziali, M. G. F. Vaz, F. S. Nunes, *J. Braz. Chem. Soc.* **2010**, *21*, 1195–1200; b) E. Faggi, R. Gavara, M. Bolte, L. Fajarí, L. Juliá, L. Rodríguez, I. Alfonso, *Dalton Trans.* **2015**, *44*, 12700–12710.

[43] a) Y. Oh, S. Bag, C. D. Malliakas, M. G. Kanatzidis, *Chem. Mater.* **2011**, *23*, 2447–2456; b) I. Pérez-Toro, A. Domínguez-Martín, D. Choquesillo-Lazarte, E. Vílchez-Rodríguez, J. M. González-Pérez, A. Castiñeiras, J. Niclós-Gutiérrez, *J. Inorg. Biochem.* **2015**, *148*, 84–92.

[44] *Coelho Software*, Topas Academics 4.2 Brisbane **2007**.

[45] A. Altomare, M. Camalli, C. Cuocci, C. Giacovazzo, A. Moliterni, R. Rizzi, *J. Appl. Crystallogr.* **2009**, *42*, 1197–1202.

[46] Accelrys Inc. Materials Studio Version 5.0, San Diego **2009**.

[47] A. K. Rappe, C. J. Casewit, K. S. Colwell, W. A. Goddard, W. M. Skiff, *J. Am. Chem. Soc.* **1992**, *114*, 10024–10035.

[48] A. L. Speck. *Platon*, A Multipurpose Crystallographic Tool **2010**.

[49] A. March, *Z. Kristallogr. - Cryst. Mater.* **1932**, 81.

Received: August 27, 2019

3.4 “Room temperature synthesis of new thiostannates by slow interdiffusion of different solvents”

The preparation of the new compounds $[Ni(L_1)][Ni(L_1)Sn_2S_6]_n \cdot 2H_2O$ (**I**) and $[Ni(L_2)]_2[Sn_2S_6] \cdot 4H_2O$ (**II**) was achieved using a new synthetic approach at room temperature. In this approach, an aqueous solution of $Na_4SnS_4 \cdot 14H_2O$ was overlayed with a solution of the complex $[Ni(L_1)](ClO_4)_2$ dissolved in CH_3CN or a solution of the complex $[Ni(L_2)](ClO_4)_2$ dissolved in DMSO was overlayed with an aqueous solution of $Na_4SnS_4 \cdot 14H_2O$ (L_1 = 1,8-dimethyl-1,3,6,8,10,13-hexaazacyclotetradecane and L_2 = 1,8-diethyl-1,3,6,8,10,13-hexaazacyclotetradecane). Both compounds crystallized in the interface region of the solvents. The structure of compound **I** consists of $[Ni(L_1)]^{2+}$ centered complexes and $[Sn_2S_6]^{4-}$ anions, whereby the Ni^{2+} cations exhibit different coordination geometries. One Ni^{2+} cation features octahedral environment of four N atoms of the L_1 ligand and two S atoms of the $[Sn_2S_6]^{4-}$ anion leading to the formation of chains along the a-axis. The second Ni^{2+} cation is in a square-planar environment und is located between the chains. Compound **II** composes of isolated $[Ni(L_2)]^{2+}$ cations and $[Sn_2S_6]^{4-}$ anions. The Ni^{2+} cations are in a square-planar coordination environment of four N atoms of the L_2 ligand. The calculation of volumes and spaces of both complexes indicates the differences of the space requirements of the ligands. This may be the reason why the crystal structures of **I** and **II** are different. Both structures were stabilized by intermolecular S···H, N···H, O···H and H···H interactions. The importance of these interactions was confirmed by Hirshfeld surface analysis.

Reprinted with permission from A. Benkada, C. Näther, W. Bensch, Room Temperature Synthesis of New Thiostannates by Slow Interdiffusion of Different Solvents, *Z. Anorg. Allg. Chem.*, **2020**. Accepted 15.06.2020. DOI: 10.1002/zaac.202000199.

Journal of Inorganic and General Chemistry
ZAAC
Zeitschrift für anorganische und allgemeine Chemie

DOI: 10.1002/zaac.202000199

ARTICLE

Room Temperature Synthesis of New Thiostannates by Slow Interdiffusion of Different Solvents

Assma Benkada,[a] Christian Näther,[a] and Wolfgang Bensch*[a]

Dedicated to Professor Christian Robl on the Occasion of his 65th Birthday

Abstract. The new compounds $[Ni(L_1)][Ni(L_1)Sn_2S_6]_n \cdot 2H_2O$ (**I**) and $[Ni(L_2)]_2[Sn_2S_6] \cdot 4H_2O$ (**II**) containing the macrocyclic ligands L_1 (L_1 = 1,8-dimethyl-1,3,6,8,10,13-hexaazacyclotetradecane) and L_2 (L_2 = 1,8-diethyl-1,3,6,8,10,13-hexaazacyclotetradecane) were prepared at room temperature by overlaying an aqueous solution of $Na_4SnS_4 \cdot 14H_2O$ with the $[Ni(L_1)](ClO_4)_2$ complex dissolved in CH_3CN (**I**) or by overlaying a solution of the $[Ni(L_2)](ClO_4)_2$ complex dissolved in DMSO with an aqueous solution of $Na_4SnS_4 \cdot 14H_2O$ (**II**). The slow interdiffusion of the two solvents guarantees supersaturation in the interface region of the solvents so that crystallization of the compounds occurs. In the structure of **I** one Ni^{2+} cation has bonds to S^{2-} anions of the thiostannate anion thus generating chains along [100]. This cation is in an octahedral environment of four N atoms of L_1 and two S atoms of the $[Sn_2S_6]^{4-}$ anion. The second $[Ni(L_1)]^{2+}$ complex exhibits a square-planar coordination geometry. These $[Ni(L_1)]^{2+}$ complexes and water molecules are located between the chains. In the structure of **II** isolated $[Sn_2S_6]^{4-}$ anions and $[Ni(L_2)]^{2+}$ cations are observed. The Ni^{2+} cations are fourfold coordinated by N atoms of the L_2 ligand and feature also a square planar environment.

Introduction

Traditionally, thiostannates containing TM^{n+} cations (TM = transition metal) or TM^{n+} centered complexes are prepared from the elements Sn and S or from SnS_2, salts like $SnCl_4 \cdot 5H_2O$ and transition metals or transition metal salts in aqueous amine solution applying the solvothermal approach.[1] A solvothermal reaction requires special vessels and is a complex system. What compound is formed depends on many parameters, such as temperature, concentration of starting materials, pH value, nature of the solvent, structure directing molecule and others.[2] In addition, very often by-products are formed leading to a reduction of the yield of the desired product and require manual separation of the different compounds. Hence, predicting the nature of a compound that crystallizes under solvothermal conditions is not possible.

To avoid solvothermal conditions, room temperature syntheses were performed leading to crystallization of e.g. $(dda)_4[Sn_2S_6] \cdot 2H_2O$ (dda = dodecylamine),[3] $[CH_3C(NH_2)_2]_8Sn_2S_6SnS_4$, $(CH_3)_2NH_2(NH_4)SnS_3$ and $(NH_4)_6Sn_3S_9 \cdot 1.3H_2O$.[4] $(dda)_4[Sn_2S_6] \cdot 2H_2O$ was prepared by the reaction of $SnCl_4 \cdot 5H_2O$ with $Na_2S \cdot 9H_2O$ in H_2O and a mixture of dodecylamine dissolved in ethanol.[3] $[CH_3C(NH_2)_2]_8Sn_2S_6SnS_4$, $(CH_3)_2NH_2(NH_4)SnS_3$, and $(NH_4)_6Sn_3S_9 \cdot 1.3H_2O$ were synthesized by reacting amorphous SnS_2 with $(NH_4)_2S$ in an aqueous solution. For the crystallization of these compounds solvents like acetonitrile and *N*,*N*-dimethylformamide were added and a crystallization time of several months was required.[4]

Recently, we explored solvothermal syntheses using different thiostannate sources and transition metal complexes as reactants for the generation of thiostannates. For example, the reaction of $Na_4SnS_4 \cdot 14H_2O$ with $[Mn(2,2'\text{-bipy})_3](ClO_4)_2$, $[Ni(cyclam)](ClO_4)_2$, $[Ni(cyclen)](ClO_4)_2$, or $[Ni(cyclen)(H_2O)_2](ClO_4)_2 \cdot H_2O$ in H_2O led to crystallization of four new tin-sulfur compounds, e.g. $[Mn(2,2'\text{-bipy})_2]_2[Sn_2S_6]$ (2,2′-bipy = 2,2′-bipyridin), $\{[Ni(cyclam)]_2[Sn_2S_6]\}_n \cdot 2nH_2O$ (cyclam = 1,4,8,11-tetraazacyclotetradecane),[5] $\{[Ni(cyclen)]_6[Sn_6S_{12}O_2(OH)_6]\} \cdot 2(ClO_4) \cdot 19H_2O$,[6] and $[Ni(cyclen)(H_2O)_2]_4[Sn_{10}S_{20}O_4] \cdot \sim 13H_2O$[7] (cyclen = 1,4,7,10-tetraazacyclododecane). In another room temperature based synthesis approach, $\{[Ni(tren)]_2[Sn_2S_6]\}_n$ (tren = tris(2-aminoethyl)amine) was used as precursor in aqueous amine solution and the two new thiostannates $[Ni(tren)_2]_2[Sn_2S_6] \cdot 8H_2O$ and $[Ni(2amp)(tren)]_2[Sn_2S_6]$ (2amp = 2-(aminomethyl)pyridine) could be synthesized. For the generation of both compounds, a breakage of the Ni–S bonds in the precursor is necessary, so that free coordination sites on the Ni^{2+} cation are generated to which N atoms of the amine molecules can coordinate.[8] But the product diversity is limited using $\{[Ni(tren)]_2[Sn_2S_6]\}_n$ as precursor. Hence, a further synthetic approach at room tem-

* Prof. Dr. W. Bensch
Fax: +49-431-880-1520
E-Mail: wbensch@ac.uni-kiel.ded
[a] Institut für Anorganische Chemie
Christian-Albrechts-Universität zu Kiel
Max-Eyth-Str. 2
24118 Kiel, Germany

Supporting information for this article is available on the WWW under **http://dx.doi.org/10.1002/zaac.202000199** or from the author.

Journal of Inorganic and General Chemistry
ZAAC
Zeitschrift für anorganische und allgemeine Chemie

ARTICLE

perature was developed in our group to synthesize thiostannates with a large variety of chemical compositions. Applying $Na_4SnS_4 \cdot 14H_2O$ and the $[Ni(amine)_3]^{2+}$ complexes [amine = ethylenediamine (en), 1,2-diaminocyclohexane (1,2-dach), 1,2-diaminopropane (1,2-dap), 2amp] in aqueous tren solution, six new compounds crystallized between 1 and 7 days: $[Ni(tren)(en)]_2[Sn_2S_6] \cdot 2H_2O$, $[Ni(tren)(en)]_2[Sn_2S_6] \cdot 6H_2O$, $[Ni(tren)(1,2\text{-dach})]_2[Sn_2S_6] \cdot 3H_2O$, $[Ni(tren)(1,2\text{-dach})]_2[Sn_2S_6] \cdot 4H_2O$, $[Ni(tren)(1,2\text{-dap})]_2[Sn_2S_6] \cdot 4H_2O$, and $[Ni(tren)(2amp)]_2[Sn_2S_6] \cdot 10H_2O$.[9] In these compounds two bidentate amine ligands (en, 1,2-dach, 1,2-dap, and 2amp) were replaced by one tetradentate tren ligand during the reaction, so that two kinds of amine molecules are coordinated to the Ni^{2+} cation instead of only one. However, the octahedral environment of the Ni^{2+} cations by the N donor atoms remained unchanged. Using this synthesis strategy the formation of Ni sulfides is prevented, because the presence of tren suppresses the generation of $[Ni(H_2O)_6]^{2+}$ complexes in water.[9]

Most of the ligands used in our group or by others for the generation of new thiostannate or tin-sulfur compounds containing TM^{n+} complexes exhibit a reasonable good solubility in water. To enhance the structural diversity, integration of more bulky TM^{2+} complexes is a promising route. In this respect macrocyclic polyaza ligands are suitable candidates. The synthetic challenge is the low solubility of complexes with such ligands in water. Because the solubility is much better in organic solvents, syntheses were performed at room temperature using an aqueous phase containing the thiostannate and an organic phase containing the Ni^{2+} complexes. The slow interdiffusion of the two solvents afforded crystallization of the new compounds $[Ni(L_1)][Ni(L_1)Sn_2S_6]_n \cdot 2H_2O$ (**I**) and $[Ni(L_2)]_2[Sn_2S_6] \cdot 4H_2O$ (**II**). Herein we report the synthetic procedure, the crystal structures, the thermal behavior, spectroscopic properties and a Hirshfeld surface analysis.

Experimental Section

$Na_4SnS_4 \cdot 14H_2O$[10] and $[Ni(L_n)](ClO_4)_2$ (n = 1 and 2)[11] were synthesized according to literature procedure. Generally, the reaction products were filtered, washed with water and dried at ambient conditions. Caution: Perchlorate anion containing compounds are potentially explosive if heated and must be handled with care.

Synthesis of $[Ni(L_1)][Ni(L_1)Sn_2S_6]_n \cdot 2H_2O$ (I): $Na_4SnS_4 \cdot 14H_2O$ (59.1 mg, 0.1 mmol) was dissolved in 2 mL H_2O and $[Ni(L_1)](ClO_4)_2$ (48.4 mg, 0.1 mmol) in 2 mL CH_3CN. The $Na_4SnS_4 \cdot 14H_2O$ solution was overlayed with the CH_3CN solution and was kept at room temperature. Small brown crystals are already observed after 2 h at the interface between the aqueous and organic phases and after 1 d single crystals are formed (ca. 32 %, 0.032 mmol and 33.4 mg yield based on Sn). Note: compound **I** could also be obtained using a DMSO solution of the complex, but in this case the yield is very low. Elemental analysis: calcd. C: 23.01 %, H: 5.41 %, N: 16.10 %; found C 22.84 %, H: 5.48 %, N: 15.90 %.

Synthesis of $[Ni(L_2)]_2[Sn_2S_6] \cdot 4H_2O$ (II): Compound **II** was prepared by dissolving $Na_4SnS_4 \cdot 14H_2O$ (59.1 mg, 0.1 mmol) in 0.5 mL H_2O and $[Ni(L_2)](ClO_4)_2$ (51.6 mg, 0.1 mmol) in 1.0 mL DMSO. The $Na_4SnS_4 \cdot 14H_2O$ solution was carefully added to the $[Ni(L_2)](ClO_4)_2$ solution and the mixture was kept at room temperature. The first larger crystallites appear after about 2 to 3 d and brown crystals suitable for single crystal determination were formed after 7 d (ca. 22 %, 0.022 mmol and 24.9 mg yield based on Sn). Elemental analysis: calcd. C: 25.37 %, H: 6.03 %, N: 14.79 %; found C 24.03 %, H: 5.53 %, N: 13.66 %

Structure Determination: Data for compounds **I** and **II** were collected using a STOE IPDS-II (Imaging Plate Diffraction System) with graphite monochromated Mo-K_α radiation (λ = 0.7107 Å) at 170(2) and 200(2) K, respectively. The structures were solved with direct methods using the program SHELXS-97,[12] and the refinements were done with SHELXL-2018.[13] All non-hydrogen atoms were refined anisotropically. The C–H and N–H H atoms were positioned with idealized geometry (methyl H atoms allowed to rotate but not to tip) and refined isotropic with $U_{iso}(H) = 1.2\ U_{eq}(C)$ (1.5 for methyl H atoms) using a riding model. The O–H H atoms in compound **I** were located in difference maps, their bond lengths were set to ideal values and afterwards they were refined using a riding model with $U_{iso}(H) = 1.5\ U_{eq}(O)$. The oxygen position of one water molecule is only half occupied. In compound **II** the O–H H atoms were located in difference maps and the bond lengths were set to ideal values and finally, they were refined isotropically with $U_{iso}(H) = 1.5\ U_{eq}(O)$ using a riding model. Details of data collection and refinement results are summarized in Table S1 (Supporting Information).

Crystallographic data (excluding structure factors) for the structures in this paper have been deposited with the Cambridge Crystallographic Data Centre, CCDC, 12 Union Road, Cambridge CB21EZ, UK. Copies of the data can be obtained free of charge on quoting the depository numbers CCDC-1950867 (**I**) and CCDC-1950765 (**II**) (Fax: +44-1223-336-033; E-Mail: deposit@ccdc.cam.ac.uk, http://www.ccdc.cam.ac.uk).

X-ray Powder Diffraction (XRPD): The powder diffraction patterns were recorded on a STOE Stadi-P diffractometer equipped with a MYTHEN 1 K detector (DECTRIS) using monochromatized Cu-$K_{\alpha1}$ radiation (λ = 1.540598 Å). Comparison of the experimental and the calculated patterns using the results of the single-crystal X-ray data indicates phase purity of the samples (Figures S1 and S2, Supporting Information).

Energy Dispersive X-ray Spectroscopy (EDX): EDX analysis (Table S2, Supporting Information) was performed with a Philips Environmental Scanning Electron Microscope ESEM XL30 equipped with an EDX detector.

Elemental Analysis: CHNS elemental analyses were done with an EURO EA Elemental Analyzer (EURO VECTOR Instruments and Software).

Infrared Spectroscopy: IR spectra were collected at room temperature from 80 to 6000 cm^{-1} with a Bruker Vertex70 FT-IR spectrometer.

Raman Spectroscopy: The Raman spectra were measured at room temperature on a Bruker RAM II FT-Raman spectrometer equipped with liquid nitrogen cooled, highly sensitive Germanium detector. The radiation and the resolution are 1064 nm and 3 cm^{-1}, respectively.

UV/Vis Spectroscopy: UV/Vis analyses of the powdered samples were performed at room temperature with an UV/Vis/NIR two channel spectrometer Cary 5 (Varian Techtron Pty., Darmstadt, 200–3000 cm^{-1}) using $BaSO_4$ as reference material. The UV/Vis data were transformed applying the Kubelka-Munk function. To determine the solubility of

Journal of Inorganic and General Chemistry
ZAAC
Zeitschrift für anorganische und allgemeine Chemie

ARTICLE

the complexes in H_2O, CH_3CN and DMSO, UV/Vis spectra were recorded on an Agilent 8453 spectrometer in a range of 190 nm to 1100 nm with deviation of ± 0.5 nm and wavelength reproducibility of ± 0.02 nm.

Thermogravimetric Analysis: Thermogravimetric measurements were performed with a Linseis STA PT1600 instrument. The samples were heated in a nitrogen atmosphere with a heating rate of 4 K·min^{-1}.

Supporting Information (see footnote on the first page of this article): Single crystal data, X-ray powder patterns, EDX data, Tables with bond lengths and angles, additional figures, IR, Raman, UV/Vis spectra and DTA-TG curves.

Results and Discussion

Synthetic Aspects

Recently, we performed syntheses under hydrothermal conditions with the complexes $[Ni(cyclen)](ClO_4)_2$ and $[Ni(cyclen)(H_2O)_2](ClO_4)_2{\cdot}H_2O$ in the presence of $Na_4SnS_4{\cdot}14H_2O$ as precursor leading to the formation of $\{[Ni(cyclen)]_6[Sn_6S_{12}O_2(OH)_6]\}{\cdot}2(ClO_4){\cdot}19H_2O$ and $[Ni(cyclen)(H_2O)_2]_4[Sn_{10}S_{20}O_4]{\cdot}\sim 13H_2O$.[6,7]

Cyclen is a tetraaza macrocyclic ligand that usually generates TM^{n+} complexes with two free coordination sites allowing S^{2-} of the thiostannate anion to coordinate to the TM^{n+} centers. This is indeed observed in the structure of $\{[Ni(cyclen)]_6[Sn_6S_{12}O_2(OH)_6]\}{\cdot}2(ClO_4){\cdot}19H_2O$, in which $[Ni(cyclen)]^{2+}$ cations are bound to the central cluster via S^{2-} and OH^- anions. This observation encouraged us to perform syntheses with Ni^{2+} complexes composed of even larger macrocyclic ligands that also offer free coordination sites at the Ni^{2+} center. Reacting $[Ni(L_1)](ClO_4)_2$ or $[Ni(L_2)](ClO_4)_2$ with $Na_4SnS_4{\cdot}14H_2O$ under hydrothermal conditions no crystalline compounds could be obtained. Hence, syntheses under ambient conditions were performed using H_2O as solvent for $[Ni(L_1)](ClO_4)_2$ and $[Ni(L_2)](ClO_4)_2$ leading to crystallization of these complexes only. However, when the mixture $[Ni(L_1)](ClO_4)_2/Na_4SnS_4{\cdot}14H_2O/H_2O$ is stirred for 2 d at room temperature, tiny amounts of **I** together with an amorphous phase are obtained. Stirring the slurry $[Ni(L_2)](ClO_4)_2/Na_4SnS_4{\cdot}14H_2O/H_2O$ no reaction occurred and only an amorphous sample was formed. We assumed that the solubility of the complexes may be too low in water and therefore the solubility was determined in different solvents (Table 1, Figures S3 and S4, Supporting Information) demonstrating that $[Ni(L_1)](ClO_4)_2$ and $[Ni(L_2)](ClO_4)_2$ are very well soluble in CH_3CN and DMSO. Therefore, syntheses at room temperature were carried out by overlaying an aqueous solution of the thiostannate with the $[Ni(L_1)](ClO_4)_2$ complex dissolved in CH_3CN (**I**) and overlaying a solution of the $[Ni(L_2)](ClO_4)_2$ complex dissolved in DMSO with an aqueous solution of $Na_4SnS_4{\cdot}14H_2O$ (**II**). The successful preparation of $[Ni(L_1)][Ni(L_1)Sn_2S_6]_n{\cdot}2H_2O$ (**I**) and $[Ni(L_2)]_2[Sn_2S_6]{\cdot}4H_2O$ (**II**) suggests that the complexes slowly diffuse from the organic into the aqueous phase, leading to a local supersaturation allowing nucleation and crystal growth of the new phases. Further investigations demonstrated that **I** can also be prepared by using DMSO as solvent for the complex. However, higher yields, better crystal quality and shorter synthesis times could be achieved by dissolving $[Ni(L_1)](ClO_4)_2$ in CH_3CN. Compound **II** was synthesized applying a solution of $[Ni(L_2)](ClO_4)_2$ in CH_3CN or DMSO. The structures of both compounds contain the $[Sn_2S_6]^{4-}$ anion which is *in-situ* formed in the aqueous solution of $Na_4SnS_4{\cdot}14H_2O$ in H_2O. As already demonstrated, the formation of the $[Sn_2S_6]^{4-}$ anion occurs at room temperature and is very fast.[7]

Table 1. Solubility of the Ni^{2+} complexes in H_2O, CH_3CN and DMSO.

	Solubility /g·L^{-1}		
	H_2O	CH_3CN	DMSO
$[Ni(L_1)](ClO_4)_2$	9.8	29.0	392.5
$[Ni(L_2)](ClO_4)_2$	9.0	76.2	198.1

Crystal Structures

Compound **I** crystallizes in the monoclinic space group $P2_1/c$ with two formula units per unit cell, while compound **II** crystallizes in the triclinic space group $P\bar{1}$ with one formula unit per unit cell. In compounds **I** and **II**, the Sn and S atoms of the $[Sn_2S_6]^{4-}$ anions are positioned on general and the $[Ni(L_n)]^{2+}$ cations (n = 1, 2) are located on centers of inversion. In both compounds, the $[Sn_2S_6]^{4-}$ anion is constructed by two edge-sharing $[SnS_4]^{4-}$ tetrahedra (Figure 1). The Sn–S_{term} bond lengths in both compounds scatter between 2.325(2)–2.3469(8) Å, whereas the Sn–S_{brid} bonds are in the range of 2.4440(8) to 2.460(2) Å (Tables S3 and S4, Supporting Information). The corresponding S–Sn–S angles are between 91.97(6) and 116.28(7)° [S_{term}–Sn–S_{term}: 116.24(3)–116.28(7)°, S_{brid}–Sn–S_{brid}: 91.97(6)–92.53(3)°, S_{brid}–Sn–S_{term}: 107.85(7)–115.298(7)°] suggesting a distinct distortion of the SnS_4 tetrahedra in the $[Sn_2S_6]^{4-}$ anion. All the geometric parameters are in the range of literature data.[5,9,14–26]

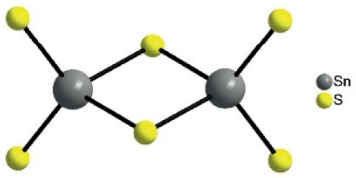

Figure 1. Structure of the $[Sn_2S_6]^{4-}$ anion in compounds **I** and **II** generated by two edge-sharing $[SnS_4]^{4-}$ tetrahedra.

The two independent $[Ni(L_1)]^{2+}$ complexes in the structure of **I** display different coordination geometries. The Ni1^{2+} cation is in an octahedral environment of four N atoms of the L_1 ligand and two S_{term} atoms of the $[Sn_2S_6]^{4-}$ moiety, while Ni2^{2+} is fourfold coordinated by N atoms of L_1 in a square-planar environment. The Ni1–N distances of 2.047(3)–2.057(3) Å are significantly longer than the Ni2–N bonds of 1.933(3)–1.936(3) Å. A comparison with literature data of Ni^{2+} centered complexes containing hexaazacycloctadecane ligands

Journal of Inorganic and General Chemistry
ZAAC
Zeitschrift für anorganische und allgemeine Chemie

ARTICLE

yields Ni–N bond lengths of 2.07(2) Å for Ni^{2+} in octahedral environment.[27–31] In compounds containing Ni^{2+} in a square-planar geometry of hexaazacyclooctadecane ligands the Ni–N bonds are significantly shorter at around 1.93 Å.[32–35] A search in the Cambridge structural database (CSD, Nov. 2019) reveals that only 29 Ni^{2+} centered complexes with the ligands L_1 and L_2 are known with mainly Ni^{2+} in octahedral environment. The Ni1–S bond length is at 2.6444(8) Å which is longer than the sum of ionic radii of 2.53 Å (Ni^{2+}_{CN6} = 0.69 Å; S^{2-}: 1.84 Å).[36] Comparable Ni–S bonds were observed for $\{[Ni(cyclam)]_2[Sn_2S_6]\}_n \cdot 2nH_2O$,[5] $[Ni(pda)_2][Cu_4Sb_2S_6]$ (pda = 1,2-propanediamine),[37] $[Ni(tren)][Sb_2S_4]$,[38] $\{[Ni(tren)]_2[Sn_2S_6]\}_n$,[39] $\{[Ni(phen)_2]_2[Sn_2S_6]\}\cdot$biph (phen = 1,10-phenanthroline, biph = biphenyl), and $\{[Ni(phen)_2]_2[Sn_2S_6]\}\cdot$phen$\cdot H_2O$.[5]

We note that the second terminal S^{2-} of the anion is 3.14 Å apart from the Ni^{2+} cation in the square-pyramidal environment of L_1. But this distance is too long for significant bonding interactions. The angles around the Ni^{2+} cations (Tables S3 and S4, Supporting Information) indicate a pronounced distortion of the ideal octahedral and of the square-planar geometry. The distortion of the $Ni1^{2+}$ centered octahedron in **I** was analyzed by the method reported by *Cumby* et al.[40] This method is based on the approximation of the shape of polyhedra by an ellipsoid (minimum bounding ellipsoid: MBE). Usually, the vertices of polyhedra with high symmetry are located on the surface of a sphere and deviation from the ideal geometry leads to the transformation of the sphere into an ellipsoid. An essential parameter to characterize the distortion of the polyhedra is the shape of the ellipsoid S, which is in the range of –1 to 1. A sphere has S = 0, for an axially compressed ellipsoid $S < 0$ and for an axially stretched ellipsoid $S > 0$. The calculated volume of the polyhedron is 46.2 $Å^3$ and the shape parameter S = 0.134 indicates an axially elongated octahedron.

In the structure of **I** two of the four S_{term} atoms of the $[Sn_2S_6]^{4-}$ anion have a bond to the $Ni1^{2+}$ cations in *trans* position leading to the generation of chains directed along the *a* axis (Figure 2). The square-planar and octahedral complexes alternate along the *b* and *c* axis (Figure 3). The $[Ni(L_1)]^{2+}$ complexes and water molecules are located between the chains and interact with them by one medium strong O–H···S_{term} interaction. Further relatively weak hydrogen bonding N–H···S and C–H···S interactions are observed (Figure S5, top; Table S5, Supporting Information).

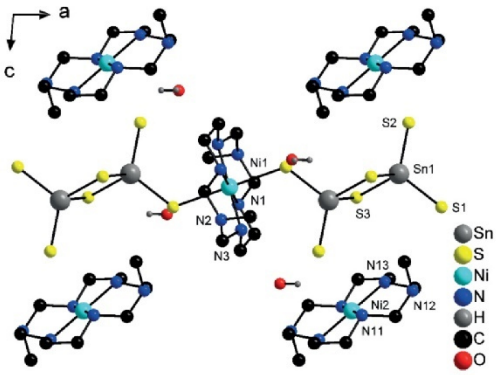

Figure 2. View of the arrangement of the chains and the square-planar $[Ni(L_1)]^{2+}$ complexes along [010] in compound **I**. Selected atoms are labeled. The H atoms of the complexes are omitted for clarity.

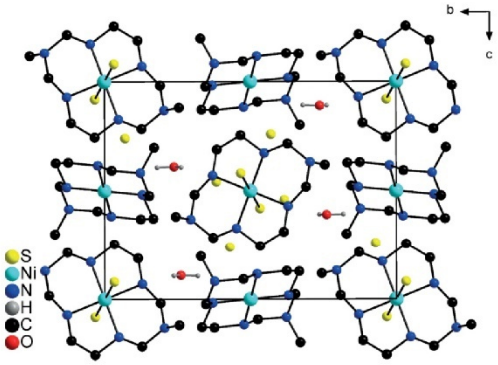

Figure 3. View of the arrangement of the square-planar and octahedral $[Ni(L_1)]^{2+}$ complexes in compound **I**. The Sn atoms are omitted and only H atoms of H_2O are shown.

The asymmetric unit of compound **II** contains one $[Sn_2S_6]^{4-}$ anion, two $[Ni(L_2)]^{2+}$ complexes and two water molecules. In contrast to compound **I**, the anion and cations are isolated (Figure 4).

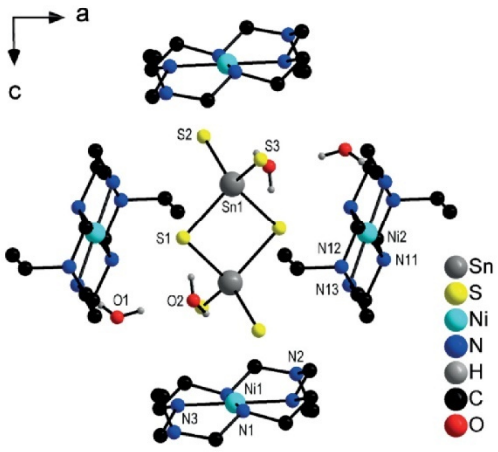

Figure 4. View of the crystal structure of compound **II** viewed along [010]. Selected atoms are labeled. The hydrogen atoms of the complexes are omitted for clarity.

The two Ni^{2+} cations are fourfold coordinated by N atoms of the L_2 ligand in a square-planar manner. The shortest Ni···S separations are 3.260 Å to the bridging S^{2-} of the anion and 3.388 Å to a terminal S^{2-}, and both values are longer than a

Journal of Inorganic and General Chemistry
ZAAC
Zeitschrift für anorganische und allgemeine Chemie

ARTICLE

typical covalent Ni–S bond, but shorter than the sum of van der Waals radii. The Ni–N bond lengths are between 1.915 and 1.932 Å, i.e. in the region observed for square-planar complexes with hexaazacycloctadecane ligands. Along [001] layers consisting of Ni2 centered cations and anions alternate with layers composed only by Ni1 centered cations, while along [100] and [010] cations and anions alternate. The two unique H_2O molecules form a dimer by strong O–H···O interaction (Table S6, Supporting Information). One of the terminal S atoms has three strong hydrogen bonds, while the second S_{term} is involved in two such contacts. In contrast to **I** the S_{brid} atom has one S···H–O interaction (Figure S5, bottom, Supporting Information).

Comparison of the crystal structures of the two compounds suggests an influence of the macrocyclic ligand surrounding the transition metal cations on the structural dimensionality. In compounds **I** and **II**, the macrocyclic ligands have either a methyl or an ethyl group as substituents. Hence, the lower steric requirement of the ligand in **I** allows the formation of chains by Ni–S bond formation. The dimensionality is reduced to isolated ions in the structure of **II**, where ethyl groups instead of methyl groups are bound to the tertiary N atoms. Indeed, the calculated volumes and surfaces of the $[Ni(L_n)]^{2+}$ complexes (n = 1 and 2) using the software Materials Studio[41] (Table 2) demonstrate that the complex $[Ni(L_2)]^{2+}$ needs more space than $[Ni(L_1)]^{2+}$. These differences may be responsible for the differences of the crystal structures of the two compounds.

Table 2. Volumes and surfaces of $[Ni(L_1)]^{2+}$ and $[Ni(L_2)]^{2+}$ complexes.

	Volume /Å^3	Surface /Å^2
$[Ni(L_1)]^{2+}$	253	249
$[Ni(L_2)]^{2+}$	283	280

Hirshfeld Surface Analysis

To get more information about the close intermolecular contacts in the structures of **I** and **II** calculation of the Hirshfeld surface was carried out using Crystal Explorer 3.1.[42–46] The important quantity of a Hirshfeld surface is the normalized distance d_{norm} which is calculated using the distances d_e and d_i, which represent the distance from the surface to the nearest atom outside the surface and the distance from the surface to the nearest atom within the molecule. In the 3D plot different areas are observed on the Hirshfeld surface. Distances shorter than the sum of the van der Waals radii are regions with the strongest intermolecular contacts and are visualized as red areas. Areas with distances longer than the sum of the van der Waals radii are displayed in white to blue. The 2D representation of the 3D surface is called fingerprint plot. The Hirshfeld surface of the cation in **I** (Figure 5) reveals that the important intermolecular contacts are H···H (70.2 %) and H···S (24.9 %) interactions. Further intermolecular contacts are N···H (2.7 %) and Ni···S (1.3 %).

Figure 6 displays the Hirshfeld surfaces and the fingerprint plots of the cations and anion in the structure of **II**. According to the fingerprint plots of both cations some differences are observed. The percentage of H···S contacts of cation 1 (21.8 %) is larger than for cation 2 (16.1 %), while more H···O interactions are found for cation 2 (6.7 %) than for cation 1 (4.1 %). Slight differences are also observed for H···H and N···H contacts (H···H: 69.9 % cation 1, 74.2 % cation 2; N···H: 1.7 % cation 1, 1.9 % cation 2). As expected, the main contributions for the intermolecular interactions of the anion are S···H bonds (90.4 %) (Figure 6, bottom, right), while minor contributions stem from S···Ni (2.8 %) and Sn···H (1.6 %) interactions.

Spectroscopic Properties

The typical bands of the macrocyclic ligands in compounds **I** and **II** are observed in the IR spectra (Figure S7, Table S7, Supporting Information). The broad absorptions at approximately 3394 and 3399 cm^{-1} are assigned to the OH vibration of H_2O molecules. The N–H stretching bands of L_1 and L_2 ligands are observed around 3228–3108 and 3202–3132 cm^{-1}, respectively and the Ni–N stretching modes in **I** are located at

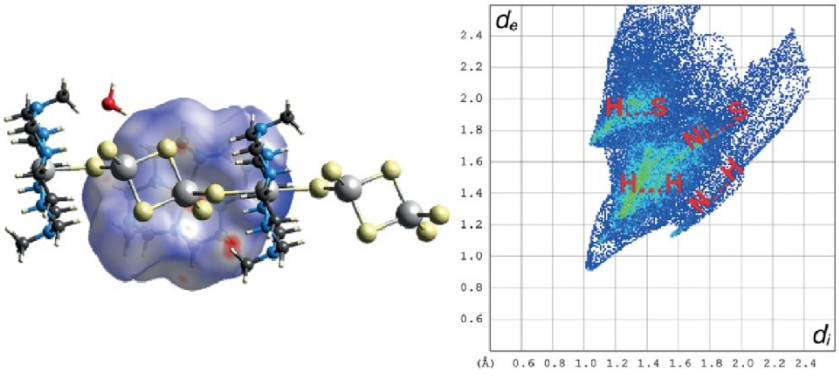

Figure 5. Hirshfeld surface (left) and 2D fingerprint plot (right) mapped with d_{norm} of the cation in the structure of compound **I**. The regions of intermolecular contacts are indicated in the fingerprint plot.

Journal of Inorganic and General Chemistry
ZAAC
Zeitschrift für anorganische und allgemeine Chemie

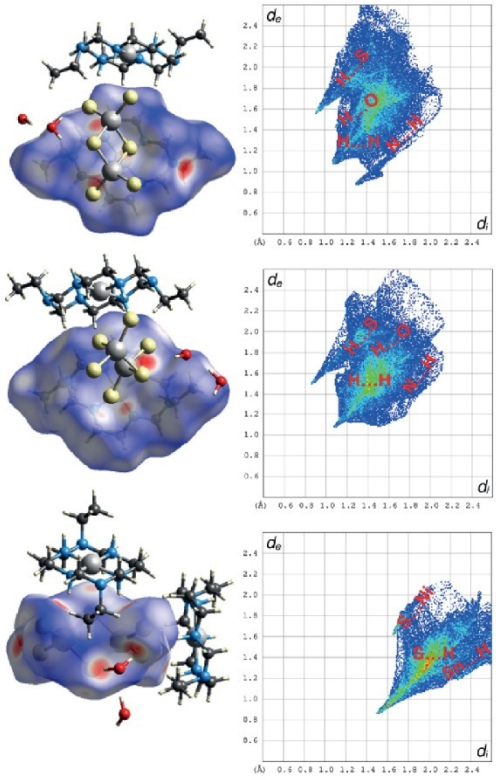

Figure 6. Hirshfeld surfaces (left) and 2D fingerprint plots (right) mapped with d_{norm} distance of cation 1 (top), cation 2 (middle), and the anion (bottom) of compound **II**. In the fingerprint plots the intermolecular contributions are indicated.

424 and 436 cm^{-1}, in accordance with two differing Ni–N bond lengths in **I**, while only one band is observed for **II** at 436 cm^{-1}. The characteristic Sn–S modes of the $[Sn_2S_6]^{4-}$ unit are observed in the Raman spectra in the region of 400 to 100 cm^{-1}. The $Sn–S_{term}$ stretching mode is observed at 374 cm^{-1} (**I**) and is split into two signals located at 378 and 393 cm^{-1} for **II**. One possible explanation for the occurrence of two signals may be the differing strengths and numbers of S···H bonding interactions in the structure of **II**. The Sn–S–Sn and Sn_2S_2 ring vibrations occur at around 336 and 272 cm^{-1} (**I**) and 338 and 275 cm^{-1} (**II**). The deformation and lattice vibrations of the $[Sn_2S_6]^{4-}$ unit are located between 200 and 100 cm^{-1}, but a definite assignment is not possible (Figure S8, Supporting Information).[47–49]

In the UV/Vis spectra of **I** and **II** the expected d–d transitions are observed (Figure S9, Supporting Information). For the high spin complex $[Ni(H_2O)_6]^{2+}$ these transitions occur at about 1.05 eV (1176 nm, $^3A_{2g} \rightarrow {}^3T_{2g}$), 1.71 eV (724 nm, $^3A_{2g} \rightarrow {}^3T_{1g}$ (F)) and 3.14 eV (395 nm, $^3A_{2g} \rightarrow {}^3T_{1g}$ (P)).[50]

For compound **I** only one defined maximum is located at 1.00 eV (1239 nm), while broad and more or less featureless signals occur between 1.5 and 3.5 eV. The molecular symmetry of the octahedrally surrounded Ni^{2+} center is D_{4h} and therefore four transitions $^3B_{1g} \rightarrow {}^3A_{2g}$, $^3B_{1g} \rightarrow {}^3E_g$, $^3B_{1g} \rightarrow {}^3B_{2g}$, and $^3B_{1g} \rightarrow {}^3A_{2g}$ can be expected.[51] In addition, the Ni^{2+} cation in the square-planar coordination has a d–d transition at about 2.75 eV (450 nm).[52] It is highly likely that the overlap of the different possible transitions leads to the very broad bands. For compound **II** with Ni^{2+} in square-planar coordination one d–d transition at about 2.75 eV (450 nm) is expected. Indeed, in the UV/Vis spectrum of **II** one signal is observed at 2.72 eV (456 nm). The strong absorptions at 4.11 eV (ca. 302 nm; compound **I**) and 3.95 eV (ca. 314 nm; compound **II**) can be assigned to charge transfer transitions.

Thermogravimetric Analysis

The thermal decomposition of compound **I** occurs in two steps (Figure S10, top, Supporting Information). The first step starts at T = 65 °C with an endothermic event at T_p = 129 °C. The mass loss of 3.3 % matches well with the expected value for the emission of two H_2O molecules (calcd. 3.4 %). In the second step the decomposition of the anhydrate formed by water removal takes place from 185 until 470 °C, in an endothermic reaction with T_p = 213 °C. The mass loss of 45.9 % probably corresponds to the emission of two L_1 molecules and a half H_2S molecule (calcd. 45.8 %). The X-ray powder pattern of the black residue recovered at 500 °C shows broad reflections indicating that nanocrystalline samples were formed. Several of the reflections can be assigned to SnS, $NiS_{1.97}$ and NiS (Figure S11, Supporting Information).

Heating compound **II** to 500 °C two mass steps are observed in the TG curve (Figure S10, bottom, Supporting Information). The first step starts at $T \approx$ 35 °C which is accompanied by an endothermic event at T_p = 92.4 °C. The mass loss of 7.1 % agrees with the removal of four H_2O molecules (calcd. 6.3 %). The anhydrate is decomposed between 180 and 500 °C, accompanied by two endothermic signals at $T_p \approx$ 190 and $T_p \approx$ 238 °C in the DTA curve. The mass loss of 46.5 % is in reasonable agreement with the emission of two L_2 molecules and a half H_2S molecule (calcd. 47 %). The X-ray powder pattern of the black residue investigated after the decomposition shows reflections of SnS, $NiS_{1.97}$ and NiS besides some not identified reflections (Figure S12, Supporting Information).

Conclusions

We presented a new synthetic approach for the preparation of thiostannate compounds at room temperature containing bulky Ni^{2+} centered complexes. Reactions of $[Ni(L_1)](ClO_4)_2$ or $[Ni(L_2)](ClO_4)_2$ with $Na_4SnS_4 \cdot 14\ H_2O$ in water at room temperature were not successful, because only the complexes could be obtained. In the structure of **I** chains of alternating $[Sn_2S_6]^{4-}$ and $[Ni(L_1)]^{2+}$ ions are observed whereas in **II** the anions and cations are isolated. The differences of the crystal structures may be explained by the differing space require-

Journal of Inorganic and General Chemistry
ZAAC
Zeitschrift für anorganische und allgemeine Chemie

ARTICLE

ments of the ligands L_1 and L_2. Hirshfeld surface analyses demonstrate the importance of intermolecular S···H, H···H, N···H and O···H interactions for the arrangement of the cations and anions. Currently we investigate whether the new synthetic protocol presented here can be applied for the preparation of new compounds with complexes which exhibit a very low solubility in H_2O, but a rather good solubility in organic solvents. This may offer the opportunity for the preparation of highly unusual materials.

Acknowledgements

Financial support by the State of Schleswig-Holstein is gratefully acknowledged. We thank *Inke Jess* for the TG measurements. Open access funding enabled and organized by Projekt DEAL.

Keywords: Room temperature synthesis; Thiostannates; Macrocyclic ligands; Single crystal structure; Spectroscopic and thermal properties

References

[1] B. Seidlhofer, N. Pienack, W. Bensch, *Z. Naturforsch. B* **2010**, *65*, 937–975.
[2] G. Demazeau, *J. Mater. Sci.* **2008**, *43*, 2104–2114.
[3] J. Li, B. Marler, H. Kessler, M. Soulard, S. Kallus, *Inorg. Chem.* **1997**, *36*, 4697–4701.
[4] P. Nørby, E. Eikeland, J. Overgaard, S. Johnsen, B. B. Iversen, *CrystEngComm* **2015**, *17*, 2413–2420.
[5] J. Hilbert, N. Pienack, H. Lühmann, C. Näther, W. Bensch, *Z. Anorg. Allg. Chem.* **2016**, *642*, 1427–1434.
[6] A. Benkada, M. Poschmann, C. Näther, W. Bensch, *Z. Anorg. Allg. Chem.* **2019**, *645*, 433–439.
[7] A. Benkada, H. Reinsch, M. Poschmann, J. Krahmer, N. Pienack, W. Bensch, *Inorg. Chem.* **2019**, *58*, 2354–2362.
[8] J. Hilbert, C. Näther, W. Bensch, *Inorg. Chim. Acta* **2017**, *459*, 29–35.
[9] J. Hilbert, C. Näther, W. Bensch, *Cryst. Growth Des.* **2017**, *17*, 4766–4775.
[10] Y. Oh, S. Bag, C. D. Malliakas, M. G. Kanatzidis, *Chem. Mater.* **2011**, *23*, 2447–2456.
[11] M. P. Suh, S. G. Kang, *Inorg. Chem.* **1988**, *27*, 2544–2546.
[12] G. M. Sheldrick, SHELXS-97, University of Göttingen, Göttingen, Germany **1997**.
[13] G. M. Sheldrick, *Acta Crystallogr., Sect. C* **2015**, *71*, 3–8.
[14] N. Pienack, H. Lühmann, B. Seidlhofer, J. Ammermann, C. Zeisler, F. Danker, C. Näther, W. Bensch, *Solid State Sci.* **2014**, *33*, 67–72.
[15] J. Hilbert, C. Näther, W. Bensch, *Dalton Trans.* **2015**, *44*, 11542–11550.
[16] J. Hilbert, C. Näther, W. Bensch, *Z. Anorg. Allg. Chem.* **2014**, *640*, 2858–2863.
[17] C. Tang, J. Lu, J. Han, Y. Liu, Y. Shen, D. Jia, *J. Solid State Chem.* **2015**, *230*, 118–125.
[18] C.-Y. Yue, X.-W. Lei, L. Yin, X.-R. Zhai, Z.-R. Ba, Y.-Q. Niu, Y.-P. Li, *CrystEngComm* **2015**, *17*, 814–823.
[19] E. Karey, K. A. Rosmus, J. A. Aitken, J. Macneil, *Acta Crystallogr., Sect. E* **2011**, *67*, m1516-m1517.
[20] R.-h. Chen, F. Wang, C.-y. Tang, Y. Zhang, D.-x. Jia, *J. Chem. Crystallogr.* **2013**, *43*, 319–324.
[21] S. Dehnen, C. Zimmermann, *Z. Anorg. Allg. Chem.* **2002**, *628*, 2463–2469.
[22] C. Zeisler, C. Näther, W. Bensch, *CrystEngComm* **2013**, *15*, 8874.
[23] B. Krebs, S. Pohl, W. Schiwy, *Z. Anorg. Allg. Chem.* **1972**, *393*, 241–252.
[24] X.-h. Lu, J.-j. Liang, J. Zhao, Y. Zhang, D.-x. Jia, *J. Chem. Crystallogr.* **2011**, *41*, 557–562.
[25] D.-x. Jia, J. Dai, Q.-Y. Zhu, Y. Zhang, X.-M. Gu, *Polyhedron* **2004**, *23*, 937–942.
[26] J. Zhou, X. Liu, G.-Q. Chen, F. Zhang, L.-R. Li, *Z. Naturforsch. B* **2010**, *65*, 1229–1234.
[27] H. Z. Kou, S. Gao, O. Bai, Z. M. Wang, *Inorg. Chem.* **2001**, *40*, 6287–6294.
[28] H.-Z. Kou, S.-F. Si, S. Gao, D.-Z. Liao, Z.-H. Jiang, S.-P. Yan, Y.-G. Fan, G.-L. Wang, *Eur. J. Inorg. Chem.* **2002**, *2002*, 699–702.
[29] H.-Z. Kou, W.-M. Bu, S. Gao, D.-Z. Liao, Z.-H. Jiang, S.-P. Yan, Y.-G. Fan, G.-L. Wang, *J. Chem. Soc., Dalton Trans.* **2000**, 2996–3000.
[30] H.-Z. Kou, S. Gao, B.-Q. Ma, D.-Z. Liao, *Chem. Commun.* **2000**, 713–714.
[31] J. W. Shin, D.-W. Kim, D. Moon, *Acta Crystallogr., Sect. E* **2016**, *72*, 223–225.
[32] Y.-W. Li, H. Xiang, T.-B. Lu, S. W. Ng, *Acta Crystallogr., Sect. E* **2004**, *60*, m309-m311.
[33] L. V. Tsymbal, Y. D. Lampeka, V. I. Boyko, V. I. Kalchenko, S. V. Shishkina, O. V. Shishkin, *CrystEngComm* **2014**, *16*, 3707–3711.
[34] Y.-W. Li, H. Xiang, T.-B. Lu, S. W. Ng, *Acta Crystallogr., Sect. E* **2004**, *60*, m312-m313.
[35] Y.-W. Li, H. Xiang, T.-B. Lu, S. W. Ng, *Acta Crystallogr., Sect. E* **2004**, *60*, m314-m316.
[36] R. D. Shannon, *Acta Crystallogr., Sect. A* **1976**, *32*, 751–767.
[37] M. Zhang, T. Sheng, X. Wang, S. Hu, R. Fu, J. Chen, Y. He, Z. Qin, C. Shen, X. Wu, *CrystEngComm* **2010**, *12*, 73–76.
[38] R. Stähler, W. Bensch, *Eur. J. Inorg. Chem.* **2001**, *2001*, 3073–3078.
[39] J. Hilbert, C. Näther, R. Weihrich, W. Bensch, *Inorg. Chem.* **2016**, *55*, 7859–7865.
[40] J. Cumby, J. P. Attfield, *Nat. Commun.* **2017**, *8*, 14235.
[41] Accelrys Inc., Materials Studio Version 5.0, San Diego **2009**.
[42] J. J. McKinnon, A. S. Mitchell, M. A. Spackman, *Chem. Eur. J.* **1998**, *4*, 2136–2141.
[43] J. J. McKinnon, M. A. Spackman, A. S. Mitchell, *Acta Crystallogr., Sect. B* **2004**, *60*, 627–668.
[44] M. A. Spackman, *Phys. Scr.* **2013**, *87*, 48103.
[45] M. A. Spackman, D. Jayatilaka, *CrystEngComm* **2009**, *11*, 19–32.
[46] M. A. Spackman, J. J. McKinnon, *CrystEngComm* **2002**, *4*, 378–392.
[47] B. Krebs, S. Pohl, W. Schiwy, *Angew. Chem.* **1970**, *82*, 884.
[48] N. Pienack, S. Lehmann, H. Lühmann, M. El-Madani, C. Näther, W. Bensch, *Z. Anorg. Allg. Chem.* **2008**, *634*, 2323–2329.
[49] N. Pienack, C. Näther, W. Bensch, *Z. Naturforsch. B* **2008**, *63*, 1243–1251.
[50] A. F. Holleman, E. Wiberg, N. Wiberg, *Lehrbuch der anorganischen Chemie*, 102nd ed., de Gruyter, Berlin **2007**.
[51] M. E. Farago, J. M. James, V. C. G. Trew, *J. Chem. Soc. A* **1967**, 820–824.
[52] M. P. Suh, *Adv. Inorg. Chem.* **1996**, *44*, 93–146.

Received: May 5, 2020
Published Online: ■

Journal of Inorganic and General Chemistry
ZAAC
Zeitschrift für anorganische und allgemeine Chemie

ARTICLE

*A. Benkada, C. Näther, W. Bensch** **1–8**
Room Temperature Synthesis of New Thiostannates by Slow Interdiffusion of Different Solvents

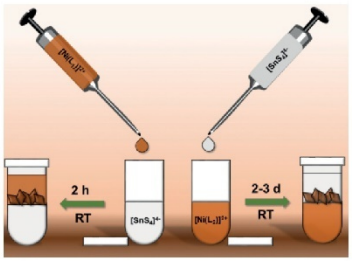

3.5 “Transformation of $Na_4SnS_4 \cdot 14H_2O$ into $Na_4Sn_2S_6 \cdot 5H_2O$ at room temperature in the solid state: Synthesis and Crystal Structure of the new compound $Na_4Sn_2S_6 \cdot 5H_2O$”

The thiostannate salt $Na_4SnS_4 \cdot 14H_2O$ was synthesized at room temperature by a new simple synthetic approach using $Na_2S \cdot 9H_2O$ and $SnCl_4 \cdot 5H_2O$ as reactants and H_2O as solvent. Storing $Na_4SnS_4 \cdot 14H_2O$ in air for 1 d led to the formation of the new compound $Na_4Sn_2S_6 \cdot 5H_2O$, whereby $Na_4SnS_4 \cdot 14H_2O$ represents the major phase. The new compound $Na_4Sn_2S_6 \cdot 5H_2O$ could be obtained by heating $Na_4SnS_4 \cdot 14H_2O$ in MeOH at 90 °C for 30 min. $Na_4Sn_2S_6 \cdot 5H_2O$ reveals a 3D network structure, in which the Na^+ cations have octahedral as well as trigonal-bipyramidal environments of O atoms and S^{2-} anions. Heat treatment of $Na_4SnS_4 \cdot 14H_2O$ led to generation of a kinetically stabilized phase of Na_4SnS_4, when fast heating rates like 4 and 16 $K \cdot min^{-1}$ were used. A mixture of Na_4SnS_4 and the kinetically stabilized phase was observed with slower heating rate of 1 $K \cdot min^{-1}$. Storing the anhydrate of $Na_4SnS_4 \cdot 14H_2O$ in air for 1 d led to the formation of $Na_4SnS_4 \cdot 14H_2O$ and $Na_4Sn_2S_6 \cdot 5H_2O$. However, $Na_4SnS_4 \cdot 14H_2O$ is the dominant phase. In contrast to $Na_4SnS_4 \cdot 14H_2O$, water uptake of the anhydrate of $Na_4Sn_2S_6 \cdot 5H_2O$ resulted in the generation of the pristine material.

A. Benkada, H. Reinsch, H. Lühmann, W. Bensch, Transformation of $Na_4SnS_4 \cdot 14H_2O$ into $Na_4Sn_2S_6 \cdot 5H_2O$ at room temperature in the solid state: Synthesis and Crystal Structure of the new compound $Na_4Sn_2S_6 \cdot 5H_2O$, *Eur. J. Inorg. Chem.*, **2020**. Submitted 15.07.2020.

WILEY-VCH

ARTICLE

Transformation of $Na_4SnS_4 \cdot 14H_2O$ into $Na_4Sn_2S_6 \cdot 5H_2O$ at room temperature in the solid state: Synthesis and Crystal Structure of the new compound $Na_4Sn_2S_6 \cdot 5H_2O$

Assma Benkada,[a] Helge Reinsch,[a] Henning Lühmann,[a] and Wolfgang Bensch[a]*

Dedication.....

Abstract: The systematic investigation of the formation, stability and thermal properties of $Na_4SnS_4 \cdot 14H_2O$ (**I**) led to the discovery of the new compound $Na_4Sn_2S_6 \cdot 5H_2O$ (**II**) which is already formed at room temperature. The transformation of **I** into **II** is most probably initiated by proton transfer from crystal water molecules to terminal S^{2-} anions in the structure of **I**. In the next step two $[SnS_3SH]^{3-}$ anions condense to form $[Sn_2S_6]^{4-}$ and H_2S is released. Phase pure samples of **II** could be prepared by heating **I** in methanol. In the structure of **II** all S^{2-} anions have bonds to Na^+ cations thus forming a 3D network structure. Heating **I** with 4 $K \cdot min^{-1}$ in N_2 until all crystal water molecules are emitted led to water free Na_4SnS_4, which represents a new polymorphic form, which is most probably a kinetically stable polymorph of Na_4SnS_4. An exothermic transition occurs at T = 563 °C and the X-ray powder pattern shows mainly reflections of the known Na_4SnS_4 phase. Hence, the compound reported in literature is the thermodynamically stable polymorph in this temperature range. Heat treatment of compound **II** led to the formation of the anhydrate which absorbs water from atmosphere resulting in recovery of the pristine material. Water uptake of the anhydrate of **I** led to generation of **I** and **II**, whereby **I** is the major phase.

Introduction

The structures of thiostannate compounds include different anionic units like $[SnS_4]^{4-}$, $[Sn_2S_6]^{4-}$, $[Sn_2S_5]^{2-}$, $[Sn_2S_7]^{6-}$,$[Sn_2S_8]^{2-}$, $[Sn_3S_7]^{2-}$, $[Sn_4S_9]^{2-}$, $[Sn_4S_{10}]^{4-}$ or $[Sn_5S_{12}]^{4-}$, which are charge compensated by metal cations.[1–8] In compounds with protonated amine molecules or transition metal complexes most often $[Sn_3S_7]^{2-}$, $[Sn_4S_8]^{2-}$ or $[Sn_2S_6]^{4-}$ anions are observed.[9] The structural versatility of thiostannate anions is due to the variable coordination number as well as the variable oxidation state of Sn. In the above-mentioned thiostannate anions Sn exhibits the coordination number 4 (tetrahedron), 5 (trigonal bipyramid) or 6 (octahedron). In addition, Sn occurs mainly in the oxidation state IV, but compounds with different oxidation states like II/IV or III/IV were also reported.[10–12]

In the overwhelming number of thiostannates the $[Sn_2S_6]^{4-}$ anion occurs, which is generated by two edge-sharing $[SnS_4]^{4-}$ tetrahedra. The anions are either isolated or linked to the metal centers to form tin-sulfide compounds. The linkage is achieved by three different modes: i) two *trans* terminal S^{2-} of $[Sn_2S_6]^{4-}$ are bound to two metal cations, ii) two S^{2-} anions are bound to one metal cation or iii) each S^{2-} anion forms a bond to one metal cation.[13] Thiostannates with metal cations as counter ions were mainly synthesized using the molten-flux approach or at elevated temperatures. For example, Au_2BaSnS_4,[14] $BaCdSnS_4$,[15] $AGaSnS_4$ (A = Na, K, Rb, Cs, Tl)[16] were obtained through the high temperature synthesis, while $A_2Sn_4S_9$ (A = K, Rb, Cs),[6] A_2CdSnS_4 (A = Li and Na) and $Na_6CdSn_4S_{12}$[17] were prepared applying the molten-flux approach. Protonated amine molecules, transition metal cations or transition metal complexes as counter ions compensating the negative charge of the $[Sn_xS_y]^{n-}$ anions were solely observed in the structures of compounds which were synthesized under solvothermal conditions.[9,18–20]

Generally, solvothermal syntheses of thiostannates were done using the elements Sn and S, SnS_2, metal salts like $SnCl_4 \cdot 5H_2O$ and $Na_2S \cdot 9H_2O$ or using a precursor like $Na_4SnS_4 \cdot 14H_2O$.[9,21–23] Recently, we performed syntheses in aqueous amine solutions applying the compound $\{[Ni(tren)]_2[Sn_2S_6]\}_n$ as educt.[24] Because the product diversity is limited with this precursor, we developed a further synthetic approach: an aqueous solution of $Na_4SnS_4 \cdot 14H_2O$ is reacted with transition metal complexes leading to crystallization of new tin sulfides like $[Mn(2,2'\text{-bipy})_2]_2[Sn_2S_6]$, $\{[Ni(cyclam)]_2[Sn_2S_6]\}_n \cdot 2nH_2O$,[13] $\{[Ni(cyclen)]_6[Sn_6S_{12}O_2(OH)_6]\} \cdot 2(ClO_4) \cdot 19H_2O$[21] and $[Ni(cyclen)(H_2O)_2]_4[Sn_{10}S_{20}O_4] \cdot \sim 13H_2O$[23] (2,2'-bipy = 2,2'-bipyridin, cyclam = 1,4,8,11-tetraazacyclotetradecane, cyclen = 1,4,7,10-tetraazacyclododecane). Notably, in the structures of these compounds either the $[Sn_2S_6]^{4-}$ anion or oxo-thio anions are observed, but not the $[SnS_4]^{4-}$ anion. The compound $Na_4SnS_4 \cdot 14H_2O$ was already reported in 1973 and was prepared in aqueous solution by reaction of $Na_2S \cdot 9H_2O$ with freshly synthesized SnS_2 or with $SnCl_4$ and by adding acetone to precipitate the product.[1] A different synthetic protocol was reported in 2011 where aqueous solutions of $Na_2S \cdot 9H_2O$ and $SnCl_4 \cdot 5H_2O$ were heated for 8 h at 45 °C and MeOH was used instead of acetone to precipitate the product.[25] Because only little is known about the stability on air and about the thermal stability, we prepared $Na_4SnS_4 \cdot 14H_2O$ using both procedures reported in literature. Applying these procedures, mainly phase mixtures were obtained. Hence, we investigated the parameters that influence product formation in detail. Furthermore, we investigated the stability of $Na_4SnS_4 \cdot 14H_2O$ at room temperature

[a] Assma Benkada, Dr. Helge Reinsch, Henning Lühmann, Prof. Dr. Wolfgang Bensch
Institute of Inorganic Chemistry
Christian-Albrechts-University of Kiel
Max-Eyth-Straße 2
24118 Kiel
Germany
E-mail: wbensch@ac.uni-kiel.de

Supporting information for this article is available on the WWW under http://dx.doi.???? or from the author.

and the thermal behavior using thermal analyses. We present a new synthetic approach to generate phase pure $Na_4SnS_4 \cdot 14H_2O$ (**I**). In addition, we report the preparation and crystal structure of the new compound $Na_4Sn_2S_6 \cdot 5H_2O$ (**II**), which is formed by a protonation and condensation reaction.

Results and Discussion

Synthetic aspects

According to the procedure reported in[25] compound I was synthesized by heating an aqueous solution of $Na_2S \cdot 9H_2O$ and $SnCl_4 \cdot 5H_2O$ for 8 h at 45 °C. The product was precipitated by addition of MeOH to the solution. X-ray powder diffraction patterns (XRPD) demonstrate that a mixture of **I** and **II** crystallized (Figure S1). Therefore, we investigated whether the temperature and/or solvent influence the formation of the two compounds. Various experiments were performed at 295 K for different reaction times and using dried acetone instead of MeOH for precipitating the product. The results of the experiments demonstrated that **I** is formed very fast after 30 min. in an aqueous solution of $Na_2S \cdot 9H_2O$ and $SnCl_4 \cdot 5H_2O$ applying a 4:1 molar ratio. The drying procedure of the product plays an important role. If the sample is dried in vacuum, the water molecules are successively removed from **I** leading to the formation of **II** (Figure S2). During this process some S^{2-} anions of the $[SnS_4]^{4-}$ anions are protonated and adjacent $[SnS_3SH]^{3-}$ units condense to generate the $[Sn_2S_6]^{4-}$ anion. The condensation requires formation of H_2S, which could be experimentally verified using humid Pb acetate paper. The decomposition of **I** can be formally described by the following chemical equation:

$$2\ Na_4SnS_4 \cdot 14H_2O \rightarrow Na_4Sn_2S_6 \cdot 5H_2O + 19\ H_2O + 2\ H_2S + 4\ NaOH$$

Storing **I** in dry Ar for 1 d no changes could be observed in the XRPD pattern, while prolongation of the time led to generation of a mixture of **I** and **II** (Figure S3). This observation indicates that an intramolecular proton transfer from H_2O to terminal S^{2-} of the $[SnS_4]^{4-}$ anion occurs leading to formation of $[Sn_2S_6]^{4-}$ as proposed above.

In further experiments with **I** we were able to crystallize **II** as phase pure product by heating **I** in MeOH at 90 °C for 30 min.

Stability of compound I at room temperature

The observations presented above prompted us to investigate the stability of **I** at room temperature on air for several days. In distinct time intervals XRPD patterns were recorded. The XRPD pattern of the starting material reveals phase purity (Figure 1). After storage for 1 d reflections of **II** appeared, but still compound **I** is the major phase (Figure 1). Further storage for 3, 6 and 11 d led to subsequent conversion of **I** into **II**. However, compound **I** is still the dominating phase indicating that the transformation process is very slow (Figure 1). Using the integrated intensities of selected reflections of the two compounds about 35 % of **I** was transformed into **II**.

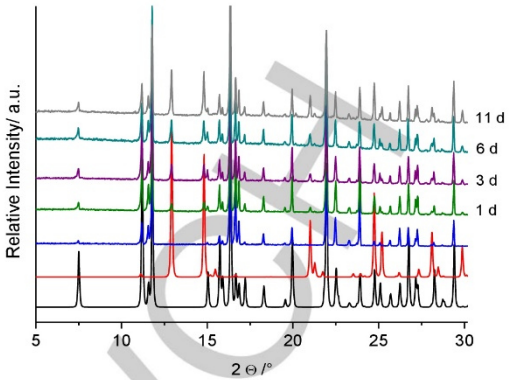

Figure 1. X-ray powder patterns recorded at different time intervals for investigation of the stability of **I** on air. Black: compound **I** (calc.), red: compound **II** (calc.) and blue: freshly prepared **I**.

Crystal Structures

Compound **I**, $Na_4SnS_4 \cdot 14H_2O$, crystallizes in the monoclinic space group *C*2/c (Z = 4, a = 8.622, b = 23.534, c = 11.347 Å and β = 110.53 °).[1] The asymmetric unit of **I** is composed of one $[SnS_4]^{4-}$ anion, seven H_2O molecules and three Na^+ cations, which are octahedrally coordinated: Na2/Na3 by six H_2O molecules and Na1 by five H_2O and one S^{2-} anion of the $[SnS_4]^{4-}$ unit (Figure 2, bottom). The Na-O bond lengths are between 2.239 and 2.587 Å (average: 2.418 Å) and the Na-S bond is at 2.873 Å. The bonds are in the range of the sum of ionic radii [r_{Na} (CN = 6): 1.02 Å, O^{2-}: 1.35 Å, S^{2-}: 1.84 Å [26]] and the values match well with those reported in literature.[2,16,17,27] The angles around the three unique Na^+ cations indicate a moderate distortion of the octahedra. The volumes of the polyhedra were calculated using the minimum bounding ellipsoid approach yielding 57.3, 57.5 and 67.3 Å^3 for Na2, Na3 and Na1 respectively.[28] According to the calculation all three polyhedra are axially stretched.

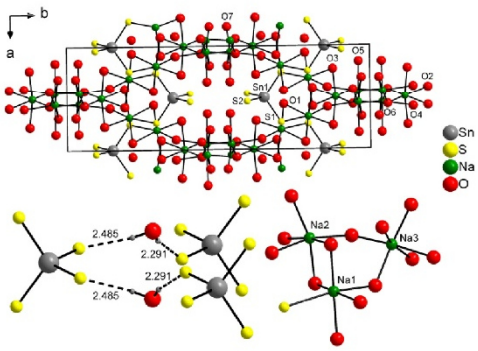

Figure 2. Top: View of the crystal structure of compound **I** along the c-axis; bottom left: H bonding interactions between H_2O molecules and the $[SnS_4]^{4-}$ anion and bottom right: coordination environments of the Na^+ cations. Only selected atoms are labelled and H atoms are omitted.

The Na^+ centered polyhedra are connected *via* common corners and edges to form a 3D crystal structure (Figure 2, top). Only two of the four S^{2-} ions of the $[SnS_4]^{4-}$ anion are involved in bonds to Na^+ cations. Between H_2O molecules, an extended H bonding network is observed, and the S^{2-} anions are also involved in H bonding interactions. The geometric parameters for O-H···S as well as O-H···O separations and angles indicate strong H bonds (Table S1).

Compound **II**, $Na_4Sn_2S_6{\cdot}5H_2O$, crystallizes in the tetragonal space group $P4_12_12$ with four formula units in the unit cell. The Sn, Na, S2, S4, O2 and O3 atoms are located on general and S1, S3 and O1 are on special positions. The asymmetric unit contains one $[Sn_2S_6]^{4-}$ anion, two Na^+ cations and three water molecules. The $[Sn_2S_6]^{4-}$ anion is constructed by two edge-sharing $[SnS_4]^{4-}$ tetrahedra. The Sn-S_{brid} bond lengths are in the range from 2.450(3) to 2.454(3) Å and are longer than the Sn-S_{term} bonds, which vary from 2.339(5) to 2.349(5) Å. This bond length distribution is typical and was observed in many $[Sn_2S_6]^{4-}$ containing compounds.[13,29–32] The S_{term}-Sn-S_{term} angles are 117.46 °, which slightly deviate from those in other $[Sn_2S_6]^{4-}$ containing compounds.[31–34] The angles in the Sn_2S_2 ring scatter from 86.33 to 93.34 Å indicating a distortion of the tetrahedra. However, all values match well with those reported in literature.[30–32,34] All S^{2-} anions of the thiostannate moiety are involved in bonds to Na^+ cations but in different fashions: the bridging S atoms (S1 and S3) have bonds to two Na^+, while the terminal S2 and S4 atoms have one respectively three bonds to Na^+ (Figure 3).

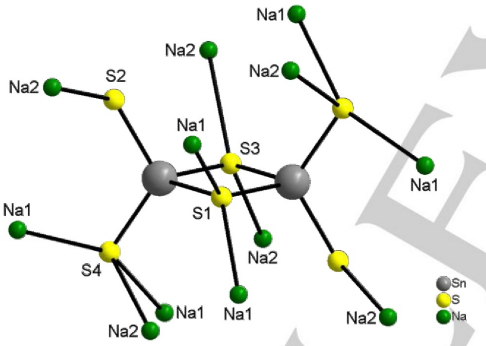

Figure 3. View of the $[Sn_2S_6]^{4-}$ anion and the bonding pattern of S^{2-} anions to Na^+ cations.

The Na^+ cations exhibit different environments: Na1 is octahedrally coordinated by three O atoms and three S^{2-} anions of $[Sn_2S_6]^{4-}$, while Na2 is in a trigonal bipyramidal environment of two O atoms and three S^{2-} anions (Figure 4). We note that this type of coordination is rare in thiostannates containing only main group cations.

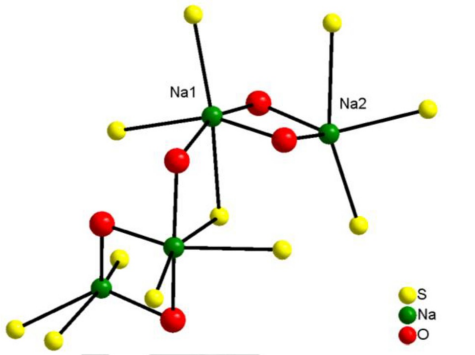

Figure 4. View of the coordination environment of the two unique Na^+ cations in the structure of compound **II**. Only selected atoms are labelled and the H atoms are not shown.

For Na1, the Na-O bond lengths are in the range from 2.406(14) to 2.558(10) Å (average: 2.499 Å) and the Na-S bonds vary between 2.973(9) and 3.138(9) Å (average: 3.045 Å). Na2 has bonds to O atoms between 2.314(14) and 2.358(15) Å (average: 2.336 Å), and Na-S bond lengths in the range from 2.862(9) to 3.244(9) Å (average: 2.997 Å). The Na-O/S bond lengths are in accordance with the sum of ionic radii [r_{Na} (CN = 6): 1.02 Å, r_{Na} (CN = 5): 1.00 Å, O^{2-}: 1.35 Å, S^{2-}: 1.84 Å[26]]. However, all these values match with those reported in literature.[1,16,17,27] The $Na1O_3S_3$ and $Na2O_2S_3$ polyhedra share common edges and a $Na_2O_3S_6$ group can be identified as secondary building unit (Figure 4). These units are further joined generating a 3D network structure (Figure 5). O···S separations are between 3.108(13) and 3.269(7) indicating strong H bonding interactions.

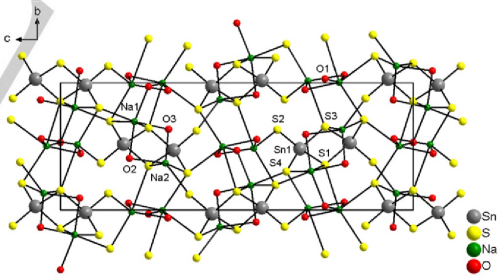

Figure 5. View of the interconnection of the different polyhedra in the structure of **II** forming a 3D network structure. Note that only some atoms are labeled.

Thermoanalytical investigations

The thermal properties of compound **I** were investigated using simultaneously thermogravimetry and differential thermoanalysis (TG-DTA). Upon heating to 300 °C two steps are observed in the TG curve which are accompanied by intense and broad endothermic events in the DTA curve (T_p = 66 and 142 °C) (Figure 6), demonstrating that the loss of water occurs in different steps. The mass loss of 42.4 % determined at 170 °C matches well with that calculated for the removal of all H_2O molecules (calc. = 42.6%). Above T ≈ 170 °C no further mass change can be observed. Interestingly, the XRPD pattern of the product obtained

at 300 °C is not in accordance with that of the fully dehydrated compound Na_4SnS_4[8] (Figure S4). One may assume that a new compound was formed at T = 300 °C and therefore a second thermal experiment was performed where the decomposition was stopped at T = 170 °C.

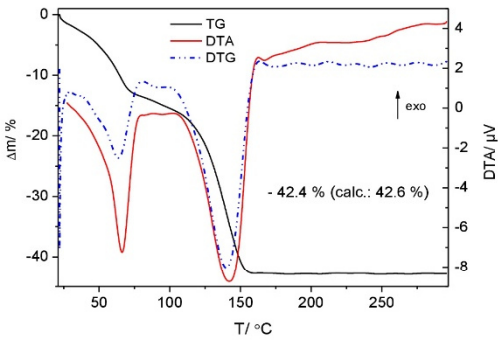

Figure 6. TG (black), DTA (red) and DTG (dashed-dotted blue) curves of compound **I** measured with a heating rate of 4 K·min^{-1} in N_2 atmosphere.

Again the XRPD pattern did not match with that of any Na thiostannate or dehydrated Na_4SnS_4 (Figure 7) but is identical with that obtained for the sample recovered at T = 300 °C (Figure S4). The reflections in the patterns of both samples are relatively broad and some exhibit an unusual shape indicating small coherently scattering domains and structural disorder, preventing structure solution from the powder data.

Increasing the heating rate to 16 K·min^{-1} did not improve crystallinity of the product (Figure S5). The observations can be summarized as follows: heating **I** with 4 or 16 K·min^{-1} generates a new compound which is most probably a new and possibly kinetically stable polymorph of Na_4SnS_4.

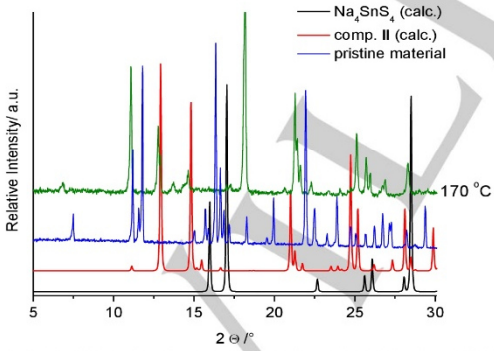

Figure 7. X-ray powder patterns of the sample recovered after heating to 170 °C (olive) and stored at 295 K for 1 d (blue). Black: Na_4SnS_4 (calc.), red: compound II (calc.), blue: pristine material.

We hypothesize that the sample formed heating **I** with a rate of 4 K·min^{-1} is kinetically stabilized. Hence, compound **I** was heated to 300 °C with the lower heating rate of 1 K·min^{-1} (Figure 8). As expected the TG curve is different compared to that obtained for 4 K·min^{-1}, showing at least three not well resolved reaction steps accompanied by two broad endothermic events in the DTA curve (T_p = 62 and 92 °C). The weight loss (41.1%) is already finished at around 105 °C (Figure 8) and is in reasonably good agreement with the emission of the crystal water molecules. A second TG run was performed by heating only to 140 °C. Independent from the final temperature (140 or 300 °C) the XRPD patterns show reflections of Na_4SnS_4 and of the unknown compound already observed in the pattern after heating **I** with 4 K·min^{-1} (Figure S6). We note that the intensity of the reflections of Na_4SnS_4 is much higher in the pattern of the sample obtained at 300 °C compared to those of the sample recovered at 140 °C. Integrating the intensities of the two reflections located at 15.9 and 17 ° 2θ (Na_4SnS_4) and of that at 18.1 ° 2θ (unknown compound) yields a ratio of 3:1 for Na_4SnS_4/unknown at T = 140 °C and of 9:1 at T = 300 °C. Isothermal annealing of the product at T = 140 °C heated with 1 K ·min^{-1} led to a successive transformation of the unknown thiostannate into the known one (Figure S7). The slower heating rate, prolonged annealing and higher final temperatures favor formation of the known Na_4SnS_4 indicating that this modification is thermodynamically more stable than the unknown compound.

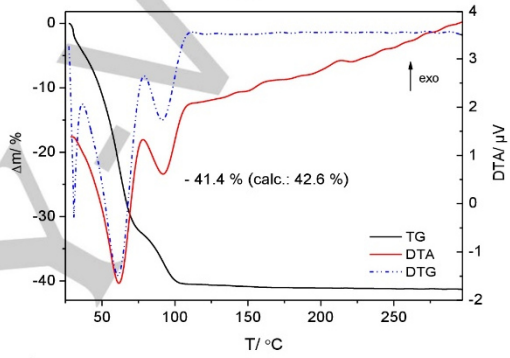

Figure 8. TG (black), DTA (red) and DTG (dashed-dotted blue) of compound **I** carried out with a heating rate of 1 K·min^{-1} in N_2 atmosphere.

A further TG experiment was performed up to 620 °C (heating rate: 1 K·min^{-1}) showing a broad exothermic event at T_P = 563 °C (Figure 9). The XRPD pattern is now clearly dominated by reflections of Na_4SnS_4 with small amounts (7 %) of the phase obtained in the experiments presented above (Figure 10).

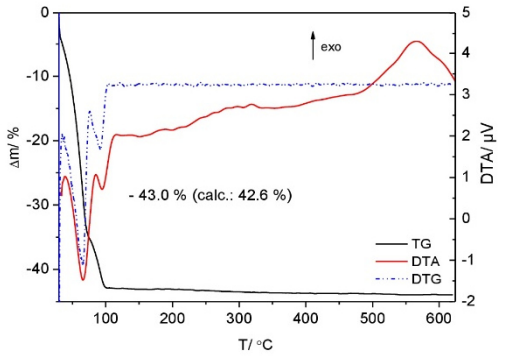

Figure 9. TG (black), DTA (red) and DTG (dashed-dotted blue) of compound **I** carried out with a heating rate of 1 K·min^{-1} in N_2 atmosphere up to 620 °C.

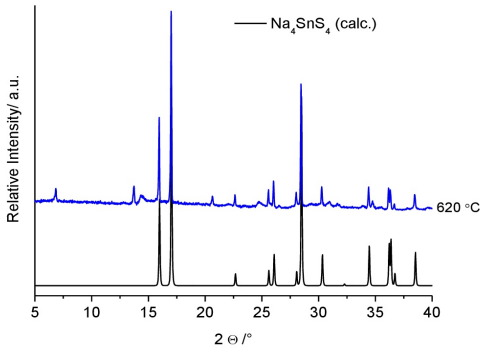

Figure 10. X-ray powder pattern of the sample recovered after heating to 620 °C (blue) compared with the calculated pattern of Na_4SnS_4 (black).

The exothermic event in the DTA curve demonstrates that the known Na_4SnS_4 is the thermodynamically stable polymorph over the entire temperature range.

The thermal stability of **II** was also investigated and the TG curve (T_{final} = 300 °C, heating rate: 4 K·min^{-1}) shows two not well-resolved mass steps (Figure 11), which are accompanied by endothermic events in the DTA curve (T_p = 95 and 132 °C). The experimental mass loss of 16.7 % is slightly larger than that calculated for the removal of all water molecules (calc.: 14.7 %). Applying a lower heating rate of 1 K·min^{-1} (Figure S8) leads to a similar mass change (16.9 %) in almost one step with an endothermic event at T_p = 128 °C. In both thermal decomposition reactions, a yellow solid was formed which may indicate a partial decomposition. The XRPD patterns are characterized by broad reflections which exhibit only a partial match with reflection positions of **II** (Figure S9). The quality of the powder pattern did not allow structure solution.

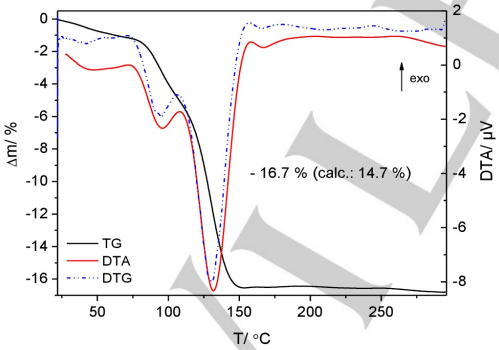

Figure 11. TG (black), DTA (red) and DTG (dashed-dotted blue) of compound **II** performed with a heating rate of 4 K·min^{-1} in N_2 atmosphere.

In the Raman spectrum of the yellow residue, the typical Sn-S modes of the $[Sn_2S_6]^{4-}$ anion are observed between 450 and 50 cm^{-1} (Figure 12). The Sn-S_{term} resonance occurs at 377 cm^{-1}, while the Sn-S-Sn bands are observed at 342 (υ_{as}) and at 304 cm^{-1} (υ_s). The Sn_2S_2 ring vibration is located at 284 cm^{-1}. The deformation and lattice vibrations are between 200 and 50 cm^{-1}, but no reasonable assignment can be performed in this region.[4]

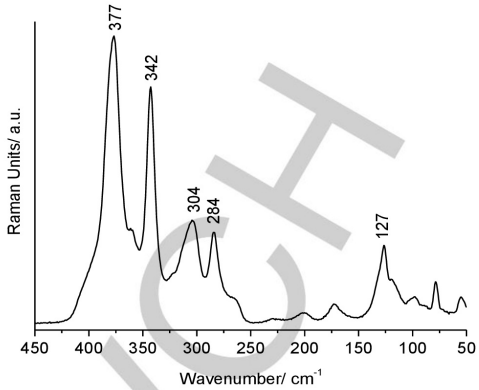

Figure 12. Raman spectrum of the anhydrate obtained by heating compound **II** to 300 °C.

To examine whether the anhydrates of compounds **I** and **II** absorb water from atmosphere, the samples obtained by heating **I** to 170 °C (4 K·min^{-1}) and 140 °C (1 K·min^{-1}) were stored in air (T = 295 K). An XRPD pattern was recorded after 1 d and reflections of **I** and **II** are present with **I** being the major phase (Figures S10 and S11). Storing the yellow anhydrate of compound **II** also on air at 295 K for 1 d led to recovery of the pristine material and the solid formed was slightly yellow (Figure S12).

Conclusions

In this work we present a new synthetic procedure for the preparation of compound **I** at room temperature. **I** could be synthesized after only 30 min. by reacting $Na_2S·9H_2O$ with $SnCl_4·5H_2O$ in water. Investigation of the stability of **I** on air demonstrated that **I** was converted to the new compound **II** after 1 d storing, but **I** represents the dominant phase. Phase pure product of **II** was obtained by a simple synthetic approach, in which compound **I** was heated in MeOH at 90 °C for 30 min. To obtain the water free Na_4SnS_4, **I** was thermally treated. Applying fast heating rates only a kinetically stabilized phase of Na_4SnS_4 was formed. However, when slower heating rate such as 1 K.min^{-1} was applied, a mixture of Na_4SnS_4 and the kinetically stable polymorph of Na_4SnS_4 were generated. A transformation of the low temperature modification into the thermodynamically most stable polymorph occurs at about 563 °C. Storing the anhydrates of **I** in water atmosphere for 1 d results in the formation of **I** and small amounts of **II**. Unlike **I**, the crystal water of compound **II** could be reversibly removed.

Experimental Section

Synthesis of $Na_4SnS_4·14H_2O$ (I)

1.80 g (7.50 mmol) $Na_2S·9H_2O$ were dissolved in 5 mL H_2O. 0.655 g (1.87 mmol) $SnCl_4·5H_2O$ also dissolved in H_2O (3 mL) were added dropwise to the $Na_2S·9H_2O$ solution. The mixture was stirred for 30 min. at RT until the generated yellow precipitate dissolved and a blue-green solution formed. To this solution, 4 mL cold (3 °C) pure acetone were added and stored at this temperature for 10 min. The colorless crystals were filtrated and kept on air for ≈ 15 min (yield ≈ 68 % based on Sn).

Synthesis of $Na_4Sn_2S_6{\cdot}5H_2O$ (II)

0.750 g (1.27 mmol) $Na_4SnS_4{\cdot}14H_2O$ was dispersed in 4 mL MeOH and heated for 30 min. at 90 °C. The white solid of $Na_4Sn_2S_6{\cdot}5H_2O$ was filtrated, washed with MeOH and dried in air at room temperature (yield ≈ 40 % based on Sn).

Structure determination

The PXRD pattern of **II** could be indexed with a tetragonal unit cell with extinction conditions suitable for the space group $P4_12_12$ using TOPAS Academics.[35] Using these parameters and an estimated composition based on EDX spectroscopy, the position of the heavy Sn, S and Na atoms could be determined using direct methods as implemented in Expo 2009.[36] This initial structure model was subsequently refined by Rietveld methods using a Thompson-Cox-Hastings profile function and a 12th order polynomial background function. Residual electron density was identified by Fourier synthesis and attributed to oxygen atoms representing water molecules coordinated to the sodium atoms. The positions of all atoms were freely refined without any restrains. The temperature factors were refined element specific. The final plot is shown in Figure S13 and some figures of merit are summarized in Table 1.

CCDC-1984037 (**II**) contains the supplementary crystallographic data for this paper. These data can be obtained free of charge from the Cambridge Crystallographic Data Centre via http://www.ccdc.cam.ac.uk/data_request/cif.

X-Ray powder diffraction

The powder diffraction patterns were measured with a STOE Stadi-P diffractometer equipped with a MYTHEN 1K detector (DECTRIS) using monochromatized Cu-$K_{\alpha1}$ radiation (λ = 1.540598 Å). The experimental and the calculated patterns using the results of the Rietveld refinement match perfectly indicating phase purity of the sample (Figure S14).

Thermogravimetry and Differential thermal analysis

Thermogravimetric experiments were performed using a Linseis STA PT1600 instrument. The samples were heated in a nitrogen atmosphere with a heating rate of 0.1, 1, 4 and 16 K·min^{-1}.

Raman spectroscopy

The Raman spectrum was measured at room temperature on a Bruker RAM II FT-Raman spectrometer equipped with a Ge detector.

Table 1. Crystallographic parameters determined by Rietveld refinement for compound **II**.

empirical formula	$Na_4Sn_2S_6{\cdot}5H_2O$
crystal system	tetragonal
space group	$P4_22_12$
$a = b$ [Å]	8.45087(3)
c [Å]	23.32912(12)
V [Å^3]	1666.10(1)
Z	4
Density (calc.) [g/cm^3]	2.40
Diffractometer	STOE Stadi P
Detector	Dectris Mythen
Radiation	Cu-$K_{\alpha1}$, λ = 154.0598 pm
Temperature [K]	293
Range of data collection	8 < 2θ < 70
Independent atoms	10
R_{WP} [%]	7.2
R_P [%]	5.5
R_{Bragg} [%]	3.8
R_{Exp} [%]	5.5
GoF	1.3

Acknowledgements

Financial support by the State of Schleswig-Holstein is gratefully acknowledged. We thank Aleksej Jochim for the numerous TG measurements.

Keywords: room temperature solid-state reaction, room temperature synthesis, crystal structure from X-ray powder data, thermal properties, thiostannate

References

[1] W. Schiwy, S. Pohl, B. Krebs, *Z. Anorg. Allg. Chem.* **1973**, *402*, 77–86.

[2] B. Krebs, S. Pohl, W. Schiwy, *Z. Anorg. Allg. Chem.* **1972**, *393*, 241–252.

[3] J. H. Liao, C. Varotsis, M. G. Kanatzidis, *Inorg. Chem.* **1993**, *32*, 2453–2462.

[4] B. Krebs, W. Schiwy, *Z. Anorg. Allg. Chem.* **1973**, *398*, 63–71.

[5] W. S. Sheldrick, B. Schaaf, *Z. Anorg. Allg. Chem.* **1994**, *620*, 1041–1045.

[6] G. A. Marking, M. Evain, V. Petricek, M. G. Kanatzidis, *J. Solid State Chem.* **1998**, *141*, 17–28.

[7] Y. Ko, C. L. Cahill, J. B. Parise, *J. Chem. Soc., Chem. Commun.* **1994**, *251*, 69–70.

[8] J.-C. Jumas, E. Philippot, F. Vermot-Gaud-Daniel, M. Ribes, M. Maurin, *J. Solid State Chem.* **1975**, *14*, 319–327.

[9] B. Seidlhofer, N. Pienack, W. Bensch, *Z. Naturforsch.* **2010**, *65b*, 937–975.

[10] M. Behrens, M.-E. Ordolff, C. Näther, W. Bensch, K.-D. Becker, C. Guillot-Deudon, A. Lafond, J. A. Cody, *Inorg. Chem.* **2010**, *49*, 8305–8309.

[11] Z. Hassanzadeh Fard, C. Müller, T. Harmening, R. Pöttgen, S. Dehnen, *Angew. Chem.* **2009**, *121*, 4507–4511.

[12] H. P. Nayek, W. Massa, S. Dehnen, *Inorg. Chem.* **2008**, *47*, 9146–9148.

[13] J. Hilbert, N. Pienack, H. Lühmann, C. Näther, W. Bensch, *Z. Anorg. Allg. Chem.* **2016**, *642*, 1427–1434.

[14] C. L. Teske, *Z. Anorg. Allg. Chem.* **1978**, *445*, 193–201.

[15] C. L. Teske, *Z. Anorg. Allg. Chem.* **1980**, *460*, 163–168.

[16] A. Kumari, K. Vidyasagar, *J. Solid State Chem.* **2007**, *180*, 2013–2019.

[17] M. S. Devi, K. Vidyasagar, *J. Chem. Soc., Dalton Trans.* **2002**, 2092–2096.

[18] N. Pienack, W. Bensch, *Z. Anorg. Allg. Chem.* **2006**, *632*, 1733–1736.

[19] N. Pienack, K. Möller, C. Näther, W. Bensch, *Solid State Sci.* **2007**, *9*, 1110–1114.

[20] N. Pienack, C. Näther, W. Bensch, *Solid State Sci.* **2007**, *9*, 100–107.

[21] A. Benkada, M. Poschmann, C. Näther, W. Bensch, *Z. Anorg. Allg. Chem.* **2019**, *645*, 433–439.

[22] A. Benkada, H. Reinsch, W. Bensch, *Eur. J. Inorg. Chem.* **2019**, 4427–4432.

[23] A. Benkada, H. Reinsch, M. Poschmann, J. Krahmer, N. Pienack, W. Bensch, *Inorg. Chem.* **2019**, *58*, 2354–2362.

[24] J. Hilbert, C. Näther, R. Weihrich, W. Bensch, *Inorg. Chem.* **2016**, *55*, 7859–7865.

[25] Y. Oh, S. Bag, C. D. Malliakas, M. G. Kanatzidis, *Chem. Mater.* **2011**, *23*, 2447–2456.

[26] R. D. Shannon, *Acta Cryst. A* **1976**, *32*, 751–767.

[27] H. Lühmann, C. Näther, I. Jess, W. Bensch, *Z. Anorg. Allg. Chem.* **2019**, *645*, 1165–1170.

[28] J. Cumby, J. P. Attfield, *Nat. Commun.* **2017**, *8*, 14235.

[29] D.-X. Jia, Y. Zhang, J. Dai, Q.-Y. Zhu, X.-M. Gu, *Z. Anorg. Allg. Chem.* **2004**, *630*, 313–318.

[30] D.-X. Jia, J. Dai, Q.-Y. Zhu, Y. Zhang, X.-M. Gu, *Polyhedron* **2004**, *23*, 937–942.

[31] Q. Jin, J. Chen, Y. Pan, Y. Zhang, D. Jia, *J. Coord. Chem.* **2010**, *63*, 1492–1503.

[32] N. Pienack, C. Näther, W. Bensch, *Z. Naturforsch.* **2008**, *63b*, 1243–1251.

[33] J. Zhou, X. Liu, L. An, F. Hu, W. Yan, Y. Zhang, *Inorg. Chem.* **2012**, *51*, 2283–2290.

[34] M. Behrens, S. Scherb, C. Näther, W. Bensch, *Z. Anorg. Allg. Chem.* **2003**, *629*, 1367–1373.

[35] Topas Academics 4.2, *Coelho Software: Brisbane,* **2007**.

[36] A. Altomare, M. Camalli, C. Cuocci, C. Giacovazzo, A. Moliterni, R. Rizzi, *J. Appl. Crystallogr.* **2009**, *42*, 1197–1202.

WILEY-VCH

ARTICLE

Entry for the Table of Contents

FULL PAPER

The new thiostannate $Na_4Sn_2S_6 \cdot 5H_2O$ was obtained at room temperature by proton transfer from water molecules to the S^{2-} anions of $Na_4SnS_4 \cdot 14H_2O$ and condensation of adjacent $[SnS_3SH]^{3-}$ anions under release of H_2S. $Na_4Sn_2S_6 \cdot 5H_2O$ exhibits a 3D network structure.

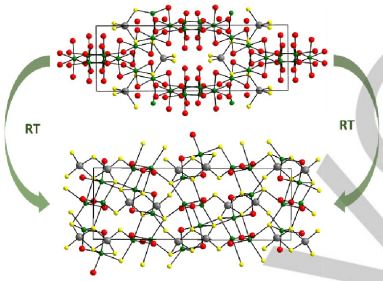

*Assma Benkada, Helge Reinsch, Henning Lühmann, and Wolfgang Bensch**

Transformation of $Na_4SnS_4 \cdot 14H_2O$ into $Na_4Sn_2S_6 \cdot 5H_2O$ at room temperature in the solid state: Synthesis and Crystal Structure of the new compound $Na_4Sn_2S_6 \cdot 5H_2O$

4. Conclusions and Outlook

The thiostannate salt $Na_4SnS_4 \cdot 14H_2O$ was applied as precursor for the formation of further Sn-S containing compounds. Investigation of the stability of $Na_4SnS_4 \cdot 14H_2O$ indicated that the transformation of $Na_4SnS_4 \cdot 14H_2O$ into the new compound $Na_4Sn_2S_6 \cdot 5H_2O$ occurs slowly at room temperature and is most probably induced by the protonation of the terminal S^{2-} anions forming the $[SnS_3SH]^{3-}$ anions, which condense to form the dimer $[Sn_2S_6]^{4-}$ under release of H_2S. $Na_4Sn_2S_6 \cdot 5H_2O$ exhibits a 3D network structure, in which the Na^+ cations are octahedrally as well as trigonal bipyramidally coordinated by S^{2-} anions of the $[Sn_2S_6]^{4-}$ unit and the O atoms of H_2O molecules. The compound $Na_4Sn_2S_6 \cdot 5H_2O$ could be obtained as phase pure product by heating $Na_4SnS_4 \cdot 14H_2O$ in MeOH. Due to the simple synthetic procedure, the good yield and the good solubility in H_2O $Na_4Sn_2S_6 \cdot 5H_2O$ can be applied as precursor to prepare further thiostannates and especially thiostannates containing the $[Sn_2S_6]^{4-}$ unit.

The reaction of $Na_4SnS_4 \cdot 14H_2O$ with $[Ni(cyclen)](ClO_4)_2$ or with $[Ni(cyclen)(H_2O)_2](ClO_4)_2 \cdot H_2O$ under hydrothermal conditions led to crystallization of two new compounds: $\{[Ni(cyclen)]_6[Sn_6S_{12}O_2(OH)_6]\} \cdot 2(ClO_4) \cdot 19H_2O$ and $[Ni(cyclen)(H_2O)_2]_4[Sn_{10}S_{20}O_4] \cdot \sim 13H_2O$. In the crystal structure of the compound $\{[Ni(cyclen)]_6[Sn_6S_{12}O_2(OH)_6]\} \cdot 2(ClO_4) \cdot 19H_2O$, the rare $[Sn_6S_{12}O_2(OH)_6]^{10-}$ cluster could be observed. The $[Ni(cyclen)]^{2+}$ cations are covalently linked to this cluster $[Sn_6S_{12}O_2(OH)_6]^{10-}$ forming the isolated cations $\{[Ni(cyclen)]_6[Sn_6S_{12}O_2(OH)_6]\}^{2+}$. $[Ni(cyclen)(H_2O)_2]_4[Sn_{10}S_{20}O_4] \cdot \sim 13H_2O$ is the first Sn(IV) oxo-sulfide compound, in which isolated anions and transition metal centered complexes arise. The Ni^{2+} cations are in an octahedral environment of four N atoms of cyclen and two O atoms of H_2O molecules thus preventing a bond formation between the $[Ni(cyclen)(H_2O)_2]^{2+}$ cations and the $[Sn_{10}S_{20}O_4]^{8-}$ anions.

Further syntheses with other macrocyclic amine molecules like 1,4,7,10-tetraazacyclododecane (cyclam), 1,8-dimethyl-1,3,6,8,10,13-hexaazacyclo-tetradecane (L_1) and 1,8-diethyl-1,3,6,8,10,13-hexaazacyclotetradecane (L_2) under hydrothermal conditions were unsuccessful. Therefore, room temperature syntheses were performed leading to the formation of three new compounds:

{[Cu(cyclam)]$_2$[Sn_2S_6]}$_n$· 2nH_2O, [Ni(L_1)][Ni(L_1)Sn_2S_6]$_n$·2H_2O and [Ni(L_2)]$_2$[Sn_2S_6]·4H_2O. In the compound {[Cu(cyclam)]$_2$[Sn_2S_6]}$_n$· 2nH_2O, the $[Cu(cyclam)]^{2+}$ cations are bound to the $[Sn_2S_6]^{4-}$ anions according to connection mode c) (see chapter 1.3 Tin-Sulfides) generating layers, while in compound [Ni(L_1)][Ni(L_1)Sn_2S_6]$_n$·2H_2O, the $[Ni(L_1)]^{2+}$ cations are linked to the $[Sn_2S_6]^{4-}$ anions following connection mode a) (see chapter 1.3 Tin-Sulfides) forming chains. Utilizing the $[Ni(L_2)]^{2+}$ cations for charge compensation only isolated cations and anions could be obtained indicating that the ethyl groups linked to N atoms of the ligand require more space as methyl groups in L_1 ligands. Hence, a bond formation between thiostannate anions and Ni^{2+} cations can be prevented.

The compound {[Cu(cyclam)]$_2$[Sn_2S_6]}$_n$·2nH_2O was obtained at room temperature by reacting Na_4SnS_4·14H_2O with [Cu(cyclam)](ClO_4)$_2$ as starting materials in aqueous solution. Applying the complex [Cu(cyclam)](ClO_4)$_2$, which is very stable (log K = 27.2[100]), the formation of aqua complexes is impeded. The crystallization of {[Cu(cyclam)]$_2$[Sn_2S_6]}$_n$·2nH_2O occurs very fast. The compound {[Cu(cyclam)]$_2$[Sn_2S_6]}$_n$·2nH_2O is the first example with Cu(II) in a S^{2-} environment. Since cyclam ligands form very stable complexes with Cu(II) the reduction of Cu(II) to Cu(I) is prevented.

The compounds [Ni(L_1)][Ni(L_1)Sn_2S_6]$_n$·2H_2O and [Ni(L_2)]$_2$[Sn_2S_6]·4H_2O were synthesized through an overlaying process, in which an aqueous solution of Na_4SnS_4·14H_2O and organic solutions of the complexes [Ni(L_1)](ClO_4)$_2$ and [Ni(L_2)](ClO_4)$_2$ were applied. Due to the poor solubility of both complexes in H_2O the solubility of the complexes was determined in organic solvents indicating that both complexes exhibit a good solubility in dimethylsulfoxid and acetonitrile. This synthetic route allowed the crystallization of thiostannate and tin-sulfide compounds in the interface region of the solvents, which are inaccessible using only H_2O as solvent. Moreover, this synthetic procedure can be used to obtain unusual materials, which could not be prepared using standard methods.

5. References

[1] P. Feng, X. Bu, N. Zheng, *Acc. Chem. Res.* **2005**, *38*, 293–303.

[2] R. L. Bedard, S. T. Wilson, L. D. Vail, J. M. Bennett, E. M. Flanigen, *Studies in Surface Science and Catalysis* **1989**, 375–387.

[3] A. K. Cheetham, G. Férey, T. Loiseau, *Angew. Chem.* **1999**, *111*, 3466–3492.

[4] A. Lafond, J. A. Cody, M. Souilah, C. Guillot-Deudon, R. Kiebach, W. Bensch, *Inorg. Chem.* **2007**, *46*, 1502–1506.

[5] N. Pienack, A. Puls, C. Näther, W. Bensch, *Inorg. Chem.* **2008**, *47*, 9606–9611.

[6] D. Zhang, G. Li, Y. Peng, L. Li, *Inorg. Chem.* **2017**, *56*, 208–212.

[7] B. Zhang, J. Li, C.-F. Du, M.-L. Feng, X.-Y. Huang, *Inorg. Chem.* **2016**, *55*, 10855–10858.

[8] M. J. Manos, K. Chrissafis, M. G. Kanatzidis, *J. Am. Chem. Soc.* **2006**, *128*, 8875–8883.

[9] M.-L. Feng, D. Sarma, X.-H. Qi, K.-Z. Du, X.-Y. Huang, M. G. Kanatzidis, *J. Am. Chem. Soc.* **2016**, *138*, 12578–12585.

[10] J. Lv, W. Wang, L. Zhang, C. Xue, D. Hu, T. Wu, *Cryst. Growth Des.* **2018**, *18*, 4834–4837.

[11] B. Krebs, *Angew. Chem.* **1983**, *95*, 113–134.

[12] W. Schiwy, S. Pohl, B. Krebs, *Z. Anorg. Allg. Chem.* **1973**, *402*, 77–86.

[13] E. Ruzin, S. Jakobi, S. Dehnen, *Z. Anorg. Allg. Chem.* **2008**, *634*, 995–1001.

[14] J. H. Liao, C. Varotsis, M. G. Kanatzidis, *Inorg. Chem.* **1993**, *32*, 2453–2462.

[15] T. Jiang, A. Lough, G. A. Ozin, R. L. Bedard, R. Broach, *J. Mater. Chem.* **1998**, *8*, 721–732.

[16] W. S. Sheldrick, *Z. Anorg. Allg. Chem.* **1988**, *562*, 23–30.

[17] K. Feng, X. Zhang, W. Yin, Y. Shi, J. Yao, Y. Wu, *Inorg. Chem.* **2014**, *53*, 2248–2253.

[18] M. Behrens, M.-E. Ordolff, C. Näther, W. Bensch, K.-D. Becker, C. Guillot-Deudon, A. Lafond, J. A. Cody, *Inorg. Chem.* **2010**, *49*, 8305–8309.

[19] H. P. Nayek, W. Massa, S. Dehnen, *Inorg. Chem.* **2008**, *47*, 9146–9148.

[20] Z. Hassanzadeh Fard, C. Müller, T. Harmening, R. Pöttgen, S. Dehnen, *Angew. Chem.* **2009**, *121*, 4507–4511.

[21] B. Krebs, S. Pohl, W. Schiwy, *Z. Anorg. Allg. Chem.* **1972**, *393*, 241–252.

[22] J.-C. Jumas, E. Philippot, M. Maurin, *J. Solid State Chem.* **1975**, *14*, 152–159.

[23] Y. Ko, C. L. Cahill, J. B. Parise, *J. Chem. Soc., Chem. Commun.* **1994**, *251*, 69–70.

[24] M. S. Devi, K. Vidyasagar, *J. Chem. Soc., Dalton Trans.* **2002**, 2092–2096.

[25] J. H. Liao, M. G. Kanatzidis, *Chem. Mater.* **1993**, *5*, 1561–1569.

[26] T. Jiang, G. A. Ozin, R. L. Bedard, *Adv. Mater.* **1994**, *6*, 860–865.

[27] T. Jiang, A. Lough, G. A. Ozin, *Adv. Mater.* **1998**, *10*, 42–46.

[28] J. B. Parise, Y. Ko, J. Rijssenbeek, D. M. Nellis, K. Tan, S. Koch, *J. Chem. Soc., Chem. Commun.* **1994**, *251*, 527.

[29] N. Pienack, D. Schinkel, A. Puls, M.-E. Ordolff, H. Lühmann, C. Näther, W. Bensch, *Z. Naturforsch. B: Chem. Sci.* **2012**, *67*, 1098–1106.

[30] M. Ø. Filsø, I. Chaaban, A. Al Shehabi, J. Skibsted, N. Lock, *Acta Crystallogr. , Sect. B* **2017**, *73*, 931–940.

[31] T. Jiang, A. Lough, G. A. Ozin, R. L. Bedard, *J. Mater. Chem.* **1998**, *8*, 733–741.

[32] S. Dehnen, C. Zimmermann, *Z. Anorg. Allg. Chem.* **2002**, *628*, 2463–2469.

[33] H. Pada Nayek, Z. Lin, S. Dehnen, *Z. Anorg. Allg. Chem.* **2009**, *635*, 1737–1740.

[34] J. Li, B. Marler, H. Kessler, M. Soulard, S. Kallus, *Inorg. Chem.* **1997**, *36*, 4697–4701.

[35] E. Karey, K. A. Rosmus, J. A. Aitken, J. Macneil, *Acta Crystallogr., Sect. E* **2011**, *67*, m1516-m1517.

[36] N. Pienack, W. Bensch, *Z. Anorg. Allg. Chem.* **2006**, *632*, 1733–1736.

[37] Y. An, B. Menghe, L. Ye, M. Ji, X. Liu, G. Ning, *Inorg. Chem. Commun.* **2005**, *8*, 301–303.

[38] M. BaiYin, L. Ye, Y. An, X. Liu, C. Jia, G. Ning, *Bull. Chem. Soc. Jpn.* **2005**, *78*, 1283–1284.

[39] W.-W. Xiong, J. Miao, P.-Z. Li, Y. Zhao, B. Liu, Q. Zhang, *CrystEngComm.* **2014**, *16*, 5989–5992.

[40] R.-C. Zhang, H.-G. Yao, S.-H. Ji, M.-C. Liu, M. Ji, Y.-L. An, *Chem. Commun.* **2010**, *46*, 4550–4552.

[41] N. Pienack, C. Näther, W. Bensch, *Solid State Sci.* **2007**, *9*, 100–107.

[42] D.-X. Jia, Y. Zhang, J. Dai, Q.-Y. Zhu, X.-M. Gu, *Z. Anorg. Allg. Chem.* **2004**, *630*, 313–318.

[43] N. Pienack, H. Lühmann, B. Seidlhofer, J. Ammermann, C. Zeisler, F. Danker, C. Näther, W. Bensch, *Solid State Sci.* **2014**, *33*, 67–72.

[44] J. Zhou, X. Liu, G.-Q. Chen, F. Zhang, L.-R. Li, *Z. Naturforsch. B: Chem. Sci.* **2010**, *65*, 1229–1234.

[45] H. Lühmann, I. Jeß, C. Näther, W. Bensch, *Z. Anorg. Allg. Chem.* **2020**, *646*, 234–240.

[46] C.-Y. Yue, X.-W. Lei, L. Yin, X.-R. Zhai, Z.-R. Ba, Y.-Q. Niu, Y.-P. Li, *CrystEngComm.* **2015**, *17*, 814–823.

[47] D.-X. Jia, J. Dai, Q.-Y. Zhu, Y. Zhang, X.-M. Gu, *Polyhedron* **2004**, *23*, 937–942.

[48] M. Behrens, S. Scherb, C. Näther, W. Bensch, *Z. Anorg. Allg. Chem.* **2003**, *629*, 1367–1373.

[49] J. Hilbert, C. Näther, W. Bensch, *Cryst. Growth Des.* **2017**, *17*, 4766–4775.

[50] J. Hilbert, C. Näther, W. Bensch, *Z. Anorg. Allg. Chem.* **2017**, *643*, 1861–1866.

[51] J. Hilbert, C. Näther, R. Weihrich, W. Bensch, *Inorg. Chem.* **2016**, *55*, 7859–7865.

[52] J. Hilbert, C. Näther, W. Bensch, *Inorg. Chim. Acta* **2017**, *459*, 29–35.

[53] N. Pienack, S. Lehmann, H. Lühmann, M. El-Madani, C. Näther, W. Bensch, *Z. Anorg. Allg. Chem.* **2008**, *634*, 2323–2329.

[54] J. Hilbert, C. Näther, W. Bensch, *Z. Anorg. Allg. Chem.* **2014**, *640*, 2858–2863.

[55] C. Zeisler, C. Näther, W. Bensch, *CrystEngComm.* **2013**, *15*, 8874.

[56] J. Hilbert, N. Pienack, H. Lühmann, C. Näther, W. Bensch, *Z. Anorg. Allg. Chem.* **2016**, *642*, 1427–1434.

[57] N. Pienack, C. Näther, W. Bensch, *Eur. J. Inorg. Chem.* **2009**, *2009*, 1575–1577.

[58] N. Pienack, C. Näther, W. Bensch, *Z. Naturforsch. B: Chem. Sci.* **2008**, *63*, 1243–1251.

[59] J. Hilbert, C. Näther, W. Bensch, *Inorg. Chem.* **2014**, *53*, 5619–5630.

[60] G.-N. Liu, G.-C. Guo, F. Chen, S.-P. Guo, X.-M. Jiang, C. Yang, M.-S. Wang, M.-F. Wu, J.-S. Huang, *CrystEngComm.* **2010**, *12*, 4035.

[61] Z. Wang, G. Xu, Y. Bi, C. Wang, *CrystEngComm.* **2010**, *12*, 3703.

[62] X.-M. Gu, J. Dai, D.-X. Jia, Y. Zhang, Q.-Y. Zhu, *Cryst. Growth Des.* **2005**, *5*, 1845–1848.

[63] J. Zhou, G.-Q. Bian, J. Dai, Y. Zhang, A.-B. Tang, Q.-Y. Zhu, *Inorg. Chem.* **2007**, *46*, 1541–1543.

[64] H.-P. Zhang, X.-W. Lei, *Chin. J. Inorg. Chem.* **2014**, 1–7.

[65] J. Hilbert, C. Näther, W. Bensch, *Dalton Trans.* **2015**, *44*, 11542–11550.

[66] T. Kaib, M. Kapitein, S. Dehnen, *Z. Anorg. Allg. Chem.* **2011**, *637*, 1683–1686.

[67] W. Schiwy, B. Krebs, *Angew. Chem.* **1975**, *87*, 451–452.

[68] J. B. Parise, Y. Ko, *Chem. Mater.* **1994**, *6*, 718–720.

[69] J. Hilbert, W. Bensch, C. Näther, *Curr. Inorg. Chem.* **2017**, *6*, 181–186.

[70] J.-J. Zhang, S.-M. Hu, X.-T. Wu, W.-X. Du, R.-B. Fu, L.-S. Wang, *Inorg. Chem. Commun.* **2003**, *6*, 744–747.

[71] L. Wu, L. Chen, J. Dai, C. Cui, Z. Fu, X. Wu, *Inorg. Chem. Commun.* **2001**, *4*, 574–576.

[72] B. Seidlhofer, N. Pienack, W. Bensch, *Z. Naturforsch. B: Chem. Sci.* **2010**, *65*, 937–975.

[73] Y. Ko, K. Tan, D. M. Nellis, S. Koch, J. B. Parise, *J. Solid State Chem.* **1995**, *114*, 506–511.

[74] Y. Wang, M. Baiyin, S. Ji, X. Liu, Y. An, G. Ning, *Chem. Res. Chin. Univ.* **2006**, *22*, 411–414.

[75] Q. Zhao, D. Jia, Y. Zhang, L. Song, J. Dai, *Inorg. Chim. Acta* **2007**, *360*, 1895–1901.

[76] N. Pienack, H. Lühmann, C. Näther, W. Bensch, *Z. Anorg. Allg. Chem.* **2016**, *642*, 25–30.

[77] B. Scott, K. J. Brewer, L. O. Spreer, C. A. Craig, J. W. Otvos, M. Calvin, S. Taylor, *J. Coord. Chem.* **1990**, *21*, 307–313.

[78] J. W. Lekse, M. A. Moreau, K. L. McNerny, J. Yeon, P. S. Halasyamani, J. A. Aitken, *Inorg. Chem.* **2009**, *48*, 7516–7518.

[79] A. Kumari, K. Vidyasagar, *J. Solid State Chem.* **2007**, *180*, 2013–2019.

[80] G. A. Marking, M. Evain, V. Petricek, M. G. Kanatzidis, *J. Solid State Chem.* **1998**, *141*, 17–28.

[81] G. A. Marking, M. G. Kanatzidis, *Chem. Mater.* **1995**, *7*, 1915–1921.

[82] W. S. Sheldrick, M. Wachhold, *Angew. Chem.* **1997**, *109*, 214–234.

[83] W.-W. Xiong, G. Zhang, Q. Zhang, *Inorg. Chem. Front.* **2014**, *1*, 292.

[84] G. Demazeau, *J. Mater. Sci.* **2008**, *43*, 2104–2114.

[85] P. Nørby, E. Eikeland, J. Overgaard, S. Johnsen, B. B. Iversen, *CrystEngComm.* **2015**, *17*, 2413–2420.

[86] G. M. Sheldrick, *SHELXS-97*, Program for the Solution of Crystal Structures; University of Göttingen, Göttingen, Germany, **1997**.

[87] G. M. Sheldrick, *SHELXL-2014,* Program for the Refinement of Crystal Structures, University of Göttingen, Göttingen, Germany, **2014**.

[88] Stoe & Cie, *WinXPow*, Stoe & Cie GmbH Darmstadt **2001**.

[89] K. Brandenburg, *Diamond*. *Crystal Impact GbR*, Bonn, Germany **2014**.

[90] *Olex²*. *OlexSys Ltd.* **2004**.

[91] Coelho Software, *Topas Academics 4.2*, Brisbane **2007**.

[92] A. Altomare, M. Camalli, C. Cuocci, C. Giacovazzo, A. Moliterni, R. Rizzi, *J. Appl. Crystallogr.* **2009**, *42*, 1197–1202.

[93] Accelrys Inc., *Materials Studio Version 5.0*, San Diego **2009**.

[94] A. L. Speck, *Platon*. *A Multipurpose Crystallographic Tool* **2010**.

[95] J. Cumby, J. P. Attfield, *Nat. Commun.* **2017**, *8*, 14235.

[96] Y. Oh, S. Bag, C. D. Malliakas, M. G. Kanatzidis, *Chem. Mater.* **2011**, *23*, 2447–2456.

[97] I. Pérez-Toro, A. Domínguez-Martín, D. Choquesillo-Lazarte, E. Vílchez-Rodríguez, J. M. González-Pérez, A. Castiñeiras, J. Niclós-Gutiérrez, *J. Inorg. Biochem.* **2015**, *148*, 84–92.

[98] J. H. Coates, D. A. Hadi, S. F. Lincoln, H. W. Dodgen, J. P. Hunt, *Inorg. Chem.* **1981**, *20*, 707–711.

[99] M. P. Suh, S. G. Kang, *Inorg. Chem.* **1988**, *27*, 2544–2546.

[100] X. Liang, P. J. Sadler, *Chem. Soc. Rev.* **2004**, *33*, 246–266.

6. Appendix

6.1 Supporting Information

6.1.1 “New Transition Metal Oxo-Thiostannate: Synthesis, Characterization, and Investigation of its Photocatalytic Properties”

Z. Anorg. Allg. Chem. **2018** · ISSN 0044–2313

SUPPORTING INFORMATION

Title: New Transition Metal Oxo-Thiostannate: Synthesis, Characterization, and Investigation of its Photocatalytic Properties
Author(s): A. Benkada, M. Poschmann, C. Näther, W. Bensch*
Ref. No.: z201800475

Supporting Information

New Transition Metal Oxo-Thiostannate: Synthesis, Characterization and Investigation of its Photocatalytic Properties

Assma Benkada, Michael Poschmann, Christian Näther, Wolfgang Bensch

Content

Table S1	Crystal and refinement data for compound **1**	p. 2
Figure S1	Experimental PXRD patterns of compound **1** compared with their simulated from single-crystal X-ray data	p. 3
Table S2	EDX data for compound **1**	p. 3
Table S3	Bond lengths and angles of the {[Ni(cyclen)]$_6$[$Sn_6S_{12}O_2(OH)_6$]} cation	p.4
Figure S2	Distribution of the SnO distances and their average values for μ_3-oxo, terminal OH, μ_3-hydroxo and terminal oxo fragments in crystal structures retrieved from the Cambridge Crystallographic Database (CSD)	p. 5
Figure S3	View of the trigonal antiprismatic arrangement of the Ni(II) cations	p. 6
Table S4	Intramolecular hydrogen bonds in compound **1**	p. 6
Table S5	Intermolecular hydrogen bonds in compound **1**	p. 7
Table S6	Bond lengths and angles around the Ni cations in compound **1**	p. 8
Figure S4	View of the chains with intermolecular C-H···S hydrogen bonding	p. 9
Figure S5	IR spectra of compound **1** and 1,4,7,10-tetraazacyclododecane (cyclen)	p. 10
Table S7	Values of the absorption observed in the IR spectrum of compound **1** together with their assignment	p. 10
Figure S6	Kubelka-Munk-Factor F^2 as function of energy retrieved form UV/Vis spectroscopic data	p. 11
Figure S7	Experimental X-ray powder patterns of compound **1**, of the dehydrated sample and of the sample after rehydration	p. 11
Figure S8	Amount of H_2 as function of time in the photocatalytic hydrogen evolution using [Ni(cyclen)$(H_2O)_2$]$(ClO_4)_2$·H_2O	p. 12

Table S1: Crystal and refinement data for compound **1**.

Crystal system	Monoclinic
Empirical formula	C48 H164 Cl2 N24 Ni6 O35 S12 Sn6
Space group	*C*2/*c*
M (g/mol)	3158.04
a (Å)	25.7223(9)
b (Å)	15.6522(3)
c (Å)	29.0703(10)
α (°)	90
β (°)	105.879(3)
γ (°)	90
V (Å^3)	11257.4(6)
Temperature (K)	170(2)
Z	4
Dcalc (g/cm^3)	1.863
μ (mm^{-1})	2.632
Scan range (deg)	1.457≤ θ ≤25.099
Reflections collected	36263
Independent reflections	9966
Observed reflections	7886
Goodness-of-fit on F^2	1.069
R values (I>2σ(I))	R1 = 0.0584, wR2 = 0.1460
R values (all data)	R1 = 0.0766, wR2 = 0.1552
Res. Elec. Dens. (e.Å^{-3})	1.080 and -0.717

2

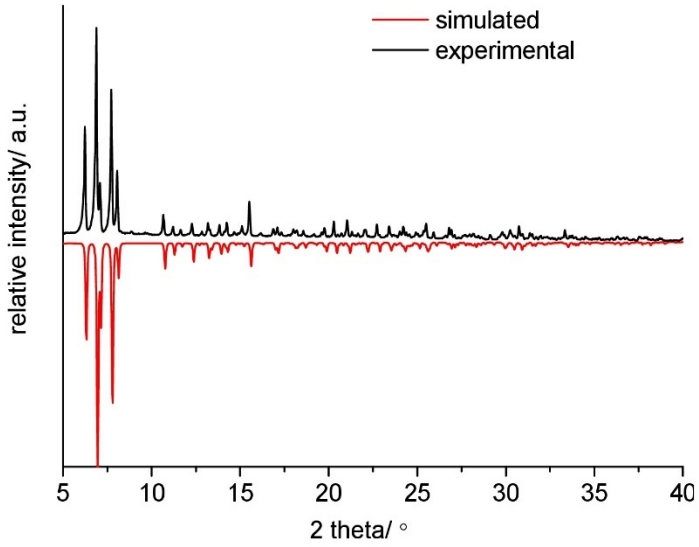

Figure S1: Experimental PXRD patterns of compound **1** (black) compared with the pattern calculated from single-crystal X-ray data (red).

Table S2: EDX data for compound **1**

		Ni	Sn	S
Compound **1**	calculated	1	1	2
	measured	0.83	1	1.90

3

Table S3: Bond lengths [Å] and angles [°] of the {[Ni(cyclen)]$_6$[$Sn_6S_{12}O_2(OH)_6$]} cation in compound **1**

Sn(1)-O(3)	2.066(6)	Sn(1)-O(2)	2.102(6)
Sn(1)-O(4)#1	2.080(5)	Sn(1)-S(2)	2.491(2)
Sn(1)-O(1)	2.097(6)	Sn(1)-S(1)	2.528(2)
O(4)-Sn(1)#1	2.080(5)	O(4)#1-Sn(1)-S(2)	93.67(16)
O(3)-Sn(1)-O(4)#1	175.4(2)	O(1)-Sn(1)-S(2)	88.33(18)
O(3)-Sn(1)-O(1)	87.9(2)	O(2)-Sn(1)-S(2)	167.01(17)
O(4)#1-Sn(1)-O(1)	95.8(2)	O(3)-Sn(1)-S(1)	93.09(18)
O(3)-Sn(1)-O(2)	87.9(2)	O(4)#1-Sn(1)-S(1)	82.74(15)
O(4)#1-Sn(1)-O(2)	90.2(2)	O(1)-Sn(1)-S(1)	169.02(18)
O(1)-Sn(1)-O(2)	78.9(2)	O(2)-Sn(1)-S(1)	90.19(16)
O(3)-Sn(1)-S(2)	89.2(2)	S(2)-Sn(1)-S(1)	102.60(7)
Sn(2)-S(4)	2.327(2)	Sn(2)-S(5)	2.394(2)
Sn(2)-S(3)	2.386(2)	Sn(2)-S(2)	2.399(2)
S(4)-Sn(2)-S(3)	114.31(9)	S(4)-Sn(2)-S(2)	109.05(9)
S(4)-Sn(2)-S(5)	105.56(9)	S(3)-Sn(2)-S(2)	108.32(8)
S(3)-Sn(2)-S(5)	105.42(7)	S(5)-Sn(2)-S(2)	114.30(8)
Sn(3)-O(4)#1	2.075(5)	Sn(3)-S(1)#1	2.525(2)
Sn(3)-O(4)	2.128(5)	Sn(3)-S(5)	2.561(2)
Sn(3)-S(6)	2.408(2)	Sn(3)-S(3)#1	2.623(2)
S(1)-Sn(3)#1	2.525(2)	S(3)-Sn(3)#1	2.623(2)
O(4)-Sn(3)#1	2.075(5)	O(4)-Sn(3)-S(5)	91.04(15)
O(4)#1-Sn(3)-O(4)	73.3(2)	S(6)-Sn(3)-S(5)	86.79(7)
O(4)#1-Sn(3)-S(6)	101.32(16)	S(1)#1-Sn(3)-S(5)	89.64(7)
O(4)-Sn(3)-S(6)	174.06(15)	O(4)#1-Sn(3)-S(3)#1	96.48(15)
O(4)#1-Sn(3)-S(1)#1	154.94(16)	O(4)-Sn(3)-S(3)#1	93.24(15)
O(4)-Sn(3)-S(1)#1	81.89(15)	S(6)-Sn(3)-S(3)#1	89.86(7)
S(6)-Sn(3)-S(1)#1	103.61(7)	S(1)#1-Sn(3)-S(3)#1	81.15(7)
O(4)#1-Sn(3)-S(5)	94.26(15)	S(5)-Sn(3)-S(3)#1	169.19(7)
Ni(2)-S(1)-Sn(3)#1	95.69(8)	Sn(2)-S(5)-Sn(3)	105.31(8)
Ni(2)-S(1)-Sn(1)	114.94(9)	Ni(3)-S(5)-Sn(3)	90.49(7)
Sn(3)#1-S(1)-Sn(1)	85.76(6)	Sn(3)-S(6)-Ni(3)	96.24(8)
Sn(2)-S(2)-Sn(1)	105.09(8)	Sn(1)-O(1)-Ni(1)	100.7(3)
Sn(2)-S(3)-Ni(2)	107.95(8)	Sn(1)-O(2)-Ni(1)	100.2(2)
Sn(2)-S(3)-Sn(3)#1	104.29(7)	Sn(3)#1-O(4)-Sn(1)#1	143.6(3)
Ni(2)-S(3)-Sn(3)#1	92.64(8)	Sn(3)#1-O(4)-Sn(3)	106.7(2)
Sn(2)-S(5)-Ni(3)	105.48(8)	Sn(1)#1-O(4)-Sn(3)	109.6(2)

4

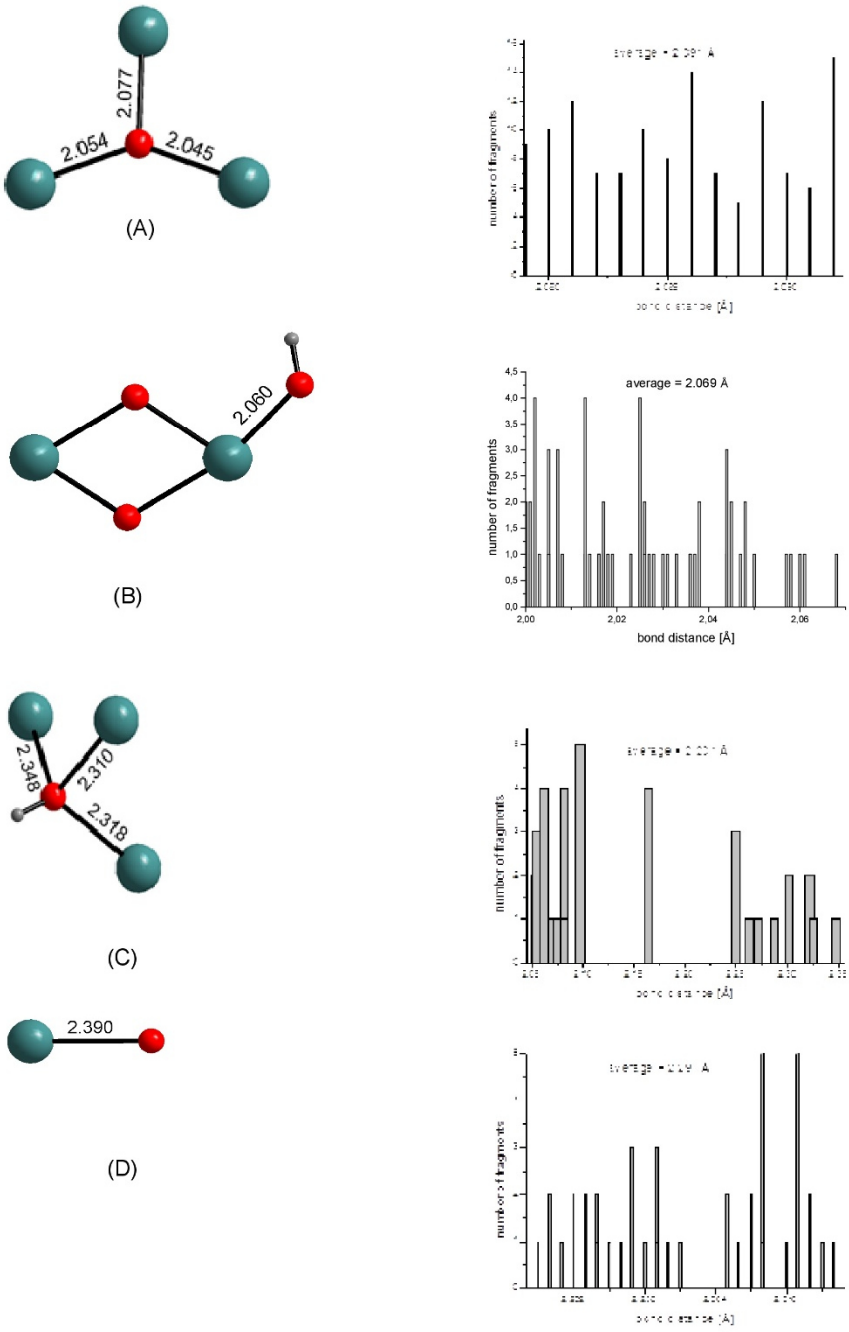

Figure S2: Distribution of the SnO distances and their average values for μ_3-oxo (A), terminal OH (B), μ_3-hydroxo (C) and terminal oxo (D) fragments in crystal structures retrieved from the Cambridge Crystallographic Database (CSD).

5

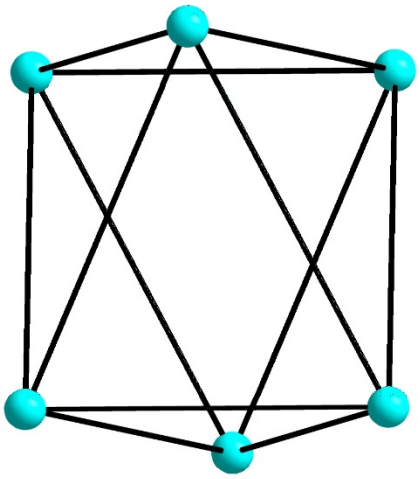

Figure S3: View of the trigonal antiprismatic arrangement of the Ni(II) cations.

Table S4: Intramolecular hydrogen bonds [Å and °] in compound **1**

D-H...A	d(D-H)	d(H...A)	d(D...A)	<(DHA)
O(1)-H(1)...S(6)	0.84	2.50	3.302(6)	160.9
O(2)-H(2)...S(5)#1	0.84	2.67	3.461(6)	156.5
N(4)-H(4N)...S(3)#1	1.00	2.37	3.297(8)	154.6
N(12)-H(12N)...S(6)#1	1.00	2.38	3.364(7)	167.7
N(14)-H(14N)...S(2)	1.00	2.30	3.270(8)	162.1
N(21)-H(21N)...S(4)	1.00	2.74	3.668(10)	155.4
N(22)-H(22N)...S(2)	1.00	2.42	3.304(9)	147.1
N(2)-H(2N)...O(3)	1.00	2.02	2.932(10)	150.2

Symmetry transformations used to generate equivalent atoms: #1 -x+3/2,-y+3/2,-z+1

6

Table S5: Intermolecular hydrogen bonds [Å and °] in compound **1**

D-H...A	d(D-H)	d(H...A)	d(D...A)	<(DHA)
N(23)-H(23N)...O(24)	1.00	2.32	3.28(3)	158.4
C(21)-H(21A)...O(11)#10	0.99	2.62	3.38(2)	133.2
C(14)-H(14B)...O(12)#8	0.99	2.44	3.37(2)	155.8
C(28)-H(28B)...O(13)#1	0.99	2.64	3.38(2)	131.2
C(3)-H(3B)...O(14)#5	0.99	2.58	3.50(2)	153.7
C(11)-H(11A)...O(14)#7	0.99	2.63	3.51(2)	149.0
C(24)-H(24A)...O(22)	0.99	2.66	3.42(2)	133.5
C(13)-H(13A)...O(24)#1	0.99	2.62	3.19(2)	116.7
O(3)-H(3)...O(39)#3	0.84	2.05	2.872(19)	167.7
N(1)-H(1N)...O(40)#3	1.00	2.24	3.20(2)	160.2
N(1)-H(1N)...O(40')#3	1.00	2.07	3.04(3)	162.0
C(3)-H(3A)...O(34)#4	0.99	2.53	3.428(19)	151.3
N(3)-H(3N)...O(37)#4	1.00	2.35	3.17(3)	138.8
N(11)-H(11N)...O(31)#6	1.00	2.63	3.450(14)	138.8
N(13)-H(13N)...O(36)#3	1.00	2.18	3.12(2)	155.5
C(16)-H(16B)...O(39)#8	0.99	2.59	3.408(19)	140.1
C(17)-H(17B)...O(38)#9	0.99	2.51	3.45(3)	157.8
C(27)-H(27B)...O(40)#11	0.99	2.63	3.57(3)	157.7
C(6)-H(6B)...S(6)	0.99	3.03	3.851(12)	141.5
C(18)-H(18A)...S(4)#6	0.99	2.93	3.752(12)	141.1
C(22)-H(22A)...S(2)	0.99	2.97	3.604(13)	122.7
C(27)-H(27B)...S(5)	0.99	2.99	3.506(12)	113.2

Symmetry transformations used to generate equivalent atoms:
#1 -x+3/2,-y+3/2,-z+1 #2 -x+1,y,-z+1/2 #3 -x+3/2,-y+1/2,-z+1
#4 -x+3/2,y+1/2,-z+3/2 #5 x+1/2,-y+1/2,z+1/2
#6 -x+2,-y+2,-z+1 #7 -x+3/2,y+1/2,-z+1/2 #8 x+1/2,y+1/2,z
#9 -x+2,y,-z+3/2 #10 x+1/2,-y+3/2,z+1/2 #11 x,y+1,z

7

Table S6: Bond lengths [Å] and angles [°] around the Ni cations in compound **1**

Ni(1)-N(1)	2.071(9)	Ni(1)-N(2)	2.108(7)
Ni(1)-N(3)	2.094(8)	Ni(1)-N(4)	2.133(7)
O(1)-Ni(1)	2.107(6)	O(2)-Ni(1)	2.115(6)
N(1)-Ni(1)-N(3)	102.9(4)	O(1)-Ni(1)-O(2)	78.4(2)
N(1)-Ni(1)-O(1)	166.8(3)	N(2)-Ni(1)-O(2)	95.0(3)
N(3)-Ni(1)-O(1)	90.0(3)	N(1)-Ni(1)-N(4)	82.8(3)
N(1)-Ni(1)-N(2)	82.8(3)	N(3)-Ni(1)-N(4)	82.4(3)
N(3)-Ni(1)-N(2)	81.9(3)	O(1)-Ni(1)-N(4)	102.2(3)
O(1)-Ni(1)-N(2)	96.2(3)	N(2)-Ni(1)-N(4)	155.8(3)
N(1)-Ni(1)-O(2)	88.6(3)	O(2)-Ni(1)-N(4)	104.0(3)
N(3)-Ni(1)-O(2)	167.6(3)	Ni(2)-N(14)	2.112(8)
Ni(2)-N(13)	2.092(7)	Ni(2)-N(12)	2.129(7)
Ni(2)-N(11)	2.110(8)	N(23)-Ni(3)-S(6)	88.2(3)
S(1)-Ni(2)	2.494(2)	S(3)-Ni(2)	2.520(2)
N(13)-Ni(2)-N(11)	100.8(3)	N(14)-Ni(2)-S(1)	98.1(2)
N(13)-Ni(2)-N(14)	82.0(3)	N(12)-Ni(2)-S(1)	101.5(2)
N(11)-Ni(2)-N(14)	80.2(3)	N(13)-Ni(2)-S(3)	166.0(2)
N(13)-Ni(2)-N(12)	81.4(3)	N(11)-Ni(2)-S(3)	88.5(2)
N(11)-Ni(2)-N(12)	83.0(3)	N(14)-Ni(2)-S(3)	110.1(2)
N(14)-Ni(2)-N(12)	153.7(3)	N(12)-Ni(2)-S(3)	89.5(2)
N(13)-Ni(2)-S(1)	87.6(2)	S(1)-Ni(2)-S(3)	83.82(7)
N(11)-Ni(2)-S(1)	171.1(3)		
Ni(3)-N(21)	2.105(9)	Ni(3)-N(22)	2.135(9)
Ni(3)-N(23)	2.109(9)	Ni(3)-N(24)	2.144(10)
S(5)-Ni(3)	2.543(2)	S(6)-Ni(3)	2.459(2)
N(21)-Ni(3)-N(23)	100.5(4)	N(22)-Ni(3)-S(6)	93.8(3)
N(21)-Ni(3)-N(22)	80.9(4)	N(24)-Ni(3)-S(6)	105.9(3)
N(23)-Ni(3)-N(22)	82.0(3)	N(21)-Ni(3)-S(5)	86.8(3)
N(21)-Ni(3)-N(24)	82.2(4)	N(23)-Ni(3)-S(5)	166.2(3)
N(23)-Ni(3)-N(24)	81.0(4)	N(22)-Ni(3)-S(5)	110.9(2)
N(22)-Ni(3)-N(24)	153.4(4)	N(24)-Ni(3)-S(5)	88.5(3)
N(21)-Ni(3)-S(6)	169.0(3)	S(6)-Ni(3)-S(5)	86.11(8)

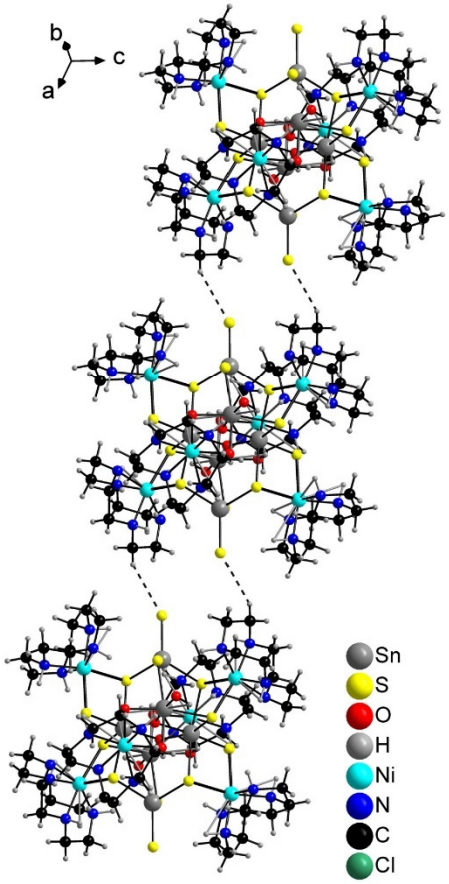

Figure S4: View of the chains with intermolecular C-H···S hydrogen bonding shown as dashed lines.

9

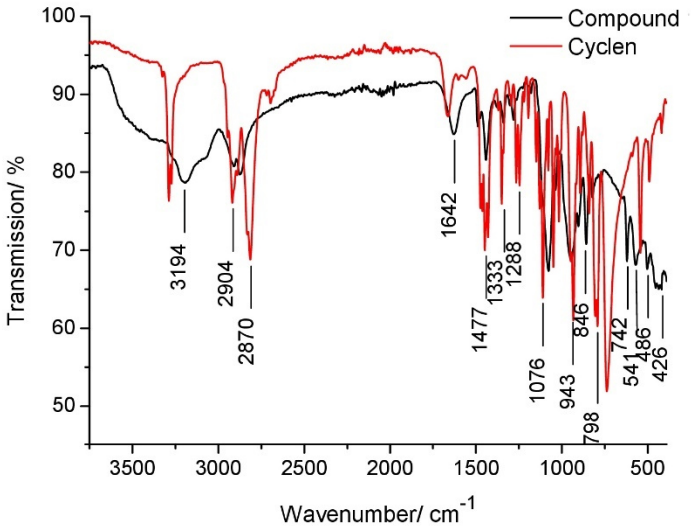

Figure S5: IR spectra of compound **1** (black) and 1,4,7,10-tetraazacyclododecane (cyclen, red).

Table S7: Values of the absorption observed in the IR spectrum of compound **1** together with their assignment

Cyclen	**Compound 1**	**Assignment**
3285m	3194m	ν (NH)
2915s, 2804s	2904w, 2870m	ν (CH_2)
1667m	1642m	δ (NH)
1433m	1477w	δ (CH_2)
1333m	1333w	δ (CH_2)
1255m	1288w	ν (C-N)
1099s	1076s	ν (C-N)
932s	943s	skeleton vib. cyclohex.
831m	864m	δ (C-C-C)
725w, 619w, 564w, 497w	798m, 742s, 541m, 486w	δ (C-C-C)
430w	426w	ν (M-N)

10

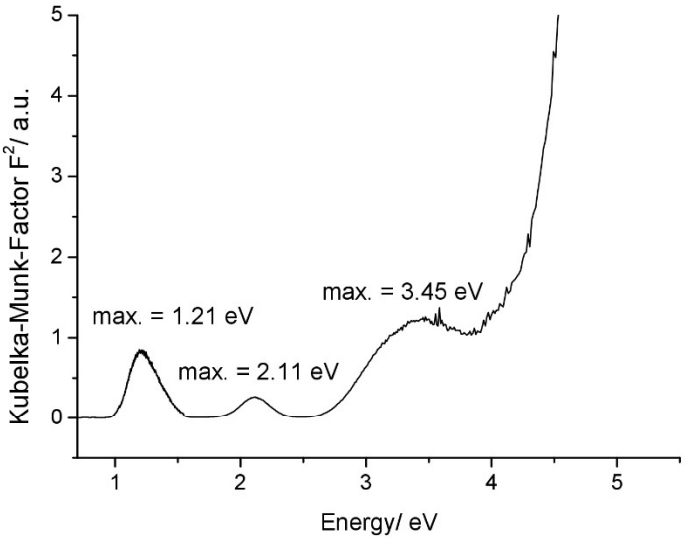

Figure S6: Kubelka-Munk-Factor F^2 as function of energy retrieved form UV/Vis spectroscopic data.

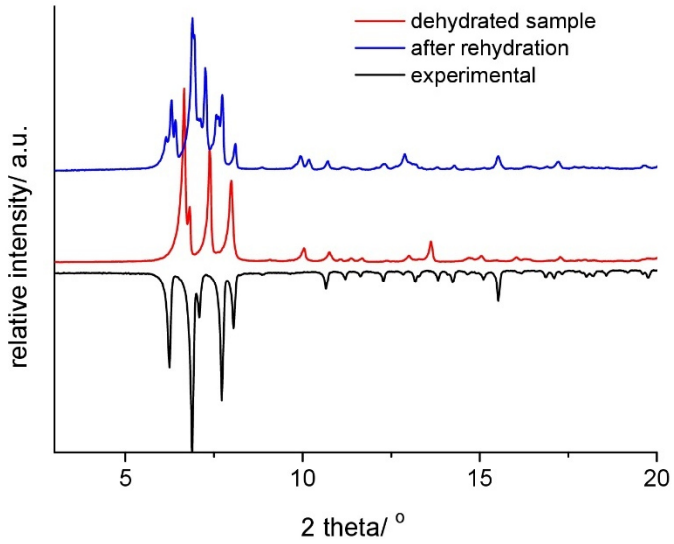

Figure S7: Experimental X-ray powder patterns of compound **1** (black), of the dehydrated sample (red) and of the sample after rehydration (blue).

11

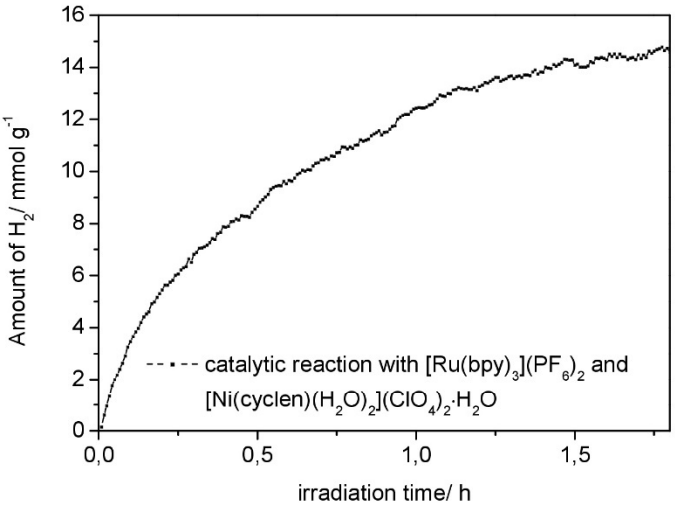

Figure S8: Amount of H_2 as function of time in the photocatalytic hydrogen evolution using $[Ni(cyclen)(H_2O)_2](ClO_4)_2 \cdot H_2O$. Triethylamine was used as sacrificial, $[Ru(bpy)_3](PF_6)_2$ as photosensitizer, water as proton donor and acetonitrile as solvent for the photosensitizer.

12

6.1.2 "Synthesis and Characterization of a Rare Transition-Metal Oxothiostannate and Investigation of Its Photocatalytic Properties"

Supporting Information

Synthesis and Characterization of a rare Transition Metal Oxo-Thiostannate and Investigation of its Photocatalytic Properties

Assma Benkada, Helge Reinsch, Jan Krahmer, Michael Poschmann, Nicole Pienack, Wolfgang Bensch

Content

Table S1	Crystallographic parameters obtained by structure solution and Rietveld refinement of the X-ray powder pattern of **1**	p. 2
Figure S1	Final Rietveld plot with experimental data shown in black, calculated fit shown in red and difference curved shown in blue. The vertical bars indicate the allowed peak positions	p. 3
Figure S2	Solvent accessible space in compound **1** calculated using OLEX2	p. 4
Figure S3	Experimental PXRD pattern of compound **1** compared with the simulated pattern calculated from the results of the Rietveld refinement	p. 5
Table S2	EDX data for compound **1**	p. 5
Figure S4	^{119}Sn-NMR spectra of the precursor $Na_4SnS_4 \cdot 14H_2O$ dissolved in D_2O measured at different temperatures in the range of 1000 to -1000 ppm	p. 6
Table S3	^{119}Sn NMR Integrals of $[SnS_4]^{4-}$ and $[Sn_2S_6]^{4-}$ anions	p. 6
Figure S5	Calculated X-ray powder pattern of compound **1** and experimental powder pattern of a sample isolated after 40 min. in an *in-situ* experiment at 90 °C.	p. 7
Figure S6	^{119}Sn-NMR spectrum of the $Na_4SnS_4 \cdot 14H_2O$ dissolved in D_2O. The pH value of the solution was adjusted to 12.3 and the solution was heated to 90 °C.	p.7
Table S4	Bond lengths and angles of **1**	p. 8
Figure S7	IR spectra of **1** and 1,4,7,10-tetraazacyclododecane (cyclen)	p. 9
Table S5	Values of the absorption observed in the IR spectrum of compound **1** together with their assignment	p. 9
Figure S8	UV-Vis spectrum of **1** plotted as Kubelka-Munk-Factor vs. energy	p. 10
Figure S9	TG, DTA and DTG curves of compound **1**	p. 10
Figure S10	Experimental X-ray powder pattern of the sample after heating to 500 °C compared with simulated X-ray powder patterns of NiO, $Ni_3Sn_2S_2$ and SnS	p. 11
Figure S11	IR-spectrum of the sample after heating to 500 °C	p. 11
Figure S12	Experimental X-ray powder pattern of compound **1**, of the dehydrated compound and calculated X-ray powder pattern for compound **1**; enlarged view of a region of the powder patterns of pristine and dehydrated sample showing the shift of the Bragg reflections	p. 12
Figure S13	Calculated X-ray powder pattern of compound **1** and experimental powder pattern of the sample after rehydration	p. 13
Figure S14	Adsorption isotherms of compound **1** with H_2O and N_2	p. 14
Figure S15	Calculated X-ray powder pattern of compound **1** and experimental powder pattern of the sample after sorption	p. 15
Figure S16	Calculated Connolly surface for **1** using water as probe molecule using Materials Studio	p. 15
Figure S17	Experimental PXRD pattern of compound **1** after phototcatalytic hydrogen evolution compared with their simulated from X-ray data	p. 16
Figure S18	Amount of H_2 as function of time in the photocatalytic hydrogen evolution using $[Ni(cyclen)(H_2O)_2](ClO_4)_2 \cdot H_2O$	p. 16

Table S1: Crystallographic parameters obtained by structure solution and Rietveld refinement of the X-ray powder pattern of **1**

Crystal system	Tetragonal
Space group	$I4_1/a$
a (Å)	26.8992(8)
b (Å)	26.8992(8)
c (Å)	12.3616(6)
V (Å^3)	8944.7(7)
Z	4
Dcalc (g/cm^3)	2.13
Diffractometer	STOE Stadi P
Detector	Dectris Mythen
Radiation	Cu-$K_{\alpha 1}$, λ = 154.0598 pm
Temperature (K)	293
Range of data collection	$3 < 2\theta < 50$
Independent atoms	24
R_{WP} (%)	8.3
R_p (%)	6.5
R_{Bragg} (%)	3.0
R_{Exp} (%)	2.9
GoF	2.9

2

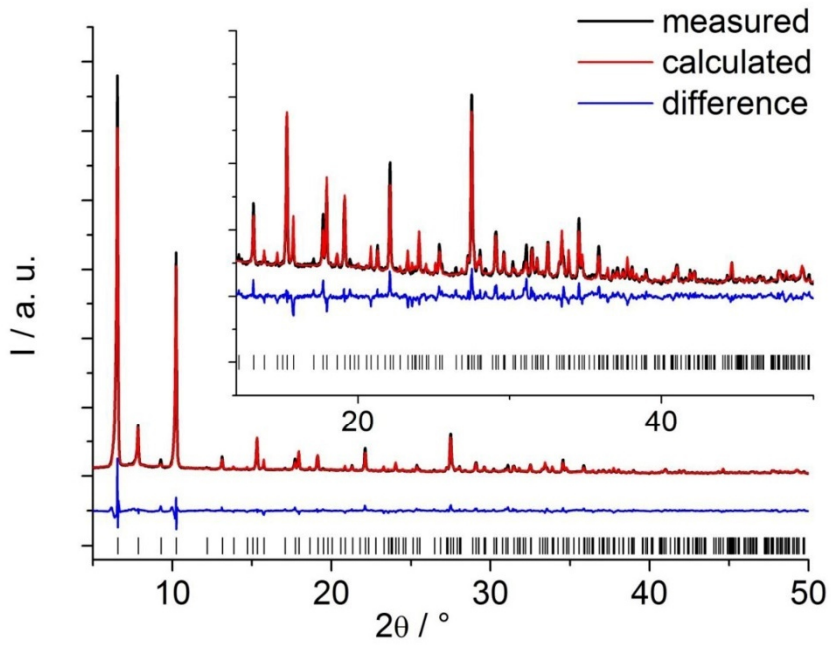

Figure S1: Final Rietveld plot with experimental data shown in black, calculated fit shown in red and difference curved shown in blue. The vertical bars indicate the allowed peak positions.

3

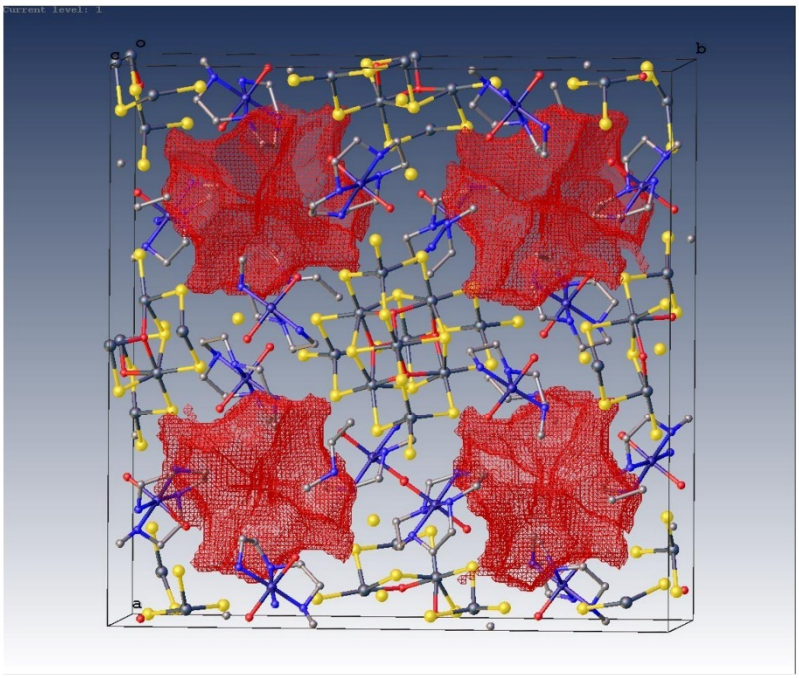

Figure S2: Solvent accessible space in compound **1** calculated using OLEX2 [1].

[1]: O. V. Dolomanov, L. J. Bourhis, R. J. Gildea, J. A. K. Howard, H. Puschmann, *J. Appl. Cryst.* **2009**, *42*, 339-341.

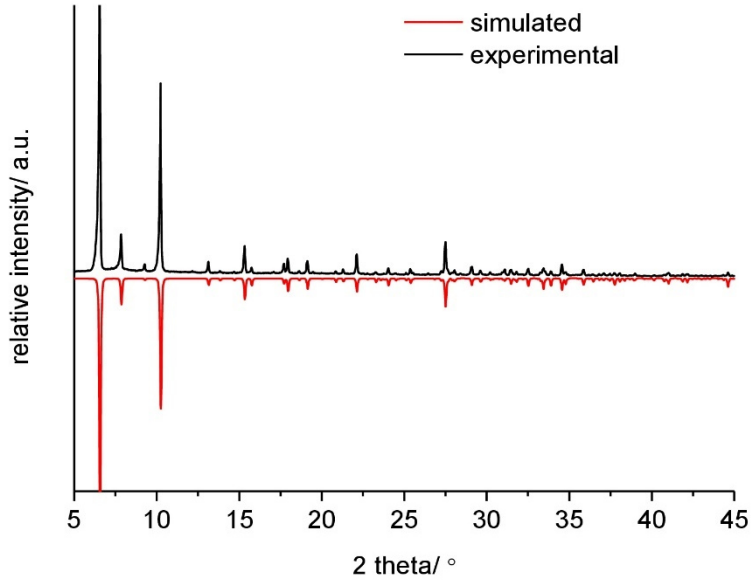

Figure S3: Experimental PXRD pattern of compound **1** (black) compared with the simulated pattern calculated from the results of the Rietveld refinement (red).

Table S2: EDX data for compound **1**

		Ni	Sn	S
Compound **1**	Calculated	4 11.38 %	10 57.54 %	20 31.08 %
	Measured	4.11 11.72 %	10.07 57.95 %	19.51 30.32 %

5

^{119}Sn-NMR

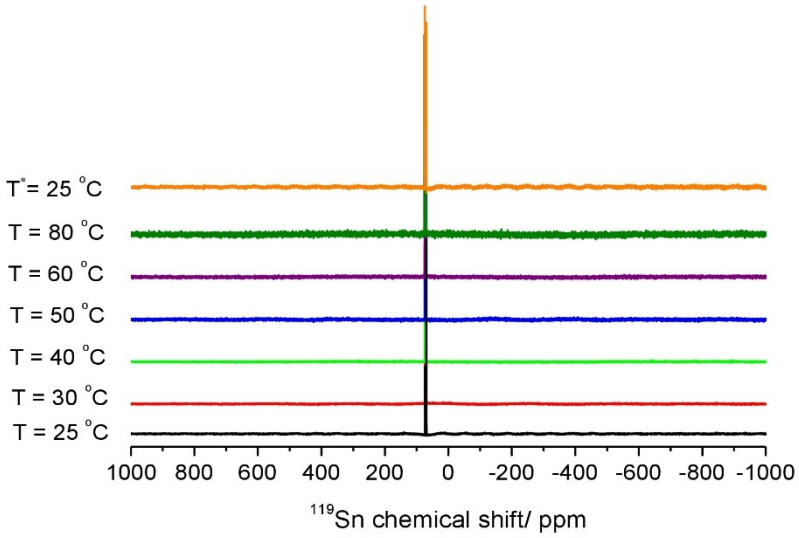

Figure S4: ^{119}Sn-NMR spectra of the precursor $Na_4SnS_4 \cdot 14H_2O$ dissolved in D_2O measured at indicated temperatures in the range of 1000 to -1000 ppm (*: ^{119}Sn-NMR spectrum of the precursor solution, which was heated at 120 °C for 1 h and cooled to room temperature).

Table S3: ^{119}Sn NMR Integrals of $[SnS_4]^{4-}$ and $[Sn_2S_6]^{4-}$ anions

T/ °C	$[Sn_2S_6]^{4-}$	$[SnS_4]^{4-}$
25	2.69	1
30	1.42	1
40	1.52	1
50	1.41	1
60	1.36	1
80	0.92	1
120	0.98	1

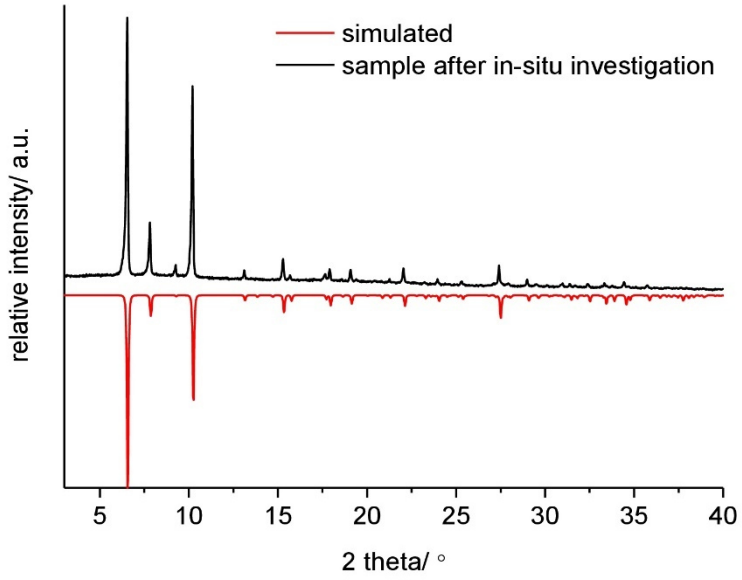

Figure S5: Calculated X-ray powder pattern of compound **1** (red) and experimental powder pattern of a sample isolated after 40 min reaction time in an *in-situ* experiment at 90°C (black).

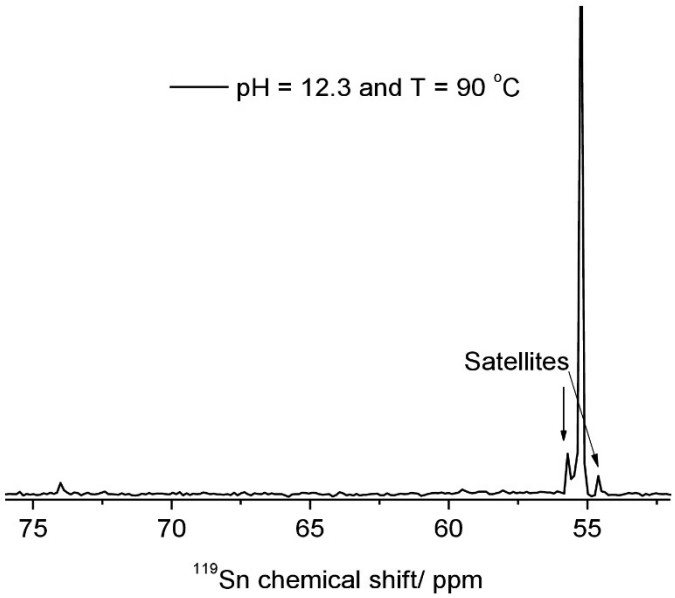

Figure S6: ^{119}Sn-NMR spectrum of the $Na_4SnS_4 \cdot 14H_2O$ dissolved in D_2O. The pH value of the solution was adjusted to 12.3 and the solution was heated to 90 °C.

Table S4: Bond lengths [Å] and angles [°] of compound **1**

Sn(1)-O(5)	2.003(6)	Sn(1)-S(7)	2.459(2)
Sn(1)-O(5)#1	2.263(7)	Sn(1)-S(8)	2.443(6)
Sn(1)-S(4)	2.419(9)	Sn(1)-S(8)#1	2.460(1)
O(5)-Sn(1)-O(5)#1	96.89(6)	O(5)-Sn(1)-S(4)	168.28(7)
O(5)-Sn(1)-S(8)	67.13(7)	O(5)-Sn(1)-S(7)	77.81(4)
O(5)#1-Sn(1)-S(4)	91.07(9)	O(5)-Sn(1)-S(8)#1	83.36(5)
O(5)#1-Sn(1)-S(8)	78.69(8)	O(5)#1-Sn(1)-S(7)	172.67(4)
S(4)-Sn(1)-S(7)	94.93(6)	O(5)#1-Sn(1)-S(8)#1	79.00(5)
S(4)-Sn(1)-S(8)	106.33(3)	S(8)-Sn(1)-S(7)	103.51(6)
S(4)-Sn(1)-S(8)#1	106.65(9)	S(8)-Sn(1)-S(8)#1	140.17(7)
S(7)-Sn(1)-S(8)#1	95.23(1)	S(6)-Sn(2)-S(4)	116.03(6)
Sn(2)-S(3)	2.493(9)	S(6)-Sn(2)-S(3)	96.49(9)
Sn(2)-S(4)	2.467(2)	S(4)-Sn(2)-S(3)	114.58(4)
Sn(2)-S(6)	2.449(8)	Sn(3)-S(3)	2.395(9)
Sn(3)-O(5)	2.001(7)	Sn(3)-S(8)	2.461(5)
O(5)-Sn(3)-O(5)#1	95.54(1)	O(5)-Sn(3)-S(8)	84.09(6)
O(5)-Sn(3)-S(3)	89.40(5)	O(5)#1-Sn(3)-S(8)	66.78(5)
O(5)#1-Sn(3)-S(3)	168.65(4)	S(3)-Sn(3)-S(8)#1	107.24(6)
S(3)-Sn(3)-S(3)#1	87.61(4)	S(8)-Sn(3)-S(8)#1	136.59(7)
S(3)-Sn(3)-S(8)	103.72(3)		
Ni(9)-O(22)	1.882(2)	Ni(9)-N(11)	1.938(3)
Ni(9)-O(23)	1.973(1)	Ni(9)-N(12)	2.021(9)
Ni(9)-N(10)	1.924(8)	Ni(9)-N(13)	1.933(1)
O(22)-Ni(9)-N(10)	87.06(8)	N(10)-Ni(9)-N(12)	91.84(1)
O(22)-Ni(9)-N(11)	90.72(2)	N(10)-Ni(9)-N(13)	88.17(3)
O(22)-Ni(9)-N(12)	89.98(2)	N(10)-Ni(9)-O(23)	93.38(1)
O(22)-Ni(9)-N(13)	95.59(3)	N(11)-Ni(9)-N(12)	87.87(7)
O(23)-Ni(9)-N(12)	82.72(8)	N(11)-Ni(9)-O(23)	88.76(9)
O(22)-Ni(9)-O(23)	172.70(6)	N(13)-Ni(9)-N(12)	174.41(9)
N(10)-Ni(9)-N(11)	177.77(9)	N(13)-Ni(9)-O(23)	91.69(9)

8

Infrared spectroscopy

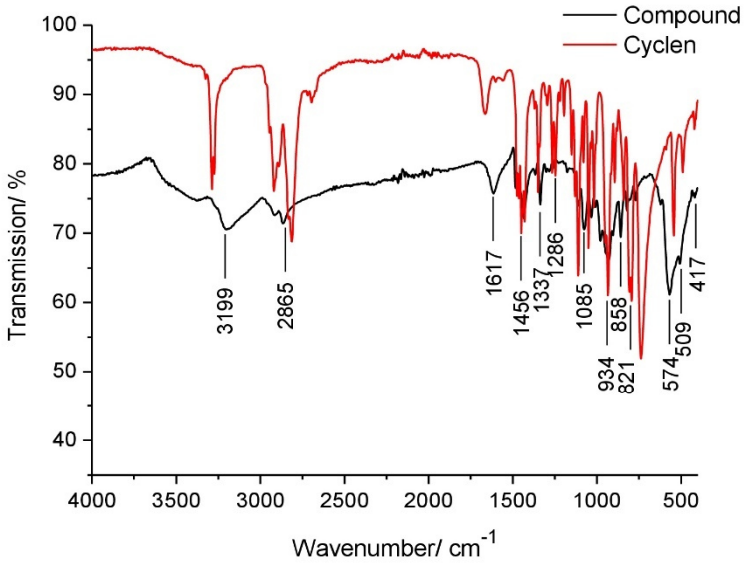

Figure S7: IR spectra of compound **1** (black) and 1,4,7,10-tetraazacyclododecane (cyclen, red).

Table S5: Values of the absorption observed in the IR spectrum of compound **1** together with their assignment

Cyclen	Compound 1	Assignment
3285m	3199m	ν (NH)
2915s, 2804s	2910w, 2865m	ν (CH_2)
1667m	1671m	δ (NH)
1433m	1456w	δ (CH_2)
1333m	1337w	δ (CH_2)
1255m	1286w	ν (C-N)
1099s	1085s	ν (C-N)
932s	934s	skeleton vib. cyclohex.
831m	858m	δ (C-C-C)
725w, 619w, 564w, 497w	821m, 574m, 509w	δ (C-C-C)
430w	417w	ν (M-N)

9

UV/Vis spectroscopy

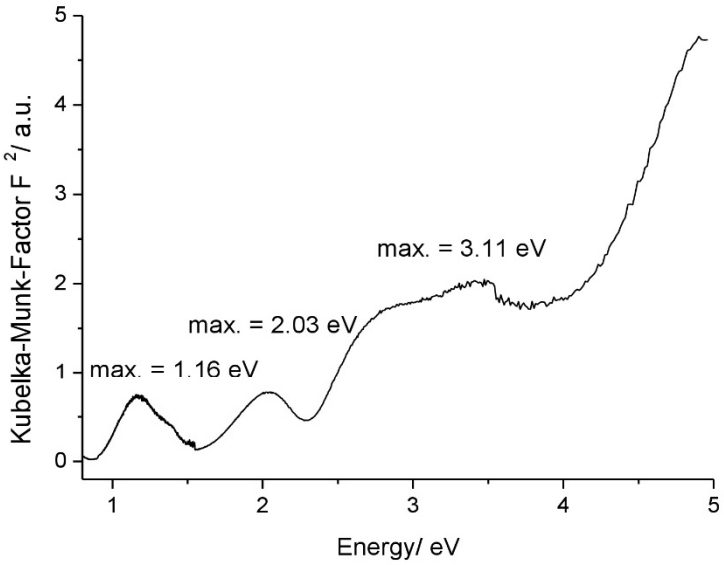

Figure S8: UV-Vis spectrum of **1** plotted as Kubelka-Munk-Factor vs. energy.

Thermogravimetric analysis

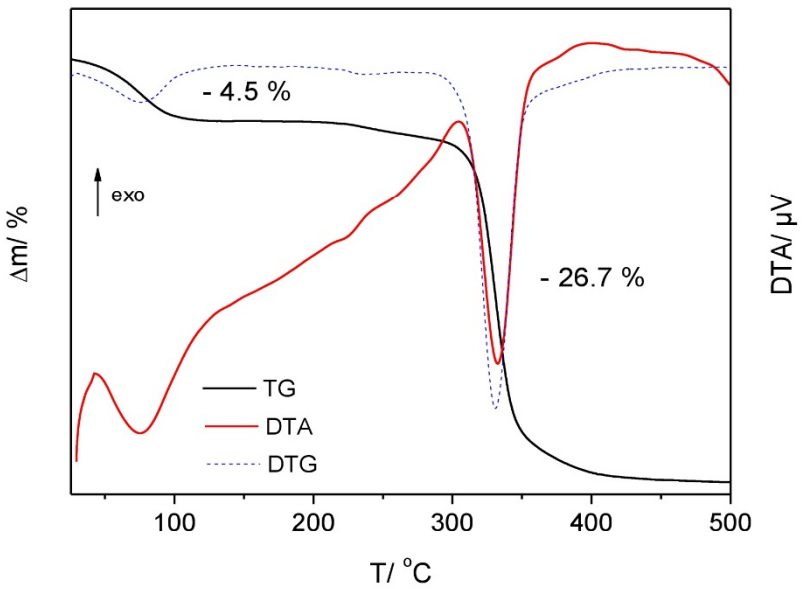

Figure S9: TG (black), DTA (red) and DTG (blue) curves of compound **1**.

10

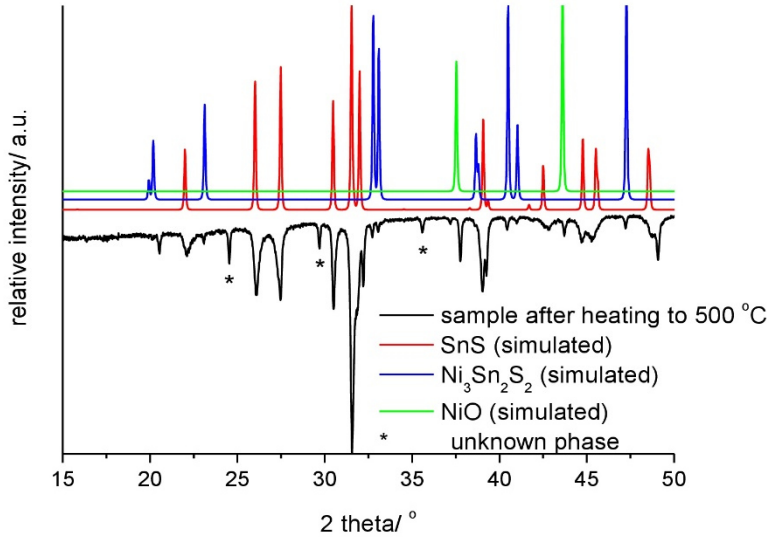

Figure S10: Experimental X-ray powder pattern of the sample after heating to 500 °C (black) compared with simulated X-ray powder patterns of SnS (red), $Ni_3Sn_2S_2$ (blue) and NiO (green).

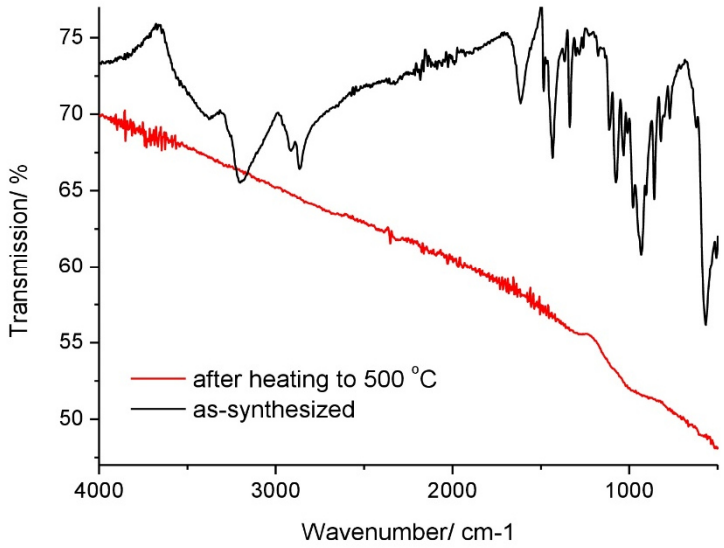

Figure S11: IR-spectra of the samples bevor (black) and after heating to 500 °C (red).

11

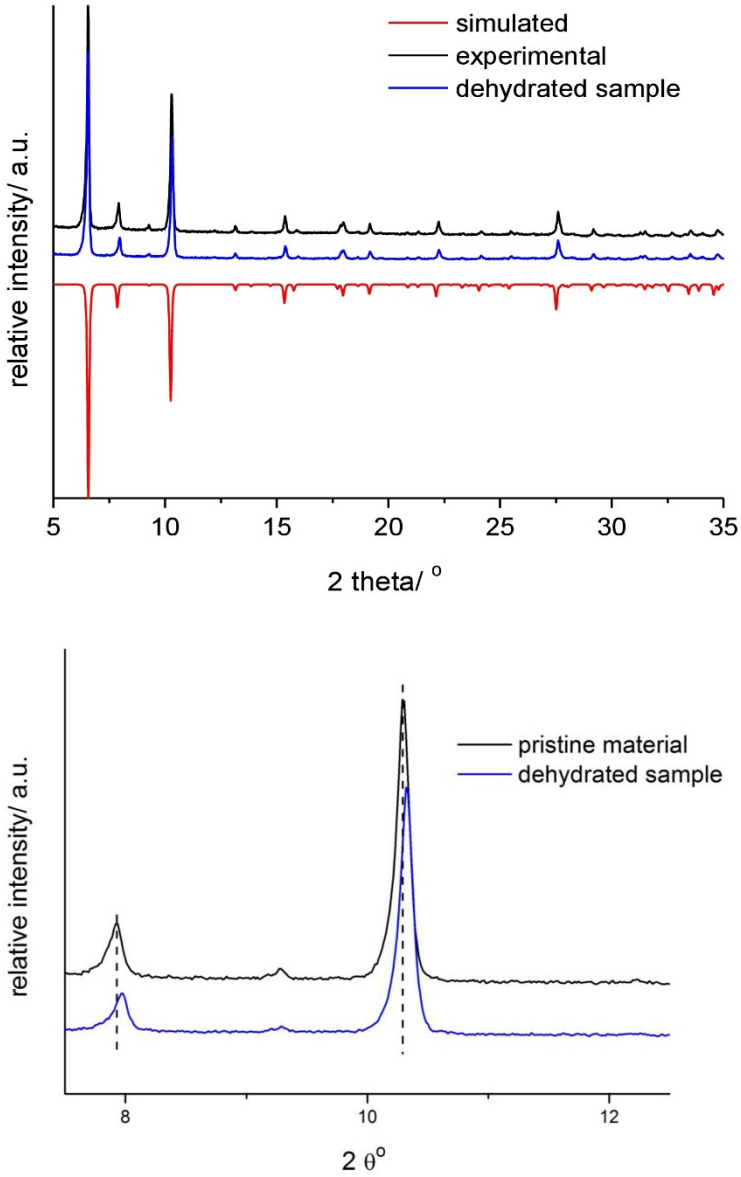

Figure S12: top: Experimental X-ray powder pattern of compound **1** (black), of the dehydrated compound (blue) and calculated X-ray powder pattern for compound **1** (red); bottom: enlarged view of a region of the powder patterns of pristine and dehydrated sample showing the shift of the Bragg reflections.

12

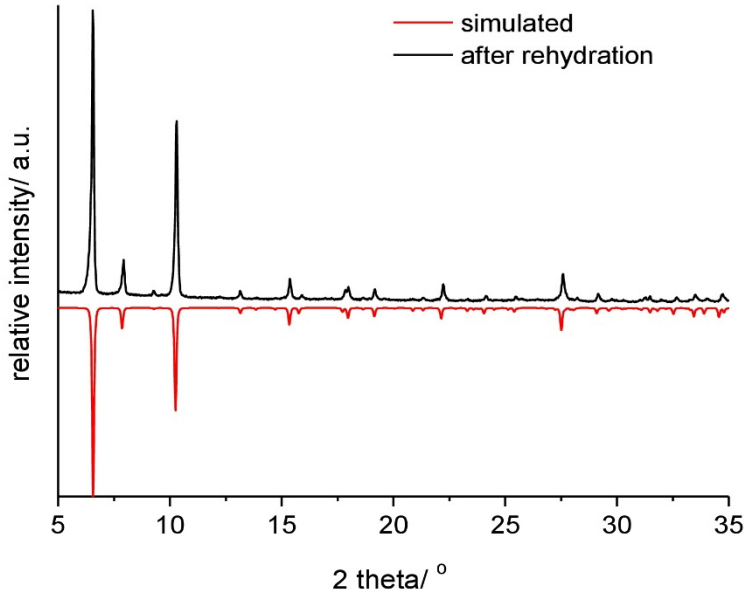

Figure S13: Calculated X-ray powder pattern of compound **1** (red) and experimental powder pattern of the sample after rehydration (black).

13

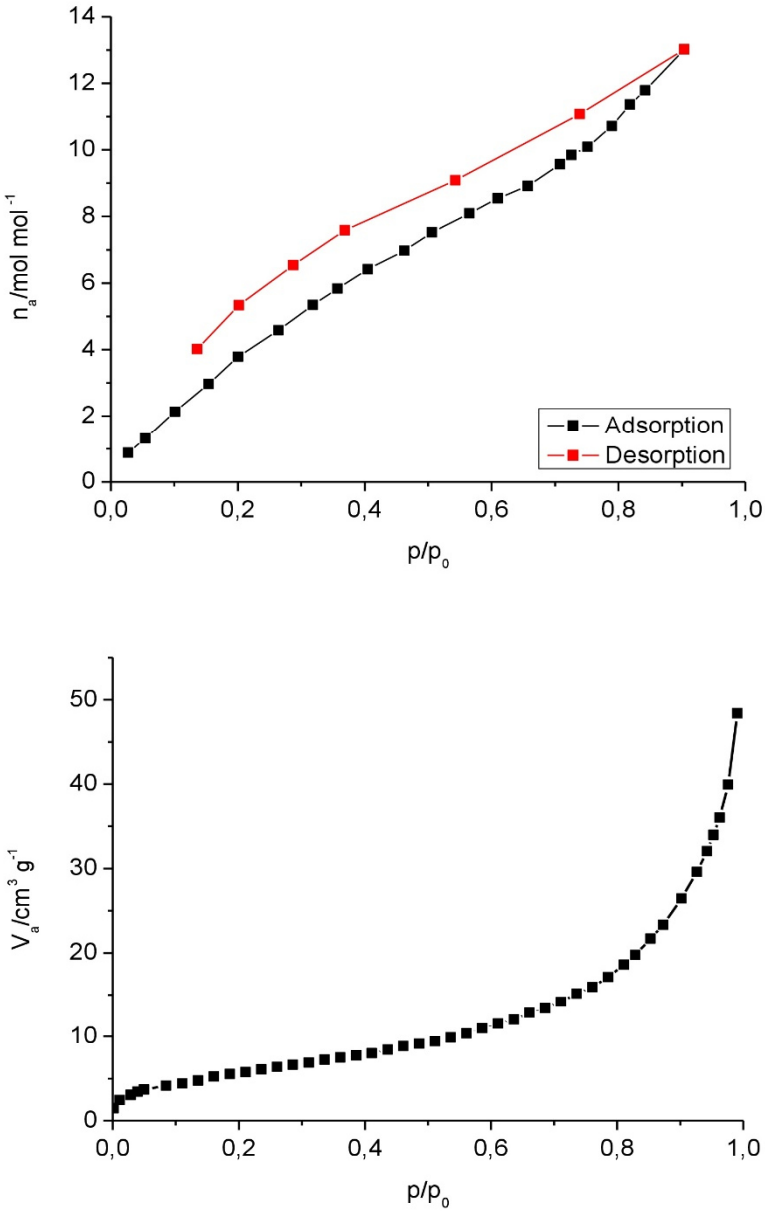

Figure S14: Adsorption isotherms of compound **1** with H_2O (top) and N_2 (bottom).

14

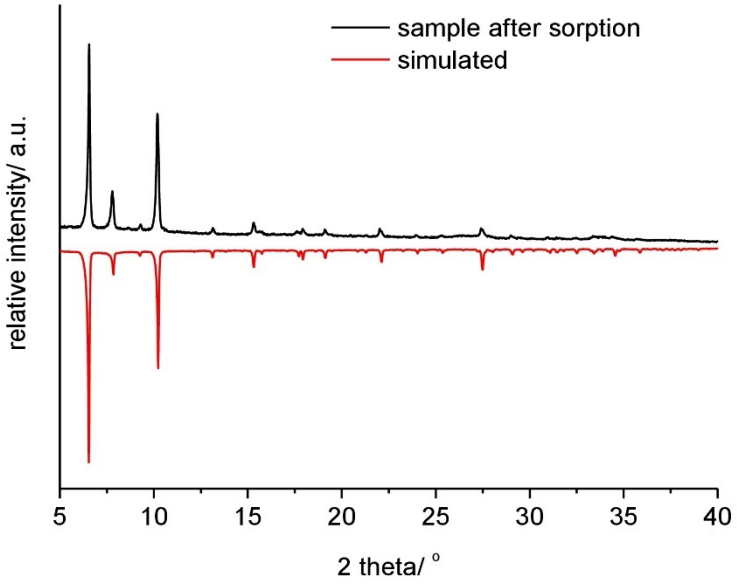

Figure S15: Calculated X-ray powder pattern of compound **1** (red) and experimental powder pattern of the sample after sorption (black).

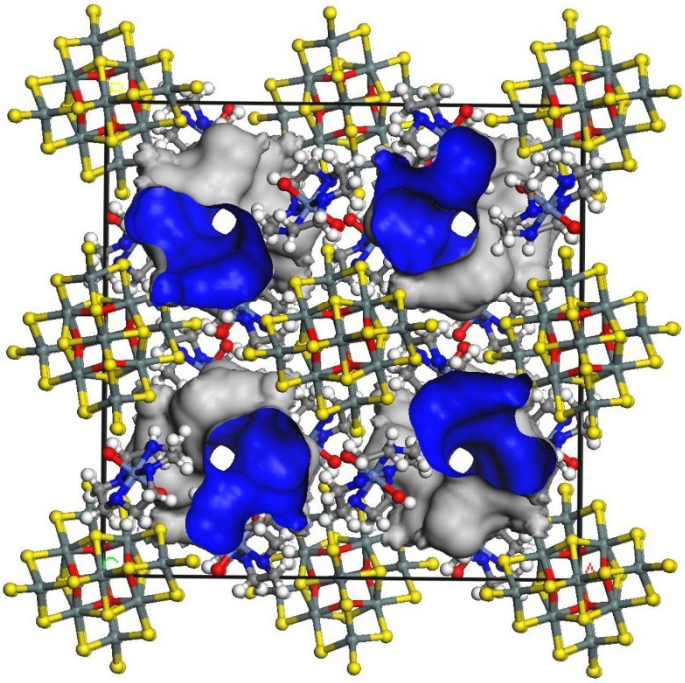

Figure S16: Calculated Connolly surface for **1** using water as probe molecule using Materials Studio.

15

Photocatalysis

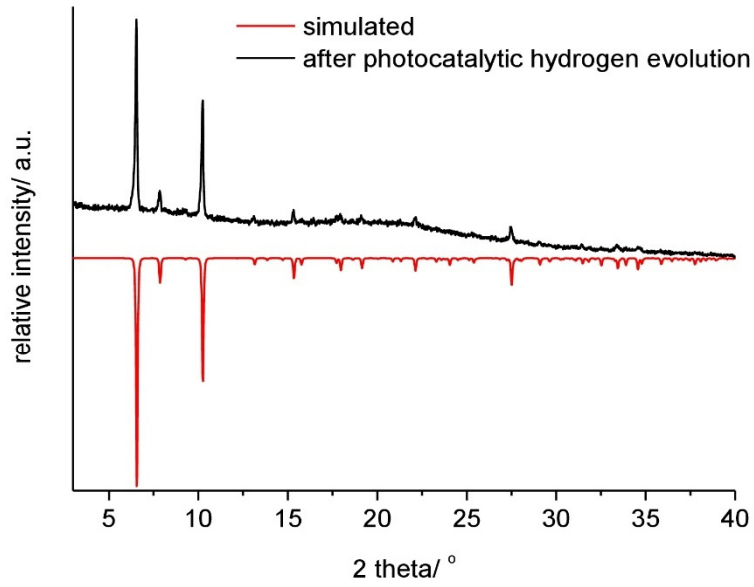

Figure S17: Experimental PXRD pattern of compound **1** (black) after phototcatalytic hydrogen evolution compared with their simulated from X-ray data (red).

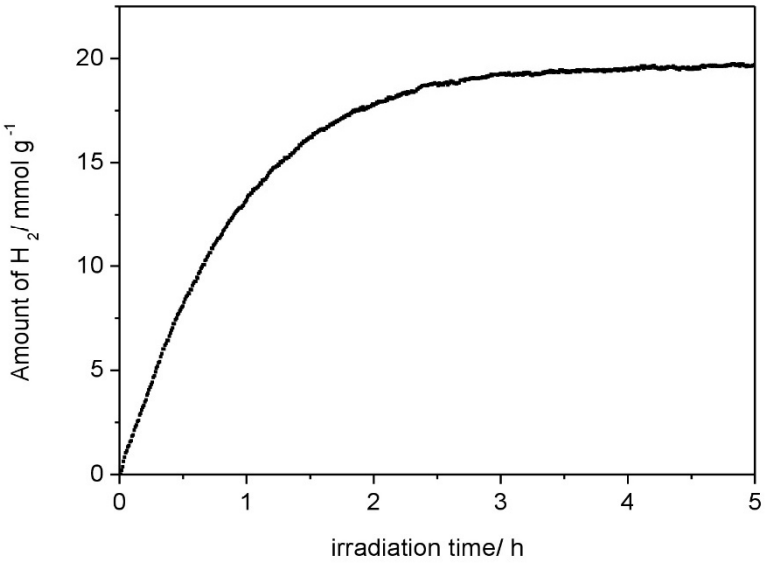

Figure S18: Amount of H_2 as function of time in the photocatalytic hydrogen evolution using $[Ni(cyclen)(H_2O)_2](ClO_4)_2 \cdot H_2O$.

16

6.1.3 "The First Thiostannate Compound with Copper(II) Synthesized Under Ambient Conditions: Crystal Structure, Electronic and Thermal Properties"

Supporting Information

The First Thiostannate Compound with Copper(II) Synthesized Under Ambient Conditions: Crystal Structure, Electronic and Thermal Properties

Assma Benkada, Helge Reinsch, and Wolfgang Bensch*

ejic201900924-sup-0001-SupMat.pdf

Content

Figure S1	UV/Vis absorbance curves of the $[Cu(cyclam)](ClO_4)_2$ complex in H_2O with different concentrations	p. 1
Table S1	Bond lengths and angles of the $[Cu(cyclam)]_2Sn_2S_6$ in compound **I**	p. 2
Figure S2	IR spectrum of compound **I**	p. 3
Table S2	Values of the absorption observed in the IR spectrum of compound **I** together with their assignment	p. 3
Figure S3	Raman spectrum of compound **I**	p. 4
Figure S4	TG, DTA and DTG curves of compound **I**	p. 5
Figure S5	Experimental X-ray powder pattern of compound **I** after heating to 500 °C, Cu_8S_5, Cu_2S, SnS Herzenbergit and SnS	p. 6
Figure S6	Experimental X-ray powder pattern of compound **I**, of the dehydrated sample and of the compound after rehydration	p. 6
Figure S7	Experimental X-ray powder pattern of compound **I**, of the dehydrated sample and of the compound after storing in MeOH	p. 7
Figure S8	Final Rietveld plot with experimental data shown in black, calculated fit shown in red and difference curved	p. 8
Table S3	Crystallographic parameters observed by Rietveld refinement for compound **I**	p. 9
Figure S9	Experimental PXRD pattern of compound **I** compared with the pattern calculated from the results of Rietveld refinement	p. 10
Table S4	EDX data for compound **I**	p. 11

Solubility of [Cu(cyclam)(ClO$_4$)$_2$]

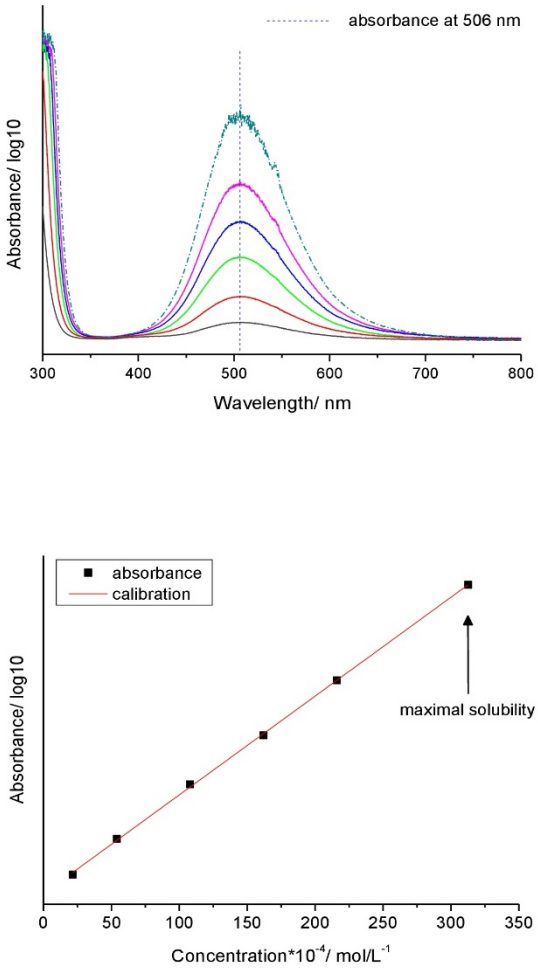

Figure S1: Top: UV/Vis absorbance curves of the [Cu(cyclam)](ClO$_4$)$_2$ complex in H_2O with different concentrations: dark gray (3 mg/ 3 mL), red (7.5 mg/ 3 mL), green (15 mg/ 3 mL), blue (22.5 mg/ 3 mL), pink (30 mg/ 3 mL) and cyan (dotted, saturated solution). Bottom: Absorbance as function of the concentration.

Table S1: Bond lengths [Å] and angles [°] of the $[Cu(cyclam)]_2Sn_2S_6$ in compound **I**

Sn(1)-S(2)	2.394(7)	Sn(1)-S(1)	2.426(9)
Sn(1)-S(3)	2.388(7)	Sn(1)-S(1)#1	2.495(7)
S(2)-Sn(1)-S(1)	110.93(28)	S(2)-Sn(1)-S(1)#1	117.25(24)
S(3)-Sn(1)-S(1)	114.35(26)	S(3)-Sn(1)-S(1)#1	108.95(26)
S(3)-Sn(1)-S(2)	111.30(25)	S(1)-Sn(1)-S(1)	93.04(26)
Sn(1)-S(2)-Cu(1)	119.02(25)	Sn(1)-S(3)-Cu(2)	123.99(24)
Cu(1)-S(2)	2.783(6)	Cu(2)-S(3)	2.765(6)
Cu(1)-N(11)	2.085(9)	Cu(2)-N(1)	1.992(13)
Cu(1)-N(15)	2.056(11)	Cu(2)-N(4)	2.000(10)
N(11)-Cu(1)-N(15)	89.32(36)	N(1)-Cu(2)-N(4)	83.01(43)
N(11)-Cu(1)-N(15)#1	90.68(36)	N(1)-Cu(2)-N(4)#1	96.99(43)
N(11)-Cu(1)-N(11)	180.00	N(1)-Cu(2)-N(1)	180.00
N(15)-Cu(1)-N(15)	180.00	N(4)-Cu(2)-N(4)	180.00
N(11)-Cu(1)-S(2)	92.59(33)	N(1)-Cu(2)-S(3)	87.71(39)
N(11)-Cu(1)-S(2)#1	87.40(33)	N(1)-Cu(2)-S(3)#1	92.29(39)
N(15)-Cu(1)-S(2)	85.95(35)	N(4)-Cu(2)-S(3)	80.99(35)
N(15)-Cu(1)-S(2)#1	94.05(35)	N(4)-Cu(2)-S(3)#1	99.01(35)
S(2)-Cu(1)-S(2)	180.00	S(3)-Cu(2)-S(3)	180.00

Infrared spectroscopy

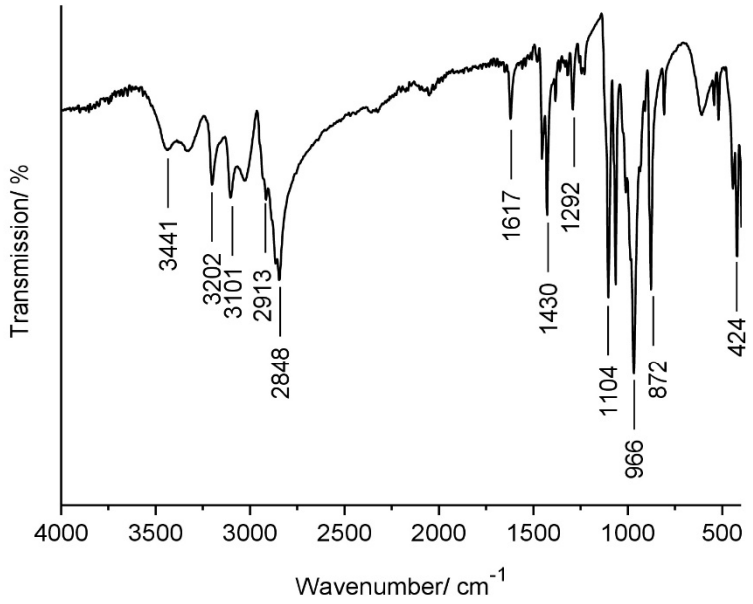

Figure S2: IR spectrum of compound **I**.

Table S2: Values of the absorption observed in the IR spectrum of compound **I** together with their assignment

Compound I	**Cyclam**[1]	**Assignment**
3202, 3101	3268, 3236	ν (NH)
2913, 2848	2917, 2873	ν (CH_2)
1617	---	ν (C-C) + ν (C-N)
1430	1434	ν (C-C) + ν (C-N)
1292	1286	ν (C-C) + ν (C-N)
1104	1110	ν (C-N) + δ (C-H)
996	997	δ (N-H)
872	894	ρ (C-H)
424	---	ν (Cu-N)

[1] G. F. Diaz, R.E. C. Clavijo, M. M. Campos-Vallette, M. S. Saavedra, S. Diez, R. Munoz, Vibrational Spectroscopy 1997, 15, 201-209.

Raman spectroscopy

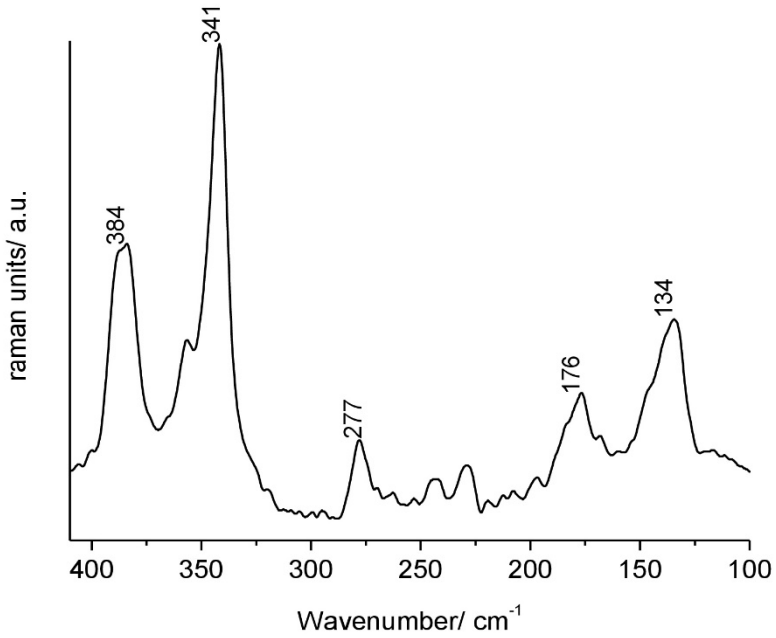

Figure S3: Raman spectrum of compound **I**.

Thermogravimetric analysis

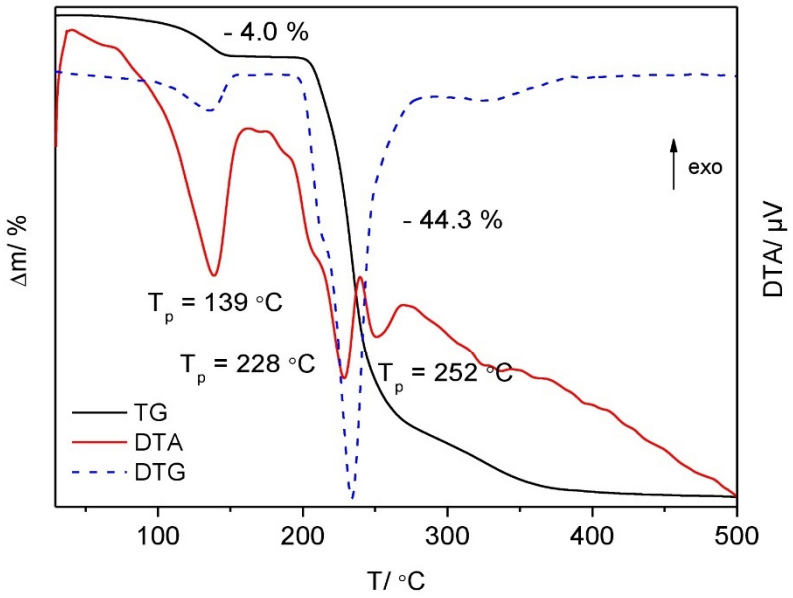

Figure S4: TG (black), DTA (red) and DTG (blue) curves of compound **I**.

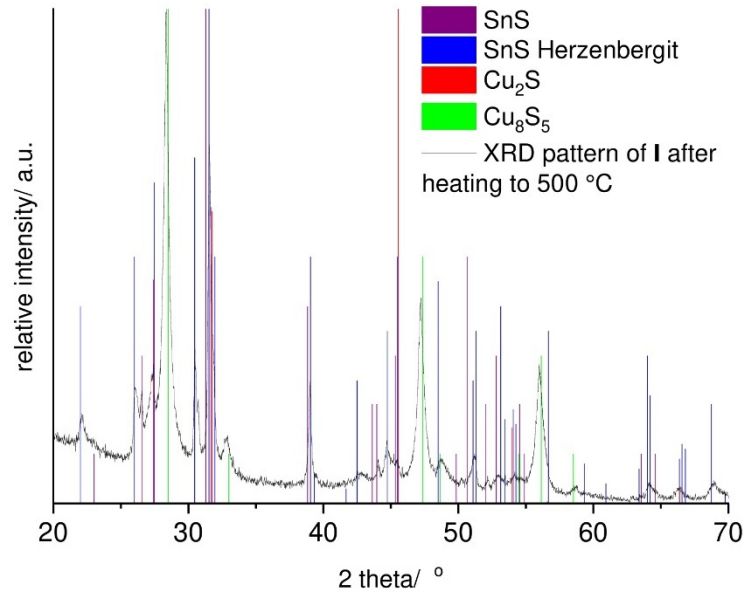

Figure S5: Experimental X-ray powder pattern of compound **I** after heating to 500 °C (black), Cu_8S_5 (green), Cu_2S (red), SnS Herzenbergit (blue) and SnS (purple).

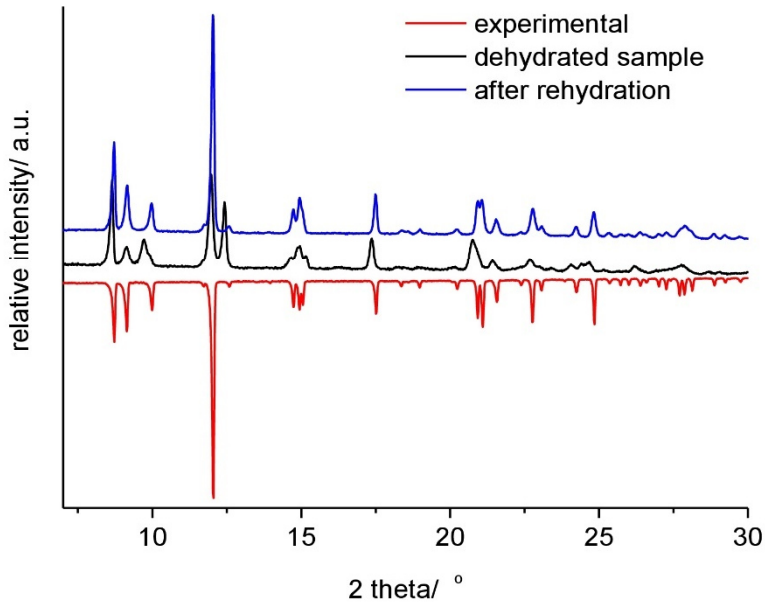

Figure S6: Experimental X-ray powder pattern of compound **I** (red), of the dehydrated sample (black) and of the compound after rehydration (blue).

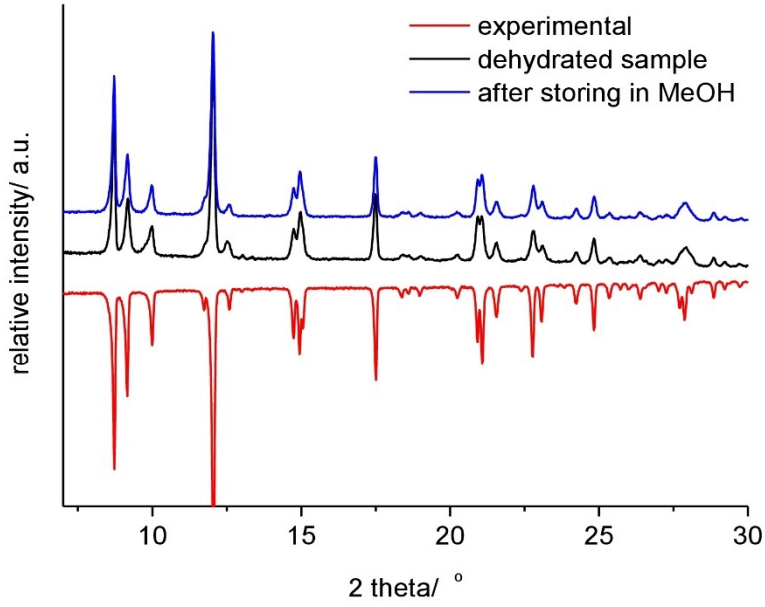

Figure S7: Experimental X-ray powder pattern of compound **I** (red), of the dehydrated sample (black) and of the compound after storing in MeOH (blue).

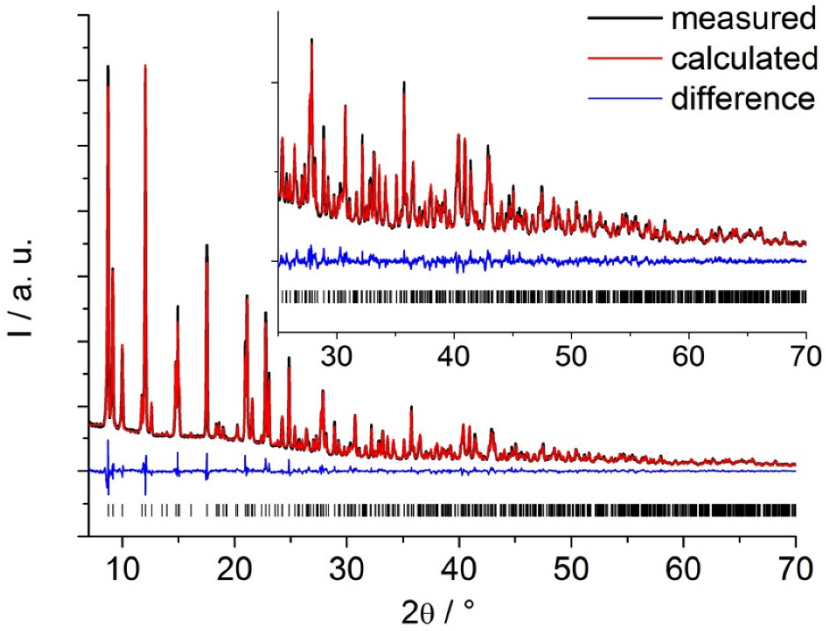

Figure S8: Final Rietveld plot with experimental data shown in black, calculated fit shown in red and difference curved shown in blue. The vertical bars indicate the allowed peak positions.

8

Table S3: Crystallographic parameters observed by Rietveld refinement for compound **I**

	I
Crystal system	Triclinic
Space group	*P*-1
a (Å)	9.0579(2)
b (Å)	9.9419(2)
c (Å)	10.2352(1)
α (°)	97.068(1)
β (°)	94.314(1)
γ (°)	101.514(1)
V (Å^3)	891.57(3)
Z	2
Density (calc.) /g·cm^{-3}	1.750
Diffractometer	STOE Stadi P
Detector	Dectris Mythen
Radiation	Cu-$K_{\alpha1}$, λ = 154.0598 pm
Temperature /K	293
Range of data collection	7 < 2Θ < 70
Independent atoms	21
R_{WP} (%)	4.7
R_{Bragg} (%)	2.2
R_{Exp} (%)	2.3

X-ray powder diffraction

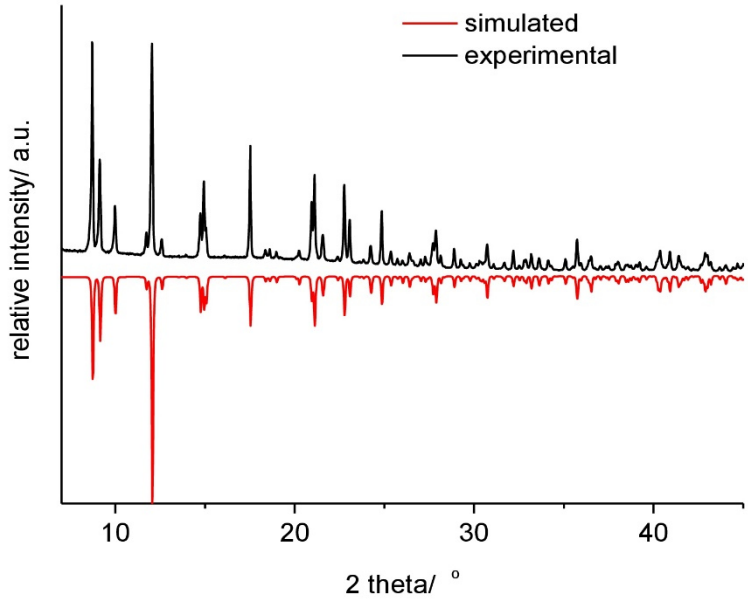

Figure S9: Experimental PXRD pattern of compound **I** (black) compared with the pattern calculated from the results of Rietveld refinement (red).

EDX spectroscopy

Table S4: EDX data for compound **I**

		Cu	Sn	S
Compound **I**	calculated	1.00	1.00	3.00
	measured	1.07	1.00	2.93

6.1.4 “Room temperature synthesis of new thiostannates by slow interdiffusion of different solvents”

Z. Anorg. Allg. Chem. **2020** · ISSN 0044–2313

SUPPORTING INFORMATION

Title: Room Temperature Synthesis of New Thiostannates by Slow Interdiffusion of Different Solvents
Author(s): A. Benkada, C. Näther, W. Bensch*
Ref. No.: z202000199

Room temperature synthesis of new thiostannates by slow interdiffusion of different solvents

Assma Benkada, Christian Näther, Wolfgang Bensch

Supporting Information

Content

Table S1	Crystal and refinement data for compounds **I** and **II**	p. 1
Figure S1	Experimental PXRD pattern of compound **I** compared with the pattern calculated from single-crystal X-ray data	p.2
Figure S2	Experimental PXRD pattern of compound **II** compared with the pattern calculated from single-crystal X-ray data	p. 3
Table S2	EDX data for compounds **I** and **II**	p. 4
Figure S3	UV/Vis absorbance curves of the $[Ni(L_1)](ClO_4)_2$ complex in H_2O, in CH_3CN and in DMSO with different concentrations	p. 5
Figure S4	UV/Vis absorbance curves of the $[Ni(L_2)](ClO_4)_2$ complex in H_2O, in CH_3CN and in DMSO with different concentrations	p. 6
Table S3	Bond lengths and angles of the $[Ni(L_1)][Ni(L_1)Sn_2S_6]_n$ in compound **I**	p. 7
Table S4	Bond lengths and angles of the $[Ni(L_2)]_2[Sn_2S_6]$ in compound **II**	p. 7
Figure S5	View of hydrogen bonding interactions between the $[Sn_2S_6]^{4-}$ unit, Ni^{2+} complexes and water molecules in compound **I** and in compound **II**	p. 8
Figure S6	ORTEP-plots of the crystal structures of compound **I** and **II**	p. 9
Table S5	Intramolecular hydrogen bonds [Å and °] in compound **I**	p. 9
Table S6	Intramolecular hydrogen bonds [Å and °] in compound **II**	p. 10
Figure S7	IR spectra of compounds **I** and **II**	p. 11
Table S7	Values of the absorption observed in the IR spectra of compounds **I** and **II** together with their assignment	p. 12
Figure S8	Raman spectra of compound **I** and **II**	p. 13
Figure S9	Kubelka-Munk-Factor F^2 as function of energy retrieved form UV/Vis spectroscopic data for compound **I** and **II**	p. 14
Figure S10	TG, DTA and DTG curves of compound **I** and **II**	p. 15
Figure S11	Experimental X-ray powder pattern of compound **I** after heating to 500 °C, SnS Herzenbergit, $NiS_{1.97}$, NiS and SnS	p. 16
Figure S12	Experimental X-ray powder pattern of compound **II** after heating to 500 °C, SnS Herzenbergit, $NiS_{1.97}$, NiS and SnS	p. 16

Table S1: Crystal and refinement data for compounds **I** and **II**

	I	**II**
Crystal system	monoclinic	triclinic
Space group	$P2_1/c$	P-1
Empirical formula	$C_{20}H_{56}N_{12}Ni_2O_2S_6Sn_2$	$C_{24}H_{68}N_{12}Ni_2O_4S_6Sn_2$
M (g/mol)	1025.91	1136.06
a (Å)	11.6481(4)	9.1562(6)
b (Å)	14.4268(3)	10.3705(7)
c (Å)	10.8450(3)	12.2897(9)
α (°)	90	66.761(6)
β (°)	95.449(2)	85.350(6)
γ (°)	90	81.308(6)
V (Å^3)	1814.21(9)	1059.67(14)
Temperature (K)	170(2)	200(2)
Z	2	1
Dcalc (g/cm^3)	1.878	1.780
μ (mm^{-1})	2.765	2.381
Scan range (deg)	1.756≤ θ ≤28.004	1.804≤ θ ≤25.195
Reflections collected	22728	8319
Independent reflections	4364	3786
Observed reflections	3946	2951
Goodness-of-fit on F^2	1.047	1.034
R values (I>2σ(I))	R1 = 0.0323, wR2 = 0.0826	R1 = 0.0579, wR2 = 0.1374
R values (all data)	R1 = 0.0370, wR2 = 0.0853	R1 = 0.0778, wR2 = 0.1470
Res. Elec. Dens. (e.Å^{-3})	0.730 and -0.816	1.589 and -0.819

X-ray powder diffraction

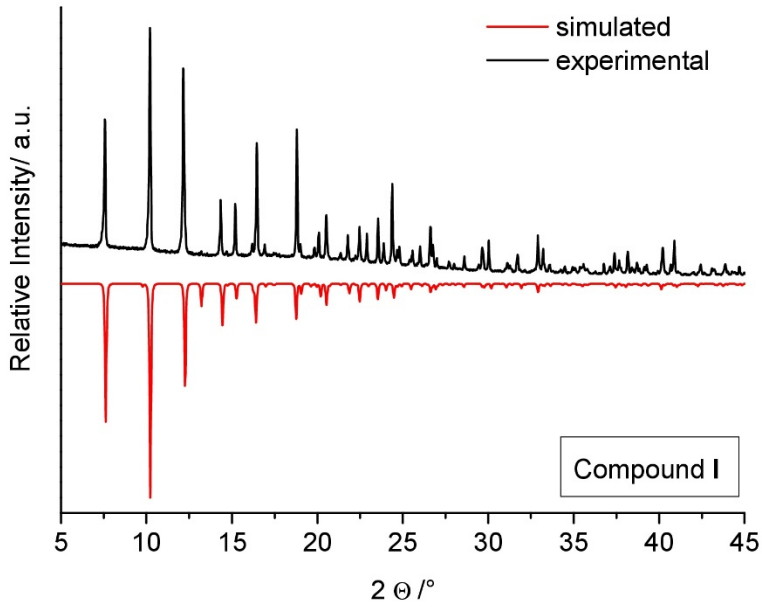

Figure S1: Experimental PXRD pattern of compound **I** (black) compared with the pattern calculated from single-crystal X-ray data (red).

2

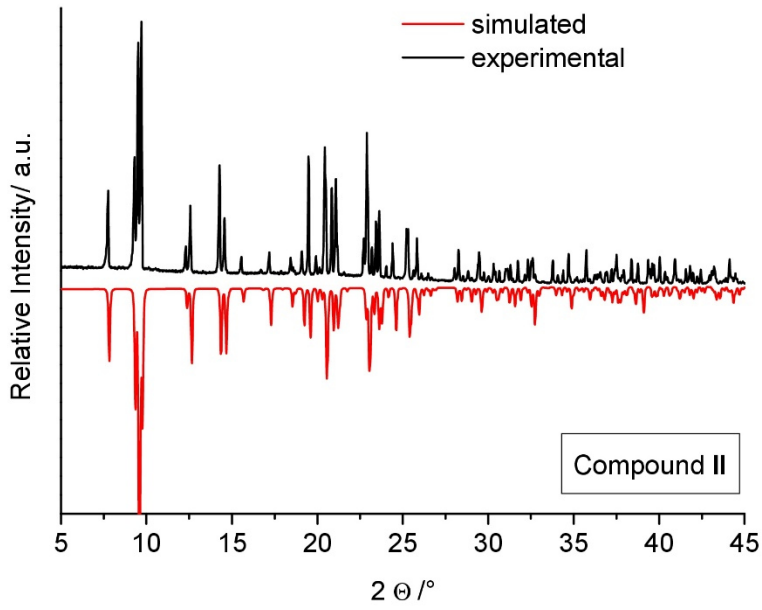

Figure S2: Experimental PXRD pattern of compound **II** (black) compared with the pattern calculated from single-crystal X-ray data (red).

EDX spectroscopy

Table S2: EDX data for compounds **I** and **II**

		Ni	Sn	S
Compound **I**	calculated	1	1	3
	measured	1.08	1.02	2.9
Compound **II**	calculated	1	1	3
	measured	0.97	0.94	3.09

Solubility of [Ni(L$_1$)](ClO$_4$)$_2$

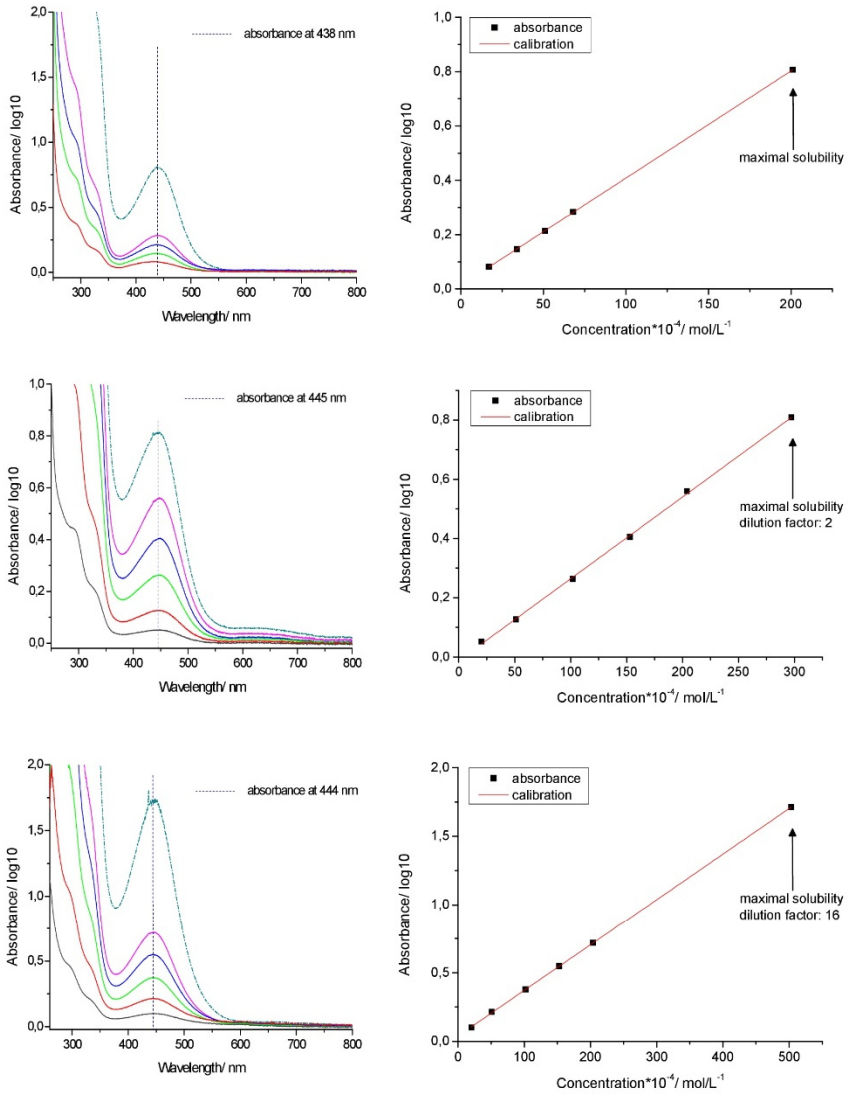

Figure S3: Left: UV/Vis absorbance curves of the [Ni(L$_1$)](ClO$_4$)$_2$ complex in H_2O (top), in CH_3CN (middle) and in DMSO (bottom), with different concentrations: dark gray (3 mg/ 3 mL), red (7.5 mg/ 3 mL), green (15 mg/ 3 mL), blue (22.5 mg/ 3 mL), pink (30 mg/ 3 mL) and cyan (dotted, saturated solution) in CH_3CN and in DMSO. In H_2O: red (2.5 mg/ 3 mL), green (5 mg/ 3 mL), blue (7.5 mg/ 3 mL), pink (10 mg/ 3 mL) and cyan (dotted, saturated solution). Right: Absorbance as function of the concentration.

Solubility of $[Ni(L_2)](ClO_4)_2$

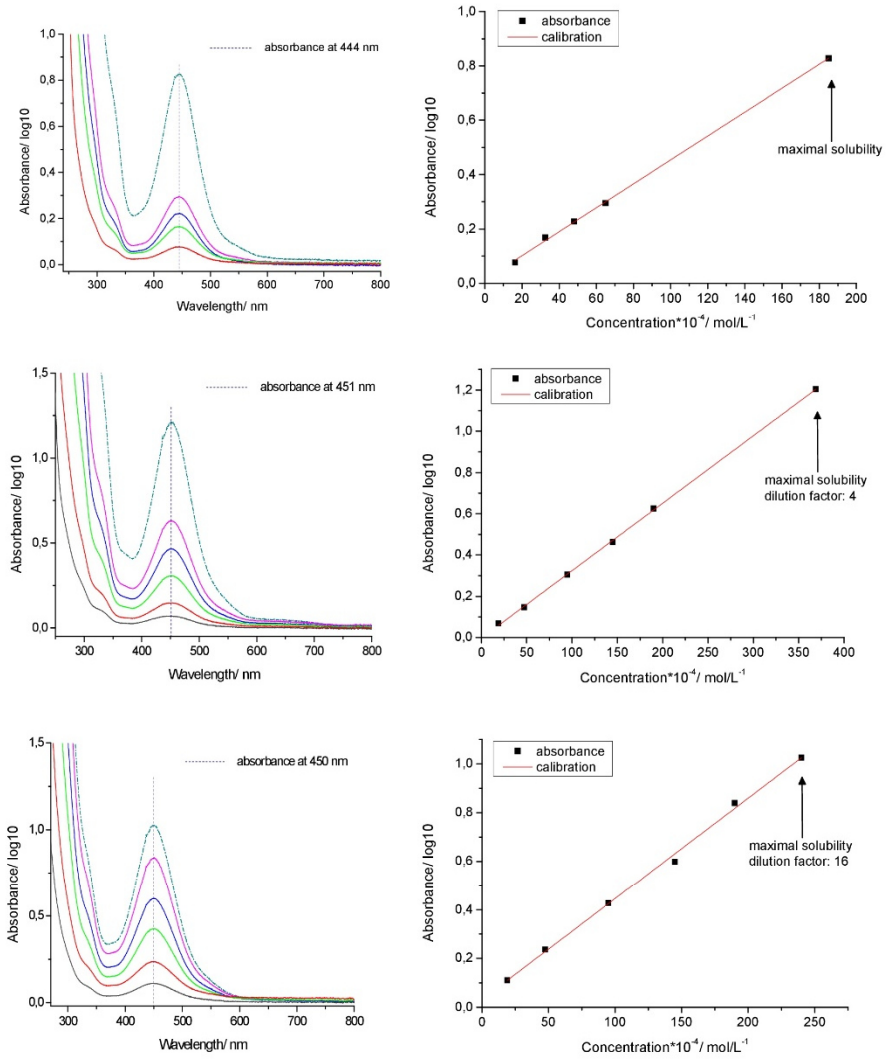

Figure S4: Left: UV/Vis absorbance curves of the $[Ni(L_2)](ClO_4)_2$ complex in H_2O (top), in CH_3CN (middle) and in DMSO (bottom), with different concentrations: dark gray (3 mg/ 3 mL), red (7.5 mg/ 3 mL), green (15 mg/ 3 mL), blue (22.5 mg/ 3 mL), pink (30 mg/ 3 mL) and cyan (dotted, saturated solution) in CH_3CN and in DMSO. In H_2O: red (2.5 mg/ 3 mL), green (5 mg/ 3 mL), blue (7.5 mg/ 3 mL), pink (10 mg/ 3 mL) and cyan (dotted, saturated solution) Right: Absorbance as function of the concentration.

Table S3: Bond lengths [Å] and angles [°] of the $[Ni(L_1)][Ni(L_1)Sn_2S_6]_n$ in compound **I**

Sn(1)-S(2)	2.3320(8)	Sn(1)-S(3)	2.4440(8)
Sn(1)-S(1)	2.3469(8)	Sn(1)-S(3)#1	2.4566(8)
S(3)-Sn(1)#1	2.4566(8)	S(2)-Sn(1)-S(3)#1	110.43(3)
S(2)-Sn(1)-S(1)	116.24(3)	S(1)-Sn(1)-S(3)#1	111.25(3)
S(2)-Sn(1)-S(3)	114.69(3)	S(3)-Sn(1)-S(3)#1	92.53(3)
S(1)-Sn(1)-S(3)	109.28(3)	Sn(1)-S(3)-Sn(1)#1	87.47(3)
Sn(1)-S(1)-Ni(1)	121.62(3)		
Ni(1)-N(1)#2	2.047(3)	Ni(1)-N(3)#2	2.057(3)
Ni(1)-N(1)	2.048(3)	Ni(1)-S(1)#2	2.6444(8)
Ni(1)-N(3)	2.057(3)	S(1)-Ni(1)	2.6444(8)
N(1)#2-Ni(1)-N(1)	180.00(16)	N(3)-Ni(1)-S(1)#2	89.44(8)
N(1)#2-Ni(1)-N(3)	85.56(14)	N(3)#2-Ni(1)-S(1)#2	90.56(8)
N(1)-Ni(1)-N(3)	94.44(14)	N(1)#2-Ni(1)-S(1)	96.40(9)
N(1)#2-Ni(1)-N(3)#2	94.44(14)	N(1)-Ni(1)-S(1)	83.60(9)
N(1)-Ni(1)-N(3)#2	85.56(14)	N(3)-Ni(1)-S(1)	90.56(8)
N(3)-Ni(1)-N(3)#2	180.00(15)	N(3)#2-Ni(1)-S(1)	89.44(8)
N(1)#2-Ni(1)-S(1)#2	83.60(9)	S(1)#2-Ni(1)-S(1)	180.0
N(1)-Ni(1)-S(1)#2	96.40(9)		
Ni(2)-N(11)#3	1.933(3)	Ni(2)-N(13)	1.936(3)
Ni(2)-N(11)	1.933(3)	Ni(2)-N(13)#3	1.936(3)
N(11)#3-Ni(2)-N(11)	180.0	N(11)#3-Ni(2)-N(13)#3	93.40(11)
N(11)#3-Ni(2)-N(13)	86.60(11)	N(11)-Ni(2)-N(13)#3	86.60(11)
N(11)-Ni(2)-N(13)	93.40(11)	N(13)-Ni(2)-N(13)#3	180.0

Symmetry transformations used to generate equivalent atoms:
#1 -x+2,-y+1,-z+1 #2 -x+1,-y+1,-z+1 #3 -x+2,-y+1,-z

Table S4: Bond lengths [Å] and angles [°] of the $[Ni(L_2)]_2[Sn_2S_6]$ in compound **II**

Sn(1)-S(3)	2.325(2)	Sn(1)-S(1A)	2.457(2)
Sn(1)-S(2)	2.335(2)	Sn(1)-S(1)	2.460(2)
S(1)-Sn(1A)	2.457(2)	S(3)-Sn(1)-S(1)	110.80(7)
S(3)-Sn(1)-S(2)	116.28(7)	S(2)-Sn(1)-S(1)	112.15(8)
S(3)-Sn(1)-S(1A)	115.29(8)	S(1A)-Sn(1)-S(1)	91.97(6)
S(2)-Sn(1)-S(1A)	107.85(7)	Sn(1A)-S(1)-Sn(1)	88.03(6)
Ni(1)-N(3B)	1.915(7)	Ni(2)-N(11C)	1.929(7)
Ni(1)-N(3)	1.915(7)	Ni(2)-N(11)	1.929(7)
Ni(1)-N(1B)	1.929(7)	Ni(2)-N(13)	1.932(6)
Ni(1)-N(1)	1.929(7)	Ni(2)-N(13C)	1.932(6)
N(3B)-Ni(1)-N(3)	180.0	N(11C)-Ni(2)-N(11)	180.0
N(3B)-Ni(1)-N(1B)	93.0(3)	N(11C)-Ni(2)-N(13)	87.7(3)
N(3)-Ni(1)-N(1B)	87.0(3)	N(11)-Ni(2)-N(13)	92.3(3)
N(3B)-Ni(1)-N(1)	87.0(3)	N(11C)-Ni(2)-N(13C)	92.3(3)
N(3)-Ni(1)-N(1)	93.0(3)	N(11)-Ni(2)-N(13C)	87.7(3)
N(1B)-Ni(1)-N(1)	180.0	N(13)-Ni(2)-N(13C)	180.0

Symmetry transformations used to generate equivalent atoms: A: -x+1,-y+1,-z+1; B: -x+1,-y,-z+2; C: -x+2,-y+1,-z+1

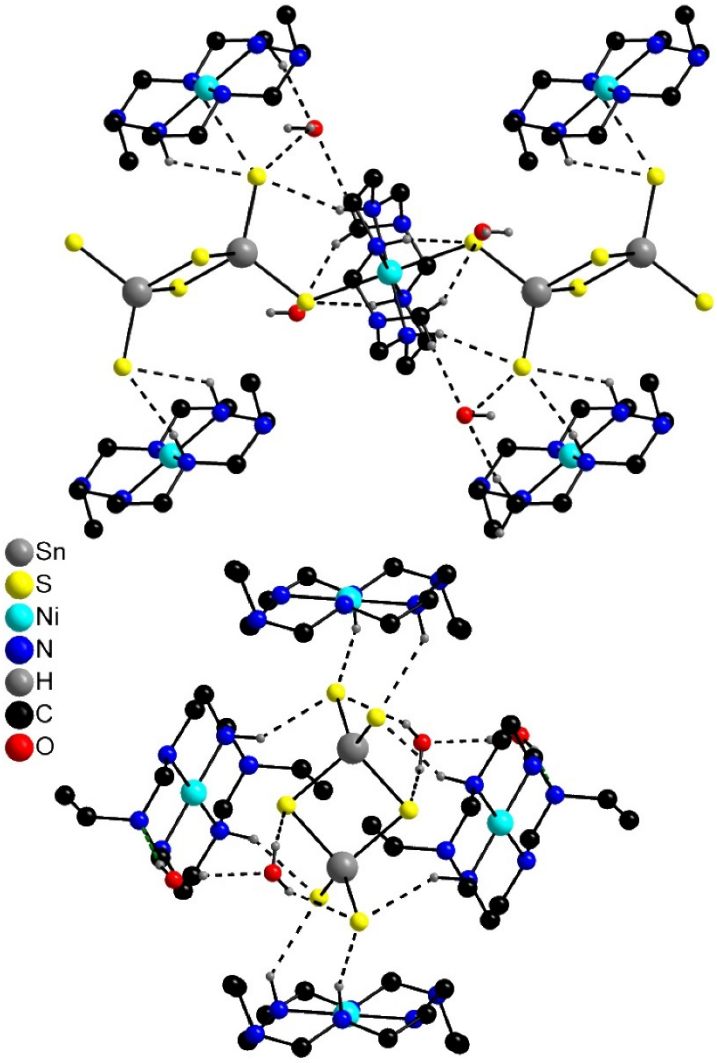

Figure S5: View of hydrogen bonding interactions (black dashed lines) between the $[Sn_2S_6]^{4-}$ unit, Ni^{2+} complexes and water molecules in compound **I** (top) and in compound **II** (bottom).

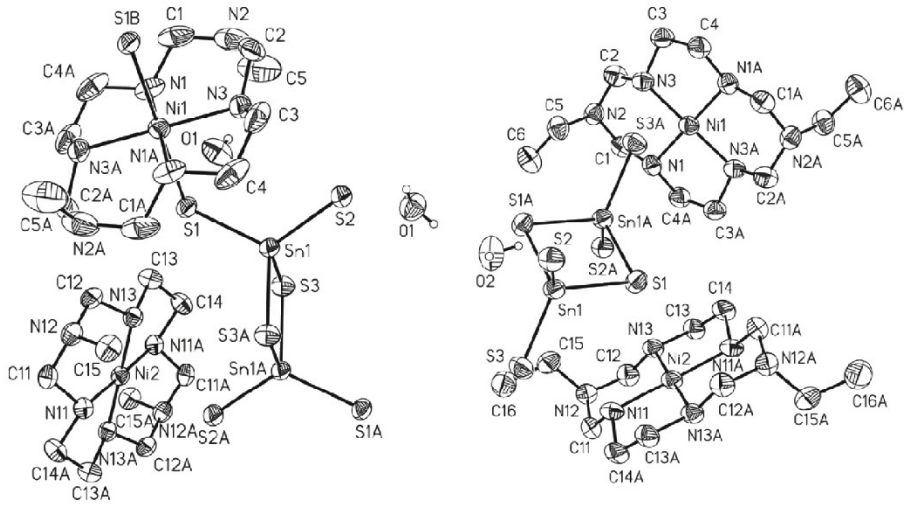

Figure S6: ORTEP-plots on the 50% probability level of the crystal structures of compound **I** (left) and of compound **II** (right).

Table S5: Intramolecular hydrogen bonds [Å and °] in compound **I**

D-H...A	d(D-H)	d(H...A)	d(D...A)	<(DHA)
N(1)-H(1)...S(1)	1.00	2.66	3.159(3)	110.7
C(1)-H(1B)...S(1)#2	0.99	2.93	3.576(4)	123.8
C(2)-H(2A)...S(1)#2	0.99	2.85	3.476(4)	122.0
N(3)-H(3)...S(2)	1.00	2.60	3.503(3)	150.0
C(3)-H(3A)...S(1)#2	0.99	2.92	3.475(4)	116.7
C(4)-H(4B)...N(2)#4	0.99	2.54	3.473(5)	157.3
C(5)-H(5A)...O(1)#5	0.98	2.31	3.208(11)	151.9
C(5)-H(5C)...O(1)	0.98	2.42	3.069(9)	123.0
N(11)-H(11)...S(2)#1	1.00	2.82	3.466(3)	122.8
C(11)-H(11B)...S(3)#6	0.99	2.97	3.736(4)	134.9
C(12)-H(12A)...S(1)	0.99	2.90	3.799(4)	151.4
N(13)-H(13)...S(2)#1	1.00	2.78	3.443(3)	124.2
C(13)-H(13B)...O(1)#7	0.99	2.45	3.417(7)	165.7
C(14)-H(14C)...S(3)#7	0.99	2.86	3.668(3)	139.9
C(14)-H(14B)...S(3)	0.99	2.82	3.638(3)	140.7
O(1)-H(1C)...S(2)#7	0.84	2.65	3.263(6)	130.8

Symmetry transformations used to generate equivalent atoms: #1 -x+2,-y+1,-z+1 #2 -x+1,-y+1,-z+1 #3 -x+2,-y+1,-z #4 -x+1,y-1/2,-z+3/2 #5 x,-y+3/2,z+1/2 #6 -x+2,y-1/2,-z+1/2 #7 x,-y+3/2,z-1/2

Table S6: Intramolecular hydrogen bonds [Å and °] in compound **II**

D-H...A	d(D-H)	d(H...A)	d(D...A)	<(DHA)
N(1)-H(1)...S(2)#1	1.00	2.37	3.295(7)	154.2
C(2)-H(2A)...O(1)#4	0.99	2.59	3.261(12)	124.8
N(3)-H(3)...S(3)#1	1.00	2.61	3.364(7)	132.3
C(4)-H(4B)...S(3)#1	0.99	2.84	3.579(10)	131.7
N(11)-H(11)...S(3)	1.00	2.48	3.391(7)	151.7
C(11)-H(11A)...S(1)#3	0.99	2.83	3.590(9)	134.5
C(11)-H(11B)...O(1)#5	0.99	2.60	3.515(12)	153.2
N(13)-H(13)...S(2)#1	1.00	2.52	3.394(7)	145.9
O(1)-H(1O1)...O(2)	0.84	2.01	2.834(11)	168.0
O(1)-H(2O1)...N(12)#6	0.84	2.30	3.128(10)	167.3
O(2)-H(1O2)...S(2)#1	0.84	2.52	3.317(8)	159.3
O(2)-H(2O2)...S(1)#1	0.84	2.60	3.317(8)	143.3

Symmetry transformations used to generate equivalent atoms:
#1 -x+1,-y+1,-z+1; #3 -x+2,-y+1,-z+1; #4 -x,-y+1,-z+2; #5 -x+1,-y+2,-z+1; #6 x-1,y,z

Infrared spectroscopy

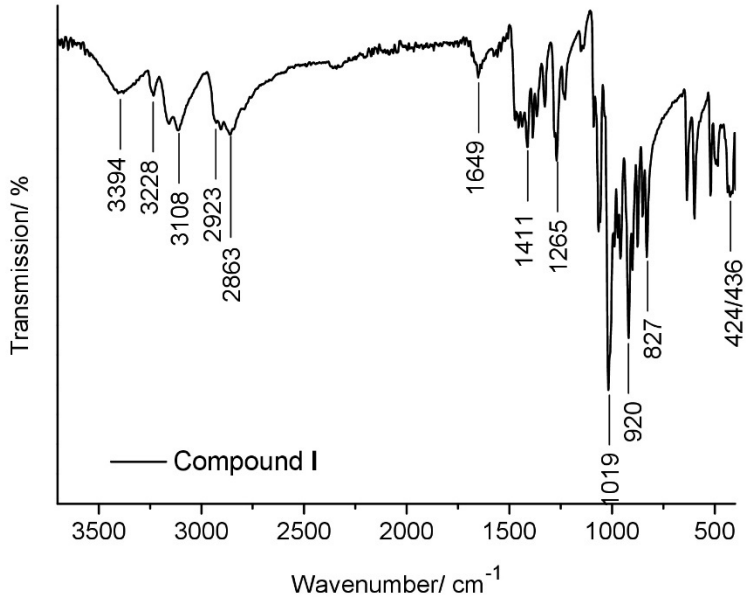

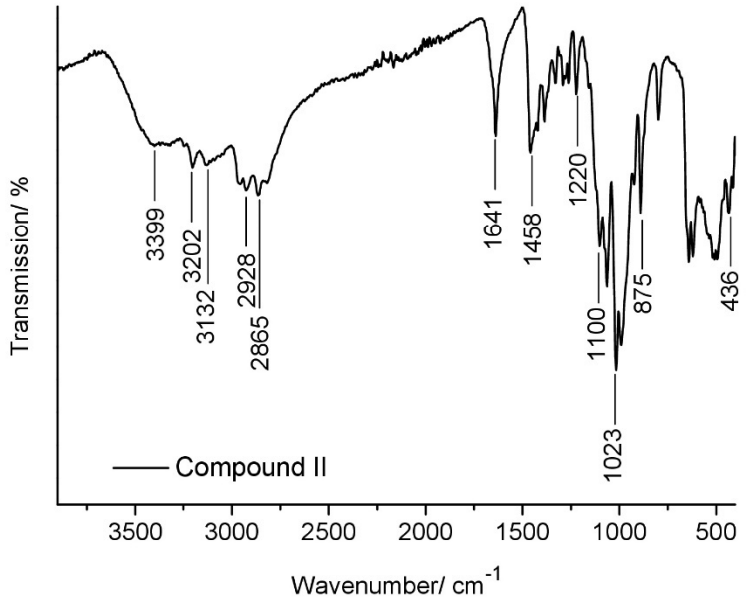

11

Figure S7: IR spectra of compound **I** (top) and **II** (bottom).

Table S7: Values of the absorption observed in the IR spectra of compounds **I** and **II** together with their assignment [1,2]

Compound I	Compound II	Assignment
3228m, 3108m	3202m, 3132m	ν (NH)
2923w	2928w	ν (CH_3)
2863m	2865m	ν (CH_2)
1649m	1641m	ν (C-C) + ν (C-N)
1411w	1458m	ν (C-C) + ν (C-N)
1265w	1220w	ν (C-C) + ν (C-N)
1019s	1100m	ν (C-N) + δ (C-H)
920s	1023s	δ (N-H)
827m	875m	ρ (C-H)
424/436w	436w	ν (Ni-N)

[1] G. F. Diaz, R.E. C. Clavijo, M. M. Campos-Vallette, M. S. Saavedra, S. Diez, R. Munoz, *Vibrational Spectroscopy* **1997**, *15*, 201-209.

[2] M. P. Suh, E. Y. Lee, B. Y. Shim, *Inorg. Chim. Acta* **1998**, *269*, 337-341.

Raman spectroscopy

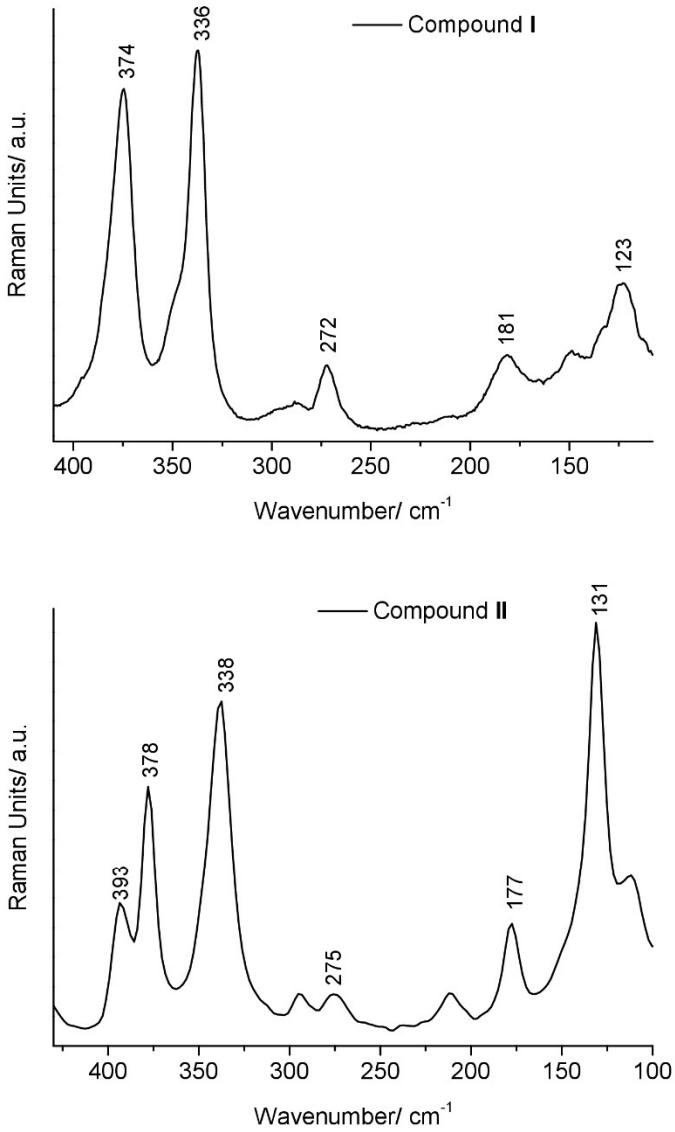

Figure S8: Raman spectra of compound **I** (top) and **II** (bottom).

13

UV/Vis spectroscopy

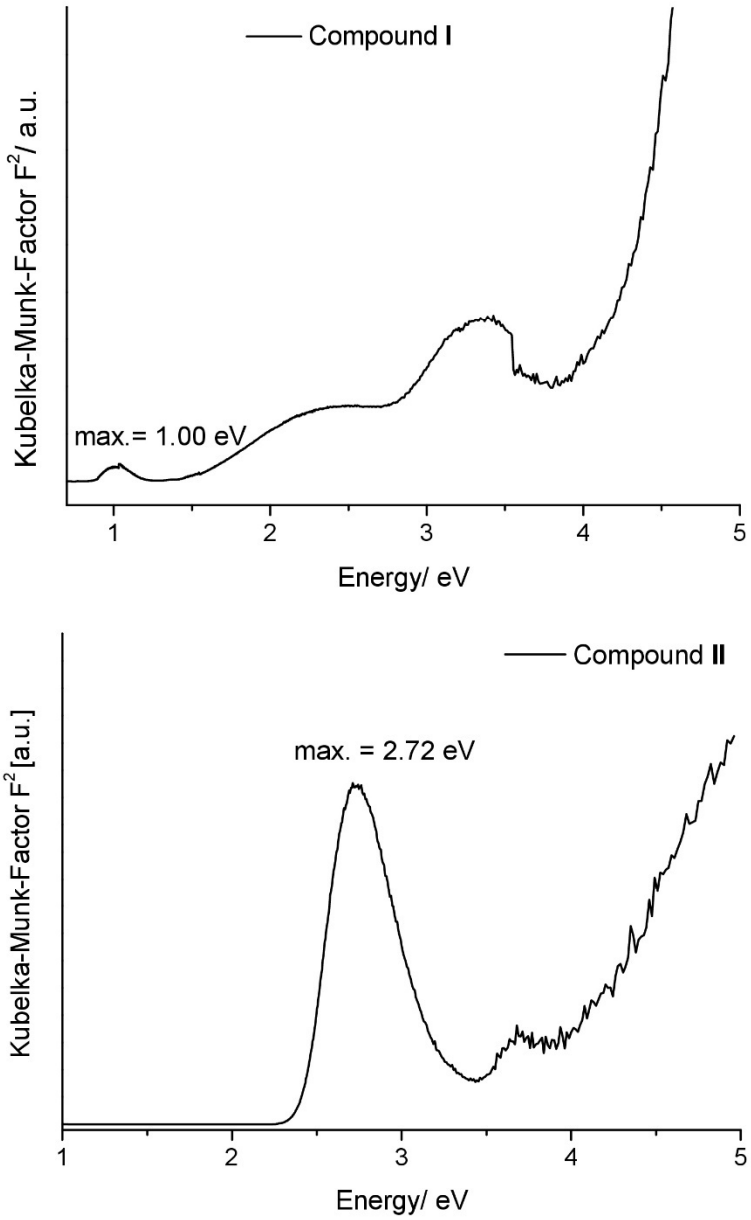

Figure S9: Kubelka-Munk-Factor F^2 as function of energy retrieved form UV/Vis spectroscopic data for compound **I** (top) and **II** (bottom).

Thermogravimetric analysis

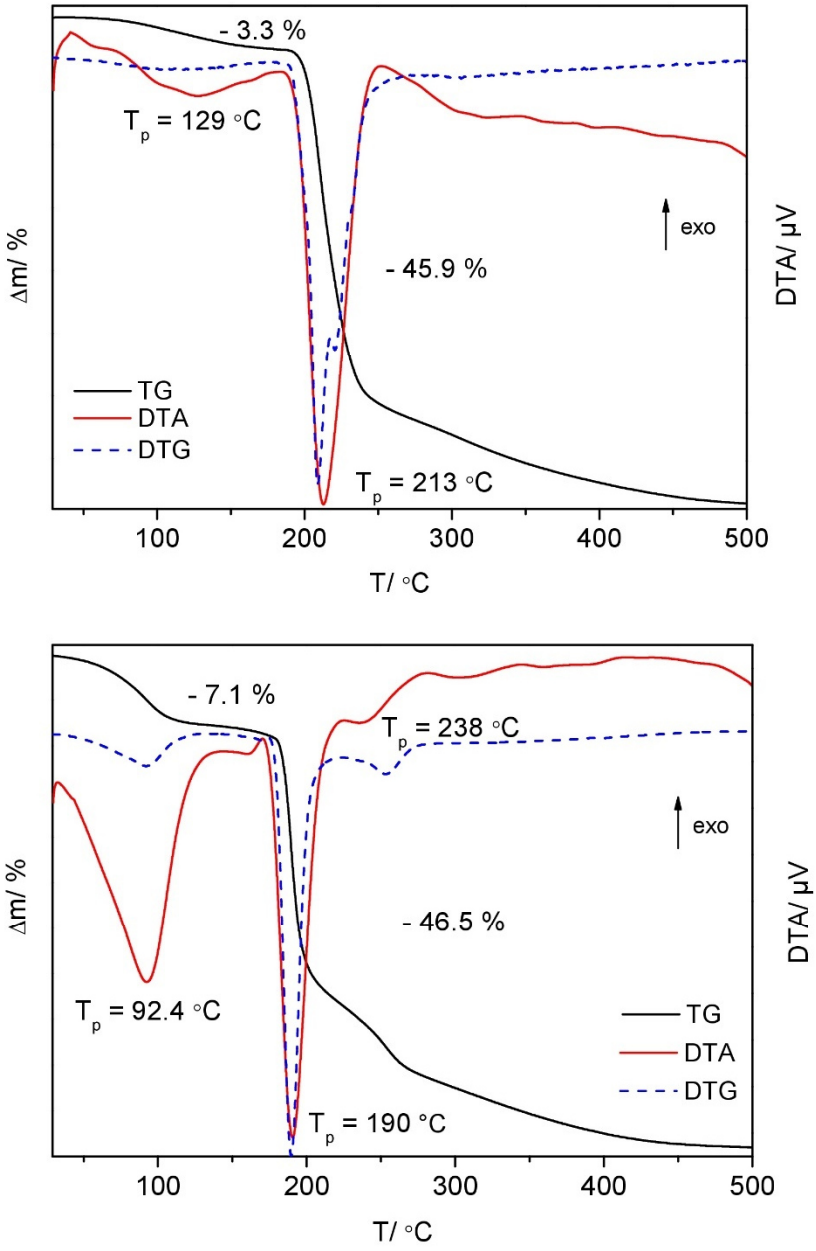

Figure S10: TG (black), DTA (red) and DTG (blue) curves of compound **I** (top) and **II** (bottom).

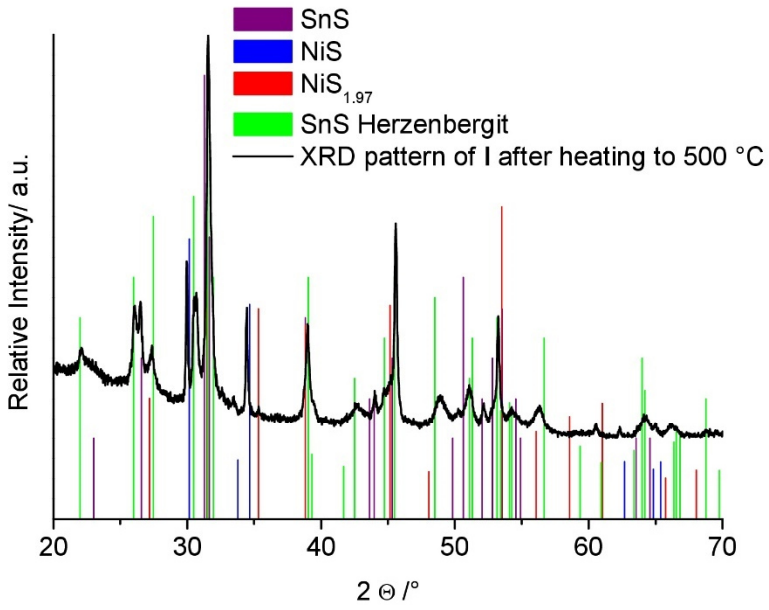

Figure S11: Experimental X-ray powder pattern of compound **I** after heating to 500 °C (black), SnS Herzenbergit (green), $NiS_{1.97}$ (red), NiS (blue) and SnS (purple).

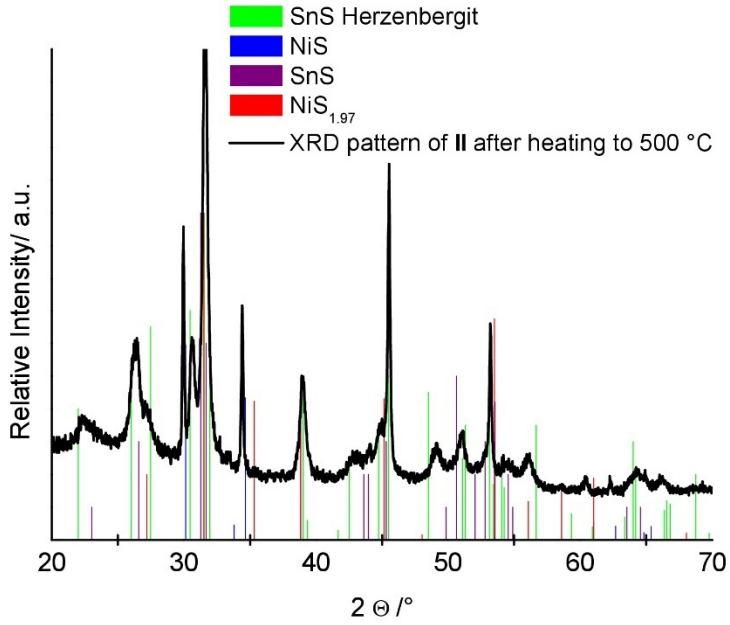

Figure S12: Experimental X-ray powder pattern of compound **II** after heating to 500 °C (black), SnS Herzenbergit (green), $NiS_{1.97}$ (red), NiS (blue) and SnS (purple).

6.1.5 "Transformation of $Na_4SnS_4 \cdot 14H_2O$ into $Na_4Sn_2S_6 \cdot 5H_2O$ at room temperature in the solid state: Synthesis and Crystal Structure of the new compound $Na_4Sn_2S_6 \cdot 5H_2O$"

submitted to the European Journal of Inorganic Chemistry

Content

Figure S1	Calculated X-ray powder patterns of compounds **I** and **II** compared with the pattern of the sample obtained according to literature procedure	p. 1
Figure S2	X-ray powder pattern of compound **I** stored in vacuum for 1 d compared with the calculated pattern of **I**, **II** and the experimental pattern of the pristine material	p. 2
Figure S3	X-ray powder pattern of compound **I** stored in Argon for 1, 2 and 5 d compared with the calculated pattern of **I**, **II** and the pattern of the pristine material	p. 3
Table S1	Geometric parameters of hydrogen bonds in compound **I**	p. 4
Figure S4	X-ray powder patterns of compound **I** heated to 170 ºC and to 300 ºC with a heating rate of 4 $K \cdot min^{-1}$ compared with the calculated pattern of Na_4SnS_4 and the experimental pattern of the pristine material	p. 5
Figure S5	X-ray powder patterns of compound **I** heated with 4 and 16 $K \cdot min^{-1}$ compared with the calculated pattern of Na_4SnS_4	p. 6
Figure S6	X-ray powder patterns of compound **I** heated to 140 ºC and to 300 ºC with a heating rate of 1 $K \cdot min^{-1}$ compared with the calculated pattern of Na_4SnS_4 and the pattern of the sample obtained by heating compound **I** to 170 °C with 4 $K \cdot min^{-1}$	p. 7
Figure S7	X-ray powder pattern of compound **I** heated to 140 ºC with 1 $K \cdot min^{-1}$ and stored at this temperature for 18 h compared with the calculated pattern of Na_4SnS_4	p. 8
Figure S8	TG, DTA and DTG of compound **II** performed with a heating rate of 1 $K \cdot min^{-1}$ in N_2 atmosphere	p. 9
Figure S9	X-ray powder patterns of the sample recovered after heating compound **II** to 300 °C with a heating rate of 4 $K \cdot min^{-1}$ and with 1 $K \cdot min^{-1}$ compared with the calculated pattern of **II**	p. 10
Figure S10	X-ray powder pattern of compound **I** heated to 170 ºC with 4 $K \cdot min^{-1}$ and stored at 295 K for 1 d compared with the calculated patterns of **I** and **II**	p. 11
Figure S11	X-ray powder pattern of compound **I** heated to 140 ºC with 1 $K \cdot min^{-1}$ and stored at 295 K for 1 d compared with the calculated patterns of **I** and **II**	p. 12
Figure S12	X-ray powder pattern of the sample recovered after heating **II** to 300 °C and stored at 295 K for 1 d	p. 13
Figure S13	Final Rietveld plot with experimental data for compound **II**	p. 14
Figure S14	Experimental X-ray powder pattern of compound **II** compared with the pattern calculated from the results of Rietveld refinement	p. 15

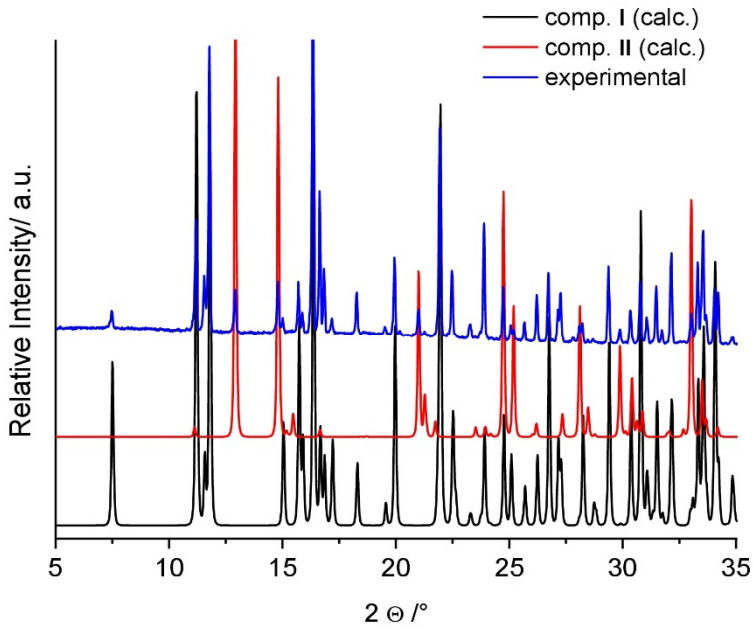

Figure S1. Calculated X-ray powder patterns of compound **I** (black) and compound **II** (red) compared with the pattern (blue) of the sample obtained according to the procedure reported in [1].

[1] Y. Oh, S. Bag, C. D. Malliakas, M. G. Kanatzidis, *Chem. Mater.* **2011**, *23*, 2447–2456.

1

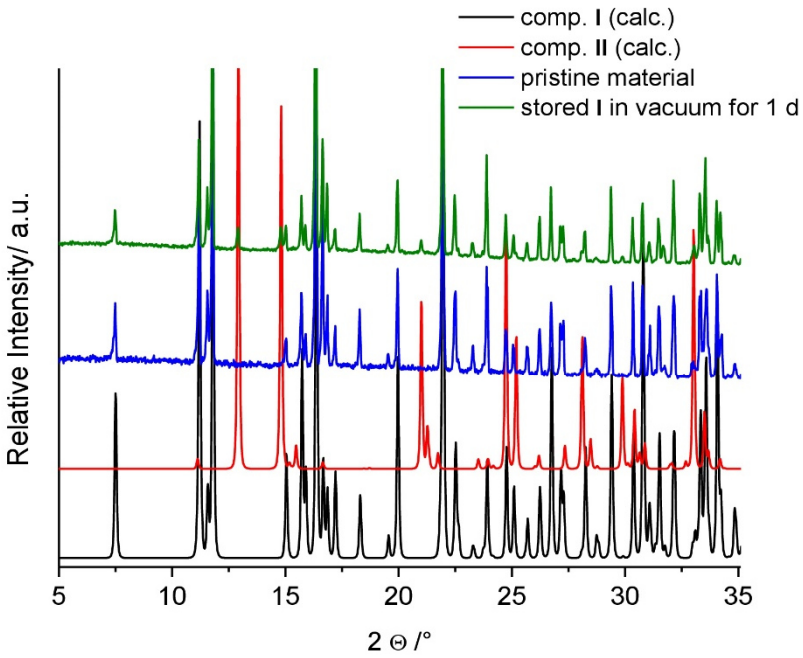

Figure S2. X-ray powder pattern of compound **I** stored in vacuum for 1 d (olive) compared with the calculated pattern of **I** (black), **II** (red) and the experimental pattern of the pristine material (blue).

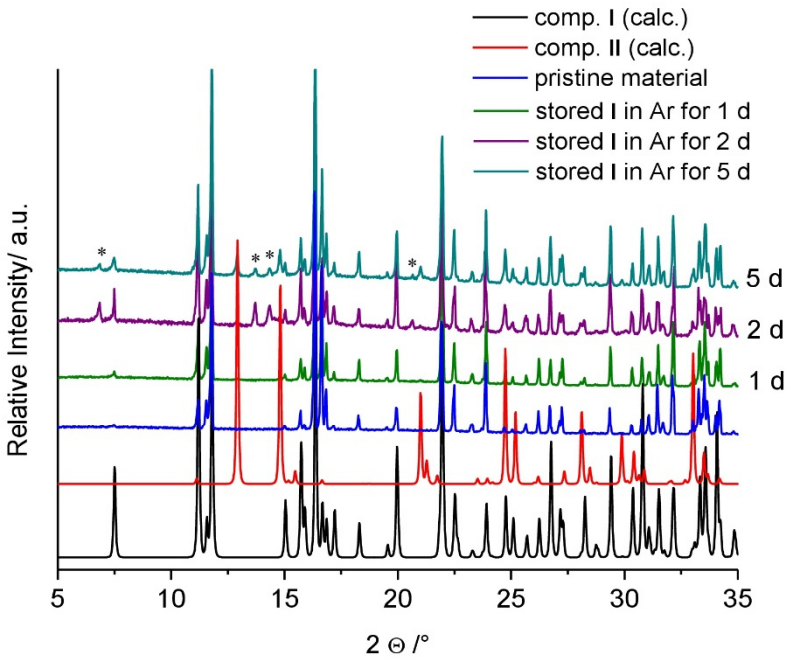

Figure S3. X-ray powder pattern of compound **I** stored in Argon for 1 d (olive), 2 d (purple) and 5 d (cyan blue) compared with the calculated pattern of **I** (black), **II** (red) and the pattern of the pristine material (blue). Asterisks indicate impurities.

Table S1. Geometric parameters of hydrogen bonds [Å and °] in compound **I**.[2]

D-H…A	d(H…A)	d(D…A)	<(DHA)
O1-H1…S1	2.420	3.320	169.4
O1-H2…S2	2.469	3.415	173.0
O2-H3…S1	2.382	3.252	170.0
O2-H4…S1	2.425	3.360	164.4
O3-H5…O5	1.779	2.792	171.3
O3-H6…S2	2.659	3.523	162.1
O4-H7…S1	2.475	3.425	169.2
O4-H8…S1	2.289	3.264	165.5
O5-H9…S2	2.291	3.206	165.4
O5-H10…S2	2.485	3.328	150.9
O6-H11…S2	2.284	3.271	175.7
O7-H13…S2	2.266	3.311	166.2

[2] W. Schiwy, S. Pohl, B. Krebs, *Z. Anorg. Allg. Chem.* **1973**, *402*, 77-86.

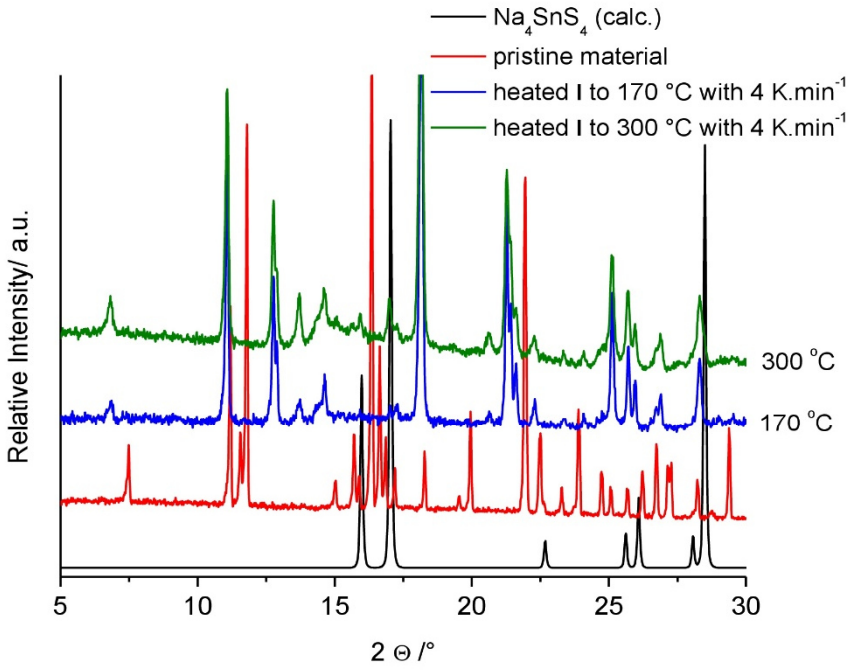

Figure S4. X-ray powder patterns of compound **I** heated to 170 ºC (blue) and to 300 ºC (olive) with a heating rate of 4 K·min^{-1} compared with the calculated pattern of Na_4SnS_4 (black) and the experimental pattern of the pristine material (red).

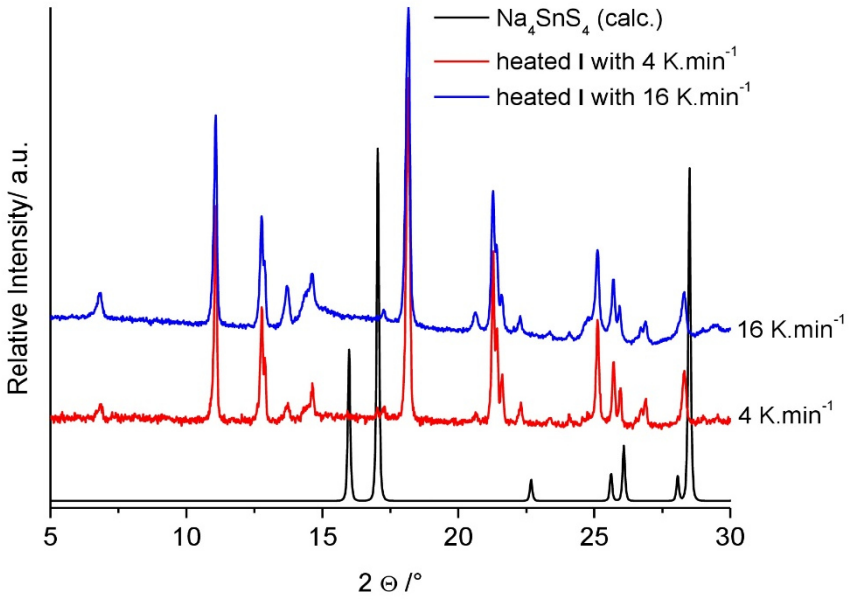

Figure S5. X-ray powder patterns of compound **I** heated with 4 K·min^{-1} (red) and 16 K·min^{-1} (blue) compared with the calculated pattern of Na_4SnS_4 (black).

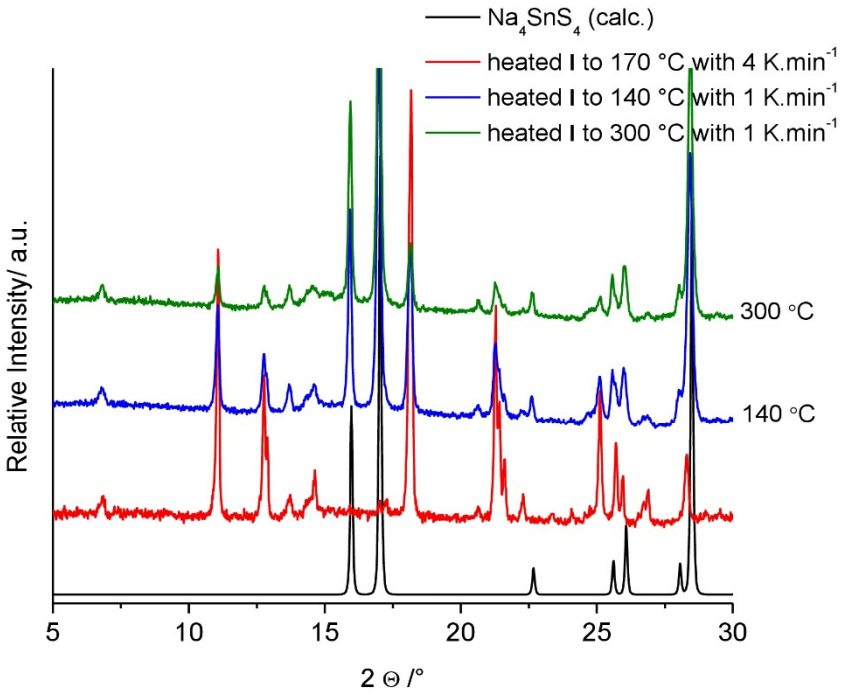

Figure S6. X-ray powder patterns of compound **I** heated to 140 ºC (blue) and to 300 ºC (olive) with a heating rate of 1 K·min^{-1} compared with the calculated pattern of Na_4SnS_4 (black) and the pattern of the sample obtained by heating compound **I** to 170 °C with a heating rate of 4 K·min^{-1} (red).

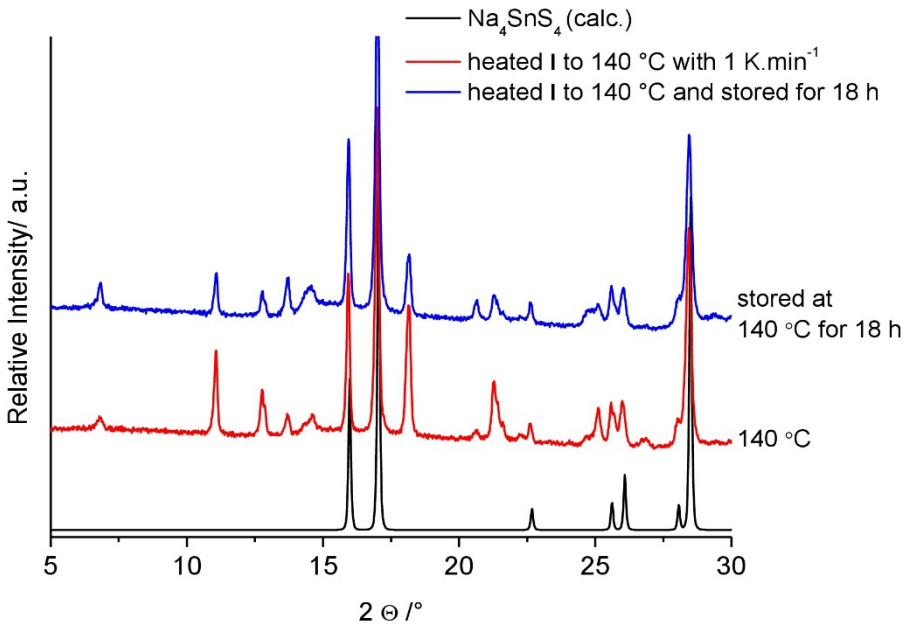

Figure S7. X-ray powder pattern of compound **I** heated to 140 ºC with 1 K·min^{-1} (red) and stored at this temperature for 18 h (blue) compared with the calculated pattern of Na_4SnS_4 (black).

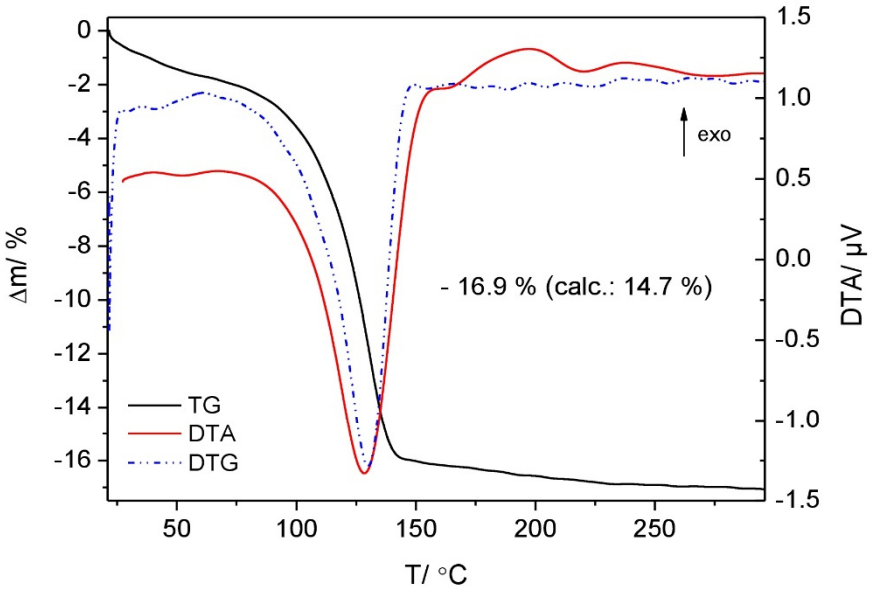

Figure S8. TG (black), DTA (red) and DTG (dashed-dotted blue) of compound **II** performed with 1 K·min^{-1} in N_2 atmosphere.

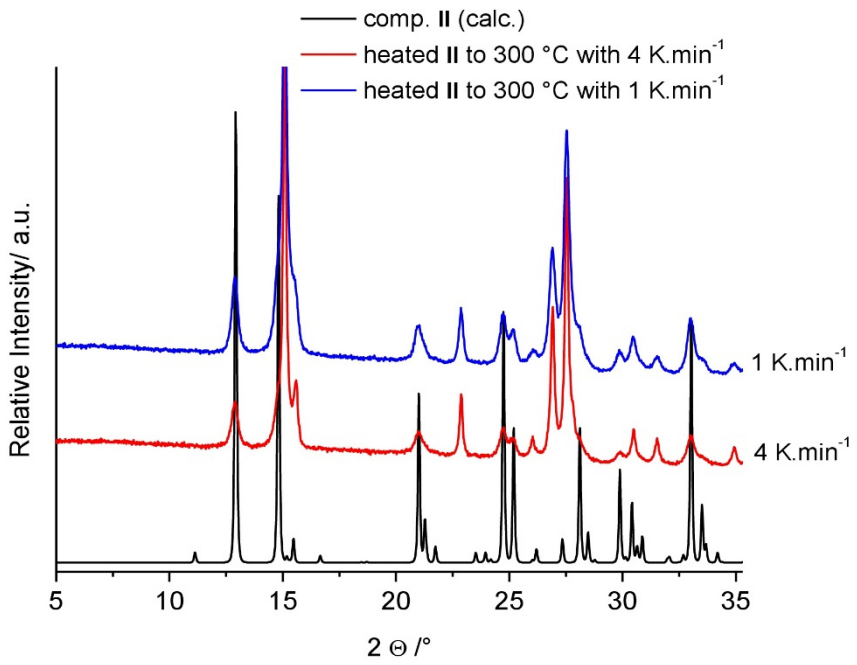

Figure S9. X-ray powder patterns of the sample recovered after heating compound **II** to 300 °C with a heating rate of 4 K·min^{-1} (red) and with 1 K·min^{-1} (blue). Black: comp. **II** (calc.).

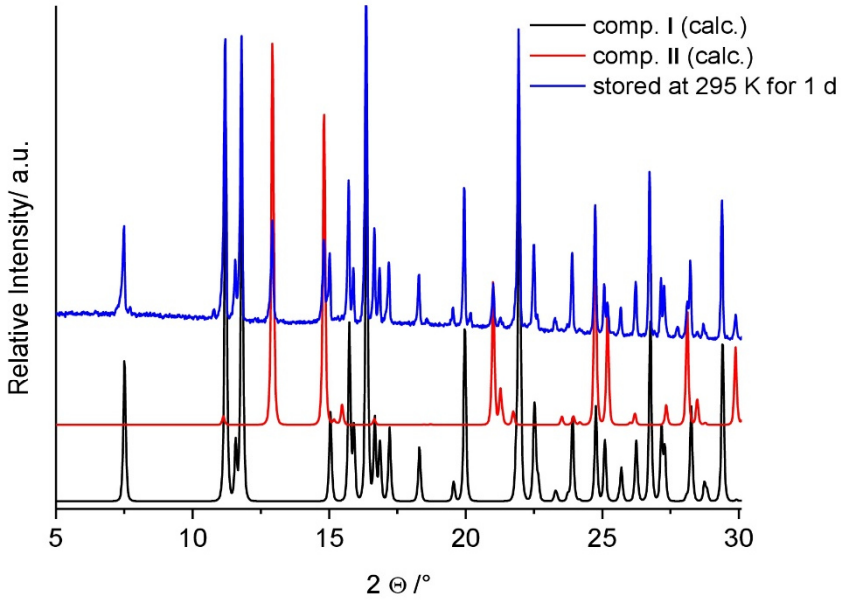

Figure S10. X-ray powder pattern of compound **I** heated to 170 ºC with a heating rate of 4 $K \cdot min^{-1}$ and stored at 295 K for 1 d (blue) compared with the calculated patterns of **I** (black) and of **II** (red).

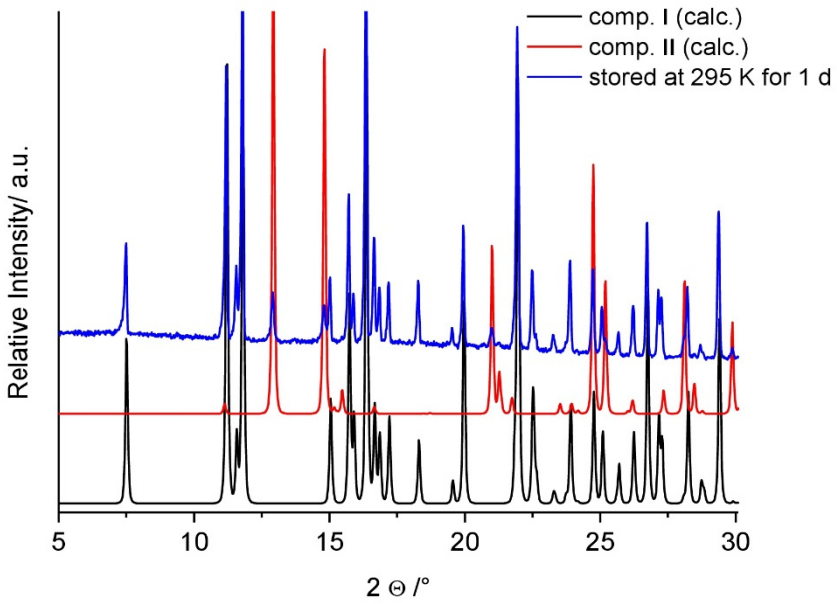

Figure S11. X-ray powder pattern of compound **I** heated to 140 ºC with a heating rate of 1 $K \cdot min^{-1}$ and stored at 295 K for 1 d (blue) compared with the calculated patterns of **I** (black) and of **II** (red).

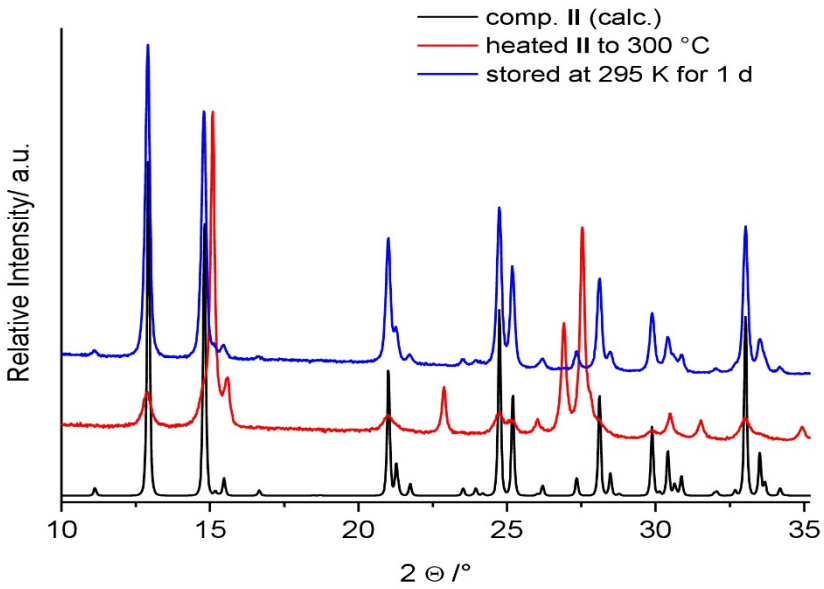

Figure S12. X-ray powder patterns of the sample recovered after heating **II** to 300 °C (red) and stored at 295 K for 1 d (blue). Black: calculated pattern of **II**.

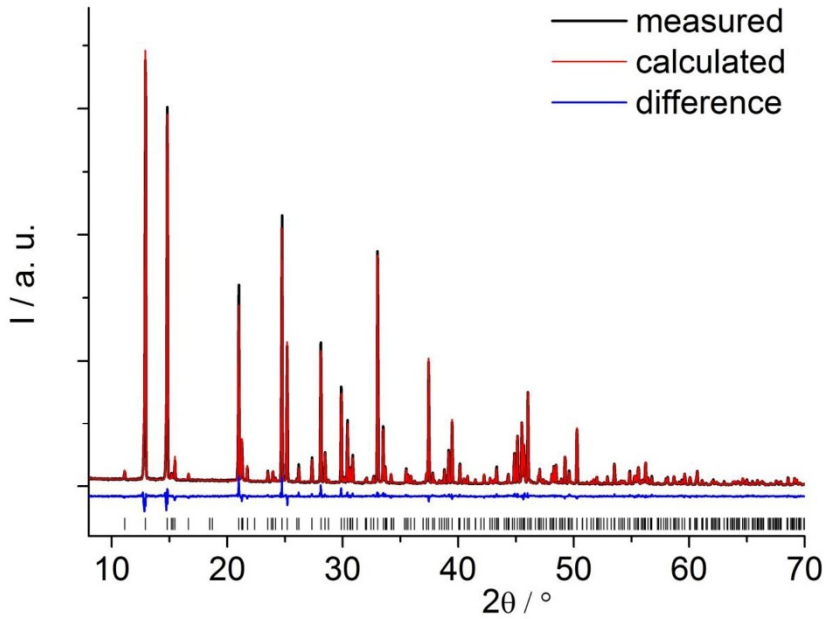

Figure S13. Final Rietveld plot with experimental data shown in black, calculated fit shown in red and difference curve shown in blue. The vertical black bars indicate the allowed peak positions for **II**.

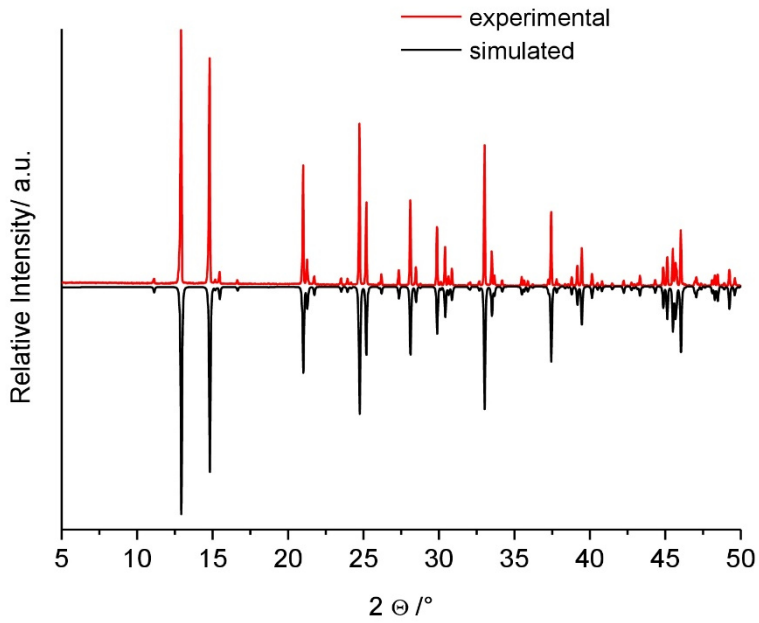

Figure S14. Experimental X-ray powder pattern of compound **II** (red) compared with the pattern calculated from the results of Rietveld refinement (black).

6.2 List of Publications

1) **Assma Benkada**, Michael Poschmann, Christian Näther and Wolfgang Bensch, *Z. Anorg. Allg. Chem.* **2019**, *645*, 433-439.
DOI: 10.1002/zaac.201800475

"New Transition Metal Oxo-Thiostannate: Synthesis, Characterization, and Investigation of its Photocatalytic Properties"

2) **Assma Benkada**, Helge Reinsch, Michael Poschmann, Jan Krahmer, Nicole Pienack and Wolfgang Bensch, *Inorg. Chem.* **2019**, *58*, 2354-2362.
DOI: 10.1021/acs.inorgchem.8b02773

"Synthesis and Characterization of a Rare Transition-Metal Oxothiostannate and Investigation of Its Photocatalytic Properties"

3) **Assma Benkada**, Helge Reinsch and Wolfgang Bensch, *Eur. J. Inorg. Chem.* **2019**, 4427-4432.
DOI: 10.1002/ejic.201900924

"The First Thiostannate Compound with Copper(II) Synthesized Under Ambient Conditions: Crystal Structure, Electronic and Thermal Properties"

4) **Assma Benkada**, Christian Näther and Wolfgang Bensch, *Z. Anorg. Allg. Chem.* **2020**, *accepted*.

"Room temperature synthesis of new thiostannates by slow interdiffusion of different solvents"

5) **Assma Benkada**, Helge Reinsch, Henning Lühmann and Wolfgang Bensch. *Eur. J. Inorg. Chem.* **2020**, *submitted*.

"Transformation of $Na_4SnS_4 \cdot 14H_2O$ into $Na_4Sn_2S_6 \cdot 5H_2O$ at room temperature in the solid state: Synthesis and Crystal Structure of the new compound $Na_4Sn_2S_6 \cdot 5H_2O$"

6.3 Acknowledgements

At first I would like to thank my supervisor Prof. Dr. Wolfgang Bensch for this exciting topic, for his time and advices. Prof. Dr. Christian Näther is grateful acknowledged for the crystal structure analyses and his support with the thermogravimetric analyses.

I want to thank Dr. Helge Reinsch for solving crystal structures from X-ray powder diffraction data.

I also want to thank Dr. Nicole Pienack for her help with the *in-situ*-experiments and her support in all questions.

I would like to thank Dr. Jan Krahmer for the numerous ^{119}Sn-NMR and EPR measurements. Aleksej Jochim and Inke Jess are grateful acknowledged for the numerous thermogravimetric analyses.

I want to say thank you to Stephanie Pehlke and Jacqueline for the elemental analysis, IR-, Raman- and UV/Vis-measurements.

I would like to thank my colleagues “Solvos”: Felix, Lisa, Dana, Joanna, Philipp and the whole working group “AK Bensch”.

A very special thank goes to my parents for the mental and financial support during my education and to offer me the opportunity to study in Germany.

A big “thank you” goes to my husband Yacir for the support and motivation in the last years.

6.4 Declaration

Hiermit versichere ich, an Eides statt, dass ich die vorliegende Dissertation: „Synthesis of Thiostannates, Oxo-Thiostannates and Tin-Sulfides Applying Transition Metal Complexes Containing Macrocyclic Amine Molecules – Development of new synthetic routes to synthesize Sn-S and S-Sn-O compounds and investigation of their properties“ selbstständig und ohne Benutzung anderer als der angegebenen Hilfsmittel angefertigt habe und dass ich alle Stellen, die ich wörtlich oder sinngemäß aus Veröffentlichungen entnommen habe, als solche kenntlich gemacht habe. Diese Arbeit wurde weder ganz noch zum Teil an anderer Prüfungsbehörde vorgelegt oder zur Veröffentlichung eingereicht.

Zusätzlich erkläre ich, dass die vorliegende Dissertation nach den Grundsätzen guter wissenschaftlicher Arbeit der Deutschen Forschungsgemeinschaft (DFG) angefertigt wurde. Außerdem bestätige ich, dass mir bisher auch kein akademischer Grad entzogen wurde.

Ich versichere, dass die eingereichte schriftliche Fassung der auf dem beigefügten Medium gespeicherten Fassung entspricht.

Kiel, 21.07.2020 Assma Benkada